Systems analysis of the CD4 T cell response induced by the novel subunit tuberculosis vaccine, H1:IC31.

Munyaradzi Nyasha Musvosvi

Thesis Presented for the Degree of

DOCTOR OF PHILOSOPHY

in the Department of Paediatrics and Child Health

Faculty of Health Sciences

UNIVERSITY OF CAPE TOWN

On the 24th of August, 2015

Supervisor: Associate Professor Thomas J. Scriba

Co-supervisor: Dr Adam Penn-Nicholson

Declaration

I, Munyaradzi Nyasha Musvosvi, hereby declare that the work on which this thesis is based is my original work (except where acknowledgements indicate otherwise) and that neither the whole work nor any part of it has been, is being, or is to be submitted for another degree in this or any other university.

I empower the university to reproduce, for the purpose of research, either the whole or any portion of the contents in any manner whatsoever.

Signature:

Date:

Acknowledgements

Finally, it's over! What an amazing journey of academic and personal growth. There are so many people I need to thank who provided encouragement, guidance, and advice throughout my PhD. This journey would not have been half as fun without you.

Firstly, I would like to thank my family. Thanks Mom and Dad for making sure that I saw the value of higher education. Watching you guys work day and night, while getting postgraduate degrees and still making time for all us kids was inspirational. I would also like to thank Tapiwa and Rufaro for being amazing siblings. You guys always brought laughter and joy after a hectic week in the lab.

Secondly, I would like to thank my awesome girlfriend, Yoliswa. You were always there for me and importantly, understood when I was late for dinner because experiments ran late.

Thank you to all the people who have supervised and mentored me during my PhD. Willem Hanekom, thank you for approaching me during my BSc honours and inviting me to join SATVI. I could not have asked for a better lab to do my PhD. Thank you Brian Abel for your supervision and showing me that an office can easily become a cricket pitch.

To Adam Penn-Nicholson, thank you for your mentorship, supervision, and lunchtime chats over Indian food.

Many thanks to my supervisor, Thomas Scriba. Your enthusiasm and passion for science is infectious. The mentorship and supervisor I have received has prepared me for life as a scientist.

I would like to give a special thank you to all the adolescents who participated and provided samples for the Adolescent Cohort Study and the THYB04 trial. This study would not have been possible without you. I would also like to thank every one of my SATVI colleagues involved in recruitment and sample processing.

Lastly, I would like to thank the Carnegie Corporation, the Bill and Melinda Gates Foundation, and Horizon2020 TBVI for funding this study.

Summary

In this study we sought to more comprehensively analyse antigen-specific CD4 T cell responses induced by vaccination and to examine the effects of latent *M.tb* infection on these responses. We had two broad objectives: Firstly, to determine the effects of latent *M.tb* infection on epitope recognition by mycobacteria-specific CD4 T cells and to design HLA class II tetramers for detection of these cells. Secondly, to characterise antigen-specific CD4 T cells following vaccination with the novel vaccine candidate, H1:IC31, by measuring transcriptomic, phenotypic and functional attributes, and to determine the effects of latent infection on these responses.

Firstly we found that acquisition of *M.tb* infection did not alter the breadth and/or pattern of Ag85A/B CD4 T cell epitopes recognised. We determined the HLA allele restriction of identified epitopes, and designed HLA class II tetramers for detection of Ag85-specific CD4 T cells. These results suggest that latent infection does not alter CD4 T cell epitope breadth within Ag85A/B elicited by BCG vaccination and/or exposure to environmental mycobacteria.

The second finding of this work is that underlying infection drives a more effector-like H1-specific CD4 T response after vaccination. Following vaccination *M.tb*-infected adolescents had higher frequencies of H1-specific CD4 T cells compared with uninfected adolescents. Additionally, H1-specific CD4 T cells from infected adolescents predominantly displayed a $CCR7^{-}CD45RA^{-}$ effector memory phenotype, had higher proportions of IFN-γ^{+}TNF-α^{+}IL-2^{+} cells, and expressed higher levels mRNA transcripts encoding effector molecules such as granzyme K and perforin, compared with uninfected adolescents. By contrast, H1-specific CD4 T cells

in uninfected adolescents displayed a less differentiated memory phenotype, and had increased expression of central memory genes, compared to cells from infected adolescents.

Thirdly, we found that Ag85B and ESAT-6-specific CD4 T cells exhibited markedly distinct transcriptomic profiles, memory phenotypes and cytokine expression patterns in *M.tb* infected adolescents. The data suggested that ESAT-6-specific cells preferentially drove the effector-like H1-specific response in *M.tb* infected adolescents.

We conclude that while underlying *M.tb* infection does not affect the epitopes recognized by mycobacteria-specific CD4 T cells, but may promote and maintain effector memory antigen-specific CD4 T cells endowed with immediate effector function and tissue homing.

List of Figures

List of Tables

List of abbreviations

ACS	Adolescent Cohort Study
ALP	Alkaline phosphatase
BAL	Bronchoalveolar lavage
BCG	Bacille Calmette-Guérin
CCR7	Chemokine receptor type 7
CM	Central memory
CMV	Cytomegalovirus
Ct	Threshold cycle
DCs	Dendritic cells
DMSO	Dimethyl sulfoxide
EBNA	Epstein–Barr nuclear antigen 1
EBV	Epstein-Bar Virus
EDTA	Ethylenediaminetetraacetic acid
EM	Effector memory cells
Et	Threshold expression
FACS	Fluorescence activated cell sorting
FCS	Foetal calf serum
FDR	False Discovery Rate
gDNA	Genomic DNA
GOI	Gene of interest
H1	Ag85B and ESAT-6
H56	Ag85B-ESAT-6-Rv2660
ICS	Intracellular cytokine staining

IFC	Integrated fluidic circuit
IFN-γ	Interferon gamma
IGRAs	IFN-g release assays
IL	Interleukin
IQR	Interquartile range
iTregs	Induced Tregs
KLK	Antibacterial cationic peptide $KLKL_5KLK$
LEF-1	Lymphoid enhancer binding factor 1
LIAI	La Jolla Institute for Allergy and Immunology
M.bovis	*Mycobacterium bovis*
M.tb	*Mycobacterium tuberculosis*
MAD	Median absolute deviations
MAIT	Mucosal associated invariant T
MMP-1	Matrix metalloproteinase 1
MVA	Modified vaccinia Ankara
nTregs	Natural Tregs
ODN1a	Phosphodiester-backboned oligodeoxynucleotide
PBMCs	Peripheral blood mononuclear cells
PBS	Phosphate buffered saline
PHA	Phytohaemagglutinin
PI3P	Phosphatidylinositol 3-phosphate
PPD	Purified protein derivative
QFT	QuantiFERON TB Gold In-Tube
qPCR	Quantitative polymerase chain reaction
R10 AB	RPMI containing 10% human AB+ serum

R10 FCS	RPMI containing 10% FCS
rBCG	recombinant BCG ΔureC::hly
RD1	Region of difference 1
RhCMV	Rhesus cytomegalovirus
ROC	Receiver operating characteristic
SATVI	South African Tuberculosis Vaccine Initiative
SEB	Staphylococcal enterotoxin
SFU	Spot forming units
STA	Specific transcript amplification
TaqMan GE	TaqMan gene expression
TCF7	Transcription factor 7
TCR	T cell receptor
Teff	Effector T cells
Tfh	Follicular helper CD4 T cells
TGFβ	Transforming growth factor beta
Th	T helper
TNF-α	Tumor necrosis factor alpha
Tregs	Regulatory T cells
TST	Tuberculin skin test
WHO	World Health Organisation

Chapter 1: Introduction

Tuberculosis burden

Tuberculosis is a major global healthcare challenge. The World Health Organisation (WHO) estimates that in 2013 there were 9.0 million cases of tuberculosis and 1.5 million deaths as a result of this disease (WHO 2014). Tuberculosis is the second leading cause of death from an infectious agent (WHO 2014). Although, tuberculosis can occur anywhere in the world the burden of disease largely affects developing counties, such as South Africa. Important discoveries such as the identification of *Mycobacterium tuberculosis* (*M.tb*) as the causative agent of tuberculosis in 1882 by Robert Koch (Daniel 2006) and the development of effective chemotherapy have helped in combating this disease but much more needs to be done (Olaru et al. 2015). The WHO has set a goal to end the tuberculosis epidemic by 2035. Although the global incidence of tuberculosis has started to fall, elimination of tuberculosis by 2035 will require the introduction of innovative and novel tools to compliment current approaches to improve the reduction rate of tuberculosis (WHO 2014). These include improvement in tuberculosis diagnosis, drug therapies, and vaccines (Abu-Raddad et al. 2009). Bacille Calmette-Guérin (BCG), the only licensed tuberculosis vaccine, is administered in many countries worldwide, including South Africa, however, for reasons discussed below there is a need for more effective vaccines to either replace BCG or boost BCG induced immunity. At the South African Tuberculosis Vaccine Initiative (SATVI) we are involved in generating knowledge and understanding about the immune responses induced by novel tuberculosis vaccines and *M.tb* infection. The main aim of this thesis was to better understand the immune responses induced by novel tuberculosis vaccines.

Better tools to diagnose active and latent tuberculosis are needed.

Pulmonary tuberculosis is the most common form of the disease, however *M.tb* is able to disseminate from the lungs and cause disease in other tissues (i.e. extrapulmonary tuberculosis) (WHO 2014). Symptoms of pulmonary tuberculosis include chronic cough, production of sputum, coughing up blood, loss of appetite, fever, loss of weight, and night sweats (Zumla et al. 2013). There are many challenges that hinder diagnosis of tuberculosis. The WHO estimates that annually only 64% of tuberculosis cases are detected (WHO 2014). Improving case detection is needed to help reduce *M.tb* transmission, because early identification and treatment of tuberculosis patients will halt the spread of the disease. A major challenge that is delaying the elimination of tuberculosis is the lack of inexpensive and quick diagnostic tools that can be used at the point of care. The most widely used method in diagnosing tuberculosis is microscopic detection of *M.tb* in sputum of patients displaying symptoms of tuberculosis (Dorman 2010). However, detection by microscopy is only possible in advanced pulmonary tuberculosis (van den Boogaard et al. 2009). It is estimated that a minimum of 5,000 – 10,000 bacilli per mL of sputum can be detected by microscopy (Tostmann et al. 2008). Another approach used to diagnose tuberculosis is detection of *M.tb* in sputum by culture. This approach has been shown to be more sensitive than microscopic detection of *M.tb* in sputum (Dorman 2010). It is also possible to detect drug resistant strains using the culture method. However, the lengthy incubation time (up to 28 days), requisite of appropriate biosafety facilities and the relatively high cost are drawbacks for performing routine *M.tb* cultures (Dorman 2010). The introduction of PCR-based methods, such as the Xpert MTB/RIF test, to detect *M.tb* nucleic acid material has been a major development in improving tuberculosis diagnosis (WHO 2014). Such methods offer the ability to

rapidly detect the presence of *M.tb* and identify mutations associated with drug resistance. However, in many low-income countries issues of affordability may result in this technology not being a true point of care test (García-Basteiro & Cobelens 2015). The lack of adequate healthcare facilities capable to perform these tests in communities affected by tuberculosis still delays diagnosis of tuberculosis. (McNerney et al. 2012; Lawn & Nicol 2011) Therefore, development of more appropriate technologies and strategies to improve tuberculosis diagnosis in resource poor settings is urgently needed.

An interesting and noteworthy feature of *M.tb* infection is that only a minority of individuals that become infected ever display symptoms of tuberculosis disease. This larger group of infected, asymptomatic people is classified as latently infected. Currently there is no test that is able to detect *M.tb* in persons not exhibiting symptoms of active tuberculosis (i.e. production of sputum). Latent *M.tb* infection is typically inferred by the presence of an immune response to mycobacterial antigens in the absence of symptoms. Traditionally, the tuberculin skin test (TST) has been used to diagnose latent *M.tb* infection. More recently, IFN-γ release assays (IGRAs), such as the QuantiFERON TB Gold In-Tube, that contain *M.tb*-specific antigens have been used to diagnose latent *M.tb* infection. Researchers, therefore, are relying on the presence of an antigen-specific immune response to *M.tb* and not the presence of *M.tb* itself to diagnosis infection. It is not possible to distinguish persons that are harbouring *M.tb* from persons that have an adaptive immune response against *M.tb*, but are not harbouring *M.tb*. However, isoniazid preventative treatment reduces the incidence of tuberculosis among TST^{+} persons, suggesting that immune sensitization is a reasonable correlate of *M.tb* infection (Akolo et al. 2010). It must be stressed that

the absence of a recall response to *M.tb* antigens does not necessarily mean the individual is not harbouring *M.tb* infection. It is possible that the anti-*M.tb* response in persons with negative TST or IGRAs may be localised and not detectable systemically (O'Garra et al. 2013).

New drugs are needed to shorten treatment and combat drug resistance.

While treatment of drug-sensitive tuberculosis is very effective (i.e. >90% cure rate), problems related to non-adherence and the emergence of drug-resistant *M.tb* strains are threatening the effectiveness of current chemotherapy regimens (Dheda et al. 2014). Addressing these challenges will help to reduce the disease burden. The challenge of non-adherence is thought to be a result of the very long duration of treatment and adverse events associated with drug treatments for tuberculosis (van den Boogaard et al. 2009). The WHO currently recommends that the duration of treatment of drug-susceptible tuberculosis should be 6 months and at least 20 months for drug-resistant tuberculosis (Zumla et al. 2015). There is a clear need to develop novel treatment regimens that shorten the treatment durations, reduce adverse events, and bolster our arsenal against drug resistant *M.tb* strains.

A more effective vaccine is required to eliminate tuberculosis.

> "The impact of vaccination on the health of the world's peoples is hard to exaggerate. With the exception of safe water, no other modality, not even antibiotics, has had such a major effect on mortality reduction and population growth." (Plotkin et al. 2008)

Vaccination is one of the most cost-effective public health interventions (Ozawa et al. 2012). Vaccines have successfully controlled many infectious diseases, with probably the most prominent success of human vaccination being the eradication of smallpox (Francis 2010). The guiding principle of vaccination is to "train" the adaptive immune system using an attenuated version or subunit components of the pathogen of interest. Successful vaccination endows the adaptive immune response with characteristics that can prevent infection or disease when the pathogen is encountered. Besides the individual benefit of preventing disease, vaccination also impacts the transmission of disease at a population level. If enough people are successfully vaccinated, even persons who do not receive the vaccine benefit; because they are not exposed.

It is therefore not surprising that after the discovery of *M.tb* in 1882, Albert Calmette and Camille Guérin began development of a vaccine against tuberculosis in 1908. They successfully produced an avirulent strain of *Mycobacterium bovis (M.bovis)*, BCG. The development of BCG was a result of *M. bovis* being passaged more than 200 times over the course of 13 years on glycerinated beef bile (Branch 1927). Vaccination of humans with BCG began in 1921 (Oettinger et al. 1999). To this day BCG remains the only licensed vaccine against tuberculosis and has extensive worldwide coverage (Kaufmann et al. 2010). It should be noted that the current BCG strains have evolved over time from the original BCG strain developed in 1921 by Calmette and Guérin (Yamamoto & Yamamoto 2007). Several genomic regions are absent in the genomes of one or more BCG strains compared to *M.bovis* or *M.tb* (Zhang et al. 2013). However, region of difference 1 (RD1) is absent is all strains of

BCG but present in *M.tb* (Lewis et al. 2003). RD1 has been linked with the reduced virulence of BCG. Introducing RD1 into BCG results in increased bacterial burdens in the lungs of mice (Majlessi et al. 2005). The absence of RD1 in BCG has prompted some investigators to use proteins, such as the early secreted antigenic target 6 kDa (ESAT-6) and culture filtrate protein 10 kDa (CFP-10), encoded by genes in RD1 as diagnostic tools or vaccine antigens.

BCG vaccination has been shown to offer consistent protection against disseminated forms of tuberculosis in infants, but BCG offers highly variable protection against adult pulmonary tuberculosis, ranging from limited to no protection (Colditz et al. 1995; Mangtani et al. 2014; WHO 2014). In a recent meta-analysis Mangtani *et. al.* observed that BCG vaccination resulted in rate ratios for pulmonary tuberculosis of 0.41 and 0.26 in infants and school aged children, respectively, indicating protection in the vaccinated group (Mangtani et al. 2014). Furthermore, the investigators reported that BCG vaccination offered substantial protection against miliary and meningeal tuberculosis (Mangtani et al. 2014). However, they did not observe consistent protection in participants older than school age (Mangtani et al. 2014). Adults have higher rates of smear positive tuberculosis compared to children and, as such, are more likely to transmit *M.tb* compared to children (Wood et al. 2012). Therefore, developing a vaccine that offers consistent protection against pulmonary tuberculosis in older persons will be key in eliminating tuberculosis. Indeed, a study that modeled the impact of hypothetical vaccines with varying levels of protection against tuberculosis identified that vaccination of adolescents/adults would have a significantly higher impact on the tuberculosis burden compared to vaccination of infants (Knight et al. 2014). In addition to the variable protection offered by BCG,

concerns have been raised about the safety of BCG in immunocompromised persons. Due to the relatively high risk of developing disseminated disease from BCG, the WHO does not recommend BCG vaccination in infants with known HIV infection (WHO 2014).

The concerns discussed above have prompted many groups to design and develop more efficacious and safer vaccines against tuberculosis. There are 15 novel vaccine candidates in various stages of clinical development (Figure 1) (WHO 2014). At SATVI, we have been involved in clinical trails assessing at least 7 of these vaccines (SATVI 2014 Annual Report http://www.satvi.uct.ac.za/sites/default/files/image_tool/images/199/Annual_Report/SATVI%20AnnualReport2014.compressed.pdf), including a recent phase IIb trial that assessed the efficacy of a modified vaccinia Ankara (MVA) expressing the mycobacterial antigen Ag85A in a cohort of BCG vaccinated infants (Tameris et al. 2013). While this trial showed disappointing results in terms of efficacy it has spurred important discussions concerning the current knowledge of the immune response to *M.tb*, the absence of minimum criteria that have to be met for vaccines to progress to efficacy trials and the need to increase diversity in vaccine concepts (Karp et al. 2015; Andersen & Woodworth 2014). A major limitation to rational development of a more effective tuberculosis vaccine is the lack of immune correlates of protection against tuberculosis or knowledge of protective immunity. There is also a lack of comprehensive knowledge of the immune response induced by novel tuberculosis vaccines in humans. Such understanding is critical in the design and clinical development of novel vaccines. In this thesis we performed a comprehensive analysis with the aim of understanding the immune responses induced by a novel tuberculosis vaccine in adolescents.

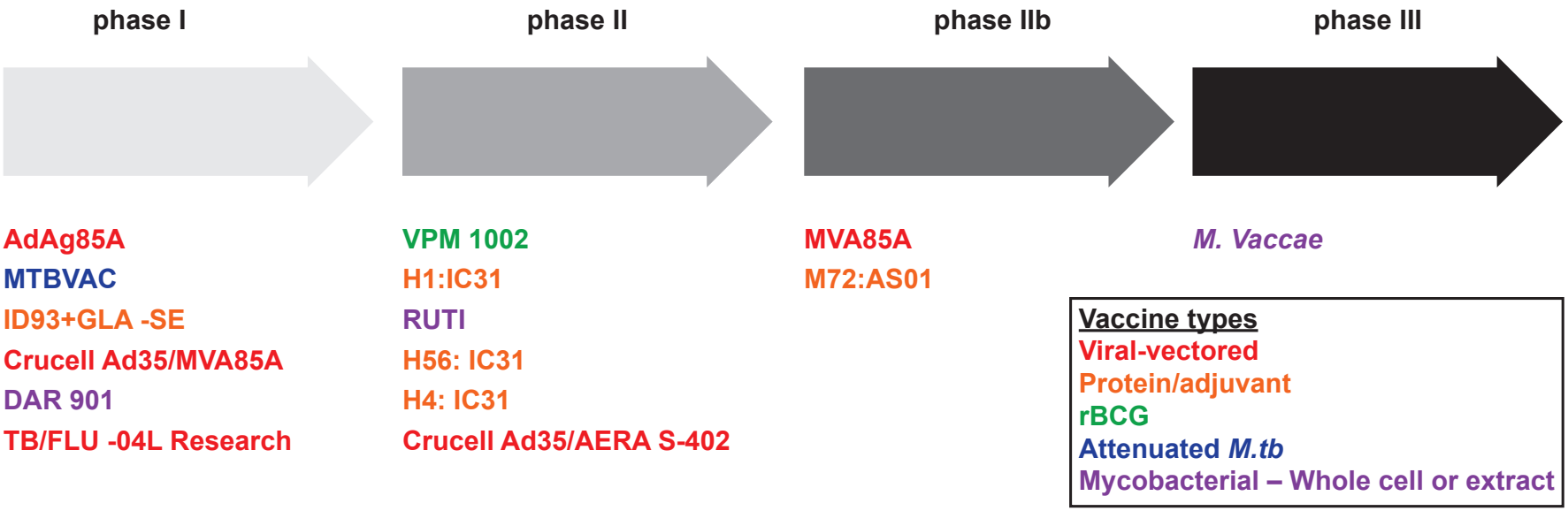

Figure 1. Tuberculosis vaccines currently in clinical development. (Adapted from WHO Global Tuberculosis Report 2014

***M.tb* is transmitted via aerosolised microdroplets to the alveoli.**

In order to rationally develop a vaccine against any pathogen, it is important to understand the events that lead to disease after exposure. Exposure to *M.tb* occurs via aerosol microdroplets coughed up by an individual with active pulmonary tuberculosis, which can remain in the atmosphere for several hours (Russell 2007). However, not all aerosolised droplets from tuberculosis patients contain viable/culturable bacteria. Fennelly *et. al* performed a study in which they collected aerosolised droplets from tuberculosis patients in order to determine the rate at which they could culture *M.tb* from collected coughs. They used cascade impactors that allowed the researchers to determine the aerosol sizes that contained the culturable *M.tb*. The researchers cultured *M.tb* from only 28% of the coughs assessed and they demonstrated that 96% of the cultured *M.tb* was collected from aerosol droplets between 0.65μm and 4.7μm (Fennelly et al. 2012). It should be noted that the rate of viable *M.tb* might have been underestimated due to a number of limitations, such as the inclusion of patients that had been on treatment for less than a week and relying on growth on selective 7H11 agar as a read-out of viable *M.tb* (Fennelly et al. 2012). Regardless of these limitations, it remains likely that natural exposure to *M.tb* occurs via droplets less than 5μm in size. Droplets smaller than 5μm can reach the alveoli of the lung (Ferron 1994). Therefore, a comprehensive understanding of the immune responses that occur in the alveoli following *M.tb* deposition is critical in identifying key events that vaccine induced responses should disrupt.

The granuloma is a hallmark feature of tuberculosis.

Alveolar macrophages function as sentinel cells in the airways, engulfing foreign particles that enter the lungs (Hussell & Bell 2014). These cells are typically viewed

as the cell type that *M.tb* first encounters following inhalation. Alveolar macrophages recognize and engulf *M.tb* using a variety of Toll-Like, scavenger, mannose, and complement receptors (van Crevel et al. 2002). Uptake of *M.tb* by alveolar macrophages initiates the production of chemo-attractants that recruit of immune cells to the site of infection (Guirado & Schlesinger 2013; Ehlers & Schaible 2013). The resulting structured aggregation of immune cells is known as a granuloma, and it is the hallmark feature of tuberculosis. The granuloma consists of infected and uninfected macrophages, epitheloid cells, foamy macrophages, neutrophils, multinucleated giant cells, fibroblast and, once an adaptive immune response has been triggered, B and T cells (Russell 2007; Guirado & Schlesinger 2013; O'Garra et al. 2013). Although the granumola is the hallmark feature of tuberculosis, it is not specific to *M.tb* infection. The immune response to other pathogens such as *Leishmania*, *Treponema pallidum*, and *Coccidioides immitis* also involves granuloma formation (Zumla & James 1996). Granuloma formation is generally viewed as a protective response initiated when acute inflammatory processes cannot destroy invading pathogen (Zumla & James 1996). Granulomas form microenvironments within the lung tissue where host defense mechanisms and *M.tb* survival mechanisms interact. The granuloma is a dynamic structure and different types of granulomas are observed in tuberculosis. The types of granulomas described include the caseous, non-necrotizing, and fibrotic granuloma, amongst others (Figure 2). The caseous (necrotic) granuloma is viewed as the classic granuloma during tuberculosis (Barry et al. 2009). At the center of this granuloma is caseum, a solid necrotic region made up of dead macrophages and where the *M.tb* is contained (Grosset 2003; Barry et al. 2009; Ramakrishnan 2012). This is surrounded by macrophages, neutrophils, T cells, B cells and enclosed by fibroblasts (Barry et al. 2009). Lack of *M.tb* control is

thought to arise from accumulation of caseum, liquefaction of the caseum and the rupturing of the granuloma releasing free *M.tb* into the airways (Kim et al. 2010). Unlike the caseous granuloma, the non-necrotizing granuloma does not have a caseum center. The non-necrotizing granuloma consists mainly of macrophages and some T and B cells (Barry et al. 2009). The fibrotic granuloma consists mostly of fibroblasts (Barry et al. 2009). The diversity of granulomas suggests that within each granuloma unique host-pathogen interactions occur (Guirado & Schlesinger 2013). Recent studies that utilized the non-human primate model of *M.tb* infection have allowed researchers to investigate and track granuloma formation and diversity in primates with latent infection or active tuberculosis (Lin et al. 2009; Gideon et al. 2015). Results from these studies suggest that the sum total of events within granulomas likely affect the outcome of *M.tb* infection (Flynn et al. 2015). Understanding these interactions and determining the effects of adaptive immune cells on granulomas is paramount for vaccine development.

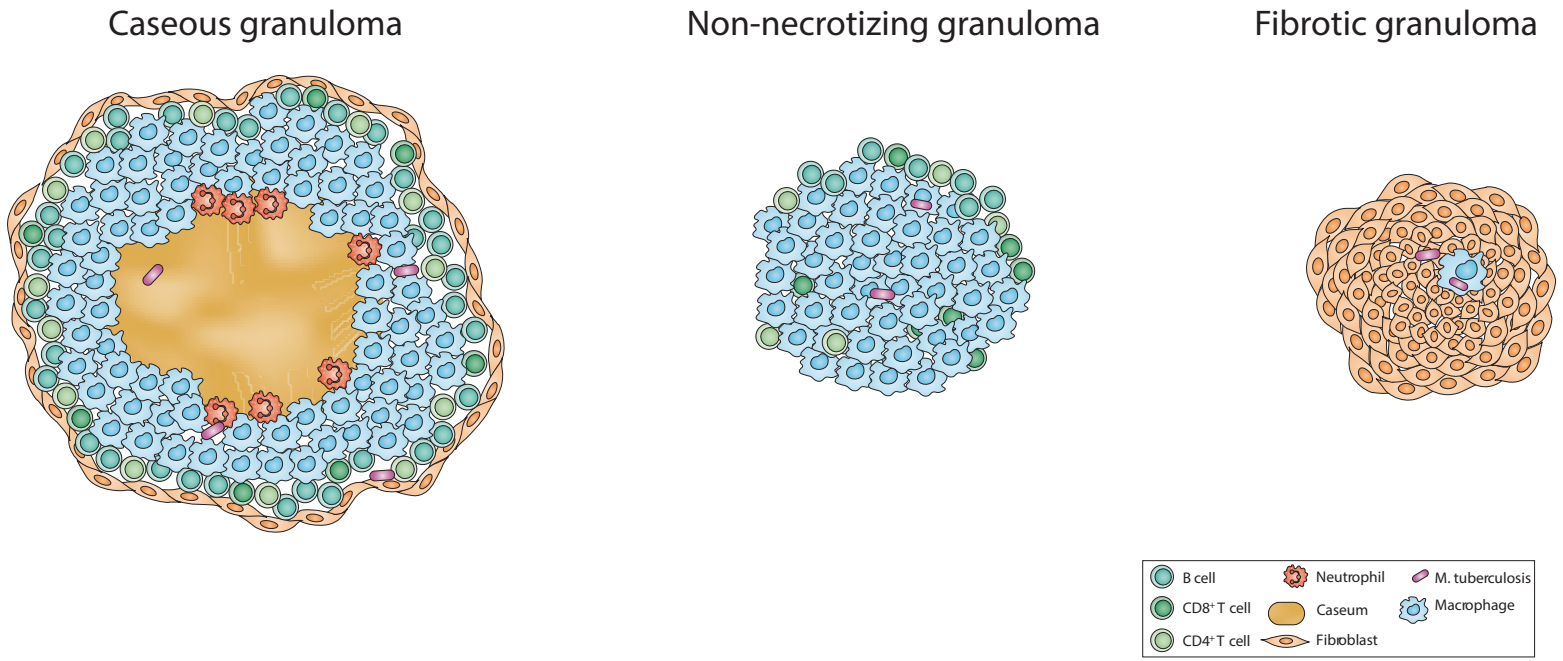

Figure 2. The cellular composition and architecture of tuberculosis granulomas. (Adapted from Barry et. al. Nature reviews. Microbiology 2009)

The antimicrobial role of macrophages and neutrophils

As discussed above, macrophages are crucial in initiating the immune response against *M.tb.* In addition to recruiting immune cells to the site of infection macrophages also initiate antimicrobial processes such as phagosome maturation, apoptosis, autophagy, and the production of antimicrobial peptides (O'Garra et al. 2013). Phagosome maturation is central to the microbicidal function of macrophages (Vieira et al. 2002). Phagosome maturation is a process that results in the fusion of a phagosome and lysosomes to form a highly acidic, antimicrobial environment (Kinchen & Ravichandran 2008). The interactions of host macrophages and *M.tb* in the context of phagosome maturation have been well-studied (Welin & Lerm 2012). *M.tb* is able to arrest phagosome maturation by inhibiting the fusion of phagosomes and lysosomes (Clemens & Horwitz 1995). A mechanism that explains this was described by Verge *et. al,* by demonstrating that *M.tb* can hydrolyse phosphatidylinositol 3-phosphate (PI3P), an essential lipid required for phagosome and lysosomal fusion (Vergne et al. 2005).

Macrophages also control *M.tb* infection through apoptosis. Apoptosis is a well-regulated process that results in macrophage death, but the plasma membrane remains intact. This is in contrast to another form of cell death, necrosis that is accompanied by plasma membrane disruption. It has been demonstrated the eicosanoid pathway is employed by macrophages to control *M.tb* bacterial burden by inducing apoptosis, whereas *M.tb* exploits the same pathway to enhance bacterial spread by inducing necrosis (Chen et al. 2008; Tobin et al. 2010; Behar et al. 2011). In addition to involvement in bacterial control, macrophage apoptosis results in greater priming of the T cell response compared to necrosis (Behar et al. 2011).

Another mechanism through which macrophages control *M.tb* is via autophagy. Autophagy is an ancient evolutionary recycling pathway that allows reusage of nutrients during starvation by degradation of protein aggregates. This pathway can also be utilised for the killing of intracellular pathogens (Songane et al. 2012; Deretic 2008). The autophagosome, which is a double-membrane vesicle, engulfs material in the cytosol and then facilitates fusion with lysosomes (Songane et al. 2012). The cytokine IFN-γ can induce autophagy in human macrophages infected with mycobacteria (Gutierrez et al. 2004). Infection of mice that lack autophagy function in macrophages resulted in increased bacterial burdens and decreased survival compared to wild-type mice (Castillo et al. 2012). In humans, vitamin D3 has also been shown to be important in inducing autophagy and the expression of the antimicrobial peptides, cathelicidin and β-defensin 2 (Fabri et al. 2011). Interestingly, tuberculosis patients have been shown to have lower levels of vitamin D compared to healthy controls (Wilkinson et al. 2000; Mahmoud & Ali 2014). Together these studies point to autophagy and the induction of antimicrobial peptides in infected macrophages as possible mechanisms that may be targeted and exploited by novel immunotherapies or vaccines aimed at controlling tuberculosis. However, more research needs to be conducted to understand of how this can be achieved.

The role of neutrophils in immune control of *M.tb* has not been characterized to the same level as macrophages (Lowe et al. 2012). There is little doubt that neutrophils are involved in the immune response to *M.tb*. These cells are readily identified in granulomas (Mattila et al. 2015). A study by Eum *et. al.* revealed that neutrophils were the predominant cell types infected with *M.tb* in the sputum and bronchoalveolar

lavage (BAL) fluid of tuberculosis patients (Eum et al. 2010). However, the answer to the question of whether neutrophils play a beneficial or detrimental role is dependent on a number of factors. Following infection neutrophils rapidly migrate to the site of infection (Eruslanov et al. 2005; Pedrosa et al. 2000). Outcomes in mouse experiments that have depleted neutrophils appear to be dependent on whether neutrophils were depleted before or during *M.tb* infection. Depleting neutrophils prior to infection resulted in increased bacterial burdens (Pedrosa et al. 2000) while depletion during chronic infection resulted in a reduction of the bacterial burden (Zhang et al. 2009). This suggests that neutrophils may have different roles early after infection and during chronic infection. Transcriptomic analysis of blood collected from tuberculosis patients revealed an interferon-inducible transcriptomic signature that was largely driven by overexpression of IFN-inducible transcripts in neutrophils (Berry et al. 2010), further highlighting the importance of this cell type during tuberculosis. It therefore appears that neutrophils may have both a beneficial and detrimental role in immune control of *M.tb* infection (O'Garra et al. 2013).

For reasons discussed below, many of the novel tuberculosis vaccines aim to induce T cell responses against *M.tb*. Given their role in T cell priming, it is important to understand the role dendritic cells (DCs) play during infection. DCs express surface receptors that allow recognition and phagocytosis of *M.tb* (O'Garra et al. 2013). A noteworthy feature of *M.tb* infection is the delayed initiation of an adaptive T cell response relative to other respiratory infections (Urdahl et al. 2011). T cells appear in the lungs of infected mice around 9 to 11 days post infection (Urdahl et al. 2011). *M.tb* has been shown inhibit antigen presentation by DCs (Wolf et al. 2007). Depleting DCs prior to *M.tb* infection results in a further delay of the T cell response

against *M.tb* and higher bacterial burden in the lungs of mice (Tian et al. 2005). It appears that the major role of DCs is to initiate the *M.tb*-specific T cell response (Buettner et al. 2005).

Interestingly, from a vaccine development point of view, lung DCs have been shown to imprint naïve T cells to traffic to the lung more efficiently upon secondary exposure compared to DCs from other tissue sites (Mikhak et al. 2013). This suggests that vaccine delivery to the lungs may allow *M.tb*-specific T cells to migrate to the lungs quicker following exposure. A recent phase I trial that compared the number of mycobacteria-specific CD4 T cells following aerosol or intradermal MVA85A showed that aerosol vaccination induced higher numbers of Ag85A-specific CD4 T cells in bronchoalveolar lavage (Satti et al. 2014). Given that the lungs are the site of *M.tb* infection and the relative delay observed in T cell migration to the lungs in animal models, more studies need to measure trafficking and homing of *M.tb*-specific T cells to the lungs following vaccination.

T cells are required for immune control of *M.tb* infection

Although the murine tuberculosis model may not accurately reflect the pathogenesis and complexity of tuberculosis in humans, this model has been essential in the study of the immune response to *M.tb*, and in particular, T cells. CD4 T cells are required to orchestrate and regulate the immune response. Therefore, it is not surprising that numerous studies have demonstrated the importance of CD4 T cells in the control of *M.tb* infection. Data showing the inhibition of antigen presentation by *M.tb* in macrophages and DCs suggests that *M.tb* benefits from inhibiting the T cell response (Baena & Porcelli 2009). Investigating the conversion of the TST in contacts of

tuberculosis patients found that TST convertion ranged from 19 to 57 days post exposure, with an average of 37 days (Menzies 1999). A possible implication of these data is that by the time a T cell response has been primed, *M.tb* has already established a stronghold in the lungs. An obvious goal of novel vaccines is the establishment of lung resident *M.tb*-specific T cells endowed with characteristics that result in rapid activation, expansion, and/or killing of *M.tb* infected cells early after exposure.

Early work investigating the role of T cells showed that mice that lack CD4 T cells had increased *M.tb* burden compared to wild-type mice (Muller et al. 1987). More recently it has been shown that antibody depletion of CD4 T cells in *M.tb* infected cynomolgus macaques also resulted in increased bacterial burden (Lin et al. 2012). Human evidence for the importance of CD4 T cells in controlling *M.tb* infection is provided by studies of HIV infected individuals. It is well established that the risk of developing tuberculosis is ±10-fold higher in HIV-infected persons compared with HIV-uninfected persons (Allen et al. 1992; Wood et al. 2000). While depletion of CD4 T cells negatively influences the level of immune control of *M.tb*, it should be stressed that killing of *M.tb* is performed by effector cells such as macrophages (Herbst et al. 2011). Therefore, removing helper CD4 T cells should be viewed as removing cells that primarily enhance macrophage killing of *M.tb*.

CD8 T cells also play a role in controlling *M.tb* infection. Mice with impaired CD8 T cells due to a mutated β_2-microglobulin gene are more susceptible to *M.tb* infection than wild-type mice (Flynn et al. 1992). Depletion of CD8 T cells during drug induced "latent infection" in mice also resulted in increased bacterial burden (Van

Pinxteren et al. 2000). *M.tb*-specific CD8 T cells express the cytotoxic molecules, granulysin, perforin, granzyme A and B (Canaday et al. 2001; Woodworth et al. 2008; Rozot et al. 2013). These molecules are critical in CD8 T cell mediated cytotoxicity. Studies have shown that *M.tb*-specific CD8 T cells have cytotoxic activity against macrophages infected with *M.tb* or splenocytes presenting *M.tb* epitopes (Serbina & Flynn 2001; Stenger 1998; Cho et al. 2000; Woodworth et al. 2008). Together, these data strongly suggest that CD4 and CD8 T cells have an integral role in the control of *M.tb* infection.

Th subset paradigm

Almost 30 years ago it was observed that antigen-specific CD4 T cells could be separated into T helper (Th) 1 or Th2 subsets, based on the expression of a unique set of cytokines termed type 1 or type 2 cytokines (Mosmann et al. 1986). The signature type 1 cytokine is interferon gamma (IFN-γ), while tumor necrosis factor alpha (TNF-α) and interleukin-2 (IL-2) are also associated with Th1 cells. The signature type 2 cytokines are IL-4, IL-5 and IL-13 (Zhu et al. 2010). It was later observed that unique transcription factors such as T-bet and GATA3, are associated with Th1 and Th2 subsets, respectively (Szabo et al. 2000; Zheng & Flavell 1997). This Th1/Th2 paradigm has been central in studies of the T cell immune response to various pathogens, including *M.tb*. More recently, additional T helper subsets, such as Th17 and regulatory T cells (Tregs), have also been identified (Kaiko et al. 2008). Surface expression of chemokine receptors can also be used to distinguish these subsets (Figure 3). For reasons explained below, investigation of the T cell response to *M.tb* have been heavily biased to the Th1 subset.

Module	Polarizing cytokine(s)	Transcription factor	Homing receptor(s)	Effector cytokine(s)
T_H1	IL-12, IFN	T-bet	CXCR3	IFN-γ
T_H2	IL-4	GATA-3	CCR4/CRTh2	IL-4, IL-5, IL-13
T_H17	IL-6,IL-1β,TGF-β	ROR-γt	CCR6 / CCR4	IL-17, IL-22
Treg	TGF-β	FOXP3	CCR7 / CCR6	TGF-β, IL-10

Figure 3. Characteristics associated with each of the CD4 T cell lineages. Polarizing cytokines prime naïve cells to differentiate into one of the CD4 T cell lineages, characterized by distint transcription factors, homing receptors, and cytokine production. (Modified from Sallusto and Lanzavecchia *European Journal of Immunology* 2009)

The role of Th1 cells in *M.tb* control

Early studies established that intact expression of type 1 cytokines is important for control of *M.tb* replication. Mice unable to produce IFN-γ, TNF-α, IL-12 have increased bacterial burden, compared with wild-type mice (Flynn et al. 1993; Flynn et al. 1995; Cooper et al. 1993).. In addition, inability to produce IL-12, a innate cytokine critical for Th1 differentiation during T cell priming, has also been shown to impair *M.tb* control in mice (Flynn et al. 1995; Cooper et al. 1997). This reduced control of *M.tb* is likely a consequence of macrophages not receiving IFN-γ signaling. As discussed above, pretreatment of macrophages with IFN-γ has been shown to enhance host defense pathways (e.g. autophagy and phagosome maturation) and expression of antimicrobial peptides (e.g. cathelicidin) in humans (Gutierrez et al. 2004; Fabri et al. 2011).

Clues from these animal models have translated well into human. Individuals with mutations in IL-12, IFN-γ receptor, or STAT1 are more susceptible to develop mycobacterial disease (Fernando & Britton 2006). Additionally, treatment of rheumatoid arthritis patients with TNF-α-blockers, who are also infected with *M.tb*,

has also been shown to increase the risk of developing TB (Keane et al. 2001; Gomez-Reino et al. 2003). Together, these studies provide strong evidence that intact Th1 responses are necessary for *M.tb* control. However, the full relevance of Th1 cells in tuberculosis remains unclear. Adoptive transfer of *M.tb*-specific IFN-γ deficient or TNF-α deficient CD4 T cells still reduced *M.tb* bacterial burden in the lungs of mice compared to mice that did not receive any T cells (Gallegos et al. 2011). Although transfer of WT *M.tb*-specific CD4 T cells resulted in the largest bacterial burden reduction, this study suggests that T cells that are lacking key Th1 mediators of control still offer some level of protection.

Mycobacteria-specific Th1 cells are readily detected following infant BCG vaccination (Soares et al. 2008). Yet, the frequencies of BCG-specific Th1 cells or their cytokine co-expression pattern measured at 10 weeks after BCG vaccination does not correlate with risk of developing tuberculosis (Kagina et al. 2010). Results from a recent phase IIb clinical trial demonstrated that in previous BCG vaccinated infants, MVA85A induced modest frequencies of Th1 cells but did not offer any protection (Tameris et al. 2013). Although the role remains unclear, many vaccine studies gauge immunogenicity by measuring the frequencies of mycobacteria-specific Th1 cells. Measuring this narrow range of parameters limits our understanding of vaccine-induced T cells responses in humans. Therefore, studies that perform more comprehensive analyses of vaccine-induced T cell responses are needed. As will be discussed below, the pathology seen in tuberculosis is driven by strong pro-inflammation, therefore a balanced vaccine induced response to *M.tb* is likely required to ensure protection.

The role of Th2 cells in *M.tb* control

Given the importance of type 1 cytokines in mediating control of *M.tb*, one might expect that down-regulation of type 1 cytokines by Th2 cells should affect outcomes in *M.tb* infection. This is supported by studies of tuberculosis patients co-infected with helminths, pathogens that induce a Th2 biased response. Co-infected patients have significantly lower IFN-γ production, compared with tuberculosis patients not infected with helminths (Resende Co et al. 2007). Further, the Th1/Th2 balance is associated with severity of disease in leprosy, caused by *Mycobacterium leprae*. Severe lepromatous lesions have more type 2 cytokine transcripts compared to controlled tuberculoid lesions, which have more Th1 cytokine transcripts (Yamamura et al. 1991). However, peripheral blood mononuclear cells (PBMCs) from latently infected and TB diseased individuals have similar levels of Th2 cytokines following stimulation with *M.tb* antigen (Zhang et al. 1995). Furthermore, mice with mutations in type 2 cytokine (e.g. IL-4 and IL-10) genes have a similar level of *M.tb* control, compared to wild type mice (North 1998). This is intriguing, because it is well established that type 2 cytokines inhibit type 1 cytokine production (Fiorentino et al. 1991; Hsieh et al. 1992). More studies are needed to better understand the role of this subset in the anti-*M.tb* immune response.

The role of Th17 cells in *M.tb* control

Signature cytokines of Th17 cells are IL-17A (often referred to as IL-17), IL-17F, IL-21, and IL-22 (Torrado & Cooper 2010). IL-17 deficient mice have been shown to have reduced control against a “hypervirulent” *M.tb* strain, HN878, compared to wild type mice, but not lab adapted or less virulent strains of *M.tb* (Gopal et al. 2014). HN878 was shown to induce higher levels of IL-17 and higher frequencies of Th17

cells compared to the lab adapted H37Rv (Gopal et al. 2014). The authors concluded IL-17 is required during HN878 infection due to this strain's ability to induce IL-17. In addition to revealing the role of IL-17 in a clinical relavent *M.tb* isolate, this study also highlights the need to also utilize clinical relevant isolates in describing immune requirement for *M.tb* control. Interestingly, adoptive transfer of *M.tb*-specific Th17 cells into naïve mice results in a significantly lower *M.tb* bacterial burden compared to mice that received *M.tb*-specific Th2 cells (Gallegos et al. 2011). This suggests that the role of Th17 cells in control of *M.tb* may not be limited to recruitment of Th1 cells only, but that IL-17 may have other, more direct effects on mycobacterial containment.

IL-17 has been shown to orchestrate trafficking of the recall response of mycobacteria-specific Th1 cells primed by vaccination. Khader et al. reported that depletion of IL-17 leads to a decrease in the recruitment of protective IFN-γ-producing CD4 T cells, primed by a subunit vaccine, to the lungs of *M.tb*-infected mice (Khader et al. 2007). It was further reported that this recruitment was mediated by IL-17-producing cells through induction of lung expression of the CXCR3 ligands, CXCL9, CXCL10, and CXCL11 (Khader et al. 2007). These results therefore suggest that novel vaccines that induce a Th17 response in the lung may offer better protection. However, mucosal pre-exposure with Th17 adjuvants was shown to result in more lung inflammation and pathology when mice were subsequently infected with influenza (Gopal et al. 2014). Therefore, caution must be taken when developing tuberculosis vaccines that aim to induce *M.tb*-specific Th17 cells in the lungs.

The CXCR3^{+} CCR6^{+} subset

Recent studies that investigated *M.tb*-specific CD4 T cells in peripheral blood of latently infected adults observed that *M.tb*-specific cells preferentially resided in the CXCR3^{+}CCR6^{+} subset (Arlehamn et al. 2014; Arlehamn et al. 2013). Furthermore, the proportion of the CXCR3^{+}CCR6^{+} population within the total CD4 T cell population was found to be larger in latently infected adults compared to uninfected BCG naïve adults (Arlehamn et al. 2014). CXCR3 and CCR6 are homing receptors associated with Th1 and Th17 cells respectively (Sallusto & Lanzavecchia 2009). This is intriguing, because of the importance that Th1 and Th17 cytokines have been shown to play in controlling *M.tb* (discussed above). CXCR3^{+} and CCR6^{+} CD4 cells have been shown to express T-bet and RORC, transcription factors associated with Th1 and Th17 differentiation (Arlehamn et al. 2014). More studies are needed to determine the origins of the CXCR3^{+}CCR6^{+} *M.tb*-specific CD4 T cells in latently infected persons, because it has been shown that conventional Th1 and Th17 cells can differentiate into CXCR3^{+}CCR6^{+} cells (Arlehamn et al. 2014; Becattini et al. 2015). There is also a need to determine the effects of BCG vaccination and tuberculosis on the *M.tb*-specific CXCR3^{+}CCR6^{+} CD4 T cell subset (Arlehamn et al. 2014). Additional work will also be required to determine the role this subset plays in immune mediated control of *M.tb*.

The role of PD-1^{+} and KLGR1^{-} cells in *M.tb* control

Several recent studies have investigated the role of *M.tb*-specific CD4 T cells expressing the PD-1^{+} KLRG1^{-} phenotype in tuberculosis. PD-1 was initially identified as a marker expressed by functionally exhausted CD8 T cells and KLRG1 as marker of terminally differentiated cells (Jonjic 2010 et al.; Day et al. 2006; Barber

et al. 2006). Therefore, it was initially surprising that PD-1^{+} *M.tb* specific CD4 T cells possessed superior proliferation and differentiation capabilities compared to PD-1^{-} cells (Reiley et al. 2010). PD-1^{+} and KLRG1$^{—}$ *M.tb* cells were found to be preferentially located in the lung parenchyma of infected mice while PD-1^{-} and KLRG1^{+} were located in the lung associated vasculature (Moguche et al. 2015; Sakai et al. 2014). Adoptive transfer into *M.tb*-infected mice resulted in preferential migration of *M.tb*-specific PD-1^{+} back to the lung parenchyma while PD-1^{-} and KLRG1^{+} cells migrated to the lung associate vasculature (Sakai et al. 2014). Transfer of PD-1^{+} CD4 T cells from *M.tb* infected mice provided superior protection compared to PD-1^{-} cells (Reiley et al. 2010). Interestingly, the frequency of IFN-γ producing cells was relatively higher in PD1^{-}KLRG1^{+} subset compared to the PD1^{+}KLRG1$^{—}$ subset (Moguche et al. 2015; Reiley et al. 2010). This result again emphasized that while IFN-γ producing is indispensible in immune mediated control of *M.tb,* additional functions performed by CD4 T cell are also required for control.

Recent work by Lindenstrøm *et. al.* also linked KLRG1$^{—}$ mycobacteria-specific CD4 T cells, induced by a boost of CAF01-adjuvanted H1 vaccine, with improved protection compared to BCG alone in mice. In this study the enhanced protection offered by KLRG1$^{—}$ cells appeared to be mediated by long-lived, IL-2 producing proliferating central memory cells during *M.tb* infection (Lindenstrom et al. 2013). Vaccination with a recombinant BCG ΔureC::hly (rBCG) vaccine also demonstrated enhanced protection in mice compared to BCG (Vogelzang et al. 2014). The authors linked the improved protection with a population of central memory cells. Together these studies suggest that establishing a self-renewing, mycobacterial-specific central

memory CD4 population that replenishes the effector CD4 T cell pool may be important in vaccine-mediated control of *M.tb* (Andersen & Woodworth 2014).

The role of Tregs in *M.tb* control

It is important that immunity mounted against a pathogen be tightly controlled. Upon T cell receptor (TCR) signaling a number of inhibitory molecules, such as PD-1, CD160 and CTLA-4, are expressed on activated T cells. Signaling through these receptors, typically via ligands expressed on antigen-presenting cells, enables negative regulation of T cell proliferation and effector functions. Another mechanism for suppressing T cell responses is through Tregs. The transcription factor FoxP3 is the signature transcription factor of Tregs (Zielinski et al. 2011). In the periphery the Treg population is comprised of natural Tregs (nTregs) and induced Tregs (iTregs). nTregs are differentiated in the thymus and migrate to the peripheral blood, while iTregs differentiate from naïve CD4 T cells in the periphery (Lafaille et al. 2009; Workman et al. 2009). Tregs are able to suppress proliferation and cytokine production by other T cells via expression of regulating cytokines such as IL-10 and transforming growth factor beta (TGFβ), or via cell receptor signaling in a cell dependent mechanism (O'Garra et al. 2004). Failure of Treg-mediated suppression of effector cells has been associated with development of sepsis, cancers, various chronic infections, and autoimmune diseases (Scalapino et al. 2006; Heuer et al. 2005; Endharti et al. 2011).

Given the importance of proinflammatory cytokines, Tregs are likely to be very important in ensuring a balanced anti-*M.tb* immune response during infection. However, depletion of Treg cells prior to *M.tb* infection in mice was shown to neither

enhance nor impair bacterial control (Quinn et al. 2006; Quinn et al. 2008; Ozeki et al. 2010). In contrast, data from the macaque model suggests that Tregs may be critical for prevention of progression of *M.tb* infection to tuberculosis. Higher peripheral blood frequencies of natural Tregs were observed before *M.tb* challenge in macaques that developed latent infection, compared with macaques that developed tuberculosis (Green et al. 2010). However, 24 weeks after *M.tb* infection, macaques with latent infection had a significantly lower frequency of Tregs compared to macaques with tuberculosis. This finding is consistent with several human studies, which report higher frequencies of Tregs in tuberculosis patients compared with healthy individuals (He et al. 2010; Guyot-Revol et al. 2006). These data suggest that a highly controlled T cell response is required after infection with *M.tb*, and Tregs are key in providing this control.

Non-conventional T cells

In addition to CD4 and CD8 T cells, unconventional T cells such as γδ T cells, CD1 restricted T cells, and mucosal associated invariant T (MAIT) cells have been shown to participate in the immune response against *M.tb*. Importantly, the observation that these unconventional cells exhibit effector functions such as cytokine production more rapidly and have a more limited polymorphic TCR repertoire, compared to conventional T cells, have made these cells attractive targets for vaccination (Lin & Flynn 2015). Furthermore, unconventional T cells are intriguing because they target non-peptide antigens thereby increasing the diversity of antigens that can be recognized. A greater understanding of the role of unconventional T cell subsets may provide valuable insights for the development of tuberculosis vaccines (Karp et al. 2015).

B cells and antibodies

B cells and antibodies are critical in mediating protection against many pathogens. However, studies that have investigated the immune response to intracellular pathogens such as *M.tb* have largely been T-cell centric (Kozakiewicz et al. 2013). This has left the roles of B cells and antibodies in *M.tb* infection understudied and underappreciated (Maglione & Chan 2009). There is growing evidence that B cells and antibodies play protective roles against intracellular pathogens (Achkar et al. 2015). B cells can help shape the CD4 T cell immune response through antigen presentation (Constant 1999) and cytokine production (Bouaziz et al. 2010). *M.tb* infection of mice that lack B cells resulted in increased immunopathology following a 100 CFU aerosol infection, and a 300 CFU dose resulted in reduced survival and increased lung bacterial burden compared to wild-type mice (Maglione et al. 2007).

Overwhelming evidence supports the critical role of CD4 T cells in control of *M.tb*, providing a sound foundation for vaccine developers to target CD4 T cells. However, this narrow focus may be insufficient to improve upon BCG. Future vaccine development will need to incorporate knowledge about B cells and non-conventional T cells when selecting vaccine antigens.

Immunopathology in tuberculosis

In developing novel tuberculosis vaccines it is important to remain cognizant that *M.tb* is an obligate human pathogen that has developed mechanisms that enable persistence and transmission in the face the host immune response (Comas et al. 2010). The pathology observed in tuberculosis is driven by the host immune response (Elkington et al. 2011). Furthermore, there is a wealth of evidence that suggests that

an intact host immune response is required for efficient transmission. It has been shown that tuberculosis patients with large cavities have higher levels of the pro-inflammatory cytokine, TNF-α, in BAL fluid, compared with patients with smaller cavities (Tsao et al. 2000). Patients with cavitary tuberculosis are known to have higher bacterial loads in their sputum compared to patients without cavities (Palaci et al. 2007). A more recent study showed higher levels of the matrix metalloproteinase 1 (MMP-1), a protease expressed by monocytes, in BAL fluid from tuberculosis patients compared to non-tuberculosis patient controls (P. Elkington et al. 2011). In the same study it was demonstrated that MMP-1 degrades components of the lung extracellular matrix (P. Elkington et al. 2011). These data suggest that a strong pro-inflammatory environment may drive tuberculosis-associated tissue damage and transmission.

Additional evidence of the paradoxical role of the immune response is provided by studies that have investigated tuberculosis in HIV infected persons. HIV infected tuberculosis patients with a CD4 T cell count below 200/μL have atypical radiographic patterns, such as decreased lung cavitation, compared with HIV uninfected tuberculosis patients (Aderaye et al. 2004). It is likely that the atypical radiographic patterns and scarcity of cavitation observed in HIV infected tuberculosis patients are due to a dampened inflammatory response resulting from immune compromise. One could imagine that restoration of the immune system would lead to an increased inflammatory response and increased tuberculosis pathology in HIV infected tuberculosis patients. Indeed, in a significant proportion of HIV infected tuberculosis patients who start antiretroviral therapy, immune restoration leads to the development of more severe tuberculosis symptoms (Meintjes et al. 2009). This has

been termed tuberculosis associated immune reconstitution inflammatory syndrome (IRIS), and further demonstrates the paradoxical role of the immune system in tuberculosis pathology.

Investigation of the genomes of *M.tb* strains that represent the global distribution revealed high levels of sequence conservation in T cell epitopes (Comas et al. 2010). This may suggest the presence of evolutionary pressure on *M.tb* to maintain T cell immune recognition for transmission. These studies suggest that the immune response to *M.tb*, tuberculosis pathology, and transmission are all connected.

Current tuberculosis vaccine pipeline

Due to the intimate relationship between the immune response and pathology, special attention must be taken when developing approaches, such as vaccination or immunomodulation, that aim to manipulate the *M.tb*-specific immune response. Rational tuberculosis vaccine design will have to acknowledge the importance of CD4 T cells in driving both immune control and immunopathogy. Therefore, it is important to ensure that vaccine induced CD4 T cells achieve a balanced response to ensure control of *M.tb*. The primary goal of any vaccine is to develop a protective immune memory response capable of preventing infection or disease prior to exposure of the disease-causing pathogen. Development of immunological memory ensures that following exposure to the pathogen an appropriate immune response will be present to clear infection.

A basic measure used by many to describe vaccine responses is the magnitude of the antigen-specific T cells induced (Seder et al. 2008). This measure allows researches

to gauge vaccine immunogenicity. However, this single attribute alone is not sufficient to describe the heterogeneity within a population of antigen-specific T cell following vaccination. Antigen-experienced T cells have been classified into distinct memory subsets based on differential functions, such as proliferative capacity, cytokine secretion and tissue homing. These subsets can be classified by surface expression of CD45RA or CD45RO and chemokine receptor type 7 (CCR7). The expression of CCR7 expression endows antigen-experienced cells with the potential for lymph node homing, which is characteristic of long-lived central memory (CM) cells. By contrast, absence of CCR7 expression allows migration to the site of infection, which is typical of short-lived effector memory cells (EM) (Sallusto et al. 1999). Unique cytokine expression patterns that associate with the differentiation state of antigen-experienced T cells have been described (Figure 4). IL-2 production, either alone or in combination with other cytokines, is typical associated with cells with higher memory potential, while cells further along the differentiation pathway with reduce memory potential preferentially express IFN-γ.

It has been proposed that the short duration of BCG-induced protection may result from the induction of a short-lived T_{EM} response, rather than long-lived T_{CM} cells (Andersen & Woodworth 2014; Orme 2010). Although BCG-specific T cells predominately express a T_{CM} ($CCR7^{+}CD45RA^{-}$) phenotype, the cytokine and cytotoxicity profile resemble T_{EM} (Soares et al. 2013). Waning of the BCG-induced recall response may also be a possible reason for the increase in tuberculosis incidence typically observed during adolescence (H Mahomed et al. 2011). As was discussed above, recent studies have observed enhanced control of bacterial burdens in animals that possess antigen-specific CD4 T cell populations with enhanced self-

renewal properties. While these characteristics do not correlate with protection against tuberculosis they remain important parameters that may be targets of vaccine induced T cell responses (Andersen & Woodworth 2014).

Another reason proposed to underlie the poor protection with BCG is exposure to non-tuberculous mycobacteria (NTM) (McShane 2014). NTM species are generally nonpathogenic in immunocompetent persons and are commonly found in the soil and water (September et al. 2004). Several studies have highlighted that NTM exposure influences the immune response induced by BCG. Mice exposed to NTMs prior to BCG vaccination had higher lung CFU upon M.tb challenge compare to mice not exposed to NTM (Brandt et al. 2002). It is noteworthy that in this study prior NTM sensitization did not affect the level of protection offered by subunit vaccination (Brandt et al. 2002). The authors also showed that the number of BCG-specific T cells was significantly lower in mice exposed to NTMs prior to BCG vaccination, suggesting that prior NTM exposure decreases BCG replication (Brandt et al. 2002). It is likely that NTM exposure happens early in life, because a study of infants from The Gambia who did not receive BCG at birth had detectable anti-mycobacterial immune response at 4 months of age (Burl et al. 2010). These data are made more intriguing as results from a meta-analysis by Mangtani and colleagues suggests that NTM exposure affects the level of BCG protection in humans. Mangtani et al reported that BCG offered greater protection at clinical trial sites further away from the equator (Mangtani et al. 2014). The authors attributed this effect to a commonly held view that NTM exposure is less common at sites far away from the equator (Mangtani et al. 2014). This finding is in agreement with the animal data that suggest that prior NTM exposure could block the protective effect of BCG. It should however

be noted that the conclusion that greater protection away from the equator was due to lower NTM exposure is not without controversy. A study that investigated sensitization to NTM antigens found similar levels of sensitization in persons closer and further away from the equator (von Reyn et al. 1993). It has been suggested by von Reyn that the finding that BCG effectiveness is affected by latitude could be confounded. The confounder is that protection offered by BCG is highest in mycobacteria-naïve infants and well-designed prospective trials in infants have been performed at sites far from the equator, therefore the observation by Mangtani et al could be a result of better discrimination of study participants with prior NTM exposure in the trials conducted away from the equator (von Reyn 2014). It is important to remember that while prior NTM exposure may have limited impact in modulating BCG induced immunity when BCG is given at birth or soon after birth, it will be critical to determine the effect of NTM exposure if older children or adolescents receive recombinant BCG (rBCG).

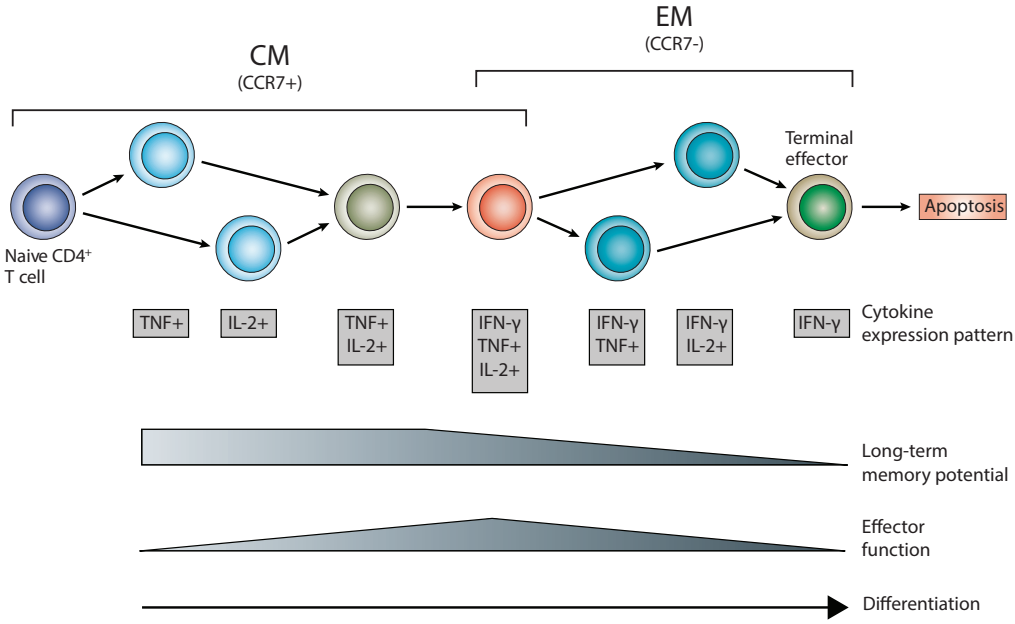

Figure 4. **Characteristics associated with differentiation of antigen-experienced CD4 T cells.** The cytokine pattern, long-term memory potential, and magnitude of effector functions of antigen-experienced CD4 T cells at various stages of differentiation. (Modified from Seder et. al *Nature Reviews Immunology* 2008)

There are several vaccine constructs in clinical development ranging from live attenuated M.tb, recombinant BCG, viral vectors expressing mycobacterial antigens, and protein subunit vaccines. The underlying idea of all these vaccines is to induce a Th1 cell response (Karp et al. 2015). Due to its efficacy in preventing disseminated tuberculosis in infants, BCG is likely to remain in the vaccine schedule. Therefore, many of the novel vaccines will be administered as booster vaccines within the context of a BCG induced primary response. However, there is growing concern about the rationale used for the selection of antigens for novel tuberculosis vaccines, especially in protein subunit and vectored vaccines. Antigen selection for subunit vaccines has been biased toward antigens recognised by T cells from persons with latent infection or persons who have been cured of tuberculosis (Kaufmann et al. 2010). To date, this strategy has resulted in the selection of "immunodominant" antigens such as Ag85A, Ag85B, TB10.4, Mtb32A, Mtb39A, and ESAT-6 in novel subunit vaccines. A recent study by Carpenter et al suggests that these current vaccine antigens are broadly recognised in populations with different HLA distribution. PBMC samples were collected from latently infected persons from five continents and it was revealed that globally 67% of persons with latent infection had an IFN-γ response to Ag85A and 100% responded to Ag85B, TB10.4, Mtb39A and ESAT-6 (Carpenter et al. 2015). Another approach used to select antigens is to identify antigens up-regulated by environmental stresses such as nutrient starvation or hypoxia. Antigens up-regulated in these environments are thought to be expressed during established latent infection (Andersen & Woodworth 2014). Latency associated antigens such as Rv2660c, Rv1813, Rv2659c, Rv1733c, and Rv3407 have been incorporated into the subunit vaccines, H56, ID93, or the recombinant BCG, rBCGΔureC::hly, in a murine study (Reece et al. 2011; Baldwin et al. 2012; Aagaard

et al. 2011). It must be highlighted that given the critical role immunopathology plays in tuberculosis (see section above), selection of immunodominant antigens that induce highly inflammatory cytokines such as IFN-γ may not be an appropriate approach.

An incredible amount of work has been performed to select the current antigens in tuberculosis vaccines, however, more comprehensive characterisation of antigen-specific T cells during human infection and understanding how host-pathogen interactions affect T cell responses is needed. Universal recognition of antigens will likely remain a requisite for inclusion into novel subunit vaccine constructs, however it is becoming clear that broad recognition alone may not be an adequate criterion. Understanding antigen expression patterns during infection will likely be critical for successful vaccine development. This is because vaccine-induced T cells can only exert protective immunity if the cognate antigen is expressed by the invading pathogen and infected cells present the relevant peptides. An experimental M.tb infection study in mice by Rogerson and colleagues exemplify the importance of understanding antigen expression patterns during infection (Rogerson et al. 2006). In this study the researchers investigated development of the Ag85B and ESAT-6-specific T cell response in mice infected with M.tb. Ag85B, a mycolyl transferases that is involved in the synthesis of the M.tb cell wall (Belisle et al. 1997), was highly expressed in the early stages of infection but wanes as infection reaches the chronic stage, while ESAT-6, a protein implicated in M.tb virulence, (Pym et al. 2002), remains highly expressed during the chronic stage of experimental M.tb infection in mice (Rogerson et al. 2006). Importantly, the expression of Ag85B by M.tb relative to ESAT-6 was lower throughout infection, and this was associated with lower Ag85B-specific T cell numbers compared to ESAT-6-specific T cells (Rogerson et al.

2006). This study demonstrates that differential antigen expression during infection might have profound effects on T cell responses and highlights the importance of understanding the role of vaccine antigens in the context of infection. One of the aims of this thesis was to determine if the ESAT-6 and the Ag85B-specific CD4 T cell responses were different in the context of human latent M.tb infection.

In addition to antigen selection, considerable effort has been made in developing adjuvants for novel subunit tuberculosis vaccines. Subunit vaccine require adjuvants to trigger innate immune cells, specifically antigen-presenting cells (APC), to induce an adaptive immune response against the vaccine antigens. Adjuvants interact with specific pattern recognition receptors, such as Toll like receptors (TLR), triggering specific signalling pathways in APC. The focus of this thesis is the H1:IC31 subunit vaccine, which is a fusion protein of Ag85B and ESAT-6 in the IC31 adjuvant. IC31 is a potent Th1 adjuvant that consists of a phosphodiester-backboned oligodeoxynucleotide (ODN1a) that signals via TLR9 and an antibacterial cationic peptide $KLKL_5KLK$ (KLK) (Agger et al. 2006). In addition, IC31 is able to prime detectable Th2 and humoral immune response to vaccine antigens (Riedl et al. 2008; Agger et al. 2006; Schellack et al. 2006). Interestingly, KLK has been shown to prolong antigen presence at the site of vaccination. OVA injected into mice in a formulation of IC31 formed a depot at the vaccination site that was present 58 days post vaccination, but removing KLK from the IC31 formulation resulted in rapid diffusion from the vaccination site (Schellack et al. 2006). IC31 has been used as an adjuvant for a variety of vaccines including vaccines against influenza, dengue, Streptococcus pneumonia, and HIV (Bernardo et al. 2011; Riedl et al. 2008; Olafsdottir et al. 2012; Pattacini et al. 2012). Other formulations used to adjuvant novel subunit tuberculosis vaccines include CAF01, AS01E, and GLA-SE. CAF01 is

a two-component adjuvant that is comprised of a cationic liposome that is stabilized with a glycolipid immunomodulator called trehalose-6,6-dibehenate (TDB) (Agger et al. 2008). TDB is a synthetic version of the mycobacterial cord factor trehalose-6, 6-dimycolate (TDM) located in the mycobacterial cell wall and interacts with the C-type lectin receptor Mincle and induces Th1/Th17 immunity (Schoenen et al. 2010). CAF01 has been used to adjuvant H1 (Ag85B and ESAT-6), H4 (Ag85B and TB10.4), H28 (Ag85B, TB10.4, and Rv2660c), and H56 (Ag85B, ESAT-6, and Rv2660c) (Elvang et al. 2009; Lindenstrom et al. 2013; Billeskov et al. 2013; Aagaard et al. 2011). It should be noted that the majority of studies performed using CAF01 as an adjuvant have been in animals. AS01E is a liposome containing a detoxified form of monophosphoryl lipid A (MPL) that interacts with TLR4 and a detoxified saponin derivative (QS21) (Alving et al. 2012). This adjuvant has been used in formulation of the M72 vaccine, which contains the mycobacterial antigens Mtb32A and Mtb39A (Day et al. 2013; Penn-Nicholson, et al. 2015). GLA-SE is comprised of the synthetic TLR4 agonist, glucopyranosyl lipid, in an oil-in-water stable emulsion and has been used to adjuvant the ID93 (Rv2608, Rv3619, Rv3620, and Rv1813) fusion protein (Baldwin et al. 2013).

Vaccination of animals with subunit vaccines consisting of fusion proteins of these immunodominant antigens enhances *M.tb* control compared to unvaccinated animals (Dietrich et al. 2006; Aagaard et al. 2011; Billeskov et al. 2013). Furthermore, boosting BCG induced immunity with a subunit vaccine consisting of Ag85B–ESAT-6–Rv2660 (H56) in a non-human primate model of *M.tb* infection resulted in improved protection compared to BCG vaccination alone (Lin, Dietrich, et al. 2012). Results from this study provide evidence that boosting BCG induced responses with a

subunit vaccine may improve immune control of *M.tb* in humans. In this thesis we aimed to perform a comprehensive analysis of the CD4 T cell immune response boosted by the subunit vaccine H1:IC31 in BCG vaccinated adolescents with or without latent infection.

H1:IC31 vaccination has been shown to be safe and immunogenic in BCG naïve, BCG vaccinated, *M.tb* uninfected, and latently infected persons (van Dissel et al. 2011; van Dissel et al. 2010). A more recent study has demonstrated improved bacterial control when the BCG vaccine immune response was boosted with a vaccine similar to H1:IC31, H1:CAF01, in mice (Lindenstrom et al. 2013). It was observed that the improved control was associated with the maintenance of an IL-2^{+} and KLRG1^{-} *M.tb*-specific CD4 T cell response during infection (Lindenstrom et al. 2013).

The aim of this thesis was to comprehensively characterise the H1:IC31 induced CD4 T cell response in BCG vaccinated uninfected and latently infected adolescents. Current methods of assessing vaccine induced response focus primarily on Th1 responses. Measuring such parameters has revealed that while novel tuberculosis vaccines readily induce these responses, induction of a Th1 *M.tb*-specific response correlate with risk of tuberculosis (Kagina et al. 2010). Therefore, it is important that in addition to describing vaccine induced T cell responses in terms of Th1 cytokine production and memory phenotypes we begin to utilise high throughput transcriptomic platforms that may allow a better understanding of these responses. Recently researchers have used these platforms to investigate complex biological systems and have revealed diversity in T cell populations that initially seemed

homogenous when measured by conventional approaches. Flatz *et. al.* demonstrated that while antigen-specific CD8 T cells induced by different HIV vaccines appeared similar based on Th1 cytokine production, analysing gene transcription patterns, key differences were observed between responses induced by the different vaccines (Flatz et al. 2011). These high throughput mRNA platforms have been used to identify molecular pathways that predict vaccine induced immune responses in humans (Querec et al. 2009). These studies demonstrate the power of such high throughput approaches.

In order to better understand the CD4 T cell immune response induced by H1:IC31 in healthy adolescents with and without *M.tb* infection, we measured the CD4 T cell immune response using conventional assays as well as an innovative high throughput transcriptomic platform. This thesis can be divided into two parts. The first part focused on (i) determining the whether *M.tb* infection affected the breadth of CD4 T cell epitopes recognised by BCG vaccinated adolescents and identifying T cell epitopes for tetramer production (ii) establishing the methods to perform transcriptomic analysis of antigen-specific CD4 T cells. Studies in mice suggest that the epitopes targeted by mycobacteria-specific CD4 T cells may be important in immune control of *M.tb* (Aagaard et al. 2009; Woodworth et al. 2014). Therefore we wanted to map epitope responses before and after infection. Additionally, determining mycobacterial CD4 T cell epitopes is necessary for the development of HLA class II tetramers. Tetramers are useful because they allow identification and interrogation of antigen-specific CD4 T cells with minimal manipulation. The second part of this thesis investigated the CD4 T cell response induced by H1:IC31 in healthy BCG vaccinated adolescents using conventional assays (e.g. whole blood intracellular

cytokine staining) and a high throughput transcriptomic approach. Results from this study provide an in-depth look at the H1:IC31-induced CD4 T cell immune response and the consequences of latent *M.tb* infection on these responses.

Objectives of this thesis

I. **To determine the effects of acquiring latent *M.tb* infection on epitope recognition by Ag85A and Ag85B-specific T cells.**

We hypothesize that acquiring latent M.tb infection will increase the number of CD4 T cell epitopes within Ag85A and Ag85B. (Chapter 2)

II. **To identify HLA alleles associated with epitope responses and to design HLA class II tetramers**.

III. **To optimise the cDNA sample preparation protocol for high throughput microfluidic qPCR quantification of mRNA levels in antigen-specific T cells.**

IV. **Characterise H1-specific CD4 T cells following H1:IC31 vaccination and determine the effects of latent *M.tb* infection on these responses.**

i.) *We hypothesize that H1:IC31 vaccination will induce a durable increase in the frequency of H1-specific CD4 T cells in adolescents with or without latent M.tb infection. Following H1:IC31 vaccination latently infected adolescents will have a higher frequency of H1-specific CD4 T cells compared to uninfected adolescents. (Chapter 4)*

ii.) *We hypothesize that H1-specific CD4 T cells from latently infected adolescents will be skewed to an effector memory phenotype and show greater effector memory functions* (*i.e. increased cytokine production and cytotoxic molecules) compared to uninfected adolescents before and after H1:IC31. (Chapter 4)*

Chapter 2: Determining the effect of underlying *M.tb* infection on epitope recognition of mycobacterial antigens.

Introduction

Determining and understanding changes in the mycobacteria-specific T cell response following *M.tb* infection may provide clues into mechanisms involved in immune control of *M.tb*. Many groups have studied mycobacteria-specific T cell responses in a cross-sectional manner in individuals with or without latent *M.tb* infection. It should be stressed that the current methods of establishing whether a person is latently infected with *M.tb* rely solely on detecting immune responses to *M.tb*-specific antigens such as ESAT-6 and CFP-10 (Aggerbeck et al. 2013). Although current methods are not able to directly measure antigen load, it is presumed that during latent infection the immune system is persistently exposed to mycobacterial antigens. Studies have revealed that the magnitude of the T cell response (measured by IFN-γ ELISPOT) to purified protein derivative (PPD) (Demissie et al. 2004), *M.tb* cell wall antigens (Adekambi et al. 2012) and Ag85A (Sander et al. 2009; Scriba et al. 2012) are significantly higher in latently infected persons compared to uninfected BCG vaccinated persons. These data suggests that persistent antigen exposure may play a role in shaping the character of antigen-specific T cell response.

Using viral models researchers have observed that the level of antigen exposure has an effect on the functionality of antigen-specific cells as well as the breadth of T cell epitopes. A study performed by Weidt *et. al.* using an acute LCMV infection model suggested that early clearance of LCMV resulted in the lack of subdominant epitopes, because T cell response to immunodominant epitopes facilitate clearance of infection (Weidt et al. 1998)while chronic infection leads to the disappearance of dominant

CD8 T cell responses as a result of exhaustion (Van Der Most et al. 2003). Given that BCG is cleared following vaccination and chronic latent infection is a common outcome following *M.tb* infection, these results offer compelling evidence to study the pattern of T cell epitope recognition following *M.tb* infection. Interestingly, in a phase II clinical trial in which participants that received a higher dose of the MVA85A vaccine recognised more Ag85A 15mer peptides compared to participants that received a lower dose (Figure 5). This data suggests that mycobacterial antigen load may affect the number of mycobacteria-specific T cell epitopes.

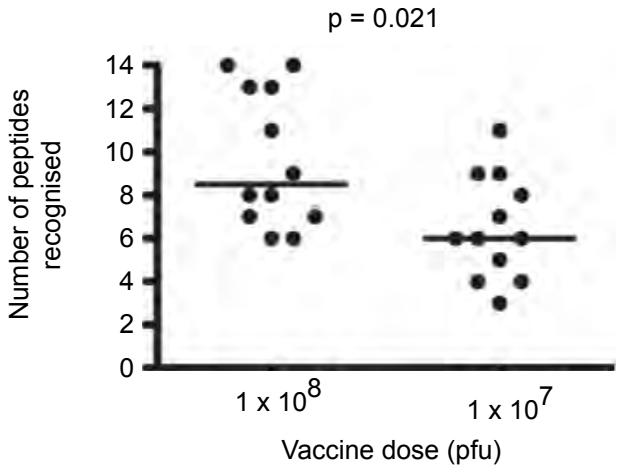

Figure 5. Peptides recognition in vaccine trial participants who received different doses of MVA85A. The number of Ag85A peptides recognised by PBMCs isolated 7 days post-vaccination was measured by IFN-γ ELISpot assay. P values were calculated using the Mann Whitney U test. (ClinicalTrials.gov Identifier: NCT00465465).

Mapping the immunogenic regions within mycobacterial antigens before and after *M.tb* infection is important in improving our understanding of how *M.tb* infection influences the T cell response to these antigens. Data from the mouse model suggests that mice that possess T cells that target subdominant ESAT-6 epitopes have enhanced control against *M.tb* infection and these T cells are more resistant to terminal differentiation during infection compared to cells that target highly immunodominant epitopes (Aagaard et al. 2009; Woodworth et al. 2014). Therefore, knowledge of the immunodominant and subdominant epitopes within mycobacterial

antigens before and after infection is likely to be useful for vaccine development.

In addition to determining the breadth of epitopes within mycobacterial antigens, mapping immunogenic regions of *M.tb* antigens is useful for designing and developing HLA class I and II tetramers. HLA tetramers allow direct monitoring and interrogation of T cell responses induced by *M.tb* and vaccines with limited manipulation. Detection of cells with tetramers does not depend on a preconceived function of the cell, so that one can perform analyses that reflect the direct ex vivo state of T cells better than current methods typically used (i.e. intracellular cytokine staining) which depend on activation of the cell for detection. Furthermore, antigen-specific cells remain functional following tetramer sorting which allows RNA analysis or clonal expansion.

We wanted to gain a better understanding of the effects of acquiring latent *M.tb* infection on the breadth and pattern of epitopes recognised by mycobacterial-specific T cells in humans. To our knowledge, no study has investigated whether the number of T cell epitopes within mycobacterial antigens expressed by both BCG and *M.tb* increase or decrease when a person previously vaccinated with BCG becomes infected with *M.tb*.

The aim of this chapter was to determine the optimal IFN-γ ELISPOT assay to map Ag85A and Ag85B-specific T cell epitopes before and after *M.tb* infection, identify associations between epitope responses and HLA allele restriction, and to design Ag85A and Ag85B-specific HLA class II tetramers.

To determine the optimal IFN-γ ELISPOT assay to map T cell epitopes we performed a pilot study in which we compared the number of ESAT-6 epitopes detected by the direct ex vivo IFN-γ ELISPOT assay and cultured IFN-γ ELISPOT assay using PBMC from latently infected adults. We selected ESAT-6 because it is a small protein compared to both Ag85A and Ag85B and can be covered by fewer 15-mer peptides, therefore fewer stimulation conditions, reagents, and PBMC would be required to determine the optimal IFN-γ ELISPOT assay to map T cell epitopes.

Specific objectives

1. To determine if the number of ESAT-6 T cell epitopes detected by the IFN-γ ELISPOT assay is higher after long-term PBMC culture with ESAT-6 compared to the direct ex vivo IFN-γ ELISPOT assay.

   We hypothesise that the number of ESAT-6 specific CD4 T cells detected by the cultured IFN-γ ELISPOT assay will be higher than those detected by ex vivo ELISPOT assay.

2. To determine if the breadth and/or pattern of Ag85A and Ag85B-specific T cell epitopes before and after *M.tb* infection are different.

   We hypothesise that the number and breadth of Ag85A and Ag85B-specific T cell epitopes will increase after M.tb infection.

3. To identify associations between HLA class II allele expression and responses to epitopes in Ag85A and Ag85B and to design HLA class II tetramers specific for Ag85A and Ag85B

Materials and Methods

Study participants

Cultured ELISPOT assay optimisation participants

Healthy adults with latent *M.tb* infection were recruited at the University of Cape Town Institute of Infectious Disease and Molecular Medicine for a pilot study to optimise the ELISPOT assay for epitope mapping. Informed consent was obtained from all participants. A positive QuantiFERON TB Gold In-Tube (QFT) (>0.35 IU/mL) assay was used to diagnose *M.tb* infection.

Adolescent Cohort Study (ACS) participants

SATVI performed a large epidemiological study, the Adolescent Cohort Study (ACS), in the Worcester district of the Western Cape (Mahomed et al. 2011). A total cohort of 6,363 adolescents were enrolled and followed up for 2 years. To investigate the effects of acquiring *M.tb* infection we selected a subgroup of adolescents who acquired *M.tb* infection during this 2 year follow up. PBMC were collected and cryopreserved at enrolment and at the end of follow-up. Included adolescents met the following inclusion criteria:

1. No evidence of *M.tb* infection at enrolment.
2. No evidence of tuberculosis throughout the study follow-up.
3. Availability of stored peripheral blood mononuclear cells (PBMC) sample.
4. *M.tb* infection at end of follow-up.

M.tb infection in these adolescents was diagnosed by QFT and a tuberculin skin test (TST). A negative QFT (<0.35 IU/mL) and TST induration of 0mm defined lack of

M.tb infection, whereas *M.tb* infection was defined as a positive QFT and a TST induration >10mm.

Blood collection and PBMC isolation

Ficoll-Hypaque method

Blood was collected from healthy adults with latent *M.tb* in heparinised tubes and PBMC were isolated by density gradient centrifugation. Briefly, blood was diluted with phosphate buffered saline (PBS) (Lonza) at a ratio of 1:1. Diluted blood was gently layered on top of Ficoll-Hypaque (Merck) and centrifuged at room temperature for 30 minutes at 800g with the brake off. The buffy coat, which contains PBMC, was carefully collected, washed with PBS, and either cryopreserved in 10% dimethyl sulfoxide (DMSO) and 40% FCS in RPMI enriched with L-Glutamine or used fresh.

BD Vacutainer CPT method

Blood was collected from adolescents and isolated by density gradient centrifugation using BD Vacutainer CPT tubes. Briefly, blood was drawn into a CPT tube and centrifuged at room temperature for 30 minutes at 1500-1800g with the brake off. PBMC were carefully collected and washed with PBS and resuspended in 1µL RPMI. PBMC cryopreserved in 10% DMSO and 40% foetal calf serum (FCS) in RPMI enriched with L-Glutamine.

Antigens

We used 15mer peptides, overlapping by 10 amino acids, spanning the entire Ag85A, Ag85B and ESAT-6 proteins (PeptideSynthetics) (Appendix Figure 1). For each individual antigen, combining all 66, 63, and 17 peptides into single pools made

Ag85A, Ag85B, and ESAT-6 peptide pools, respectively. Because PBMC numbers from ACS participants were limited, it was not possible to individually test for T cell responses to each Ag85A and Ag85B 15mer peptide. We therefore designed peptide pool matrices for Ag85A and Ag85B that allowed identification of peptide responses using 17 and 16 pools of peptides, respectively (Figure 6). Each individual peptide was represented in 2 different pools at a final concentration 2μg/mL, allowing identification of T cell epitopes by an iterative process. Tuberculin purified protein derivative (PPD, Statens Serum Institut) was used at a final concentration of 10μg/mL. Staphylococcal enterotoxin (SEB, Sigma-Aldrich) or phytohaemagglutinin (PHA, Remel) were used as positive controls at final concentrations of 1μg/mL and 10μg/mL, respectively.

Establishment of T cell lines

Cryopreserved PBMC were thawed into supplemented RPMI containing 10% human AB+ serum (R10 AB) and DNAse (10 μg/mL, Sigma-Aldrich). Viability of PBMC was measured by trypan blue exclusion staining. Two million PBMCs in R10 AB were incubated with peptide pools (final concentration of 2μg/mL per peptide) spanning the ESAT-6, Ag85A, or Ag85B proteins at 37°C in 5% CO_2. On days 3, 6, and 9, half of the culture medium (1mL) was replaced with fresh R10 AB containing IL-2 (50IU/mL, eBioscience). On day 13, the cells were washed and re-suspended in supplemented RPMI containing 10% FCS (R10 FCS) and counted manually or using a Coulter Counter (Beckman Coulter). For ELISPOT assays on the expanded cell lines, cells were rested for 6 hours at 37°C in 5% CO_2 and transferred to the IFN-γ ELISPOT plates.

Ag85A	Pool 9	Pool 10	Pool 11	Pool 12	Pool 13	Pool 14	Pool 15	Pool 16	Pool 17
Pool 1	1	9	17	25	33	41	49	57	44
Pool 2	10	2	26	18	42	34	58	50	66
Pool 3	19	27	3	11	51	59	35	43	63
Pool 4	4	12	20	28	36	65	52	60	56
Pool 5	13	5	29	21	45	37	61	53	
Pool 6	22	30	6	14	54	62	38	46	
Pool 7	7	15	23	31	39	47	55		
Pool 8	32	40	48	8	16	24	64		

Ag85B	Pool 9	Pool 10	Pool 11	Pool 12	Pool 13	Pool 14	Pool 15	Pool 16
Pool 1	1	9	17	25	33	41	49	57
Pool 2	10	2	26	18	42	34	58	50
Pool 3	19	27	3	11	51	59	35	43
Pool 4	4	12	20	28	36	44	52	60
Pool 5	13	5	29	21	45	37	61	53
Pool 6	22	30	6	14	54	62	38	46
Pool 7	7	15	55	31	39	47	23	63
Pool 8	32	40	48	8	16	24	56	

Figure 6. Peptide matrices constructed from 15mer peptides overlapping by 10 amino acids to identify peptide specific T cell responses. Numbers indicate individual 15mer peptides. Ag85A peptides were arranged into 17 unique peptide pools and Ag85B peptides into 16 unique peptide pools. *See appendix Figure 1 for amino acid sequence.*

Enzyme-linked immunospot (ELISPOT) assay

PBMC ($1x10^5$, direct ex vivo ELISPOT assay) or T cell lines ($5x10^4$, cultured ELISPOT) were stimulated with ESAT-6, Ag85A and Ag85B peptide pools (Figure 5) or single peptides (2μg/mL) in duplicate in a 96 well ELISPOT plate (Millipore) coated with an anti-IFN-γ antibody (Mabtech). For direct ex vivo IFN-γ ELISPOT assays, PPD was included as an antigen control. For all ELISPOT assays PHA or SEB was used as positive controls and media alone wells served as negative control. Cells were incubated for 18 hours in 5% CO_2 at 37°C. IFN-γ detection was performed with biotinylated anti-IFN-γ antibody and alkaline phosphatase (ALP) conjugated to streptavidin (Mabtech). Next, IFN-γ production was visualised with ALP conjugate substrate (Bio-Rad) and spot forming units (SFU) were enumerated

with an AID ELISpot plate reader using the AID ELISpot software V5.0. (AID and Cellular Technology Ltd).

Intracellular cytokine staining (ICS) assay

To confirm recognition of individual 15mer peptides and to determine which T cell subset (i.e. CD4 or CD8) mediated the epitope specific responses, ICS assays were performed on ESAT-6, Ag85A, and Ag85B-specific T cell lines. Cells were suspended in R10 FCS and stimulated with single 15-mer peptides, or complete ESAT-6, Ag85A, and Ag85B peptide pools at 37°C. PHA served as a positive control and unstimulated cells served as a negative control. After 1 hour of stimulation, Brefeldin A (Sigma-Aldrich) was added at a final concentration of 10μg/ml to each condition and cells were stimulated for a further 5 hours. Cells were stained with the viability dye, 7-AAD (3μL/100μL, BD Biosciences) prior to permeabilisation with Perm/Wash buffer (BD Biosciences) for 10 minutes, and then stained with the following fluorescent antibodies: CD3-PE (1μL/100μL, BD Biosciences), CD4-APC (1μL/100μL, BD Biosciences) and IFN-γ-FITC (5μL/100μL, BD Biosciences). Stained cells were acquired on a BD FACSCalibur flow cytometer and data was analysed using FlowJo v9.2.

DNA extraction and HLA Typing

DNA was isolated from cells recovered from plates after the IFN-γ ELISPOT assay, from PAXgene whole blood tubes (QIAGEN), or cryopreserved PBMC. DNA isolation was performed using the QIAGEN QIAamp DNA Mini or Blood Mini kit following the manufacturer's protocols. Ethanol precipitation was performed and dry

DNA pellets were sent to the La Jolla Institute for Allergy and Immunology (LIAI) for high resolution (4-digit) HLA typing.

Peptide-HLA binding prediction

Our collaborators at the LIAI performed predictions of peptide binding to HLA class II alleles. Consensus binding predictions were calculated from the following binding prediction algorithms: ARB, combinatorial library, SMM_align, and Sturniolo. Estimating a consensus prediction from multiple prediction algorithms attains the best overall prediction of binding (Wang et al. 2008). For each entered peptide sequence a consensus binding score was calculated. The results for each peptide were expressed as a percentile rank among 5 million other peptides, with peptides predicted to be the strongest binders to a particular HLA class II allele attaining the lowest percentile rank. Peptides that achieve a percentile rank below 2% were regarded as good binders.

In vitro HLA-peptide binding

To confirm HLA allele restriction, our collaborators at LIAI performed measurement of the binding affinity of immunodominant Ag85A and Ag85B peptides to a series of recombinant HLA class II molecules. This binding assay was developed specifically for measuring peptide binding to HLA class II molecules (Sidney et al. 2001). The binding assay measured inhibition caused by the peptide of interest to the binding of a radiolabeled probe peptide to soluble recombinant HLA molecules. The peptide of interest and the probe peptide were incubated with HLA molecules for 48 hours. This was followed by size exclusion gel-filtration chromatography to measure the proportion of radiolabeled probes bound to the soluble HLA molecules. From this, the

IC_{50} (i.e. the concentration which inhibits 50% of probe binding) of the test peptides was calculated.

Tetramer synthesis

Following confirmation of Ag85A and Ag85B peptide binding to HLA class II molecules, HLA class II tetramers were made by the NIH tetramer core facility at Emory University in Atlanta, GA. For each *M.tb* tetramer, the tetramer core unit facility also provided HLA-class II tetramers loaded with an epitope from the self-antigen, Clip, or the HIV envelope protein as irrelevant antigen controls.

MHC class II tetramer staining conditions

Cryopreserved PBMC were thawed as described above and incubated in 1mL of the viability dye LIVE/DEAD (1 μL/mL, Invitrogen) for 30 minutes at room temperature. PBMC were washed with 2% FCS and 2mM ethylenediaminetetraacetic acid (EDTA) in PBS and then stained with the fluorescently labelled CCR7-PerCP-Cy5.5 antibody (1μL/100μL, Clone: 150503, BD Pharmingen) for 30 minutes at 37°C. PBMC were washed again and incubated with HLA class II tetramers (1-2 μg/mL) for 60 minutes at room temperature. Following another wash, cells were incubated for 30 minutes at room temperature with the following fluorescently labelled antibodies: CD3-FITC (5μL/100μL, Clone: UCHT1, BD Pharmingen), CD4-BV421 (1μL/100μL, Clone: RPA-T4, Biolegend), CD45RA-PE-Cy7 (0.3μL/100μL, Clone: UCHL1, BD Pharmingen), CD8-BV510 (0.3μL/100μL, Clone: RPA-T8, Biolegend), CD19-BV510 (0.1μL/100μL, Clone: HIB19, Biolegend), CD14-BV510 (0.3μL/100μL, Clone: M5E2, Biolegend). CD8, CD19, and CD14 staining was performed to exclude cell populations that expressed these surface markers (dump gate). Inclusion of the

dump gate improves specificity when detecting rare tetramer+ T cells by eliminating aberrant tetramer binding events (Perfetto et al. 2010). Anti-Mouse Ig compensation beads (BD) and stained cells were acquired on a BD FACS LSRII or a BD FACS Aria II and data was analysed using FlowJo v9.2.

Data analysis

Statistical analyses were performed using R and GraphPad Prism v5.0. The Fisher's exact test was used to compare the number of 15mer peptide-specific responses detected by the direct ex vivo and cultured IFN-γ ELISPOT assays, to compare the number of adolescents responding to Ag85A and Ag85B before and after natural *M.tb* infection, and to determine the probability of peptide restriction to HLA alleles. Receiver operating characteristic (ROC) curve analysis was performed to determine the cut-off value for a positive response measured by cultured ELISPOT and ICS. The Mann-Whitney U and Wilcoxon signed-rank tests were performed to compare the number of Ag85A and Ag85B peptides recognised before and after *M.tb* infection.

Results

Cultured IFN-γ ELISPOT assay detected more ESAT-6 T cell epitopes than the direct IFN-γ ex vivo ELISPOT assay.

A common limitation of the assays currently used to identify antigen or epitope-specific T cells is the requisite of specific T cells to perform a particular function (e.g. produce cytokines, cytotoxic molecules, or proliferate) following antigen stimulation. The IFN-γ ELISPOT assay identifies antigen specific T cells by detecting production of IFN-γ following antigen stimulation. Our first goal was to determine if in vitro expansion of antigen-specific T cells would improve the sensitivity of identification of T cell epitopes.

We compared the number of 15mer ESAT-6 peptides recognised by T cells by direct ex vivo and cultured IFN-γ ELISPOT assays, performed in parallel on PBMCs isolated from 9 healthy latently *M.tb* infected individuals. A significantly higher frequency of IFN-γ producing cells was observed after 12-day culture in the presence of ESAT-6, compared to the direct ex vivo assay (Figure 7A). Culturing cells in the presence of ESAT-6 resulted in a median IFN-γ fold increase of 12.86 (IQR 8.09 - 57.55) (data not shown). Importantly, we did not observe a difference between frequencies of CFP-10-specific responses in direct ex vivo and in vitro expanded cells (Figure 7B), suggesting that we expanded cells in an antigen-specific manner. Next, we wanted to compare the number of participants with detectable response to ESAT-6 using the direct ex vivo and cultured IFN-γ ELISPOT assays. A responder was classified as having ≥50 SFU per million PBMC above the negative control. We detected 6/9 (67%) of donors as having a response to the ESAT-6 peptide pool in the direct ex vivo assay, while 9/9 (100%) of donors were classified as having a response

after 12 day culture (Figure 7C). Although the frequency of ESAT-6-specific cells increased in all 9 donors after 12 days, we did not observe a correlation between the direct ex vivo and the cultured IFN-γ ELISPOT assay (Figure 7D).

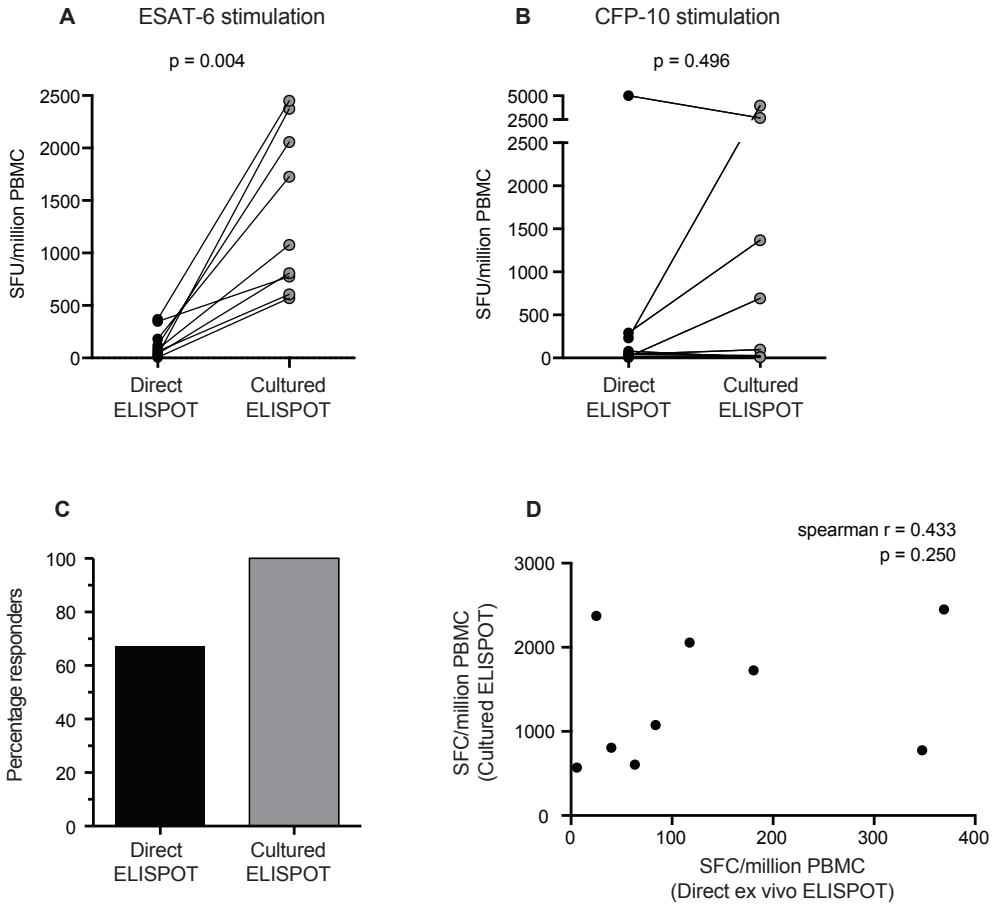

Figure 7. **Comparison of the direct *ex vivo* IFN-γ ELISPOT assay and the cultured IFN-γ ELISPOT.** Assays were performed in parallel on PBMCs from 9 QFT^+ healthy donors. Magnitudes of IFN-γ expressing T cells detected by direct *ex vivo* ELISPOT or cultured ELISPOT upon re-stimulation on ESAT-6 T cell lines with a complete ESAT-6 (A) or CFP-10 (B) peptide pool. (C) The percentage of individuals responding to individual 15mer ESAT-6 peptides and a complete ESAT-6 peptide pool (>50SFU above unstimulated), detected by direct *ex vivo* or cultured IFN-γ ELISPOT assay. (D) The correlation between the direct *ex vivo* ELISPOT and the cultured ELISPOT. P values were calculated using the Wilcoxon signed-rank test (A and B) or spearman correlation (D).

Next, we wanted to compare the number and pattern of T cell epitopes recognised within ESAT-6 when we used the direct ex vivo and the cultured IFN-γ ELISPOT assays. A significantly higher number of responses to ESAT-6 peptides were detected

by the cultured ELISPOT compared to the direct ex vivo ELISPOT. Both ELISPOT assays identified the C- and N-terminal ends of the ESAT-6 protein as most commonly recognised regions (Figure 8). This pattern was more pronounced in the epitope map generated by the cultured IFN-γ ELISPOT assay. Specific T cell responses to ESAT-6 15mer peptides p5, p10, p12, p16, and p17 were detected by cultured IFN-γ ELISPOT assay only, albeit in a single person (Figure 8).

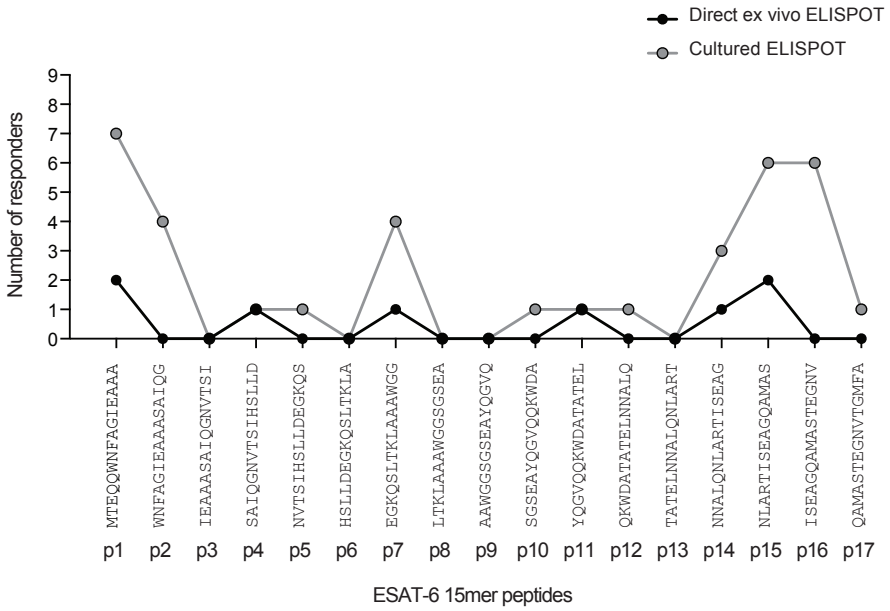

Figure 8. **ESAT-6 epitopes recognised by *M.tb* infected individuals.** The number of participants responding to individual 15mer ESAT-6 peptides (>50SFU above unstimulated) detected by direct *ex vivo* or cultured IFN-γ ELISPOT assay.

The T cell subset responding to the peptide stimulation could not be determined using the IFN-γ ELISPOT assay. Therefore, production of IFN-γ was measured by ICS to confirm and identify the T cell subset recognising the ESAT-6 15mer peptides (Figure 9). Due to the large number of cells required to perform the direct ex vivo ELISPOT and ICS, we could only perform this analysis on the PBMC cultured for 12 days. Interestingly, only CD4 T cells were observed to respond to the 15mer peptides following 12 days culture. Based on the increased sensitivity and ability to detemine

the responding T cell subset we decided to use the cultured IFN-γ ELISPOT assay for identification of epitopes in subsequent experiments.

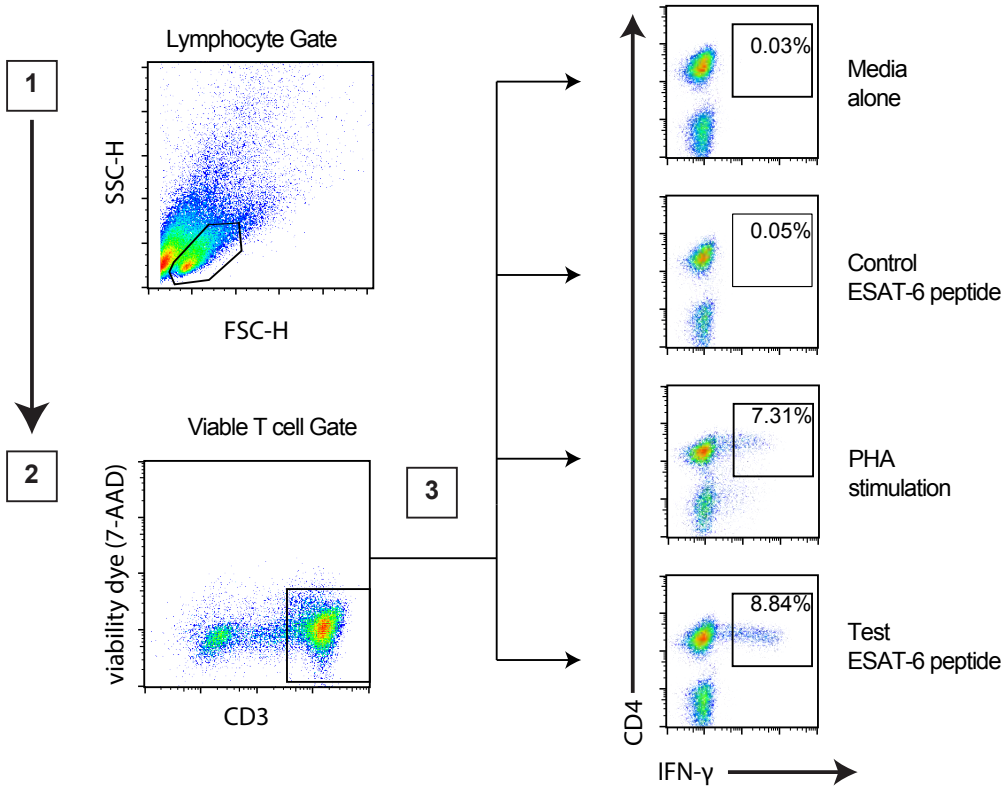

Figure 9. Gating strategy used to confirm peptide specific T cell responses identified by the cultured IFN-γ ELISPOT assay. Expanded T cells were incubated with media alone and a control ESAT-6 peptide not detected by ELISPOT assay (negative controls), PHA (positive control), and the ESAT-6 peptide detected by ELISPOT assay. The frequency of IFN-γ^+ CD4 T cells is shown in each plot.

Demographics of ACS participants who acquired M.tb infection.

We identified a total of 58 healthy adolescents who acquired *M.tb* infection during 2 years of follow-up, defined by TST and QFT conversion. Nineteen adolescents had PBMC available at both enrolment and end of study time points, 26 adolescents had PBMC from the enrolment time point only, while 13 adolescents had PBMC at the end of study only. The demographic characteristics are shown in Table 1.

Table 1. Demographic characteristics of the 58 selected adolescents who acquired *M.tb* infection during follow up. SD= standard deviation and IQR= interquartile range.

Adolescents selected (n = 58)		
Gender, n (%)	Female	30 (52)
Race, n (%)	Black	11 (19)
	Mixed race	47 (81)
Mean age, years (SD)	Enrolment	15.1 (1.37)
	End of study	17.1 (1.37)
Median TST, mm (IQR)	Enrolment	0 (0-0)
	End of study	15(13-17)
Median QFT, IU/mL (IQR)	Enrolment	0 (0-0.04)
	End of study	11.78 (3.24-21.07)

Determination of robust cut-off values using receiver operating characteristic curve (ROC) analysis.

Optimal identification of T cell epitope recognition is only possible if the T cell assay is able to differentiate between positive and negative responses to peptides. Retrospective analysis of samples from adolescents who acquired new *M.tb* infection during follow-up in the ACS allowed us to compare ESAT-6-specific T cell responses before and after *M.tb* infection. These valuable pre and post-infection samples provide the opportunity to derive robust cut-off values, since we do not expect these adolescents to have detectable T cell response to ESAT-6 before infection, and to develop positive ESAT-6 responses only after *M.tb* infection. To determine robust cut-off values for the definition of a positive T cell response measured by cultured ELISPOT and ICS assays, we used ROC curve analysis. We first determined the fold increase in ESAT-6-specific T cells, defined by the frequency of SFU or IFN-γ producing CD4 cells upon peptide stimulation divide by frequency of the negative control for the cultured ELISPOT and ICS assays, respectively. As expected, frequencies of ESAT-6-specific T cells were significantly higher for both assays after *M.tb* infection, compared with the pre-infection time-point (Figure 10).

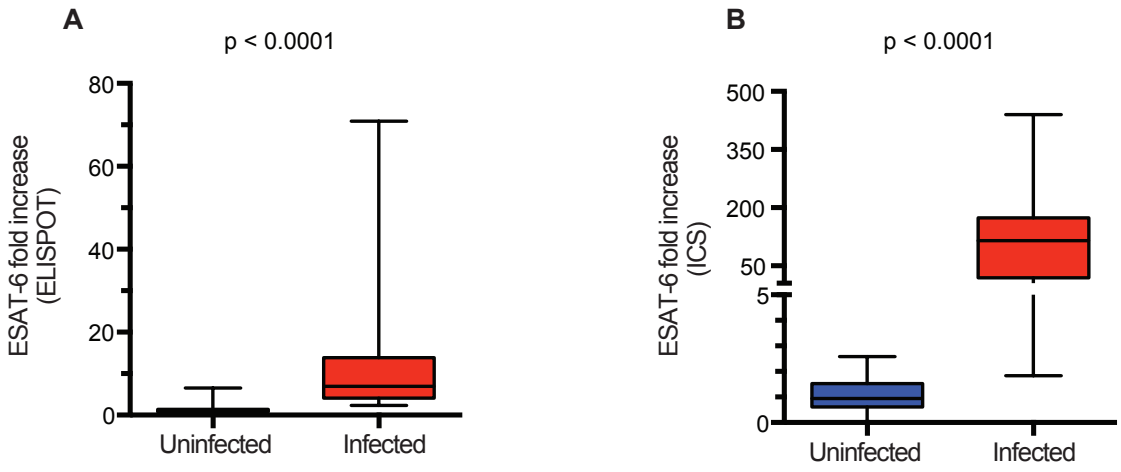

Figure 10. ESAT-6-specific T cell responses upon ESAT-6 peptide pool re-stimulation of T cell cultures generated before and after M.tb infection of adolescents. (A) Fold increase in the number of ESAT-6-specific T cells, measured by IFN-γ ELISPOT assay. (B) Fold increase in the frequency of IFN-γ+ CD4 T cells, measured by intracellular cytokine staining. Fold increase values were defined by dividing the frequency of SFU or IFN-γ producing CD4 T cells upon ESAT-6 stimulation by the frequency of the negative control. P values were calculated using the Mann Whitney U test.

Next, we generated ROC curves using the fold increase values in ESAT-6 responses measured by these assays before and after conversion of their QFT and TST tests. Excellent discrimination of the pre- and post-infection time-points was achieved by both assays, as the area under the curve (AUC) was 0.980 and 0.986 for the cultured ELISPOT and the ICS, respectively (Figure 11). We then plotted the specificity and sensitivity value for discriminating pre- and post-infection ESAT-6 responses when various fold increase values were used (Figure 12). A fold increase above the negative control of 2.5 yielded the maximum specificity and sensitivity for detecting a positive response for both assays. We therefore applied this cutoff value to define positive responses in all subsequent cultured ELISPOT and ICS assays.

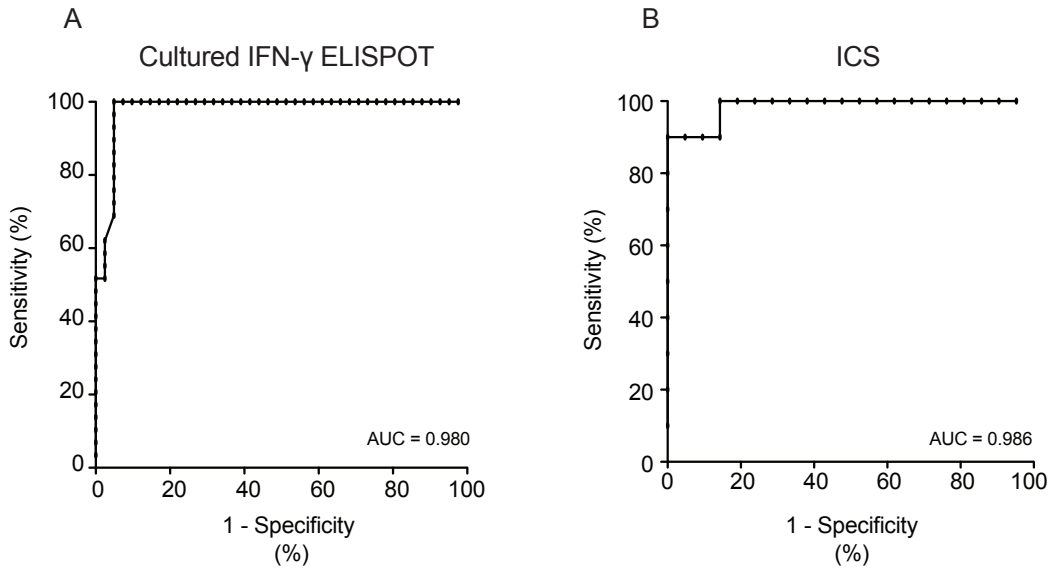

Figure 11. Receiver operating characteristic (ROC) curve analysis to determine the utility of the fold increase values to identify responders. The plots depict the true positive (sensitivity) and false positive (1-specificity) rates at different fold increase cut-off values for the (A) cultured IFN-γ ELISPOT and (B) ICS assays.

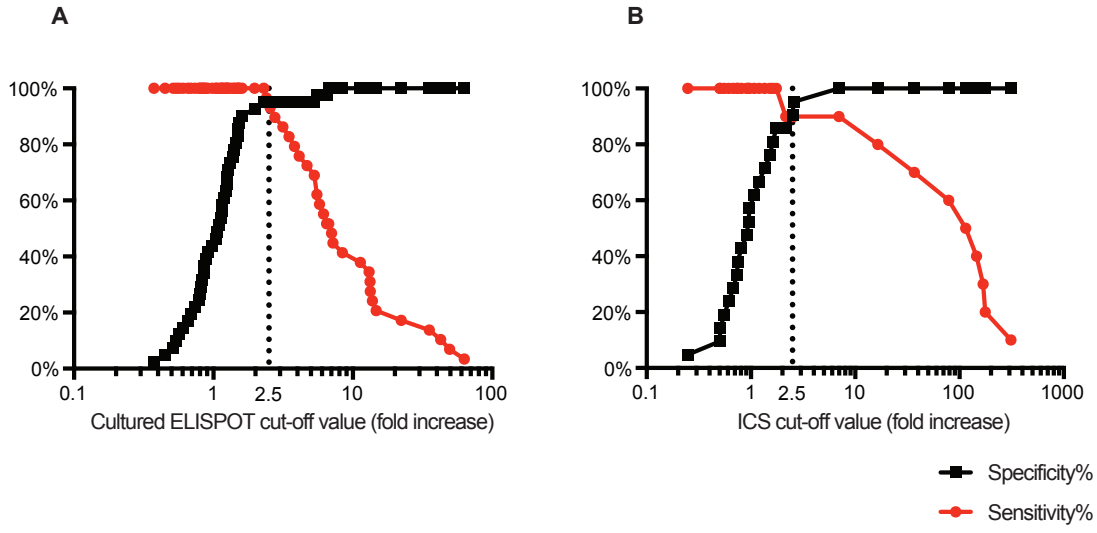

Figure 12. Determining robust cut-off values for a positive ESAT-6-specific T cell response by ROC analysis. The specificity and sensitivity were plotted at various cut-off values for ESAT-6-specific responses detected by (A) cultured IFN-γ ELISPOT assay or (B) ICS assay.

Ag85A and Ag85B epitope recognition patterns are not different before and after acquisition of M.tb infection.

We used the cultured ELISPOT to identify putative Ag85A and Ag85B T cell

epitopes. Confirmation of responses to individual 15mer peptides, as well as identification of the responding subset as CD4 or CD8 T cells, was performed by ICS. Notably, only CD4 T cells were found to respond to the 15mer Ag85A and Ag85B peptides, before and after *M.tb* infection; not a single CD8 T cell response was detected.

Due to insufficient PBMC or as a result of failed positive controls, data was available for 33 and 28 uninfected and *M.tb* infected adolescents, respectively, for Ag85A. For Ag85B data was available for 35 and 18 uninfected and *M.tb* infected adolescents, respectively. We did not observe a significant difference in the total number of peptides recognised when we performed a cross-sectional analysis of uninfected and *M.tb* infected adolescents for Ag85A and Ag85B (Figure 13A and Figure 13B). Comparing the number of Ag85A or Ag85B 15mer peptides recognised by the same adolescent before and after acquisition of *M.tb* infection revealed a trend of increased peptide recognition following infection, but these differences were not significant ($p > 0.05$) (Figure 13C and Figure 13D).

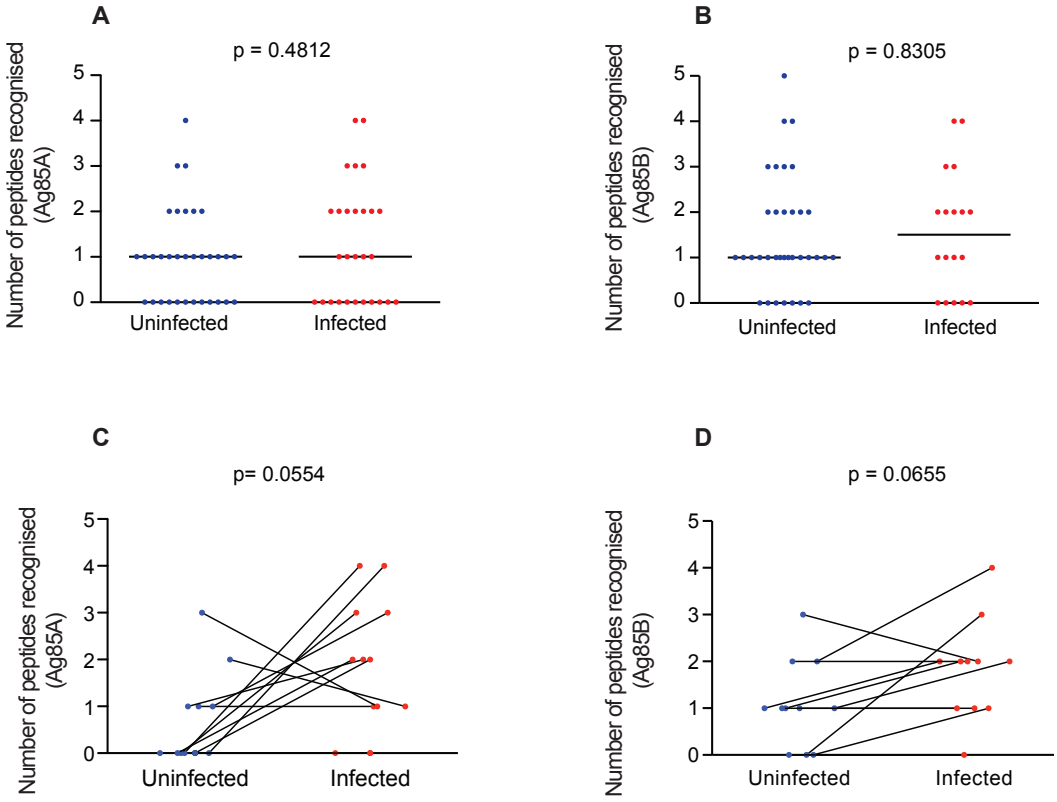

Figure 13. Number of Ag85A and Ag85B peptides recognised by uninfected and M.tb infected adolescents. Cross-sectional analysis of the number of (A) Ag85A and (B) Ag85B peptides recognised by uninfected and infected adolescents. Longitudinal analysis of the number of (C) Ag85A and (D) Ag85B peptides recognized before and after acquired M.tb infection. P values were calculated using the Mann Whitney U test (A and B) or the Wilcoxon signed-rank test (C and D).

Next, we constructed Ag85A and Ag85B T cell epitope maps. These show which regions of these proteins are recognised by CD4 T cells before and after *M.tb* infection (Figure 14A and Figure 14B). Although multiple 15-mer peptides were recognised throughout the sequences of both proteins, three regions were immunodominant. For Ag85A, peptides p13, p27 and p62 were the most frequently recognized before and after infection. It was not surprising that similar regions, namely p12/p13, p27, and p61/62 were frequently recognised within Ag85B before and after acquisition of *M.tb* infection because Ag85A and Ag85B are homologous, sharing 78% amino acids (Appendix Figure 2).

MHC class II binding algorithms predicted HLA restriction of immunodominant regions

In order to identify which HLA class II alleles most likely restrict peptides within these three immunodominant regions of Ag85A and Ag85B, peptide binding predictions to HLA class II alleles were performed. Predictions were performed for DRB1, DRB3/4/5, DQA/B, and DPA/B loci (Figure 15). Peptides that achieved a consensus percentile rank of below 2% were considered possible binders to that particular HLA allele. For ease of interpretation data is presented as the reciprocal of the consensus percentile rank. The p13 region (PSMGRDIKVQFQSGGNNSPA) was previously predicted to bind strongly to the DRB1*03:01 allele, an allele that we successfully developed a class II tetramer bearing this peptide (Dintwe et al. 2013). The p27 region (GKAGCQTYKWETFLTSEL) was predicted to bind with moderate strength to DPA1*01-DPB1*04:01 and very strongly to DPA1*02:01-DPB1*05:01. The p61/62 region (FPPNGTHSWEYWGAQLNAMK) did not achieve a consensus percentile rank below 2% for any of the HLA class II alleles tested, however, the highest predicted binding allele was DRB3*01:01 (consensus percentile rank = 3.57%).

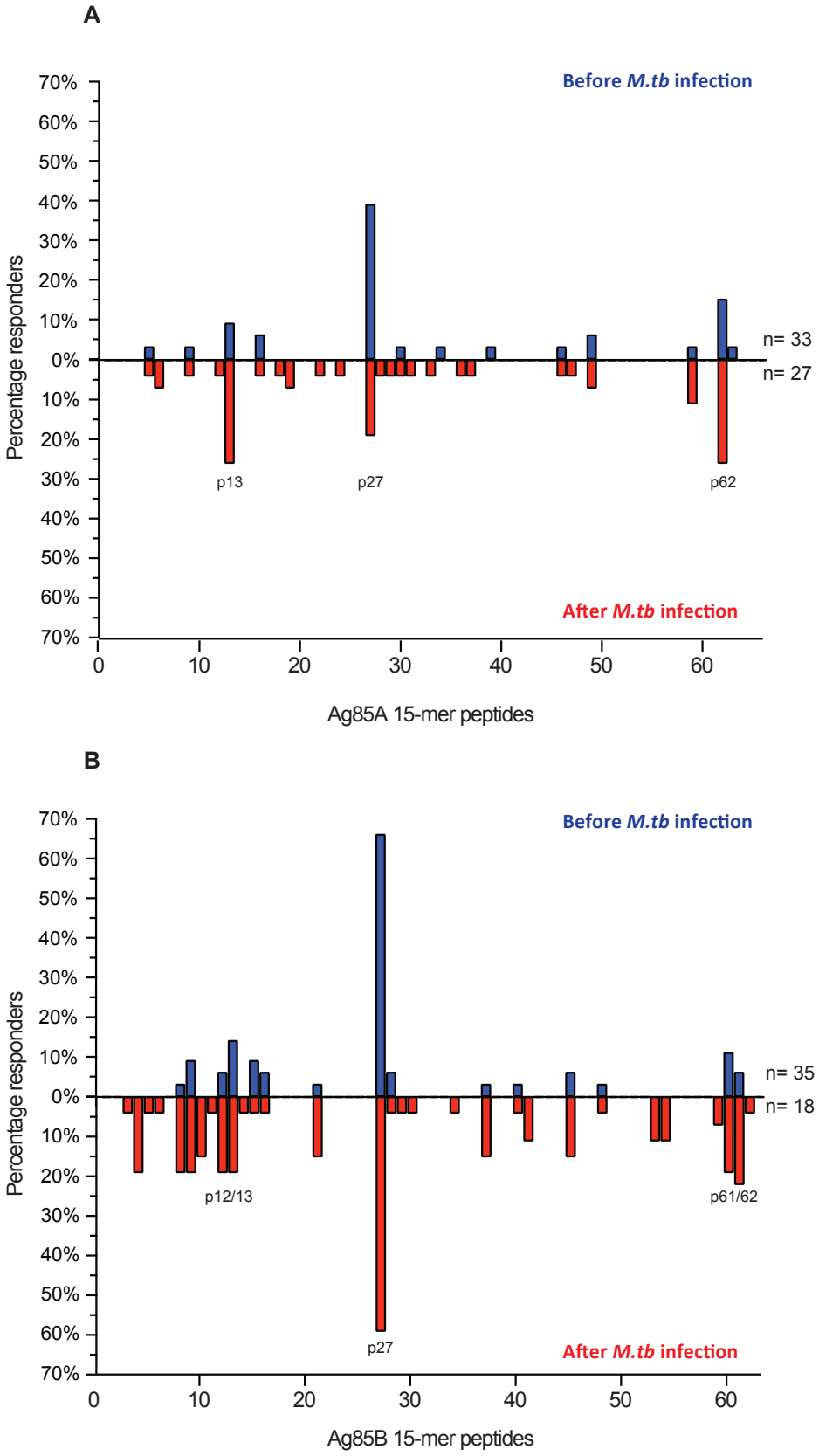

Figure 14. Ag85A and Ag85B epitope recognition by CD4 T cells. Proportions of adolescents with positive (>2.5 fold increase above unstimulated) CD4 T cell responses to single (A) Ag85A and (B) Ag85B 15mer peptides at the pre and post-infection time points. Only responses confirmed with the ICS assay were included in the epitope maps.

Guided by the binding prediction results, we investigated associations between positive ELISPOT and ICS responses to immunodominant Ag85A and Ag85B peptides by persons who either expressed HLA class II alleles predicted to bind these peptides, or not. In this cohort of adolescents there was no significant association between responses to the p13 regions of Ag85A and Ag85B and the expression of the DRB1*03:01 allele ($p = 0.221$ and $p = 0.136$, respectively). Not a single adolescent in this cohort bore the DPA1*02:01/DPB1*05:01 allele, an allele predicted to bind strongly to the p27 region of both Ag85A and Ag85B. Expression of the DPA1*01-DPB1*04:01 allele combination was associated with responses to p27 in the Ag85A protein ($p = 0.032$). However, a significant association between the expression of the DPA1*01-DPB1*04:01 alleles with responses to p27 in the Ag85B protein was not observed ($p = 0.441$).

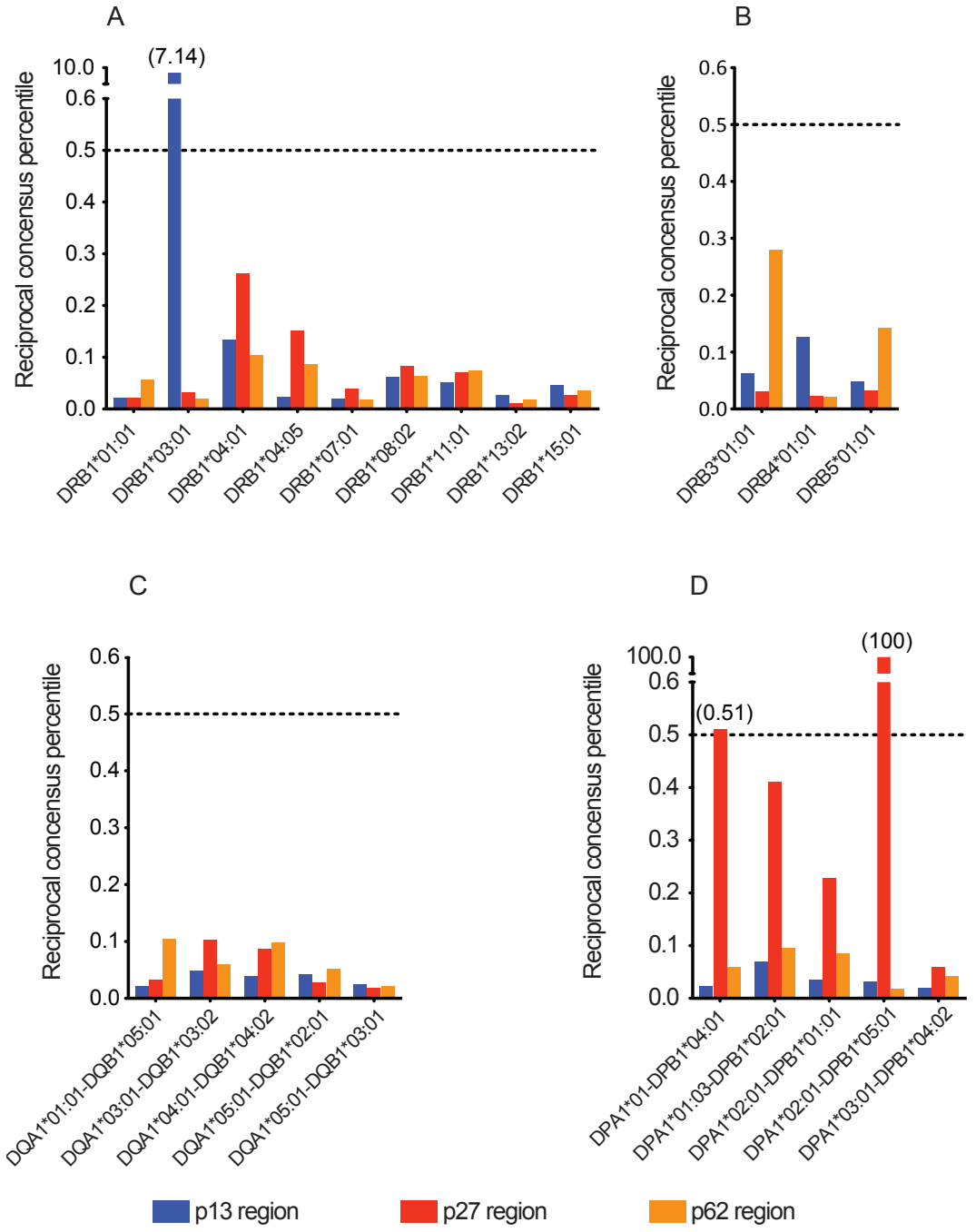

Figure 15. Predictions of Ag85A and Ag85B peptide binding to HLA class II alleles. Binding prediction was performed for immunodominant regions to class II alleles and consensus percentile ranks were determined. A higher reciprocal consensus percentile rank indicates stronger predicated binding of the peptide of interest to the HLA allele: (A) HLA DRB1, (B) HLA DRB3/4/5 , (C) HLA DQA/B, and (D) HLA DPA/B. A reciprocal consensus percentile rank value of ≥0.5 was selected as a cut off value for peptide binding.

In vitro HLA-peptide binding and Ag85A/B-specific class II tetramer development

The predictions and associations with HLA allele expression and peptide response

provided encouraging evidence that these particular peptides and HLA alleles could be targeted for HLA class II tetramer design. However, these results required in vitro confirmation. Using an in vitro binding assay, the affinity of the immunodominant Ag85A and Ag85B peptides to the HLA class II alleles was investigated. Peptides that achieved an IC_{50} ≤1000nM were classified as having a high binding affinity to the HLA class II allele (personal communication, Dr. John Sidney at LIAI). It was observed that Ag85Bp12 had an IC50 value of 422nM to the DRB1*03:01 molecule (Figure 16A), a result that was predicted by various MHC class II binding algorithms. Ag85Ap27 and Ag85Bp27 had a high binding affinity to DPA1*01:03/DPB1*04:01 and DPA1*02:01/DPB1*05:01 (Figure 16B and Figure 16C).

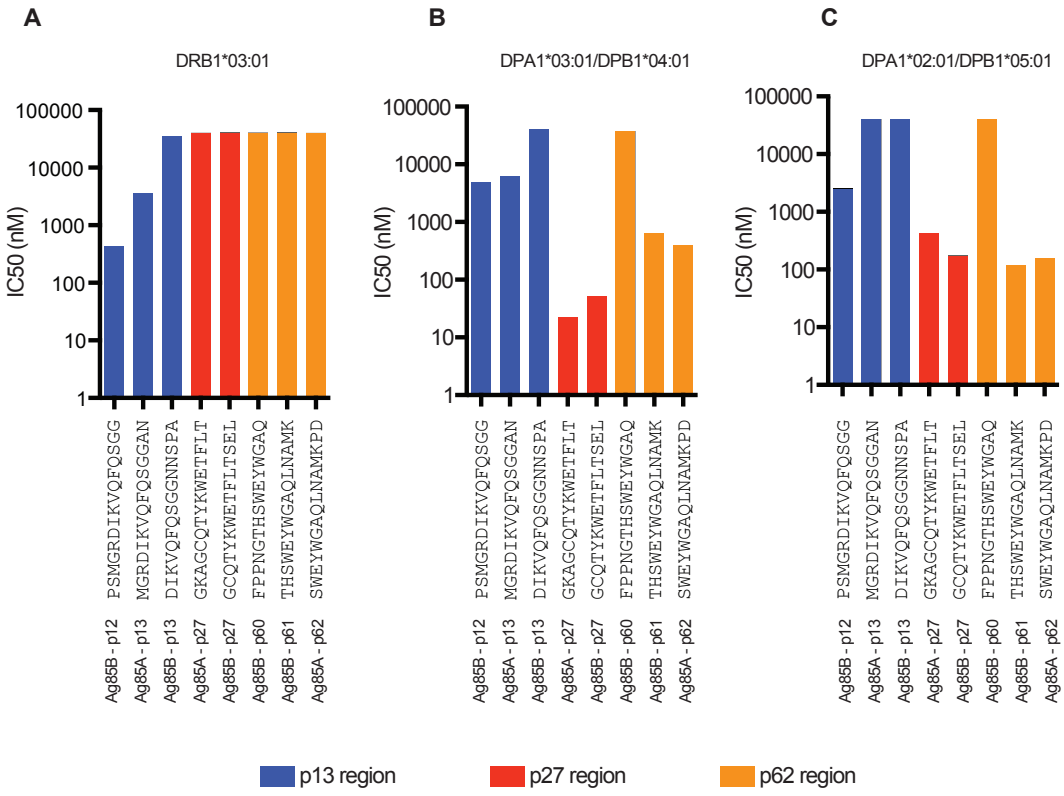

Figure 16. *In vitro* binding assays of HLA class II molecules predicted to bind the immunodominant regions of Ag85A and Ag85B. A low IC50 (<1000nM) indicates high affinity binding to the HLA allele: (A) DRB1*03:01, (B) DPA1*03:01/DPB1*04:01, and (C) DPA1*02:01/DPB1*05:01.

The binding data suggested that the following HLA class II allele: DRB1*03:01, DPA1*01:03/DPB1*04:01, and DPA1*02:01/DPB1*05:01 could be targeted for designing Ag85-specific HLA class II tetramers. From prior work performed in our lab we had already designed an Ag85-specific tetramer that had $Ag85A_{VPSPSMGRDIKVQFQSGGAN}$ loaded into DRB1*03:01 (Dintwe et al. 2013) (Figure 17A). Due to the lack of expression of the DPA1*02:01/DPB1*05:01 allele within the cohort of adolescents this allele was not targeted for tetramer development. A DPB1*04:01 tetramer was synthesised by the NIH tetramer core facility loaded with $Ag85B_{GKAGCQTYKWETFLTSE}$, and a DPB1*04:01 tetramer loaded with HIVenv $_{TEKLWVTVYYGVPVW}$ served as a negative control (Figure 17A). Based on work performed by Dintwe et al. who identified ESAT-6 epitopes and their HLA class II restriction, a DQB1*06:02 tetramer loaded with ESAT-$6_{EGKQSLTKLAAAWGG}$ was also synthesized, and a DQB1*06:02 tetramer loaded with $Clip_{PVSKMRMATPLLMQA}$ served as a negative control (Figure 17A). We confirmed specific binding of mycobacteria-specific CD4 T cells with these HLA class II tetramers (Figure 17B).

A

HLA allele	Mycobacterial antigen	Peptide sequence	Irrelevant antigen	Peptide sequence
DRB1*03:01	Ag85	VPSPSMGRDIKVQFQSGGAN	ApoB	ISNQLTLDSNTKYFHKLN
DPB1*04:01	Ag85	GKAGCQTYKWETFLTSE	HIV env	TEKLWVTVYYGVPVW
DQB1*06:02	ESAT-6	EGKQSLTKLAAAWGG	Clip	PVSKMRMATPLLMQA

B

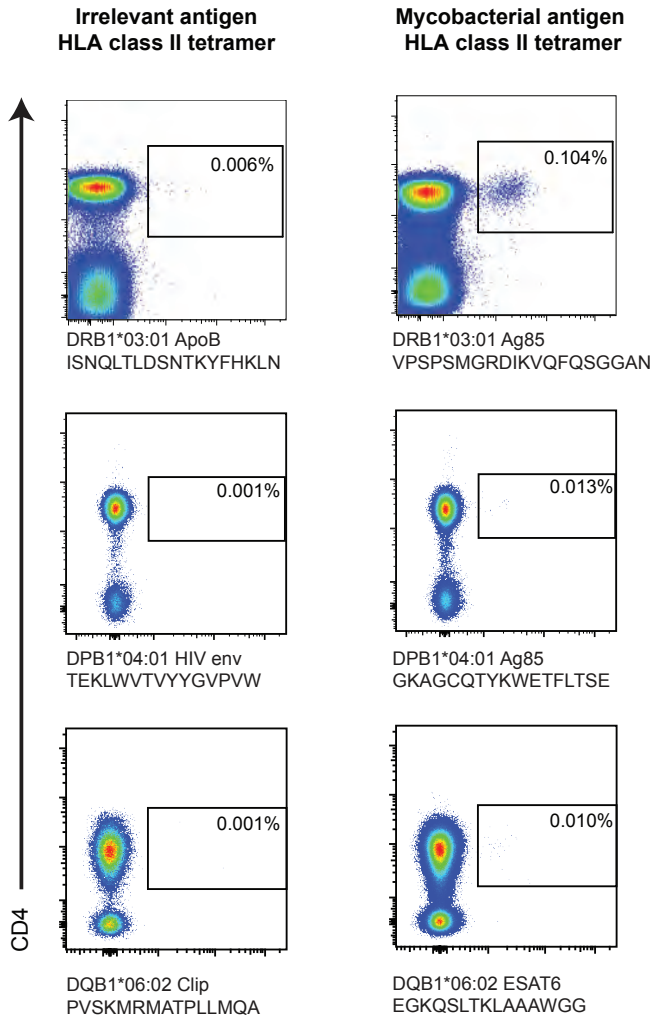

Figure 17. Panel of HLA class II tetramers designed to identify mycobacteria-specific CD4 T cells. (A) HLA class II molecules loaded with mycobacteria-specific peptides or an irrelevant antigen. (B) Example of PBMC staining using a DRB1*03:01, DPB1*04:01, or DQB1*06:02 HLA class II tetramer.

Discussion

The primary aim of the experiments in this chapter was to investigate whether natural infection with *M.tb* in adolescents affected the number of epitopes recognised by T cells and/or the breadth of epitope recognition within the immunodominant antigens,

Ag85A and Ag85B. In order to optimally identify the epitopes targeted by T cells, we chose to use the IFN-γ ELISPOT assay. This assay is frequently used to measure T cell response to antigens, however it does have limitations. The IFN-γ ELISPOT assay detects antigen-specific T cells that produce detectable levels of IFN-γ. Therefore, antigen-specific T cells that do not produce IFN-γ will not be detected. Consequently, using the ELISPOT may underestimate the real frequencies of antigen-specific T cells circulating in blood. Using intracellular IL-2, TNF-α and/or IL-17 staining, we have detected antigen-specific T cells that do not produce IFN-γ in a number of studies (Day et al. 2011; Soares et al. 2008; Scriba et al. 2008; Rozot et al. 2014). Nevertheless, IFN-γ remains one of the best cytokines to detect epitope responses. This is because most epitopes identified by ELISPOT assays that measure other cytokines (i.e. IL-2 or TNF-α) are also identified by the IFN-γ ELISPOT (personal communication, Dr. Alessandro Sette at LIAI). Similarly, soluble levels of IL-2 and TNF-α strongly correlate with IFN-γ levels following stimulation with ESAT-6 and CFP-10 (Penn-Nicholson et al. 2015).

The IFN-γ ELISPOT assay readily detects antigen specific T cell responses following overnight stimulation of PBMC with mycobacterial antigens. However, we were concerned that single epitope-specific responses might not be detected following such short-term stimulation of PBMC. We investigated whether the sensitivity to detect peptide specific responses with the IFN-γ ELISPOT assays could be increased if antigen-specific T cell cultures were generated prior to the IFN-γ ELISPOT. Indeed, the IFN-γ ELISPOT assay detected more peptide specific responses following generation of ESAT-6 T cell cultures, compared to direct ex vivo testing. This

suggests that the cultured assay expanded antigen-specific T cell populations and allowed identification of antigen-specific T cells present at very low frequencies in peripheral blood. The expansion of rare antigen-specific T cells, at undetectable levels prior to 12-day culture, may help explain the lack of correlation between the magnitudes of ESAT-6-specific T cell before and after the 12-day culture observed in Figure 7D. It is also possible that during the 12-day culture not all epitope-specific responses expanded uniformly and therefore could result in the lack of concordance between the two ELISPOT assays. The sensitivity of IFN-γ release assays has been shown to increase when the incubation time of antigen stimulation increases (Leyten et al. 2007). Concern has been expressed that this increase may be a result of de novo priming of peptide-specific T cell response from naïve T cells during the 12-day culture. However, we did not observe any ESAT-6-specific T cells responses in *M.tb* uninfected adolescents when using the cultured IFN-γ ELISPOT assay, strongly supporting that de novo priming did not occur during the 12-day culture. These data suggest that the cultured IFN-γ ELISPOT assay detected genuine epitope-specific T cell populations circulating in the blood.

Having determined the appropriate assay to measure epitope-specific T cell responses, the regions within Ag85A and Ag85B targeted by T cells before and after infection were identified. Three major points emerged: 1) acquisition of *M.tb* infection did not significantly change the breadth of T cell epitope recognition of Ag85A and Ag85B; 2) three distinct regions of immunodominance were identified in each of the Ag85A and Ag85B proteins; 3) peptides within these immunodominant regions were exclusively recognised by CD4 T cells and, therefore, restricted by HLA class II alleles. These data suggest that BCG vaccination and/or exposure to environmental

mycobacteria elicit CD4 T cell responses within Ag85A/B with similar epitope breadth to natural infection with *M.tb*. However, we did observe a trend toward recognition of more epitopes following *M.tb* infection in a subset of participants that had cells available before and after infection. Perhaps by increasing the sample size we would have observed a difference.

Within Ag85A, the 15-mer peptides Ag85A-p13, Ag85A-p27, and Ag85A-p62 were most commonly targeted before and after *M.tb* infection. Similarly, Ag85B-p12/13, Ag85B-p27, and Ag85B-p60/61 were immunodominant before and after *M.tb* infection. It was not surprising that similar epitope maps for Ag85A and Ag85B were generated, given that 78% of the amino acid sequence of Ag85A and Ag85B is identical.

To our knowledge, this is the first study to map T cell epitopes within Ag85A or Ag85B epitopes before and after *M.tb* infection in the same individuals. However, others have generated Ag85A and Ag85B epitope recognition maps in healthy BCG vaccinated persons and adults after vaccination with the novel tuberculosis vaccine, MVA85A. In BCG vaccinated persons, Ag85B-p13 and Ag85B-p27 were reported to be frequently recognised (Mustafa et al. 2000), and Ag85A-p13 and Ag85A-p27 were shown to be commonly recognised by CD4 T cells from healthy adults after MVA85A vaccination (McShane et al. 2004). Our data on epitope identification in natural mycobacterial infection and those observed by other investigators suggest that immunodominance of the regions within Ag85A and Ag85B are at least in part independent of the genetic background and nature of antigen exposure.

Our results may have implications for vaccine development and the epitopes that novel vaccines should aim to target. Data from the mouse model suggest that targeting subdominant epitopes within ESAT-6 may be beneficial in immune control of *M.tb* infection. Vaccination of mice with a truncated ESAT-6 protein lacking the N-terminal immunodominant epitope induced responses to subdominant epitopes (Aagaard et al. 2009). Furthermore, mice that recognised the subdominant epitope had enhanced control of *M.tb* infection compared to mice that recognised the N-terminal immunodominant epitope (Aagaard et al. 2009). Interestingly, CD4 T cells that recognised subdominant epitopes had smaller proportions of cells expressing KLRG1, a marker of terminally differentiation,,compared to CD4 T cells that recognised the immunodominant epitope (Woodworth et al. 2014). Furthermore, 12 weeks after *M.tb* infection a larger proportion of CD4 T cells that recognised the subdominant epitope were polyfunctional, simultaneously producing IFN-γ, TNF-α, and IL-2 compared to CD4 T cells that recognised the immunodominant epitope (Woodworth et al. 2014). We observed that p27 was dominant in our study. It would be interesting to compare the cytokine response of p27-specific CD4 T cells with the response of CD4 T cells targeting the more subdominant regions of Ag85A and Ag85B.

It was striking that CD4 T cells mediated all responses to Ag85A and Ag85B, especially following *M.tb* infection, because previously we have observed Ag85B or TB10.4-specific CD8 T cell responses in BCG vaccinated children (Tena-Coki et al. 2010). Furthermore, using CD4 depleted PBMCs, others in our group detected IFN-γ responses upon ESAT-6 stimulation using a direct *ex vivo* IFN-γ ELISPOT assay (Moshi *et. al* unpublished), demonstrating that the direct IFN-γ ELISPOT assay can

detect ESAT-6-specific CD8 T cells in *M.tb* infected persons. These results may suggest that the cultured ELISPOT assay preferentially expand CD4 T cell responses. CD8 and CD4 T cells interact with epitopes in the context of MHC class I and II molecules, respectively. The loading grooves of MHC class I and II have distinct characteristics, which dictate the length of peptides loaded. The MHC class I groove is closed and accommodates peptides of 8 to 10 amino acids in length (Simon et al. 2000). The MHC class II groove is not closed and can accommodate much longer peptides (Simon et al. 2000). Since we used peptide pools comprised of 15-mer peptides spanning Ag85A and Ag85B, it is likely that the CD4 T cells were preferentially expanded, while CD8 T cells were not optimally activated.

The development of HLA tetramers is vital for future studies that aim to study the mycobacteria-specific T cell immune response with minimum perturbation of cells. We have already successfully utilised a DRB1*03:01 HLA class II tetramer to investigate mycobacterial immune response following MVA85A vaccination (Dintwe et al. 2013). A major drawback of using tetramers to probe the T cell immune responses is the prerequisite that study participants must express cognate HLA alleles (Nepom 2012). Therefore, in order to study a human population with a diverse class II HLA repertoire, a set of tetramers that allow good coverage of the population are required. We successfully designed a DPB1*04:01 HLA class II tetramer to identify Ag85-specific CD4 T cells. Using a panel of mycobacteria-specific HLA class II tetramers specific for Ag85B and ESAT-6, we aimed to probe vaccine-induced Ag85B and ESAT-6-specific CD4 T cells in *M.tb* infected and uninfected adolescents.

Chapter 3: Optimisation of transcriptomic analysis of tetramer-sorted CD4 T cells.

Introduction

A better, more comprehensive appreciation of vaccine-induced mycobacteria-specific CD4 T cells will require simultaneous quantification of many parameters. Although typical immunogenicity measures, such as frequencies or cytokine co-expression profiles of Th1 cytokine-expressing CD4 T cells are important and measurement of these outcomes has led to a greater understanding of vaccination, they do not correlate with risk of TB disease (Kagina et al. 2010). In a recent phase IIb trial assessing the efficacy of MVA85A vaccination in a cohort of BCG vaccinated infants, Ag85A-specific Th1 cytokine-expressing cells were increased in MVA85A vaccinated infants compared to placebo control, yet MVA85A vaccination did not reduce incidence of tuberculosis (Tameris et al. 2013). Characterisation of T cell attributes beyond expression of the typical Th1 cytokines is necessary to expand our understanding of immune responses induced by vaccines. In this regard, high throughput transcriptomic platforms offer an appealing approach to comprehensively characterize vaccine induced immune responses. Such platforms have been used to identify a transcriptomic signature that predicted the immune response induced by the yellow vaccine, YF-17D, in humans (Querec et al. 2009). High throughput platforms have also been used to better understand immune responses induced by different vaccination strategies. In a study performed by Flatz et al. vaccination of mice with three different prime-boost vector combinations induced HIV envelope-specific CD8 T cells that appeared similar based on conventional parameters, such as magnitude, memory phenotype, or co-expression of IFN-γ, TNF-α and IL-2. However,

microarray analysis revealed heterogeneity at the transcriptomic level within T cell populations induced by the different vector combinations (Flatz et al. 2011). These studies support our rationale, that by expanding the parameters measured, we may gain new insights into the character of antigen-specific CD4 T cells induced by novel tuberculosis vaccines.

Recently, a scalable and cost-effective microfluidic qPCR platform, the BioMark HD System (Fluidigm), has been used to perform gene expression measurement in as few as one cell (White et al. 2011; Dominguez et al. 2013). This high level of sensitivity makes the BioMark HD System an ideal platform to measure expression of mRNA transcripts by circulating antigen-specific CD4 T cells, even if these cells are present at very low frequencies. The BioMark HD technology can measure expression of 96 mRNA transcripts in 96 samples, simultaneously, amounting to 9,216 qPCR reactions. Although, the BioMark HD System measures far fewer parameters compared to microarray or RNASeq and is not a truly unbiased assessment of the character of vaccine induced CD4 T cells, the number of parameters measured by the BioMark HD System is much more than has been traditionally measured in tuberculosis vaccine clinical trials.

By combining traditional approaches with the BioMark HD System comprehensive characterisation of vaccine-induced CD4 T cell responses can be performed. This chapter describes the optimisation of protocols to identify, sort and characterize vaccine-induced CD4 T cell responses with the BioMark HD System. We also investigated possible effects of short-term incubation of CD4 T cells with HLA class II tetramers on the expression of mRNA within antigen-specific CD4 T cells to

determine if the tetramer staining procedure perturbs the transcriptomic programme of cells of interest.

The aims of this chapter were to determine the optimal cDNA synthesis protocol to quantify mRNA transcripts in HLA class II tetramer sorted mycobacteria-specific CD4 T cells and to determine the effects of tetramer staining on mRNA expression by antigen-specific CD4 T cells.

Specific objectives

1. To perform a pilot experiment to determine the effect of cell number on the proportion of mRNA transcripts detected by the BioMark HD System.

   We hypothesized that the proportion of detected mRNA transcripts will be reduced in samples with fewer cells compared to samples with more cells.

2. To determine if performing RNA extraction, cDNA synthesis, and specific transcript amplification in the same PCR tube (one-step RT-PCR) would increase the proportion of mRNA transcripts detected by the BioMark HD System compared to performing RNA extraction and cDNA synthesis sequentially in separate PCR tubes (two-step RT-PCR) prior to specific transcript amplification.

   We hypothesized that a higher proportion of mRNA transcript will be detected following *one-step RT-PCR compared to two-step RT-PCR.*

3. To determine the amplification efficiency of each qPCR primer/probe set selected to measure gene expression profiles within antigen-specific CD4 T cells.

4. To verify that the protocol for generating cDNA for BioMark HD System analysis accurately detects transcriptomic differences in populations of naïve, central memory, and effector memory CD4 T cells.

   We hypothesized that the optimal cDNA protocol will readily distinguish naïve, central memory, and effector memory CD4 T cells, based on transcriptomic patterns, in agreement with the known functions of these CD4 T cell subsets.

Methods and Materials

TaqMan Gene Expression (GE) assays

We reviewed the literature to identify mRNA transcripts associated with a range of CD4 T cell functions. Broadly, mRNA could be categorized into T cell activation, apoptosis, chemokine receptors, cytokine receptors, cytokines, cytotoxic molecules, inhibition, and transcription factors (Table 2). We also incorporated genes based on discussion with Dr. Holden Maecker, Stanford University, who has extensive experience with transcriptional profiling of T cells as part of the Human Immunophenotyping platform. TaqMan primer/probe sets found not to perform well in the Maecker lab were not included. Although, the BioMark HD System simultaneously quantifies the expression of 96 transcripts, we selected a total of 101 transcripts because we anticipated that some primers and probe sets would have poor amplification efficacy (*see qualification section below*). We searched Life Technologies predesigned TaqMan gene expression (TaqMan GE) assays database to identify primer/probe sets specific for the 101 mRNA transcripts of interest. TaqMan GE assays are a set of forward and reverse primers and a FAM/TAMRA labelled probe. TaqMan GE assays classified as "Best Coverage" by Life Technologies and probes spanning exons were selected. Best Coverage assays are recommended by Life Technologies because for standard gene expression experiments they detect the maximum number of transcripts. If a gene did not have a TaqMan GE assay classified as "Best Coverage", we selected assays with probes that spanned exons.

Table 2. 101 TaqMan GE assays that were included in the qualification experiments.

	Gene Name	TaqMan ID
1	*ARHGEF18*	Hs00248726_m1
2	*AXIN2*	Hs00610344_m1
3	*B2M*	Hs00984230_m1
4	*BCL2*	Hs00608023_m1
5	*BCL2L11*	Hs00708019_s1
6	*BID*	Hs00609632_m1
7	*BID*	Hs01026791_m1
8	*BTLA*	Hs00699198_m1
9	*CAMK4*	Hs00174318_m1
10	*CCR2*	Hs01560352_m1
11	*CCR4*	Hs00747615_s1
12	*CCR5*	Hs00152917_m1
13	*CCR6*	Hs01890706_s1
14	*CCR7*	Hs01013469_m1
15	*CCR9*	Hs01890924_s1
16	*CD137*	Hs00155512_m1
17	*CD154*	Hs00163934_m1
18	*CD160*	Hs00199894_m1
19	*CD27*	Hs00386811_m1
20	*CD28*	Hs00174796_m1
21	*CD38*	Hs01120071_m1
22	*CD4*	Hs01058407_m1
23	*CD69*	Hs00934033_m1
24	*CD8A*	Hs00233520_m1
25	*CTLA4*	Hs03044418_m1
26	*CXCL10*	Hs01124251_g1
27	*CXCR3*	Hs01847760_s1
28	*CXCR6*	Hs00174843_m1
29	*EPHA4*	Hs00177874_m1
30	*FAS*	Hs00236330_m1
31	*FCER1G*	Hs00175408_m1
32	*FOXO3A*	Hs00818121_m1
33	*FOXP3*	Hs01085834_m1
34	*G6PD*	Hs00166169_m1
35	*GAPDH*	Hs02758991_g1
36	*GATA3*	Hs00231122_m1
37	*GNLY*	Hs00246266_m1
38	*GPR15*	Hs00922903_s1
39	*GZMA*	Hs00989184_m1
40	*GZMB*	Hs01554355_m1
41	*GZMK*	Hs00157878_m1
42	*HBB*	Hs00747223_g1
43	*HPRT*	Hs01003267_m1
44	*ICOS*	Hs00359999_m1
45	*IFNG*	Hs00989291_m1
46	*IFNGR1*	Hs00988304_m1
47	*IL10*	Hs00961622_m1
48	*IL12RB1*	Hs00538167_m1
49	*IL12RB2*	Hs01548202_m1
50	*IL15*	Hs00542571_m1
51	*IL15*	Hs01003716_m1
52	*IL17A*	Hs00174383_m1
53	*IL2*	Hs00174114_m1
54	*IL21*	Hs00222327_m1
55	*IL22*	Hs01574154_m1
56	*IL2RA*	Hs00907779_m1
57	*IL2RB*	Hs01081697_m1
58	*IL2RG*	Hs00953624_m1
59	*IL4*	Hs00174122_m1
60	*IL5*	Hs01548712_g1
61	*IL6*	Hs00985639_m1
62	*IL7*	Hs00174202_m1
63	*IL7R*	Hs00902334_m1
64	*ITGAL*	Hs00158218_m1
65	*ITGAX*	Hs01015070_m1
66	*ITK*	Hs00950634_m1
67	*JNK*	Hs00177083_m1
68	*KI67*	Hs01032443_m1
69	*LDLRAP1*	Hs00296701_m1
70	*LEF1*	Hs01547250_m1
71	*LTK*	Hs01587788_m1
72	*MAN1C1*	Hs00220595_m1
73	*MCAM*	Hs00174838_m1
74	*NFKB1*	Hs00765730_m1
75	*PDCD1*	Hs01550088_m1
76	*PKIA*	Hs00738983_m1
77	*PRF1*	Hs00169473_m1
78	*PRKCA*	Hs00925195_m1
79	*PRR5L*	Hs01029928_m1
80	*PTPRC*	Hs00365634_g1
81	*RASGRF2*	Hs00394798_m1
82	*RHOH*	Hs00180265_m1
83	*RORA*	Hs00536545_m1
84	*RORC*	Hs01076112_m1
85	*SELL*	Hs00174151_m1
86	*SOCS1*	Hs00705164_s1
87	*STAT1*	Hs01013996_m1
88	*STAT3*	Hs01047580_m1
89	*STAT4*	Hs01028017_m1
90	*STAT5A*	Hs00234181_m1
91	*STAT5B*	Hs00273500_m1
92	*STAT6*	Hs00598625_m1
93	*TBX21*	Hs00203436_m1
94	*TCF3*	Hs00413032_m1
95	*TCF7*	Hs00175273_m1
96	*TCF7L2*	Hs01009044_m1
97	*TFRC*	Hs00951083_m1
98	*TGFB1*	Hs00998133_m1
99	*TNFA*	Hs99999043_m1
100	*TNFSF10*	Hs00921974_m1
101	*ZAP70*	Hs00896347_m1

PBMC

PBMC isolation was performed by Ficoll density gradient separation as described in Chapter 2.

Specific transcript amplification (STA) cDNA preparation

One of the objectives of this chapter was to determine the optimal protocol to prepare antigen-specific CD4 T cell cDNA for analysis on the BioMark system. We compared the two-step and the one-step RT-PCR, described below.

Two-Step RT-PCR

RNA was extracted from cells and converted into cDNA (step 1) and then cDNA was transferred into another PCR tube for STA (step 2).

RNA extraction

RNA was extracted from cells using the RNeasy mini or the RNeasy micro kits (Qiagen), following the manufacturer's protocols. The NanoDrop 2000 spectrophotometer (Thermo Scientific) was used to measure RNA concentrations and purity.

cDNA synthesis

cDNA was synthesised from RNA using the SuperScript III First-Strand Synthesis System for RT-PCR (Life Technologies). 100ng of RNA, oligo-dTs, dNTP mixture, and molecular grade water were combined to make a 10µL mixture in a 200µL PCR tube. The mixture was incubated at 65°C for 5 minutes and then placed on ice for 1 minute. Next, 10µL of cDNA synthesis mix (2µL 10X RT buffer, 4µL 25nM $MgCl_2$, 2µL 0.1M DTT, 1µL RNaseOUT, and 1µL SuperScript III reverse transcriptase) was added into the PCR tube and incubated at 50°C for 50 minutes. The cDNA synthesis reaction was terminated at 85°C for 5 minutes. cDNA was either used immediately or stored at -20°C.

Specific Transcript Amplification (STA)

Transcripts of interest were amplified prior to microfluidic qPCR. Amplification of

specific transcripts was required to ensure even distribution of cDNA originating from rare mRNA transcripts into each of the 96 microchambers of the 96.96 Dynamic Array chip (Dominguez et al. 2013). Amplification of specific transcripts was performed as follows: 2.5µL of cDNA was added to 5µL 2x Fermentas PCR mix and 2.5µL 0.2xTaqMan GE assay mix (mixture which contained all 96 TaqMan GE assays) in a 200µL PCR tube. PCR tubes were incubated at 95°C for 10 minutes followed by 14 cycles of 95°C for 15 seconds and 60°C for 4 minutes. STA-cDNA was diluted 1:5 with molecular grade water and stored at -20°C.

One-Step RT-PCR

Using the CellsDirect one-step RT-PCR method, RNA isolation, cDNA synthesis, and STA all occur in the same PCR tube. Prior to optimization of protocols we used the following protocol: Cells (1µL) were pipetted directly into a mixture of 25µL 2X Reaction Mix, 2µL of SuperScript III RT/ Platinum Taq Mix, and 12.5µL of 0.2X TaqMan GE assay mix and made up to 50µL with molecular grade water. The PCR tube was incubated at 50°C for 20 minutes, followed by 95°C for 2 minutes and then by 14 cycles of 95°C for 15 seconds and 60°C for 4 minutes. STA-cDNA was diluted 1:5 with molecular grade water and stored at -20°C. The optimal reaction volume and number of STA cycles were determined as described in the results.

Confirmation of specific transcript amplification (STA) using conventional qPCR

The presence of STA-cDNA was confirmed by conventional qPCR. 4µL of STA-cDNA from randomly selected samples was placed in a 200µL PCR tube containing

10µL TaqMan Universal PCR Master Mix, 1µL of *CD4*, *GAPDH, or B2M* 20X TaqMan GE assay mix, and 5µL molecular grade water. The PCR tube was place in a Rotor-Gene 6000 (QIAGEN) and the following thermal profile was initiated; 50°C for 120 seconds, then 95°C for 600 seconds, followed by 40 cycles of 95°C for 15 seconds and 60°C for 60 seconds. Only samples with detectable levels of transcripts were loaded onto a 96.96 Dynamic Array chip.

BioMark HD System qPCR

TaqMan GE assays and STA-cDNA samples were loaded onto a 96.96 Dynamic Array chip according to the manufacture's instructions. Briefly, control line fluid was injected into each accumulator on the 96.96 Dynamic Array chip. The chip was placed in the integrated fluidic circuit (IFC) controller and the Prime 136x script was run to load the control line fluid into the chip. Next, 2.5µL of each 20X TaqMan GE assay and 2.5µL assay loading reagent (Fluidigm) were loaded into each assay inlet on the 96.96 Dynamic Array chip. 2.25µL of STA-cDNA, 2.5µL TaqMan Universal PCR Master Mix, and 0.25 sample-loading reagent (Fluidigm) were loaded into each sample inlet on the 96.96 Dynamic Array chip. To ensure consistency, a master mix of TaqMan Universal PCR Mix and sample-loading reagent was prepared and dispensed into a 96 well plate containing STA-cDNA. Loading into the assay inlets and the sample inlets was performed with a multipipette. The chip was placed in the IFC controller and the Load Mix 136x script was run. Upon completion of sample and assay loading, the chip was placed in the BioMark HD system and the GE 96x96 standard v1 thermal profile (Table 3) was initiated.

Table 3. The GE 96x96 standard v1 thermal profile used to measure relative mRNA transcript levels.

Thermal Mix			UNG	Hot Start	PCR cycles (40X)	
50°C	**70°C**	**25°C**	**50°C**	**95°C**	**95°C**	**60°C**
120 seconds	**1800 seconds**	**600 seconds**	**120 seconds**	**600 seconds**	**15 seconds**	**60 seconds**

Qualification of TaqMan GE assays

Qualification of TaqMan GE assays was performed to determine the amplification efficacy of each TaqMan GE assay, using a modified approach described by Dominquez et al. (Dominguez et al. 2013). Briefly, PBMC were stimulated with PMA/Ionomycin, PHA, or media alone. All stimulations were performed at 37°C in 5% CO_2. For PMA/Ionomycin stimulation PBMC were incubated with PMA (50ng/mL) and Ionomycin (500ng/mL) for 2 hours. For PHA stimulation PBMCs were incubated with 10µg/mL PHA for 4 hours. PBMC from the different stimulation conditions were combined and twelve 2-fold serial dilutions were made, starting with 10,240 cells to 5 cells. This was done for a total of 8 replicates. Cells (1µL) were pipetted directly into a mixture of 5µL of CellsDirect 2X reaction Mix, 0.5µL SuperScript III RT/ Platinum Taq Mix, and 2.5µL of 0.2X TaqMan GE assay mix and 1µL Low TE buffer. The mixture was incubated for 50°C for 20 mins. Threshold expression (Et) values (40-Ct) were calculated for each gene. For a TaqMan GE assay to qualify, a linear relationship with a slope between 3.1-3.6 and an R^2 value greater than 0.97 had to be achieved.

Fluorescence-activated cell sorting (FACS)

Using the FACSAria^{TM} (BD Biosciences) the following cell types were sorted from PBMC isolated from healthy donors: memory T cells ($CD45RA^-$ only), effector memory (EM) ($CCR7^-CD45RA^-$), central memory (CM) ($CCR7^+CD45RA^-$), naïve

($CCR7^+CD45RA^+$), and CFP10-specific CD4 T cells. Cryopreserved PBMC were thawed as described in Chapter 2. For bulk memory, EM, CM, and naïve CD4 T cells, PBMC were stained with the antibody panel shown in Table 4, except for antibodies in the dump gate. The full antibody panel shown in Table 4 was used for CFP-10-specific CD4 T cell staining with the DRB1*04:01 CFP-10_{71-85} tetramer as described in Chapter 2. Anti-Mouse Ig compensation beads (BD) were acquired prior to acquiring stained PBMC in order to perform fluorescence compensation.

Table 4. Antibodies and dye used to stain and identify naïve, CM, EM, and CFP-10-specific CD4 T cells from PBMC.

Surface Marker	**Clone**	**Manufacture**	**Fluorochrome Conjugates**	**Volume**
Live/dead	NA	Invitrogen	NA	1µL/mL
CCR7	150503	BD Pharmingen	PerCP-Cy5.5	1µL/100µL
CD3	UCHT1	BD Pharmingen	FITC	5µL/100µL
CD4	RPA-T4	Biolegend	BV421	1µL/100µL
CD45RA	UCHL1	BD Pharmingen	PE-Cy7	0.3µL/100µL
CD8 (dump)	RPA-T8	Biolegend	BV510	0.3µL/100µL
CD14 (dump)	M5E2	Biolegend	BV510	0.3µL/100µL
CD19 (dump)	HIB19	Biolegend	BV510	0.1µL/100µL

Magnetic bead sorting CD4 T cells

For some experiments bulk CD4 T cells were sorted using a negative selection $CD4^+$ T cell isolation kit (Miltenyi Biotec) according to the manufacturer's protocols. Briefly, PBMC were thawed, counted, and suspended in a solution of PBS with 0.5% fetal calf serum (FCS) and 2mM EDTA (40µL of buffer per 10^7 cells) and kept on ice throughout. PBMC were incubated with $CD4^+$ T Cell Biotin-Antibody Cocktail for 5 minutes. Next, 30µL of buffer and 20µL of $CD4^+$ T Cell MicroBead Cocktail per 10^7

cells was added and incubated for 10 minutes. LS MACS columns were rinsed and the cell suspension was added to the column and CD4 T cells were collected in the flow through.

Generation of CFP-10 and Epstein–Barr nuclear antigen 1 (EBNA) specific CD4 T cell clones

CFP-10 and EBNA-specific CD4 T cell clones were generated as described by Mariotti et al. (Mariotti & Nisini 2009). Briefly, CFP-10 and EBNA-specific CD4 T cells were identified by HLA class II tetramer staining and FACS-sorted into sterile PBS using FACS. The concentration and viability of sorted cells was determined manually using Trypan blue exclusion staining. A set of 96 well U-bottom plates with each well containing $2x10^5$ irradiated, heterologous PBMC in 100µL culture medium (10% AB, 1% L-glutamine, 1% Penicillin-Streptomycin in RPMI) was prepared. Using limiting dilution, sorted cells were pipetted into each well of the 96 well plate at an average concentration of a single cell per well, so that only a subset of wells contained a single, viable CD4 T cell. Wells were visually assessed daily and media was replaced when it changed colour due to cell growth. After 10 ~ 14 days, 20µL aliquots from each well with possible clonal expansion were collected from culture wells and assessed by CD4 and HLA class II tetramer staining and flow cytometry to determine if expanded CFP-10 or EBNA-specific CD4 T cell clones were detected. Cultures that had enriched clonal tetramer+ CD4 T cell populations were transferred into additional wells supplemented with IL-2, irradiated heterologous PBMC and culture medium to further allow proliferation of clonal CD4 T cells.

Data Analysis

Statistical analyses were performed using R and GraphPad Prism v5.0. The BioMark HD System software automatically determined a single threshold line per 96.96 Dynamic Array chip using linear derivative baseline correction. For ease of interpretation, Ct values were transformed to Et values (40-Ct), because a higher Et value indicates higher mRNA expression. Delta Et values were calculated by subtracting Et values of the reference (housekeeper) gene from the Et value of the gene of interest (GOI). A higher delta Et value reflects relatively higher mRNA expression. We initially used GAPDH as a reference gene, however, further investigation of the qPCR literature suggested that *B2M* is a more appropriate reference gene to use when analysing CD4 T cells (Mane et al. 2008; Wang et al. 2012). Fold-change values were calculated using the comparative Ct ($2^{-\Delta\Delta CT}$) method with *B2M* serving as the reference gene. The relative fold change in the expression of the GOI in the treated sample compared to the untreated sample was calculated as follows:

[(C_T value of GOI − C_T value of reference gene) treated sample –

(C_T value of GOI − C_T value of reference gene) un-treated sample]

To visualise the multidimensional transcriptomic data the heatmap.2 package was used (Warnes et al. 2015).

Results

Quantifying mRNA expression in naïve and memory CD4 T cells

Our first aim was to determine how well the BioMark HD system could detect mRNA transcripts within small populations of CD4 T cells that varied in cell numbers. PBMC were stimulated with PMA/ionomycin or PBS and bulk naïve ($CCR7^+$ and $CD45RA^+$) and memory ($CD45RA^-$) CD4 T cells were sorted. The cells were counted microscopically and 10-fold serial dilutions made performed, resulting in samples ranging from 1 million to 10 CD4 T cells. The RNeasy kit was used to isolate RNA from cells. cDNA synthesis was performed using the SuperScript III First-Strand Synthesis System for RT-PCR kit and specific transcripts were amplified as described above. Samples that had 1 million cells had the highest proportion of expressed genes with detected Et values, with a median of 94% of the 96 genes detected (Figure 18A). The proportion of genes with detectable Et values decreased as cell numbers decreased (Figure 18B and Figure 18C). There was poor detection of mRNA transcripts (below 50%) at low cell numbers (i.e. 10 - 1,000) using the two-step RT-PCR protocol (Figure 18A).

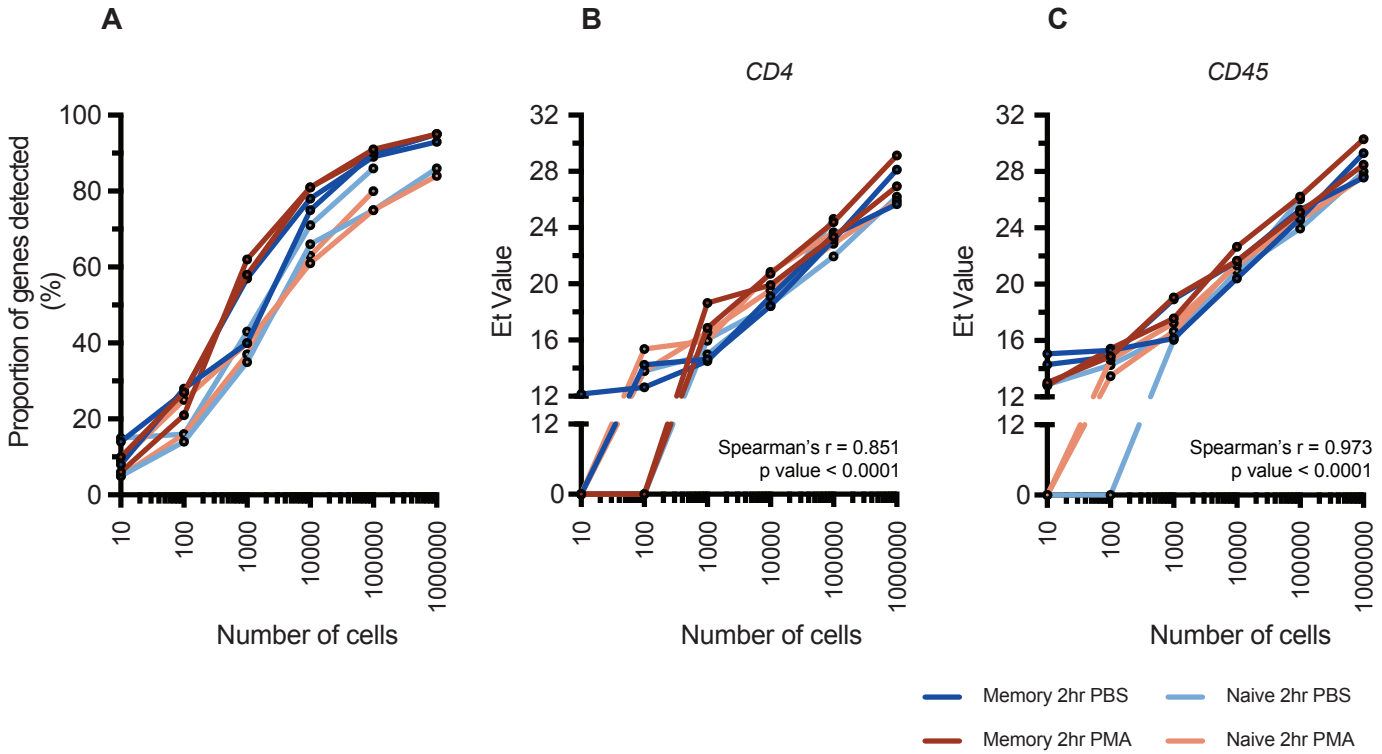

Figure 18. Initial sensitivity achieved with the BioMark HD system using sorted memory and naïve CD4 T cells stimulated with PMA-Ionomycin or PBS using the two-step protocol. (A) The proportion of mRNA transcripts detected (Ct value < 40, or Et value > 0) within CD4 T cell populations consisting of different cell numbers. Representative plots showing (B) CD4 (*CD4*) and (C) CD45 (*PTPRC*) transcript Et values obtained from different numbers of CD4 T cells. P and r values were calculated using the Spearman rank correlation and are unadjusted for multiple comparisons.

We then investigated differences in mRNA transcript levels within bulk populations of naïve and memory CD4 T cells. Given that detection of transcripts was highly dependent on the number of cells, we only analysed data from 10,000 cells or more. Relative gene expression was calculated using *GAPDH* as a reference gene. We identified a total of 51 genes that had differential (FDR < 5%) expression in naïve CD4 T cells compared to memory CD4 T cells. mRNA transcripts encoding cytokines, cytotoxic molecules, and apoptosis markers were among those expressed at a higher level in memory cells (Figure 19A) and *CCR7* and *SELL* (CD62L) expression was higher in naïve cells compared to memory cells (Figure 19B). These results were consistent with published literature. This data confirmed that accurate measurement of mRNA transcript levels within T cell populations could be performed using the BioMark HD System.

Improving the sensitivity to detect mRNA expression in low numbers of cells

While the proportion of genes detected was high when we sorted ≥10,000, the sensitivity was poor when fewer than 100 were sorted. Based on literature and previous experience (Dintwe et al. 2013; Scriba et al. 2005; Scriba et al. 2005), we anticipated that frequencies of antigen-specific CD4 T cells detected with HLA class II tetramers would be very low, in the region of 10-250 cells. Therefore, given the low number of tetramer+ cells we would be able to sort we needed to optimise the protocol to improve transcript detection in the 10-250 range of cell numbers. The CellsDirect one-step RT-PCR protocol has been used previously to quantify mRNA transcripts even at the single cell level (Flatz et al. 2011; Guo et al. 2010). Cells are sorted directly into the CellsDirect master mixture and reverse transcription and specific target amplification is performed in a single PCR tube.

The standard CellsDirect reaction volume is 50µL. We wanted to determine if we could use a reaction volume of 10µL to preserve reagents and reduce cost. We compared the proportion of transcripts detected and the average Et values obtained from 10 or 100 sorted CD4 T cells using 50µL or 10µL reaction volumes (Figure 20). We did not observe a difference in the proportions of genes detected (Figure 20A) or the average Et value of detected genes (Figure 20B). Therefore, we opted to use the 10µL CellsDirect protocol in all subsequent experiments. However, the low number of genes with detectable Et values suggested that the protocol required substantial further optimisation to allow acceptable gene expression profiling. On closer examination, we observed that a suboptimal thermal cycle profile was run on the BioMark HD System instead of the Fluidigm recommend thermal cycle profile. Use of the suboptimal thermal cycle profile may have reduced the BioMark HD System sensitivity.

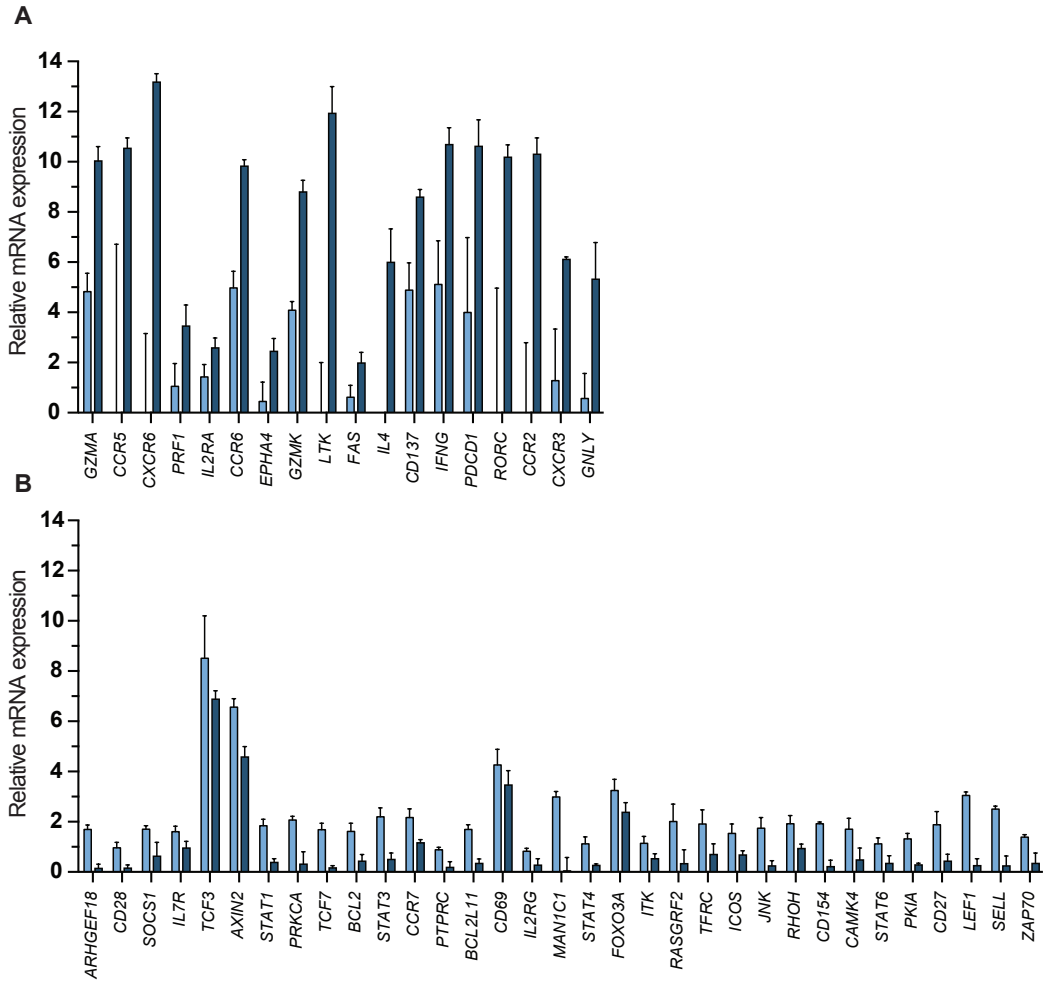

Figure 19. mRNA transcripts that were differentially expressed between naïve and memory CD4 T cells (FDR < 0.05). (A) mRNA transcripts with higher expression levels in unstimulated memory ($CD45RA^{-}$) CD4 T cells. (B) mRNA transcripts with higher expression in unstimulated naïve ($CD45RA^{+}$) CD4 T cells. Medians and upper IQR are shown. p values were calculated using the Wilcoxon signed-rank and adjusted for multiple comparisons using the Benjamini-Hochberg method.

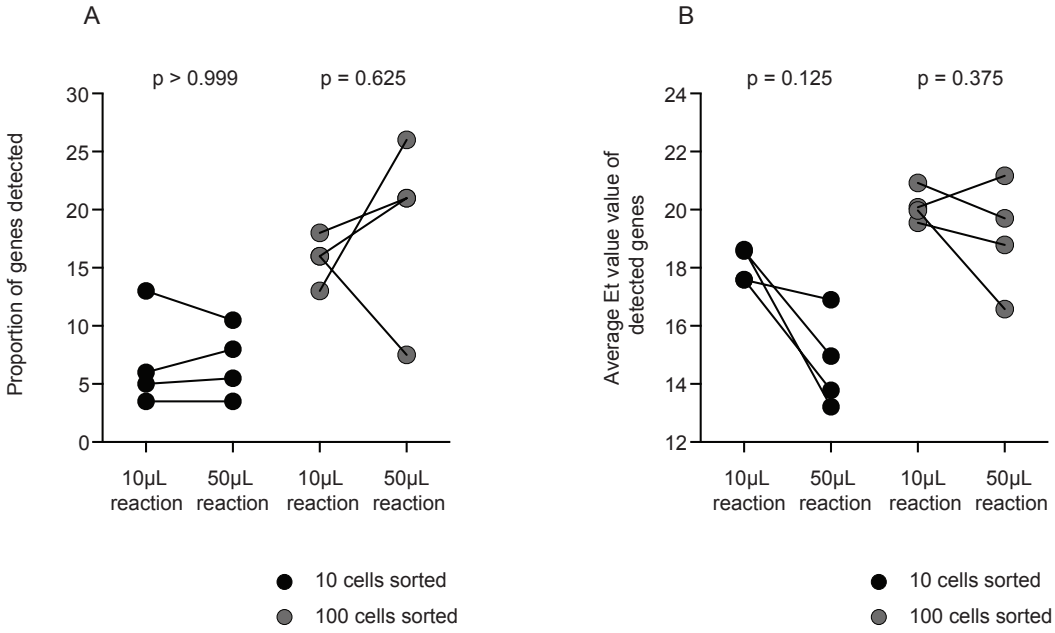

Figure 20. Sensitivity achieved with the BioMark HD system using the CellsDirect one-step RT-PCR kit to generate STA-cDNA. (A) The proportion of mRNA transcripts detected (Ct value < 40) within CD4 T cell populations and the (B) mean Et value of detected genes. P values were calculated using the Wilcoxon signed-rank and are unadjusted for multiple comparisons.

Since we were not satisfied with the assay sensitivity, we compared our protocol with a STA-cDNA protocol used by Guo *et. al.* to quantify mRNA expression in single cells (Guo et al. 2010). We identified three differences, namely duration of reverse transcription, concentration of reverse transcriptase and Taq polymerase enzymes, and using low TE buffer to make up the total reaction volume instead of water, which we reasoned may increase sensitivity of transcript detection. We therefore determined the effect of these individual variables on the number of detected transcripts. MACS beads were used to sort CD4 T cells and conventional qPCR was used to measure Et values. We found that prolonging the duration of reverse transcription from 15 to 20 minutes resulted in a significant increase of both CD4 and GAPDH Et values (Figure 21A). Increasing the amount of reverse transcriptase and Taq polymerase enzymes also resulted in an increase of both *CD4* and *GAPDH* Et values (Figure 21B). Finally,

using TE buffer instead of water also resulted in a significant increase in the Et value only for CD4, but not GAPDH (Figure 21C). We therefore incorporated all these changes into our final STA-cDNA protocol (Table 5 and Table 6) and used this protocol to synthesise STA-cDNA for all experiments going forward.

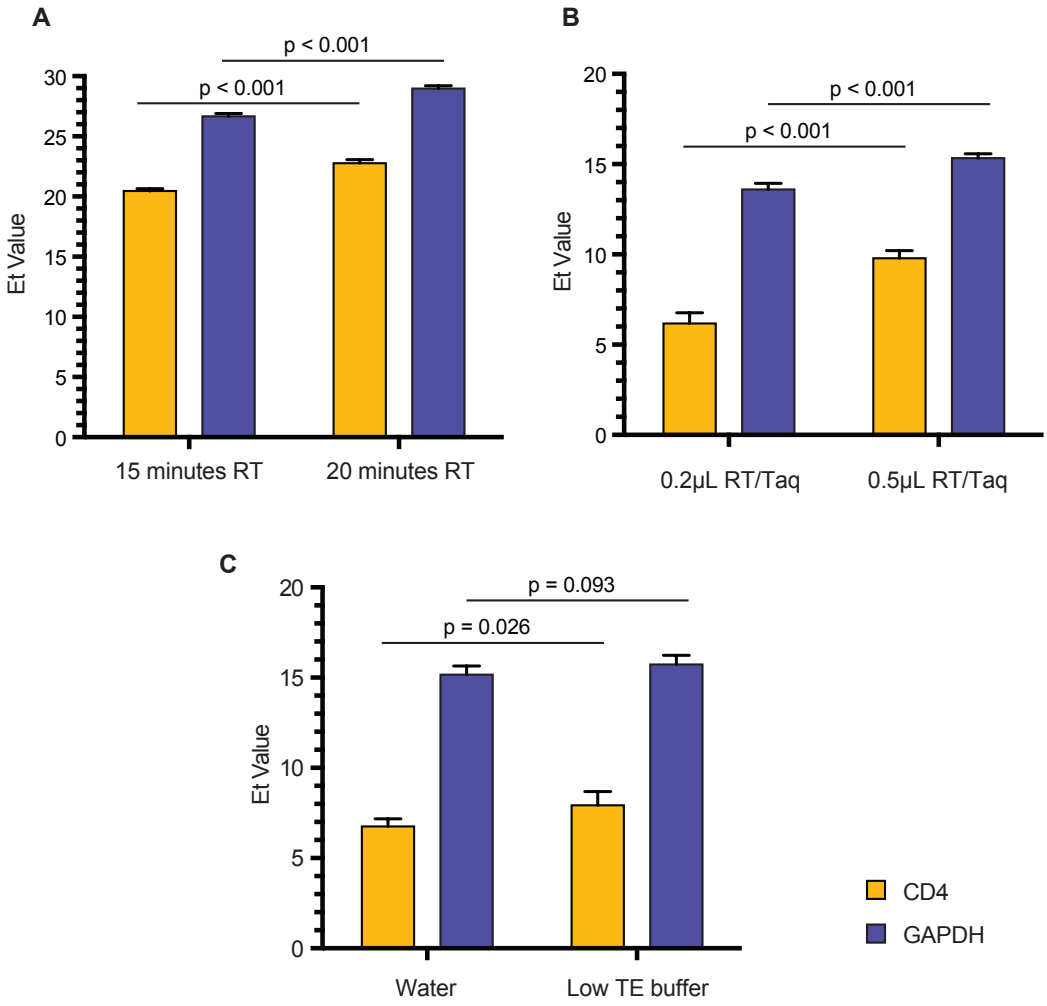

Figure 21. Optimisation of the CellsDirect One-Step qPCR STA-cDNA protocol by exploring 3 different variables. (A) Et values of CD4 (yellow) and GAPDH (blue) when applying reverse transcription incubation 50°C for 15 or 20 minutes. (B) Et values of CD4 and GAPDH detected when 0.2uL or 0.5uL of the reverse transcriptase/Taq polymerase was used. (C) Et values of CD4 and GAPDH when 1uL water or 1uL TE buffer was used to make up a total volume of 9uL of the CellsDirect master mix. Medians and IQR are shown. P values were calculated using the Mann-Whitney U test and are unadjusted for multiple comparisons.

Table 5. CellsDirect one-step RT-PCR master mix used for STA-cDNA synthesis.

Reagent	**Per well volume (µL)**
CellsDirect 2X Reaction Mix	5 µL
SuperScript™ III RT/Platinum® Taq Mix	0.5µL
0.2X Primer/Probe Mix*	2.5 µL
DNA Suspension Buffer (10 mM Tris, pH 8.0, 0.1 mM EDTA)	1 µL

Table 6. Thermal profile used to perform reverse transcription and specific target amplification

	RT	Taq Activation	Specific target amplification (18x)	
Temperature	50°C	95°C	95°C	60°C
Time	20 mins	2 mins	15 sec	4 mins

Qualification of TaqMan GE assays

The amplification efficiencies of all TaqMan GE assays must be close to 100% (± 10%) in order to use the comparative Ct method to quantify relative gene expression (Schmittgen & Livak 2008). We determined the amplification efficiency of each of 101 TaqMan GE assays that we selected to characterise mycobacteria-specific CD4 T cells. To determine the efficiencies we modified a method described by Dominguez et al. (Dominguez et al. 2013). A total of twelve, 2-fold serial dilutions of PBMC were made, and the slope and R^2 value for each TaqMan GE assay was determined. Assays had to achieve a slope between 3.1 to 3.6 and a very strong correlation ($r^2 >$ 0.97) across at least 5 consecutive dilution points (Figure 22). A slope between 3.1 and 3.6 corresponds to efficiencies ranging from 90% to 110%. Using these criteria we determined that 95 of 101 TaqMan GE assays qualified. However, 4 TaqMan GE assays (*CXCL10*, *GAPDH*, *IL-5*, and *PTPRC*) in our panel could potentially detect genomic DNA (gDNA) according to Life Technologies. While we included 96 TaqMan GE assays on each 96.96 Dynamic Array chip, we did not analyse data obtained from the 5 TaqMan GE assays that failed qualification or detected gDNA

from analysis. Therefore, analysis was performed for 91 TaqMan GE assays (Table 7).

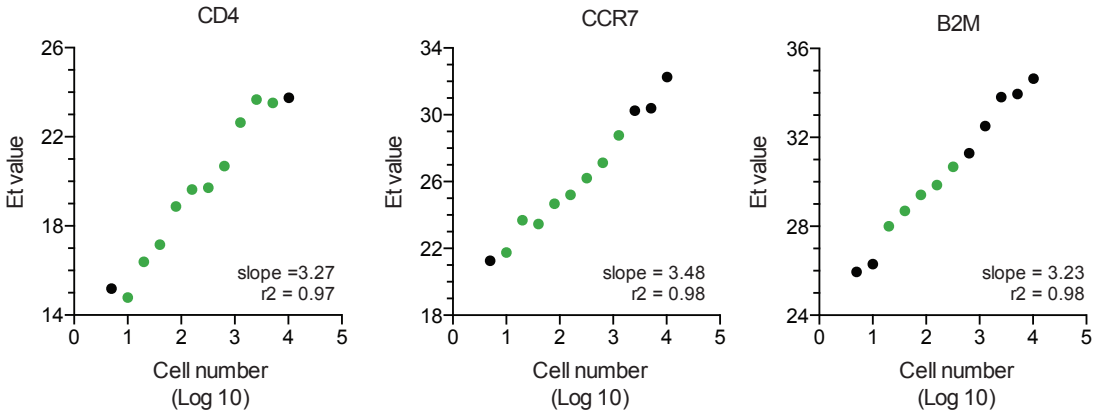

Figure 22. Representative plots showing the approach used to qualify TaqMan GE assays. Twelve 2-fold serial dilutions were performed using PBMC starting from 10,240 to 5 cells and STA-cDNA was synthesised from cells. Segments of five or more points were analysed and a TaqMan GE assays was qualified if any of these segments achieved a slope between 3.1–3.6 and R^2 >0.97 (green points).

Table 7. 91 TaqMan GE assays included in the panel of genes used to assess CD4 T cell responses.

	Gene Name	TaqMan ID
1	*ARHGEF18*	Hs00248726_m1
2	*AXIN2*	Hs00610344_m1
3	*B2M*	Hs00984230_m1
4	*BCL2*	Hs00608023_m1
5	*BCL2L11*	Hs00708019_s1
6	*BID*	Hs01026791_m1
7	*BTLA*	Hs00699198_m1
8	*CAMK4*	Hs00174318_m1
9	*CCR2*	Hs01560352_m1
10	*CCR4*	Hs00747615_s1
11	*CCR5*	Hs00152917_m1
12	*CCR6*	Hs01890706_s1
13	*CCR7*	Hs01013469_m1
14	*CCR9*	Hs01890924_s1
15	*CD137*	Hs00155512_m1
16	*CD154*	Hs00163934_m1
17	*CD160*	Hs00199894_m1
18	*CD27*	Hs00386811_m1
19	*CD28*	Hs00174796_m1
20	*CD38*	Hs01120071_m1
21	*CD4*	Hs01058407_m1
22	*CD69*	Hs00934033_m1
23	*CD8A*	Hs00233520_m1
24	*CTLA4*	Hs03044418_m1
25	*CXCR3*	Hs01847760_s1
26	*CXCR6*	Hs00174843_m1
27	*EPHA4*	Hs00177874_m1
28	*FAS*	Hs00236330_m1
29	*FCER1G*	Hs00175408_m1
30	*FOXO3A*	Hs00818121_m1

	Gene Name	TaqMan ID
31	*FOXP3*	Hs01085834_m1
32	*G6PD*	Hs00166169_m1
33	*GATA3*	Hs00231122_m1
34	*GNLY*	Hs00246266_m1
35	*GPR15*	Hs00922903_s1
36	*GZMA*	Hs00989184_m1
37	*GZMB*	Hs01554355_m1
38	*GZMK*	Hs00157878_m1
39	*HPRT*	Hs01003267_m1
40	*ICOS*	Hs00359999_m1
41	*IFNG*	Hs00989291_m1
42	*IFNGR1*	Hs00988304_m1
43	*IL10*	Hs00961622_m1
44	*IL12RB1*	Hs00538167_m1
45	*IL12RB2*	Hs01548202_m1
46	*IL15*	Hs01003716_m1
47	*IL17A*	Hs00174383_m1
48	*IL2*	Hs00174114_m1
49	*IL21*	Hs00222327_m1
50	*IL22*	Hs01574154_m1
51	*IL2RA*	Hs00907779_m1
52	*IL2RB*	Hs01081697_m1
53	*IL2RG*	Hs00953624_m1
54	*IL6*	Hs00985639_m1
55	*IL7*	Hs00174202_m1
56	*IL7R*	Hs00902334_m1
57	*ITGAL*	Hs00158218_m1
58	*ITGAX*	Hs01015070_m1
59	*ITK*	Hs00950634_m1
60	*JNK*	Hs00177083_m1

	Gene Name	TaqMan ID
61	*KI67*	Hs01032443_m1
62	*LEF1*	Hs01547250_m1
63	*MAN1C1*	Hs00220595_m1
64	*MCAM*	Hs00174838_m1
65	*NFKB1*	Hs00765730_m1
66	*PDCD1*	Hs01550088_m1
67	*PKIA*	Hs00738983_m1
68	*PRF1*	Hs00169473_m1
69	*PRKCA*	Hs00925195_m1
70	*PRR5L*	Hs01029928_m1
71	*RASGRF2*	Hs00394798_m1
72	*RHOH*	Hs00180265_m1
73	*RORA*	Hs00536545_m1
74	*RORC*	Hs01076112_m1
75	*SELL*	Hs00174151_m1
76	*SOCS1*	Hs00705164_s1
77	*STAT1*	Hs01013996_m1
78	*STAT3*	Hs01047580_m1
79	*STAT4*	Hs01028017_m1
80	*STAT5A*	Hs00234181_m1
81	*STAT5B*	Hs00273500_m1
82	*STAT6*	Hs00598625_m1
83	*TBX21*	Hs00203436_m1
84	*TCF3*	Hs00413032_m1
85	*TCF7*	Hs00175273_m1
86	*TCF7L2*	Hs01009044_m1
87	*TFRC*	Hs00951083_m1
88	*TGFB1*	Hs00998133_m1
89	*TNFA*	Hs99999043_m1
90	*TNFSF10*	Hs00921974_m1
91	*ZAP70*	Hs00896347_m1

Unique mRNA expression profiles in naïve, central memory and effector memory CD4 T cells

To determine if our optimised STA-cDNA synthesis protocol and selection of mRNA transcripts was adequate for transcriptional profiling in a relatively low number of cells, we sought to test the method's utility to differentiate between bulk naïve ($CD45RA^{+}CCR7^{+}$), central memory (CM) ($CD45RA^{-}CCR7^{+}$), and, effector memory (EM) ($CD45RA^{-}CCR7^{-}$) cells (Figure 23A). We also were interested in determining the sensitivity of our optimized protocol at detecting mRNA transcripts in sorted CFP-10-specific $tetramer^{+}$ CD4 T cells at different cell input numbers (Figure 23B). We observed that naïve CD4 T cells had the lowest proportion of detected mRNA transcripts, then central memory had intermediate detection of transcripts, and effector memory CD4 T cells had the highest proportion of detected mRNA transcripts (Figure 23C). We observed a high level of variability in the proportion of mRNA transcripts detected when we sorted 2 CFP-10-specific CD4 T cells, ranging from 0% to 72% (Figure 23D). Sorting 10 CFP-10-specific CD4 T cells increased the proportion of mRNA transcripts detected. We observed that not a single mRNA transcript was detected in one of the three sorts of the 50 CFP-10-specific CD4 T cells sort (Figure 23D). This was likely due to cells not being successfully sorted into the PCR tube. We did not observe any difference in the proportions of detected transcripts from 50, 100, and 250 cells (Figure 23D). When we compared the proportions of mRNA transcripts detected in 10 or 100 CFP-10-specific CD4 T cells using our optimized protocol with the proportions detected in 10 or 100 cells in our initial run, we observed higher proportions in CFP-10-specific CD4 T cells (Figure 24).

Although, the one-step RT-PCR protocol increased the proportion of detected mRNA transcripts, we were still not satisfied with the relatively low level of transcript detection at the lower cell numbers (i.e. 2 and 10 cells). Data generated by colleagues in the lab using the same one-step RT-PCR protocol showed no difference in the proportion of mRNA transcripts detected when 25 or 50 cells were sorted (Dintwe unpublished). All together the data suggested that the proportion of detected mRNA transcripts likely reached a plateau at approximately 25 cells.

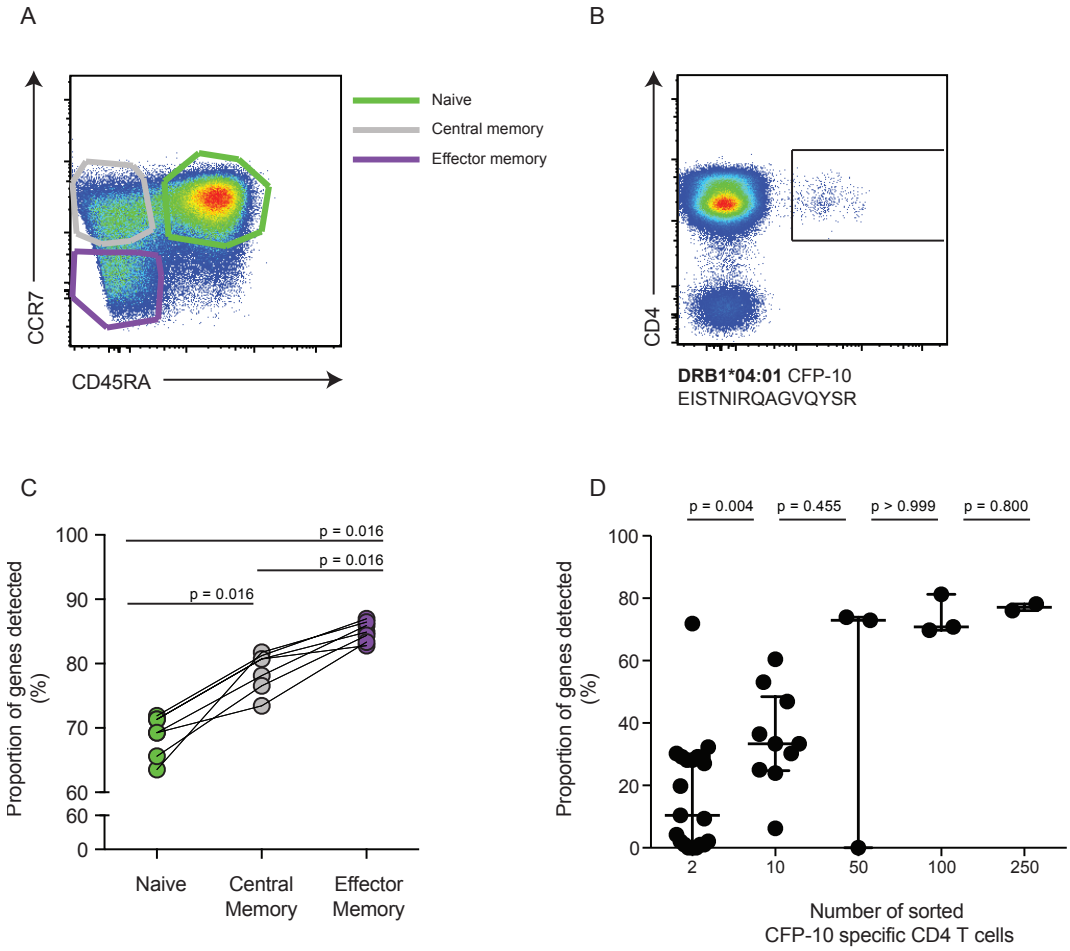

Figure 23. Proportions of mRNA transcripts detected with the BioMark HD system using the optimal STA-cDNA protocol in populations of FACS-sorted bulk naïve, central memory, effector memory and CFP-10 specific CD4 T cells. Representative flow plot showing gating on the (A) bulk naïve, central memory and effector memory CD4 T cell subsets or (B) CFP-10-specific CD4 cells detected with the DRB1*04:01-CFP-$10_{71\text{-}85}$ HLA class II tetramer. Proportions of mRNA transcripts detected in (C) 250 bulk naïve, central memory and effector memory CD4 T cells or (D) in different numbers of CFP-10 specific CD4 T cells. Medians (horizontal line) and IQR are shown. P values were calculated using the Wilcoxon signed-rank (C) or Mann Whitney U (D) tests and are unadjusted for multiple comparisons.

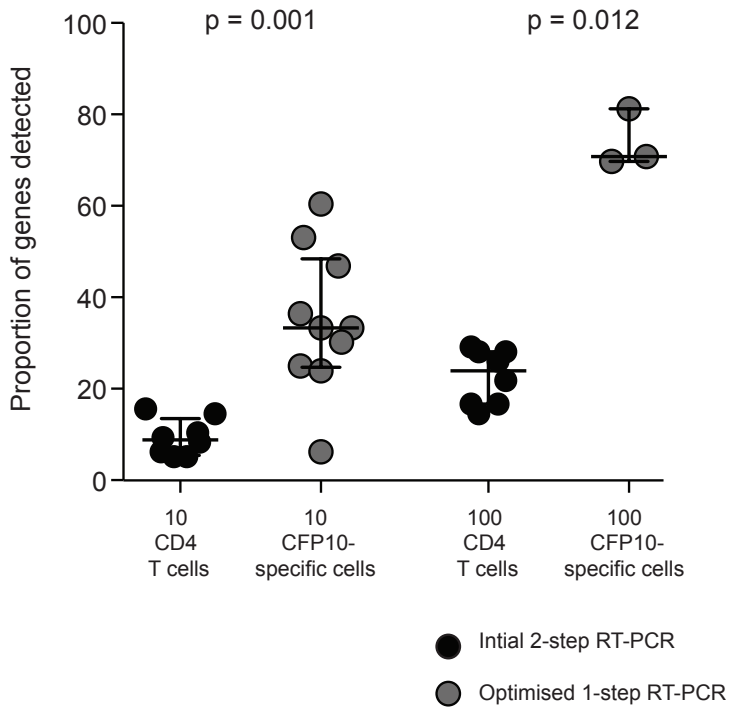

Figure 24. Comparison of the proportions of mRNA transcripts detected in cDNA synthesised using the 2-step RT-PCR or 1-step RT-PCR protocols in 10 and 100 cells. Median (horizontal line) and IQR shown. P values were calculated using the Mann Whitney U test and are unadjusted for multiple comparisons.

We then investigated whether the transcriptomic profiles measured in bulk naïve, CM, and EM was consistent with the known functions and characteristics of these cells. As expected, we observed differential expression in numerous mRNA transcripts between the groups. A total of 56 genes were differentially expressed (FDR < 5%) between the naïve, CM and EM T cell subsets (Figure 25). As expected we observed that *CCR7* and *SELL* (CD62L) were differentially expressed, as these markers are commonly used to distinguish the subsets (Haining et al. 2008). We also observed higher expression of mRNA transcripts encoding effector molecules, such as IFN-γ, TNF-α, granulysin, granzyme A, B, K and perforin in EM. The chemokine receptors, CCR2, CCR5, CCR6, CCR9, CXCR3, and CXCR5 were expressed a higher levels in EM compared to naïve CD4 T cells. By contrast, naïve CD4 T cells expressed the

transcription factors, STAT1, STAT3, and STAT6, and the surface marker IL-7R at higher levels compared to EM. Given that the naïve, CM, and EM CD4 T cell subsets were define by surface expression of CCR7 and CD45RA, we expected that mRNA expression would reflect the protein expression of CCR7. We observed a strong correlation between mRNA and protein expression of CCR7, measured by median fluorescence intensity (MFI) (Figure 26). The overall transcriptomic expression profiles appeared to reflect that naïve and EM CD4 T cells are at opposite ends of a linear differentiation path and CM cells fall somewhere in-between.

Effect of short-term tetramer staining on mRNA expression

Next, we wanted to determine the effect of tetramer staining on mRNA expression. We wanted to utilise HLA class II tetramers for detection and sorting of antigen-specific CD4 T cells because ex vivo tetramer staining results in less activation or perturbation of the cells compared to other commonly used methods that rely on cytokine expression or proliferation for detection (Wooldridge et al. 2009). Despite this, several studies have shown that TCR engagement with soluble HLA class I or class II tetramers may initiate T cell signaling (Boniface et al. 1998; Cochran et al. 2000; Irvine et al. 2002). We therefore wanted to determine if HLA class II tetramer staining of antigen-specific CD4 T cells significantly affected mRNA expression levels which may thus affect the outcomes of our planned studies. We generated CFP-10 and Epstein-Bar Virus (EBV) nuclear antigen 2 (EBNA2) specific CD4 T cell clones to allow evaluation of effects of tetramer staining on an identical population of cells.

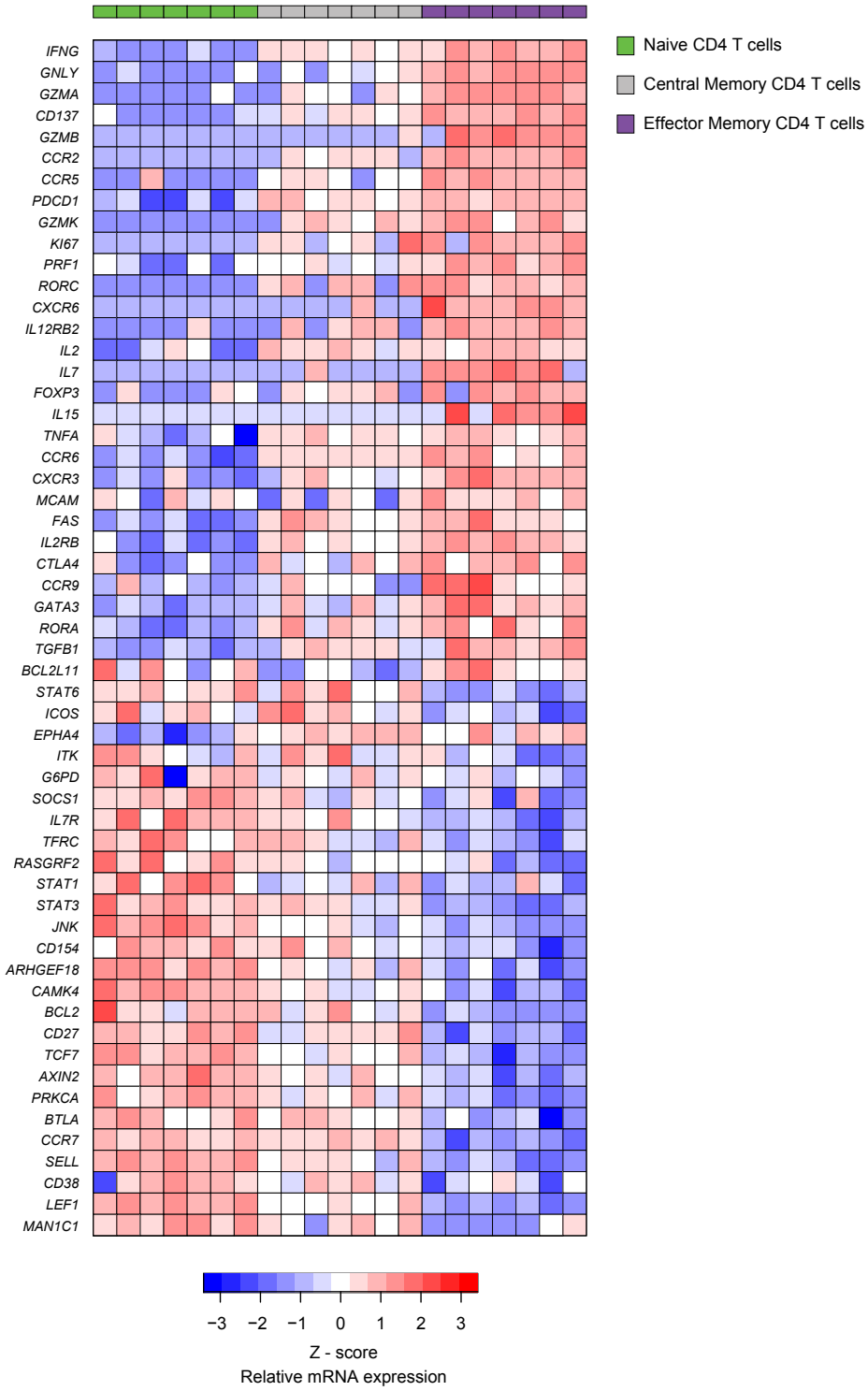

Figure 25. **Differential mRNA transcript expression between CD4 T cell subsets.** Transcriptomic profiles of FACS-sorted, bulk naïve (CD45RA+CCR7+), central memory (CD45RA-CCR7+) and effector memory (CD45RA-CCR7-) CD4 T cells from 7 donors. p values were calculated using the Kruskal Wallis H test and adjusted using the Benjamini-Hochberg method. Only mRNA transcripts (n = 56) found to be differentially expressed between naïve, central memory, and effector memory CD4 T cells are shown ($p < 0.05$ and $fdr < 0.05$).

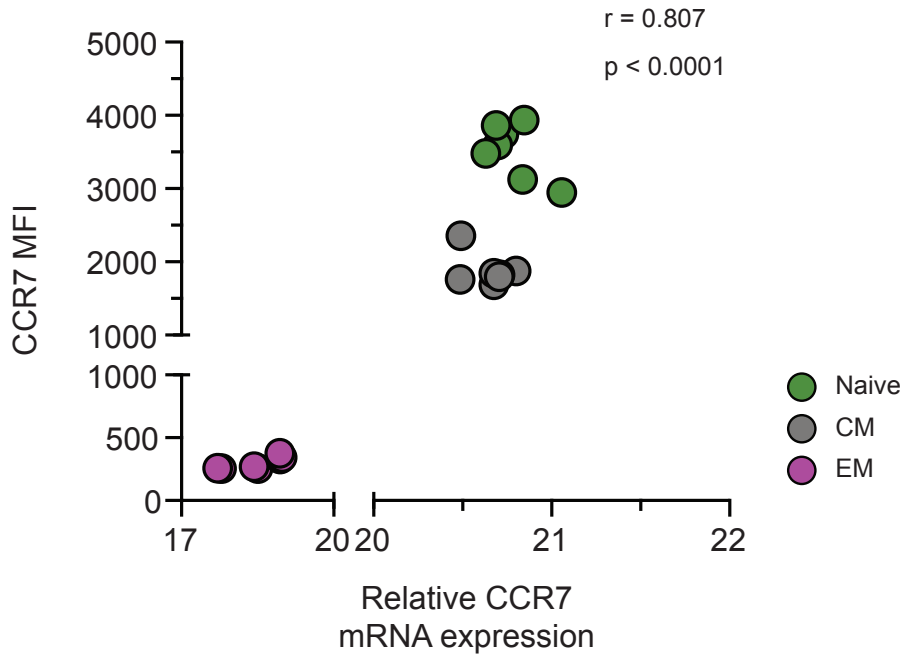

Figure 26. **Confirmation of differential expression of CCR7 at the protein level.** Plot showing the correlation of CCR7 mRNA and surface protein expression. The spearman correlation was used to determine the level of association.

We established two EBNA2-specific CD4 T cell clones and two CFP-10-specific CD4 T cells clones (Figure 27). Transcript levels were measured in a thousand clonal cells before (baseline) and after incubation for 60 minutes with cognate HLA class II tetramer or tetramer staining media alone, and compared the fold change in expression following incubation with cognate tetramer and staining media (Figure 28A and Figure 28B). While we observed trends of increased or decreased expression in 19 mRNA transcripts (Figure 28B *black or dark grey bars respectively*), we did not observe a significant difference in any of the mRNA transcripts tested.

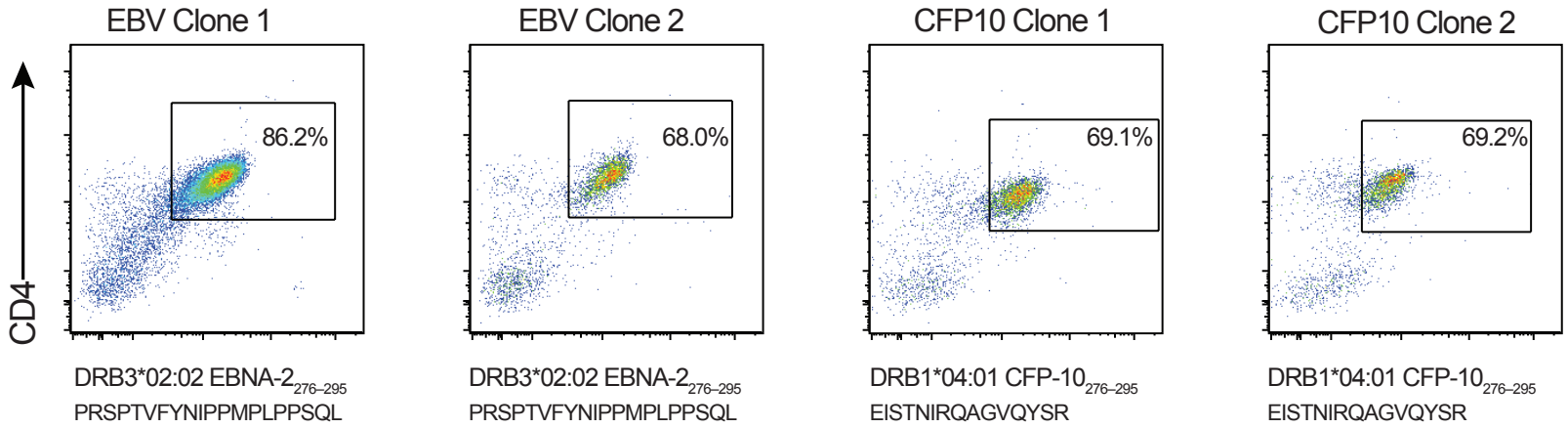

Figure 27. Flow cytometry plots showing tetramer staining of (A) EBNA-2 (B) and CFP-10 specific CD4 T cell clones.

Given that sample processing duration has been shown to influence the expression of many genes in human peripheral blood cells (Baechler et al. 2004), we asked if expression of any of the mRNA transcripts in our panel correlated with the duration of tetramer staining. T cell clones were incubated with tetramer for 5, 10, 20, 30, or 60 minutes and mRNA expression levels were measured (Figure 28C). We observed that 25 genes had strong to moderate correlations with the duration of tetramer staining (Figure 28D *red bars*), while another 8 genes displayed significant but weak correlations with the duration of tetramer staining (Figure 28D *orange bars*).

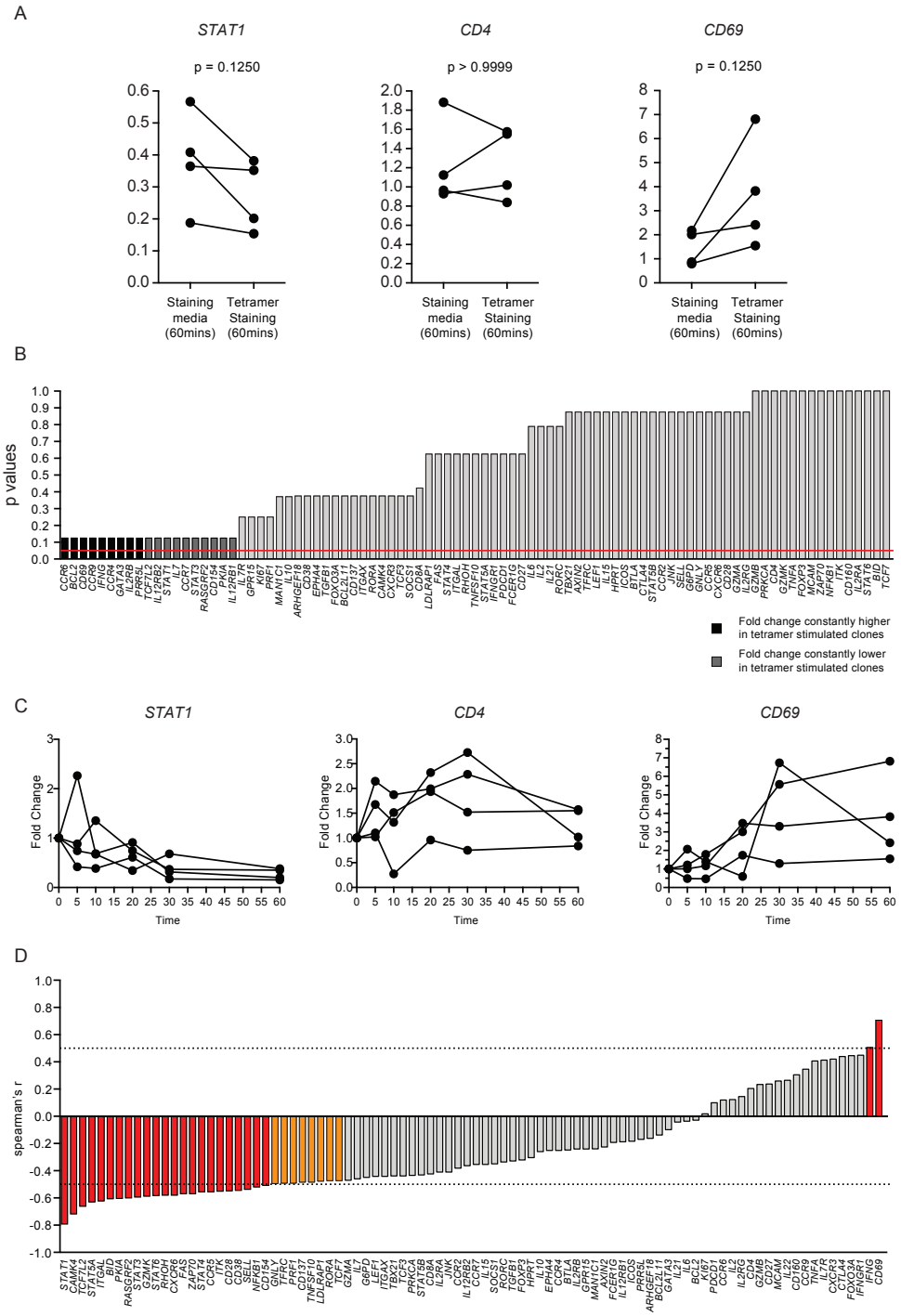

Figure 28. Determining the effect of HLA class II tetramer staining on gene expression levels in EBNA-specific and CFP10-specific CD4 T cell clones. (A) Examples of fold change from baseline (0 mins) comparison in EBNA-specific and CFP10-specific CD4 T cell clones after incubation for 60 minutes in tetramer staining media alone or with cognate tetramer. (B) Summary result of comparisons between CD4 T cell clones incubated with cognate class II tetramer for 60 minutes or incubated with PBS for 60 minutes. Red line indicates p = 0.05. (C) Examples showing fold change in mRNA expression transcripts that was negatively correlated with time (*STAT1*), did not correlate with time (*CD4*), or positively correlated with time (*CD69*). (D) The correlation coefficients between mRNA expression and duration of tetramer staining. Red bars indicate genes with a a strong to moderate correlation(FDR < 5% and r-value > 0.5 or < -0.5) and orange bars indicate genes with a weak correlation (FDR< 0.5% and r-value < 0.5 or > -0.5). P-values were calculated using the Wilcoxon signed-rank and are unadjusted for multiple comparisons (A and B). p and r values were calculated using the Spearman rank correlation (D).

Discussion

High throughput microfluidic qPCR is an excellent platform to comprehensively investigate immune responses, including antigen-specific CD4 T cells. A major advantage of such platforms over conventional approaches such as ICS and flow cytometry or IFN-γ ELISPOT, is the ability to simultaneous measure a large number of parameters within a population of antigen-specific T cells. The BioMark HD System has already shown utility in studying the T cell response induced by different HIV vaccine constructs in mice (Flatz et al. 2011). Using such powerful approaches may greatly improve our understanding of the immune response by revealing novel functions and phenotypes of cells induced by novel tuberculosis vaccines in humans.

Our aim is to comprehensively characterise the antigen-specific CD4 T cell response induced by the novel tuberculosis vaccine, H1:IC31, by using the BioMark HD System. To achieve this we had to establish and optimise a protocol to quantify relative mRNA transcript expression in small numbers of mycobacteria-specific CD4 T cells. First, we determined that the one-step CellsDirect RT-PCR approach was more sensitive at detecting mRNA transcripts within a small population of CD4 T cells. Second, we determined that by increasing the concentration of reverse transcriptase and Taq polymerase, using low TE buffer instead of molecular grade water, as well a prolonging the duration of STA, we improved the sensitivity of the assay.

We designed a panel of TaqMan GE assays that allowed probing of a range of T cell functions, phenotypes, signalling pathways and lineages. While naïve and memory CD4 T cells have over 95% similarity in their transcriptomic profiles, differential

mRNA expression has been observed in these subsets (Weng et al. 2012). We utilised this differential expression of genes to validate our RT-PCR methodology by confirming that sorted memory T cell subsets clustered based on mRNA transcript levels measured by the BioMark HD System. Our results were in accordance with the differentiation pathway of CD4 T cells. The CXC- and CC chemokine receptors, CXCR3, CXCR5, CCR5, and CCR6, the cytotoxic molecules, granyzme A, granzyme B, granzyme K, perforin, and the cytokines IFN-γ and TNF-α have previously been reported to be highly expressed in memory T cells (Weng et al. 2012). CCR7 and SELL (CD62L) are reported to be highly expressed on naïve cells compared to EM CD4 T cells (Berard & Tough 2002). Although we did not perform confirmation at the protein level for the genes that were differentially expressed, we were able to correlate the surface expression of CCR7, measure by MFI because CCR7 in conjunction with CD45RA was used to identify and sort the different memory subsets, suggesting our transcriptomic data was accurate. The lymphoid enhancer binding factor 1 (LEF-1) and transcription factor 7 (TCF7) have also been reported to be highly expressed in naïve cells (Willinger et al. 2006). Reassuringly, we observed differential expression of these genes in the expected direction among others. Based on these results we are confident that the STA-cDNA protocol that we have established allows reliable and accurate measurement of mRNA expression levels in as few as 25 sorted cells.

It is generally accepted that identification of antigen-specific T cells by tetramer staining results in minimal manipulation of the activation or functional state of the cells (Wooldridge et al. 2009). Binding of HLA molecule and TCR is considered to be “signal one” in the activation of T cells, which can initiate T cell signalling. The

traditional two-signal or more contemporary three-signal T cell activation suggests that activation of CD4 T cells is unlikely with soluble HLA class II tetramer. The two-signal model requires interaction of co-stimulatory molecules, such as CD28 with CD80 or CD86 (signal 2) in addition to the MHC-peptide interaction (Goral 2011). The three-signal model requires the presence of cytokines for optimal T cell activation (signal 3) (Goral 2011). It is therefore unlikely that CD4 T cells would be fully activated because of the lack of signals 2 and 3 in our experiments. Interestingly, a study by Boniface *et. al.* demonstrated that incubating antigen-specific T cells with APC presenting the cognate epitope resulted in sustained elevation of intracellular calcium, while soluble tetramers resulted in only transient elevation of calcium signalling (Boniface et al. 1998). The authors concluded that the TCR-tetramer interaction may be adequate to initiate signalling but may be insufficient to sustain full T cell activation. However, in another study, a 12 hour incubation of soluble HLA-DR1 tetramers loaded with influenza virus hemagglutinin epitope with a CD4 T cell clone resulted in up-regulation of the T cell activation surface marker CD69 (Cochran et al. 2000). Given these results, we wanted to determine if short-term (1 hour) tetramer staining at room temperature would influence the expression of mRNA transcripts. We did not observe any statistically significant differences in the expression levels in clones treated with tetramer for 60 minutes compared to clone treated with staining media only. However we did observe trends towards higher or lower expression for 19 genes. It should be noted that we had reduced statistical power due to the limited number of T cell clones. Perhaps by increase the sample size these differences would have been significant.

Work by others has shown that duration of *ex vivo* handling of PBMC influences the expression levels of many genes (Baechler et al. 2004). We observed significant correlations between increased or decreased mRNA expression levels and the duration of tetramer staining for a number of genes. Unfortunately, we did not have a matching "media only" condition at all time points to control for time in staining media in the absence of HLA class II tetramer. Therefore, we were unable to discern whether mRNA expression correlated with the duration only or duration in the presence of tetramers. However, because we did not observe any differences in gene expression after 60 minutes in the presence or absence of tetramer, we reasoned that mRNA expression correlated with the duration only. Interestingly, the majority of genes that correlated with time were in the negative direction, echoing results described by Baechler et. al. who found that *ex vivo* incubation prior to RNA isolation resulted in lower level of expression for a large number of genes (Baechler et al. 2004). The authors suggested that this could be due to mRNA decay or cellular responses to stress (Baechler et al. 2004). Together these data suggest that staining antigen-specific CD4 T cells with soluble tetramers had minimal effects on mRNA expression levels, but the duration of *ex vivo* processing appeared to affect mRNA expression. Nonetheless, unique transcriptomic signatures were identified in populations of naïve, CM, and EM cells that underwent similar processing procedures, suggesting that discernable differences in mRNA transcript levels in T cell populations can still be detected despite ex vivo processing.

Taken together, we conclude that the STA-cDNA protocol we developed to measure mRNA expression in sorted tetramer$^+$ CD4 T cells provides an accurate measure of the direct *ex vivo* transcriptional state of antigen-specific CD4 T cells. Our next aim

was to apply this methodology to comprehensively characterise the antigen-specific CD4 T cell response induced by the novel tuberculosis vaccine, H1:IC31, and to determine effects of underlying *M.tb* infection on this response.

Chapter 4. Characterisation of the H1:IC31 vaccine-induced response and determining effects of underlying *M.tb* infection

Introduction

Elimination of tuberculosis will require the development of a more efficacious vaccine. Current knowledge highlights the critical role that T cells perform in the control of *M.tb* infection. Furthermore, the production of Th1 cytokines has been shown to be necessary for immune control of infection. Guided by this knowledge, many novel tuberculosis vaccines aim to induce a Th1 biased mycobacteria-specific T cell response. However, this response does not correlate with protection against tuberculosis. The lack of correlates of protection has hampered rational development of a more efficacious vaccine. In the absence of correlates of protection, phase I and II clinical trials typically assess vaccine-induced immunogenicity by measuring the frequencies, cytokine-expression profiles, and/or memory phenotypes of mycobacteria-specific Th1 cells. However, while these measures of immunogenicity have been informative we lack a comprehensive understanding of the immune response induced by novel tuberculosis vaccines in humans. Furthermore, we lack full appreciation of the effects of underlying *M.tb* infection on these vaccine-induced T cell responses. A more comprehensive understanding of these responses and the effects of underlying infection may yield valuable insights into vaccine design and vaccination strategies.

While numerous clinical trials have been completed to assess novel tuberculosis vaccines, there is a paucity of studies that have compared the immune response in healthy persons with or without *M.tb* infection in the same trial design. Studies that

have investigated T cell responses following vaccination with MVA85A, a viral vectored vaccine expressing Ag85A, have shown similar frequencies of Ag85B-specific T cells (Sander et al. 2009; Scriba et al. 2012), while subunit vaccines appear to induce higher frequencies of antigen-specific T cells in persons with underlying infection compared with uninfected persons (Penn-Nicholson et al. 2015; van Dissel et al. 2011; Day et al. 2013; Luabeya et al. 2015). Underlying infection has also been found to influence the functional profile of vaccine-induced CD4 T cells. Penn-Nicholson et. al and Luabeya et. al reported that persons with underlying infection had a larger proportion of polyfunctional (e.g. simultaneously producing multiple cytokines) vaccine-induced CD4 T cells compared to uninfected persons (Penn-Nicholson et al. 2015; Luabeya et al. 2015).

Effects of underlying infection on the memory phenotypes of antigen-specific T cells induced by novel tuberculosis vaccines has been studied to a lesser extent than vaccine induced frequencies and cytokine profiles. Recent studies have demonstrated the importance of maintaining a subset of memory cells capable of self-renewal and resisting terminal differentiation during *M.tb* infection (Reiley et al. 2010; Sakai et al. 2014; Moguche et al. 2015; Lindenstrom et al. 2013). These results highlight the need to better understand memory phenotypes of mycobacteria-specific T cells following vaccination. One proposed reason for the lack of sustained protection through BCG vaccination is that BCG may induce short-lived EM responses instead of long-lived CM responses (Orme 2010; Andersen & Woodworth 2014). While BCG preferentially induces antigen-specific cells with a CM phenotype (e.g $CCR7^{+}CD45RA^{-}$), the functional attributes of these cells resembles an EM phenotype, expressing mostly IFN-γ, while tetanus toxoid-specific cells, induced a

subunit vaccine that is readily cleared and induced central memory response characterised by TNF-α and IL-2 production (Soares et al. 2013). Clearly this study demonstrates the need for holistic analyses that include measurement of cytokine expression profiles in addition to memory surface marker expression in the definition of T cell memory following vaccination. Further highlighting this point are numerous studies that have identified a subset of mycobacteria-specific CD4 T cells with a phenotype typically associated with naïve cells ($CCR7^{+}CD45RA^{+}$) (Caccamo et al. 2006; Dintwe et al. 2013; Soares et al. 2013; Tena-Coki et al. 2010). These cells circulate in the peripheral blood at levels well above those typical for truly naïve cells (Kwok et al. 2012). They also express cytokines following ex vivo stimulation with peptides or whole mycobacterium; a function typically not associated with naïve cells (Seder et al. 2008). More recently, colleagues at SATVI performed a comprehensive transcriptomic analysis of *M.tb*-specific tetramer sorted cells and found that *M.tb*-specific cells displaying a $CCR7^{+}CD27^{+}CD45RA^{+}$ naïve phenotype were transcriptomically distinct from truly naïve cells, but had a transcriptomic signature that was more similar to *M.tb*-specific CM cells (Dintwe unpublished). In light of the recent studies that highlight memory self-renewal and resistance to terminal differentiation as favourable outcomes following vaccination (Lindenstrom et al. 2013), understanding the character of human memory T cells induced by novel tuberculosis vaccine is important.

In this thesis we hypothesised that by utilising innovative tools and high throughput transcriptomic approaches we could interrogate vaccine induced CD4 T cell responses to degrees of detail that traditional approaches do not allow. Such in-depth analysis is required to better understand immune responses to *M.tb* infection and vaccination. In

order to perform this analysis we developed a panel of HLA class II tetramers (Chapter 2) and optimised a microfluidic high throughput qPCR approach (Chapter 3) to detect and sort mycobacteria-specific CD4 T cells and perform transcriptomic analysis of these cells. We combined this transcriptional analysis with multiparameter flow cytometry to address our aims.

We recently conducted a phase II clinical trial assessing the safety and immunogenicity of H1:IC31 under four different vaccination strategies that differed in the dosage and number of vaccinations administrated to adolescents with or without latent *M.tb* infection (South African National Clinical Trials Register NHREC number: DOH-27-0612-3947 and Pan African Clinical Trial Registry number: PACTR201403000464306). This trial provided an ideal opportunity to obtain a more comprehensive understanding of the H1:IC31 induced CD4 T cell response, while also investigating effects of underlying *M.tb* infection.

H1:IC31 is a subunit vaccine comprised of a fusion protein of Ag85B and ESAT-6 (H1) formulated in the adjuvant, IC31. Ag85B is expressed in all mycobacterial species including BCG, while ESAT-6 is expressed by *M.tb* and not BCG (Lewis et al. 2003). Interestingly, ESAT-6 is expressed at higher levels relative to Ag85B in the lungs of mice infected with *M.tb* (Rogerson et al. 2006). This difference in expression has been proposed to underlie the appearance of ESAT-6-specific CD4 T cells in larger numbers in infected mice, compared to Ag85B-specific cells (Rogerson et al. 2006). Therefore, characterisation of Ag85B and ESAT-6-specific CD4 T cells in persons with *M.tb* infection may yield valuable insights into the effect of differentially expressed antigens during infection.

The adjuvant, IC31, is a potent Th1 adjuvant that consists of ODN1a and an antibacterial cationic peptide KLK (Agger et al. 2006). H1:IC31, along with other subunit vaccine derivatives, such as H4 (Ag85B and TB10.4) and H56 (Ag85B, ESAT-6, and Rv2660) were developed by the Statens Serum Institut and have been through advanced stages of clinical development. These subunit vaccines have to date shown acceptable safety profiles in BCG naïve, previous BCG vaccinated, and *M.tb* infected persons (Luabeya et al. 2015; Reither et al. 2014; van Dissel et al. 2011; van Dissel et al. 2010; Geldenhuys et al. 2015). In animal models, boosting the pre-existing BCG immune response with these subunit vaccines improves *M.tb* control (i.e. lower bacterial burdens) (Aagaard et al. 2011; Lin et al. 2012; Lindenstrom et al. 2013). Understanding the H1:IC31 boosted CD4 T cell response in BCG vaccinated adolescents with and without *M.tb* infection from a setting endemic for tuberculosis, such as the Western Cape of South Africa, is the next step for clinical development of these vaccines.

The aim of this chapter is to investigate the HI:IC31 induced CD4 T cell response in BCG vaccinated adolescents with or without latent *M.tb* infection. We focused our analysis on adolescents enrolled into Group 1 only. This group comprised of QFT^{-} and QFT^{+} adolescents who received two doses of 15μg of H1:IC31 in 500 nmol KLK and 20 nmol ODN1a.

Specific objectives:

1. To determine the characteristics of circulating Ag85B and ESAT-6-specific CD4 T cells from QFT^{+} and QFT^{-} adolescents prior to H1:IC31 vaccination.
   We hypothesized that prior to vaccination QFT^{+} adolescents will have higher frequencies of Ag85B and ESAT-6-specific CD4 T cells and these cells will possess a more effector memory phenotype compared to QFT^{-} adolescents.

2. To determine the frequency and kinetics of H1-specific CD4 T cells following two doses of H1:IC31 vaccination in QFT^{+} and QFT^{-} adolescents.
   We hypothesized that following primary and secondary H1:IC31 vaccination QFT^{+} adolescents will have greater frequencies of H1-specific CD4 T cells compared to QFT^{-} adolescents.

3. To compare the transcriptomic, phenotypic and functional attributes of H1-specific CD4 T cells in QFT^{-} and QFT^{+} adolescents following H1:IC31 vaccination.

   We hypothesized that following primary H1:IC31 vaccination H1-specific CD4 T cells from QFT^{+} adolescents will possess a more effector transcriptomic, phenotypic, and functional profile compared to QFT^{-} adolescents. Secondary vaccination will induce a greater H1:IC31-specific CD4 T cell effector response in QFT^{-} compared to QFT^{+} adolescents.

4. To compare the transcriptomic, phenotype and functional profiles of Ag85B and ESAT-6-specific CD4 T cells in QFT^{+} adolescents following H1:IC31 vaccination.

Methods and Materials

Participants

Adolescents from the Worcester district of the Western Cape were enrolled in a phase II clinical trial (Trial code: THYB-04) designed to assess the safety and immunogenicity of H1:IC31 (South African National Clinical Trials Register NHREC number: DOH-27-0612-3947 and Pan African Clinical Trial Registry number: PACTR201403000464306). This trial aimed to enroll 120 *M.tb* uninfected and 120 latently infected adolescents. Diagnosis of latent infection was performed by QFT as described in chapter 2. Participants had to meet the following inclusion criteria:

1. Healthy based on medical examination
2. Between 12 and 18 years old
3. Signed informed consent from the parents/legal representative
4. Signed assent from the participant

Exclusion criteria included:

1. Evidence of current or prior active tuberculosis disease
2. Vaccinated with any vaccine 3 months before the first H1:IC31 vaccination
3. Participation in other experimental tuberculosis vaccine trials
3. Administration of immune modulating drugs
4. HIV seropositive

The Human Research Ethics Committee of the University of Cape Town and the Medicines Control Council of South Africa reviewed and approved the study.

H1:IC31 vaccinations

Adolescents were randomised into one of four vaccination groups.

Group 1: 15µg vaccine (day 0) + 15 µg vaccine (day 56)

Group 2: 50µg vaccine (day 0) + 50 µg vaccine (day 56)

Group 3: 15µg vaccine (day 0) + placebo (day 56)

Group 4: 50µg vaccine (day 0) + placebo (day 56)

IC31 dosing (500 nmol KLK and 20 nmol ODN1a) was consistent across all groups.

PBMC sample collection

Blood samples were collected from adolescents prior to vaccination (day 0) and on days 14, 56, 70, 112, and 224 post vaccination. PBMC were isolated from blood samples using the BD Vacutainer CPT method and cryopreserved in 10% DMSO and 40% FCS in RPMI enriched with L-Glutamine as described in Chapter 2.

HLA typing of adolescents

DNA was isolated from cells collected from QFT tubes after harvesting plasma. DNA extractions were performed using the QIAamp DNA Blood Mini Kit (Qiagen) according to the manufacturer's protocol. DNA was sent to the La Jolla Institute for Allergy and Immunology (LIAI) for high resolution (4-digit) HLA typing of class II alleles.

Whole blood intracellular cytokine staining (ICS)

One mL of whole blood from adolescents was stimulated with 15mer peptides

spanning Ag85B (2μg/mL Staten Serum Institute), ESAT-6 (2μg/mL Staten Serum Institute), PHA (5μg/mL Bioweb), or media alone for 12 hours in the presence of the co-stimulatory antibodies, anti-CD28 and CD49d (0.25μg/mL BD). After 7 hours brefeldin A (10μg/mL Sigma Aldrich) was added and incubated for a further 5 hours. After stimulation, red blood cells were lysed with FACS Lysing solution (BD), white cells were fixed, and frozen to allow for batch intracellular cytokine staining (ICS). Cells were thawed and permeabilised with Perm/Wash buffer (BD) and stained with the antibodies listed in Table 8. Anti-Mouse Ig compensation beads (BD) were acquired prior to acquiring stained fixed white blood cells on an LSRII (BD).

Table 8. Whole blood ICS antibody staining panel

Surface Marker	**Clone**	**Manufacture**	**Fluorochrome Conjugates**	**Volume**
CD3	UCHT1	BD	BV421	0.25μL/100μL
CD4	S3.5	Life Technologies	QDot605	0.3μL/100μL
CD8	SK1	BD	PerCP-Cy5.5	3μL/100μL
IFNg	B27	BD	AlexaF700	0.5μL/100μL
TNF	MAb11	eBioscience	PE-Cy7	0.6μL/100μL
IL-2	5344.111	BD	FITC	2.5μL/100μL
IL-17	SCPL1362	BD	Alexa-647	2μL/100μL
CCR7	150503	BD	PE	3μL/100μL
CD45RA	HI100	BioLegend	BV570	0.25μL/100μL

MHC class II tetramer staining

A single vial of cryopreserved PBMC was thawed as described in Chapter 2 and incubated in 1mL of the LIVE/DEAD fixable aqua viability dye (1 μL/mL, Invitrogen) for 30 minutes at room temperature. PBMC were washed with 2% FCS and 2mM EDTA in PBS and then stained with the fluorescently labelled CCR7-PerCP-Cy5.5 antibody (1μL/100μL, Clone: 150503, BD Pharmingen) for 30 minutes

at 37°C. PBMC were washed again and resuspended in 2% FCS and 2mM EDTA (100µL). PBMC were then incubated with DRB1*03:01$_{VPSPSMGRDIKVQFQSGGAN}$ (Ag85B), DPB1*04:01$_{GKAGCQTYKWETFLTSE}$ (Ag85B), or DQB1*06:02$_{EGKQSLTKLAAAWGG}$ (ESAT-6) HLA class II tetramers (1-2 µg/mL) for 60 minutes at room temperature. For some experiments 10µL (10%) of PBMC were aliquoted prior to staining with antigen-specific tetramers and stained with HLA class II tetramers loaded with an irrelevant epitope (negative control staining). Following another wash, cells were incubated for 30 minutes at room temperature with the following fluorescently labelled antibodies: CD3-FITC (5µL/100µL, Clone: UCHT1, BD Pharmingen), CD4-BV421 (1µL/100µL, Clone: RPA-T4, Biolegend), CD45RA-PE-Cy7 (0.3µL/100µL, Clone: UCHL1, BD Pharmingen), CD8-BV510 (0.3µL/100µL, Clone: RPA-T8, Biolegend), CD19-BV510 (0.1µL/100µL, Clone: HIB19, Biolegend) CD14-BV510 (0.3µL/100µL, Clone: M5E2, Biolegend). CD8, CD19, and CD14 staining was performed to exclude cell populations that expressed these surface markers (dump gate). Anti-Mouse Ig compensation beads (BD) and stained cells were acquired on the BD FACS Aria II and HLA class II tetramer$^+$ CD4 T cells were sorted. A minimum of 25 tetramer$^+$ CD4 T cells had to be sorted for reliable transcriptomic analysis to be performed on the samples. In order to control for the level of variability in the transcriptomic data due to the number of cells, we limited the number of cell sorted to 50.

Specific Transcript Amplification (STA) cDNA synthesis

STA-cDNA synthesis was performed using the optimized one-step qPCR protocol described in Chapter 3. Briefly, HLA class II tetramer$^+$ CD4 T cells were sorted

directly into a 200µL PCR tube containing 5µL 2X CellsDirect Reaction Mix (Invitrogen), 0.5µL of SuperScript III RT/ Platinum Taq Mix (Invitrogen), and 2.5µL of 0.2X TaqMan GE assay (Life Technologies) mix and 1µL Low TE buffer. The PCR tube was incubated at 50°C for 20 minutes, followed by 95°C for 2 minutes and then 18 cycles of 95°C for 15 seconds and 60°C for 4 minutes. STA-cDNA was diluted 1:5 with molecular grade water and stored at -20°C.

Confirmation of specific transcript amplification using conventional qPCR

The presence of STA-cDNA was confirmed by conventional qPCR. 4µL of STA-cDNA from randomly selected samples was placed in a 200µL PCR tube containing 10µL TaqMan Universal PCR Master Mix, 1µL of *CD4 or B2M* 20X TaqMan GE assay mix, and 5µL molecular grade water. The Rotor-Gene 6000 (QIAGEN) was used to perform conventional qPCR. The following thermal profile was initiated; 50°C for 120 seconds, then 95°C for 600 seconds, followed by 40 cycles of 95°C for 15 seconds and 60°C for 60 seconds.

BioMark HD System qPCR

TaqMan GE assays and STA-cDNA samples were loaded onto a 96.96 Dynamic Array chip according to the manufacturer's instructions. Microfluidic multiplexed qPCR was performed as described in Chapter 3.

Data analysis

The BioMark HD System software automatically determined a single threshold value per 96.96 Dynamic Array chip. Samples had to have detectable levels of *CD4*, *B2M*, *HPRT*, and *G6PD* to be included for analysis. Relative mRNA levels (delta Et) in H1-specific CD4 T cells were determined by subtracting *B2M* Et values from the gene of interest Et value. A higher delta Et value reflects relatively higher mRNA expression. Fold change values were calculated using the delta delta Ct ($2^{-\Delta\Delta CT}$) method as described in Chapter 3. Flow cytometry data was analysed using FlowJo V9.2 or V10.

Statistical analyses were performed using R and GraphPad Prism v6.0. To visualise the multidimensional transcriptomic data from ESAT-6 and Ag85B-specific CD4 T cells the heatmap.2 (Warnes et al. 2015) and prcomp (R Development Core Team 2014) functions in R were used to generate heatmap and PCA plots, respectively. The Mann Whitney U test was used to compare QFT^{-} and QFT^{+} adolescents, while the Wilcoxon signed-rank test was used to compare results within each group. P values describing difference in the frequency, proportion of cytokine producing subset, and proportion of memory phenotypes were corrected using the Bonferroni correction, while p values describing difference in mRNA expression levels were corrected using the Benjamini Hochberg method (FDR).

Results

Enrollment and demographics

A total of 240 adolescents were enrolled and QFT^{-} and QFT^{+} adolescents were randomised into 1 of 4 different vaccination groups (Figure 29). For the analysis described here, we focused on participants enrolled into Group 1 only. However, we also utilized data collected from QFT^{-} and QFT^{+} adolescents in Groups 2, 3, and 4, as well as data from an independent trial that assessed the H56:IC31 induced CD4 T cell response in QFT^{-} and QFT^{+} adults (Luabeya et al. 2015) to confirm some of the results observed in Group 1. We did not observe any significant differences in the demographic characteristics measured between QFT^{-} and QFT^{+} adolescents enrolled in Group 1 (Table 9).

A main objective of this thesis was to measure the mRNA transcript expression in mycobacteria-specific CD4 T cells sorted using a panel of HLA class II tetramers (described in Chapter 2). To detect specific cells using tetramer we had to determine the HLA allele expressed by adolescents in Group 1. We HLA typed 51 of the 60 adolescents; we were unable to HLA type 9 adolescents because QFT tubes were discarded prior to DNA isolation. In total we identified 31 adolescents who expressed one or more HLA alleles that matched our tetramers (Table 10).

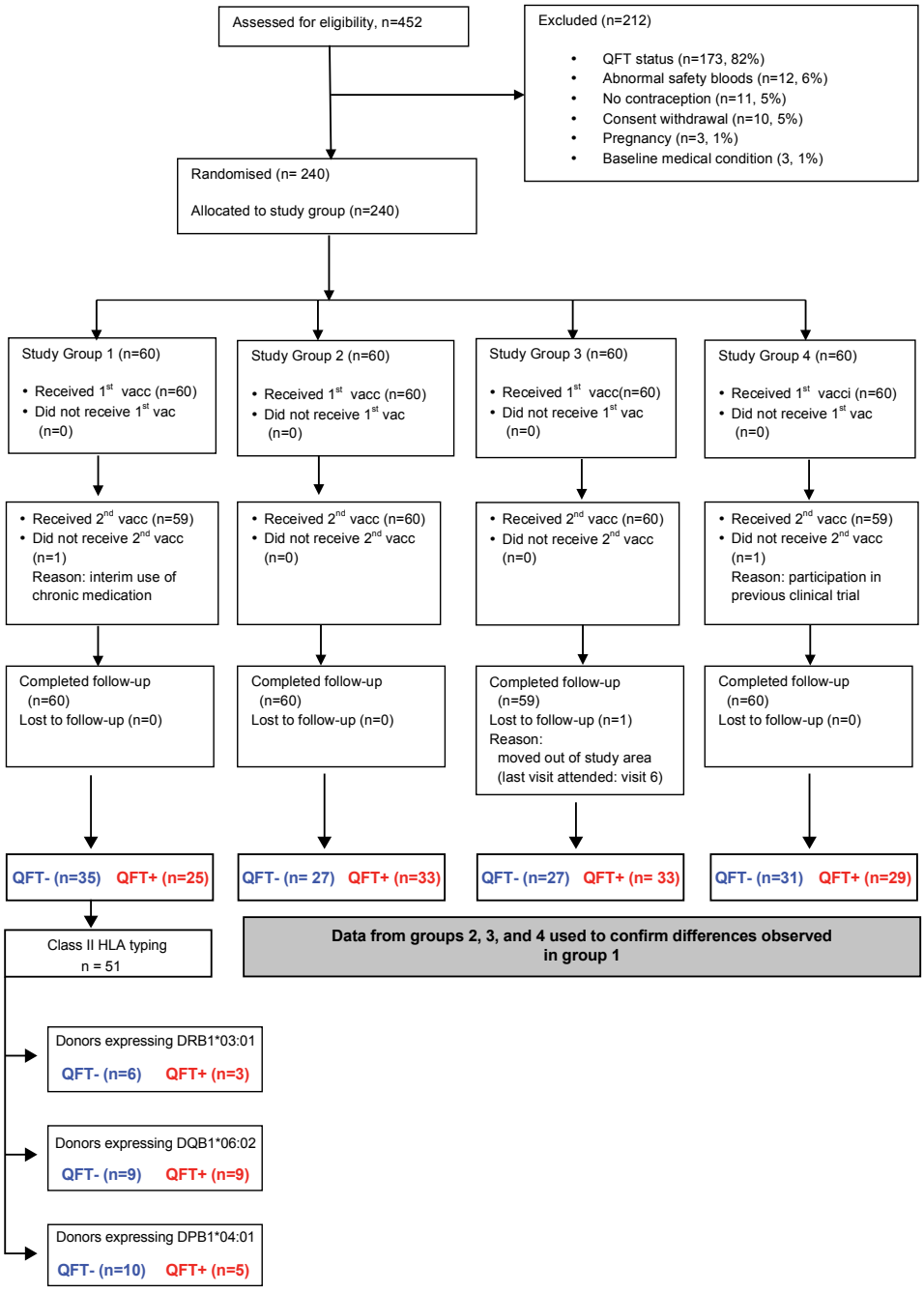

Figure 29. Consort diagram of the adolescents screened and enrolled into the H1:IC31 phase II trial (THYB-04).

Table 9. Demographic characteristics of adolescents enrolled into Group 1

	QFT-	QFT+	
n	35	25	
female, n (%)	18 (51)	14 (56)	p = 0.726
male, n (%)	17 (49)	11 (44)	
Age, median (IQR)	15 (14-16)	15 (15-16)	p = 0.420

Table 10. Adolescents enrolled in Group 1 who expressed the cognate HLA alleles required for tetramer staining. DRB1*03:01 and DPB1*04:01 tetramers were loaded with Ag85B-specific peptides and the DQB1*06:02 tetramer was loaded with an ESAT-6-specific peptide.

Donor ID	Screening QFT	DRB1 Ag85B	DQB1 ESAT6	DPB1 Ag85B
THYB-04-ID0110	NEG		DQB1*06:02	DPB1*04:01
THYB-04-ID0113	NEG			DPB1*04:01
THYB-04-ID0117	NEG	DRB1*03:01		
THYB-04-ID0014	NEG	DRB1*03:01		
THYB-04-ID0019	NEG			DPB1*04:01
THYB-04-ID0002	NEG	DRB1*03:01		DPB1*04:01
THYB-04-ID0028	NEG	DRB1*03:01		
THYB-04-ID0029	NEG		DQB1*06:02	
THYB-04-ID0033	NEG		DQB1*06:02	DPB1*04:01
THYB-04-ID0034	NEG		DQB1*06:02	
THYB-04-ID0037	NEG		DQB1*06:02	
THYB-04-ID0005	NEG		DQB1*06:02	DPB1*04:01
THYB-04-ID0062	NEG		DQB1*06:02	
THYB-04-ID0069	NEG		DQB1*06:02	
THYB-04-ID0070	NEG		DQB1*06:02	DPB1*04:01
THYB-04-ID0074	NEG	DRB1*03:01		DPB1*04:01
THYB-04-ID0079	NEG			DPB1*04:01
THYB-04-ID0080	NEG	DRB1*03:01		DPB1*04:01
THYB-04-ID0135	POS		DQB1*06:02	
THYB-04-ID0138	POS	DRB1*03:01	DQB1*06:02	DPB1*04:01
THYB-04-ID0143	POS		DQB1*06:02	
THYB-04-ID0146	POS		DQB1*06:02	DPB1*04:01
THYB-04-ID0147	POS			DPB1*04:01
THYB-04-ID0152	POS			DPB1*04:01
THYB-04-ID0157	POS	DRB1*03:01	DQB1*06:02	
THYB-04-ID0166	POS		DQB1*06:02	
THYB-04-ID0189	POS		DQB1*06:02	
THYB-04-ID0195	POS			DPB1*04:01
THYB-04-ID0201	POS		DQB1*06:02	
THYB-04-ID0211	POS		DQB1*06:02	
THYB-04-ID0230	POS	DRB1*03:01		

At baseline QFT+ adolescents had a more effector-like Ag85B-specific CD4 T cell response compared to QFT— adolescents.

Our first objective was to determine the effects of underlying *M.tb* infection on the H1-specific CD4 T cell response at baseline. We determined the frequencies of circulating CD4 T cells specific to the antigens in H1 (i.e. Ag85B and ESAT-6) in healthy adolescents with or without *M.tb* infection. Whole blood collected from adolescents was stimulated with 15mer peptides spanning Ag85B and ESAT-6 and frequencies of Th1 cytokine$^+$ (IFN-γ, TNF-α, and IL-2) CD4 T cells were measured (Figure 30 and Figure 31A). QFT$^+$ adolescents had higher frequencies of Th1 cytokine$^+$ ESAT-6-specific CD4 T cells compared to QFT$^-$ (Figure 31B). This result was expected because ESAT-6-specific responses are used to define *M.tb* infection in the QFT assay. Interestingly, the frequencies of Th1 cytokine$^+$ Ag85B-specific CD4 T cells in QFT$^-$ and QFT$^+$ adolescents prior to vaccination were not different (Figure 31C). However, when we analysed combined data from adolescents enrolled groups 2, 3, and 4 we did observe that QFT$^+$ adolescents had higher frequencies of Th1 cytokine$^+$ Ag85B-specific CD4 T cells (Figure 31D).

Next, we wanted to assess cytokine co-expression profiles of H1-specfic CD4 T cells by comparing proportions of Th1 cytokine$^+$ Ag85B-specific CD4 T cells expressing each combination of IFN-γ, TNF-α, and/or IL-2 in QFT$^-$ and QFT$^+$ adolescents. We did not assess the proportions ESAT-6-specific CD4 T cells because, by definition, QFT$^-$ adolescents do not have an ESAT-6 specific response. We found larger proportions of triple positive, IFN-γ^+TNF-α^+IL-2^+, cells within the Ag85B-specific CD4 T cell population in QFT$^+$ adolescents, compared to QFT$^-$ adolescents. Proportions of single IL-2 producing cells were larger in QFT$^-$, compared to QFT$^+$,

adolescents (Figure 31E). However, these differences in the proportions of IFN-γ^+TNF-α^+IL-$2^+$and single IL-2^+ cells were not significant following correction for multiple comparisons using the Bonferroni correction (p = 0.14 and p =0.08, respectively). Notably, there was also a trend toward higher frequencies of single IL-2 producing Ag85B-specific CD4 T cells in QFT$^-$ compared to QFT$^+$ (p = 0.086, unadjusted p value). Using data obtained from Groups 2, 3, and 4 we confirmed that QFT$^+$ adolescents had a significantly larger proportion of IFN-γ^+TNF-α^+IL-2^+ cells, compared to QFT$^-$ adolescents (Figure 31F) (p <0.001, adjusted p value). The latter had larger proportions (p < 0.001, adjusted p value) and higher frequencies of single IL-2^+ cells compared to QFT$^+$ adolescents (Figure 31F and Figure 31G). Importantly, these differences remained significant after correcting for multiple comparisons.

Due to the larger proportions of IFN-γ^+TNF-α^+IL-2^+ and single IL2^+ Ag85B-specific CD4 T cells in QFT$^+$ and QFT- adolescents, respectively, we hypothesized that QFT$^+$ adolescents would have larger proportions of Ag85B-specific cells expressing an effector memory (EM) phenotype, while QFT$^-$ adolescents would have larger proportions of cells expressing a central memory (CM) phenotype. Memory phenotypes of Ag85B-specific CD4 T cells were determined by measuring expression of CCR7 and CD45RA (Figure 32A). Proportions of Ag85B-specific Th1 cytokine$^+$ cells expressing a EM (CCR7$^-$CD45RA$^-$), CM (CCR7$^+$CD45RA$^-$), naïve (CCR7$^+$CD45RA$^+$), and terminally differentiated effector (CCR7$^-$CD45RA$^+$) phenotypes were not statistically different between QFT$^-$ and QFT$^+$ adolescents when p values were corrected using the Bonferroni method (Figure 32B). However, we did observe a trend toward higher proportions of Ag85B-specific cells expressing a “naïve” phenotype (p = 0.052 after Bonferroni correction). We again utilized data

from Groups 2, 3, and 4 to confirm our results and determine whether trends observed in Group 1 would be statistically different in a larger dataset. QFT^{-} adolescents in Groups 2, 3, and 4 had larger proportions of Ag85B-specific CD4 T cells expressing a "naïve" phenotype compared to QFT^{+} adolescents. In this larger dataset, QFT^{+} adolescents also had larger proportions of cells expressing an EM phenotype (Figure 32C). Although not significant, a trend for higher EM had been seen in QFT^{+} adolescents in Group 1.

The relatively large proportion of Ag85B-specific CD4 T cells expressing a "naïve" phenotype in QFT^{-} adolescents was intriguing for a number of reasons. Firstly, these cells were circulating at frequencies higher than would be expected for truly naïve cells (Kwok et al. 2012). Secondly, cytokine expression was readily detected in these cells, with some cells simultaneously expressing multiple cytokines, a function not typically associated with naïve cells (Seder et al. 2008). BCG, which expresses Ag85B, would have been administered at birth in this cohort. Although evidence of BCG vaccination was not an inclusion criterion, in this setting we would expect the vast majority of adolescents to have received BCG at birth (Hesseling et al. 2009). Mycobacteria-specific CD4 T cells displaying a "naïve" phenotype have been described in other cohorts of BCG vaccinated individuals (Dintwe et al. 2013; Soares et al. 2013; Tena-Coki et al. 2010). We therefore investigated the cytokine profile of Ag85B-specific cells expressing the naïve phenotype in both QFT^{-} and QFT^{+} adolescents. The majority of these "naïve" Ag85B-specific Th1 CD4 T cells in QFT^{-} adolescents were single IL-2 producing cells (Figure 32D). We also found a significant correlation between the proportion of single IL-2 producing Ag85B-specific CD4 T cells and the proportion of "naïve" Ag85B-specific CD4 T cells on

day 0 (Figure 32E). Altogether these data suggest that adolescents with underlying *M.tb* infection have a more effector-like Ag85B-specific CD4 T cell response compared to uninfected adolescents.

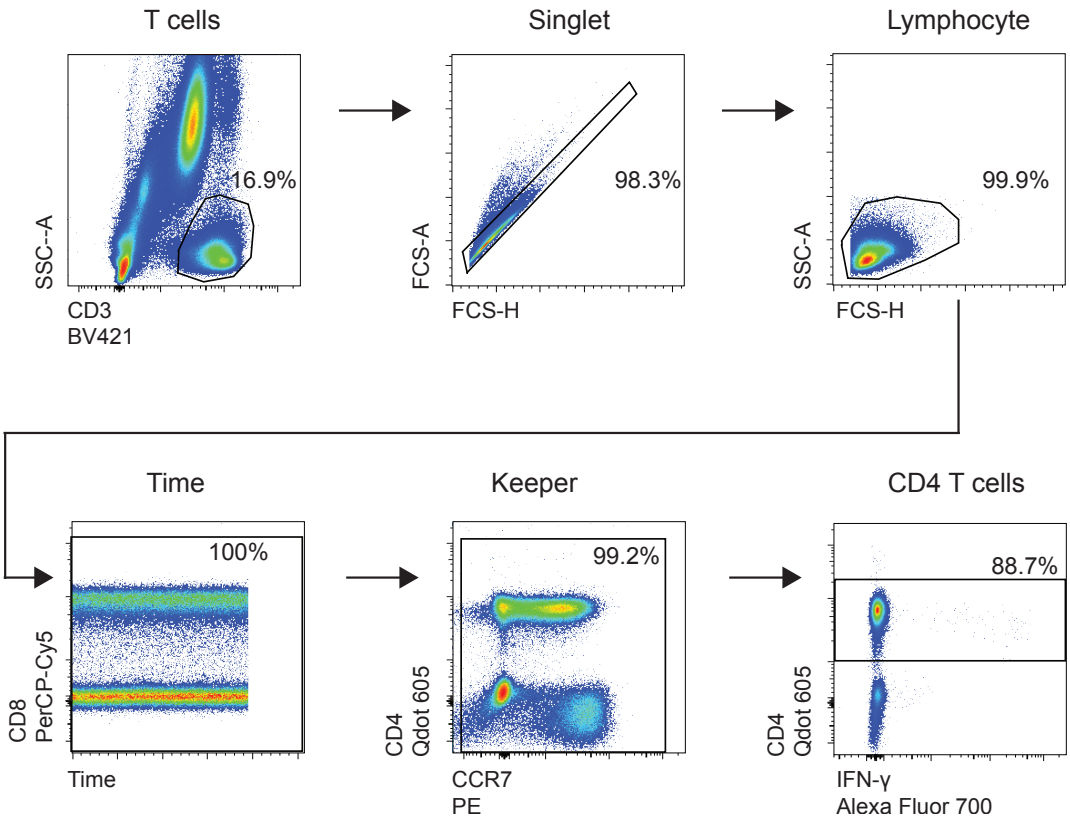

Figure 30. Gating strategy for analysis of H1-specific CD4 T cell response. Representative flow plots depicting the gating strategy used to identify CD4 T cells expressing Th1 cytokines following Ag85B or ESAT-6 peptide pool stimulation.

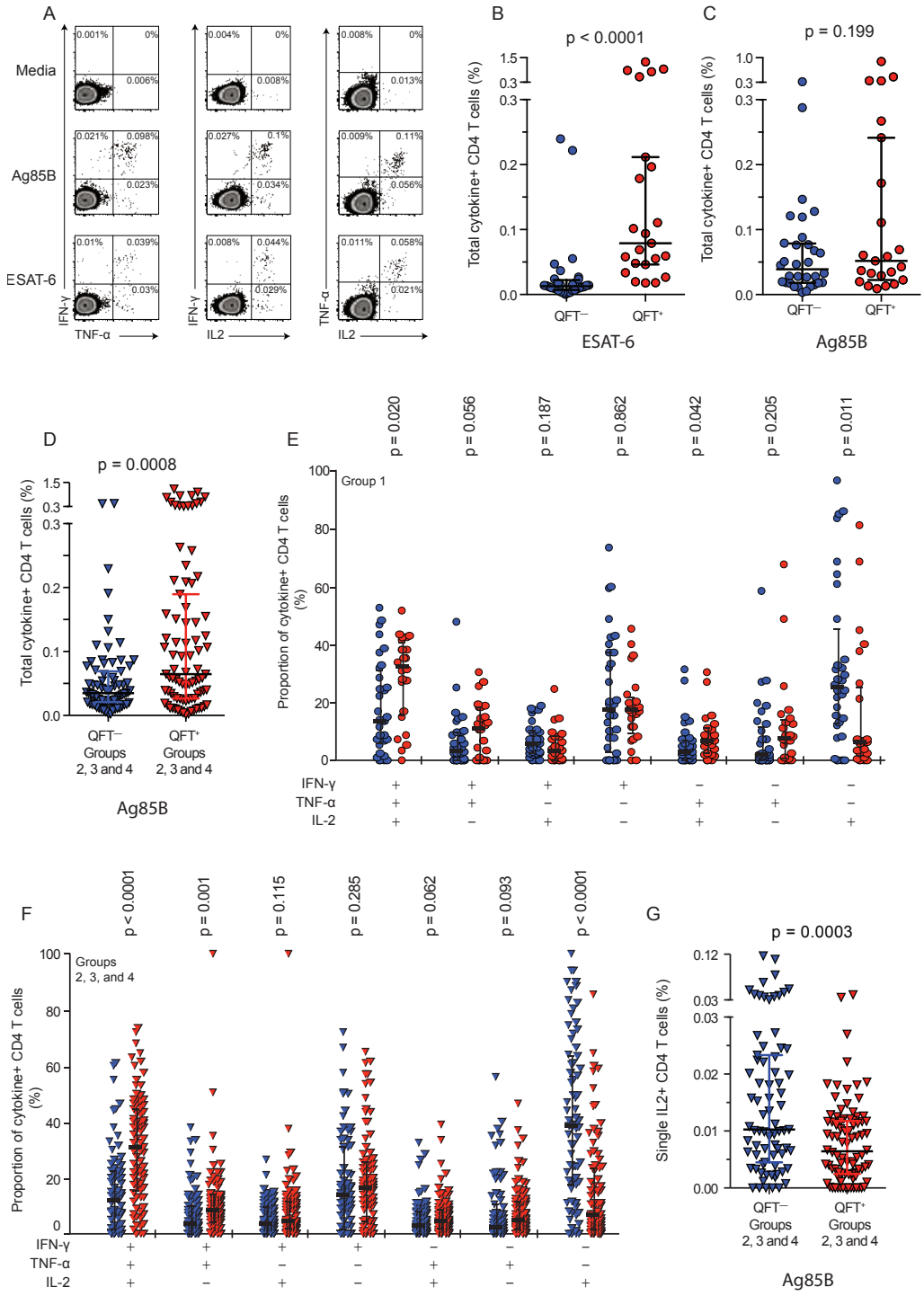

Figure 31. Baseline frequencies and cytokine profile of H1-specific CD4 T cells in QFT^{-} and QFT^{+} adolescents. (A) Representative flow cytometry plots showing intracellular staining of IFN-γ, TNF-α, and IL-2 following 12hr whole blood stimulation with media alone, Ag85B, or ESAT-6 peptides prior to H1:IC31 vaccination. Total frequencies of Th1 cytokine^{+} ESAT-6-specific (B), Ag85B-specific CD4 T cells in QFT^{+} and QFT^{-} adolescents enrolled in Group 1 (C), or Ag85B-specific cells in Groups 2, 3, and 4 (D) prior to H1:IC31 vaccination. The relative proportions of Ag85B-specific CD4 T cells expressing each combination of IFN-γ, TNF-α, and/or IL-2 in QFT^{-} and QFT^{+} adolescents in Group 1 (E) or Groups 2, 3, and 4 (F) prior to H1:IC31 vaccination. (G) The frequencies of single IL-2^{+} Ag85B-specific CD4 T cells in QFT^{-} and QFT^{+} adolescents in Groups 2, 3, and 4. Horizontal lines indicate medians and error bars indicate IQR. P-values were calculated using the Mann Whitney U test and are unadjusted for multiple comparisons.

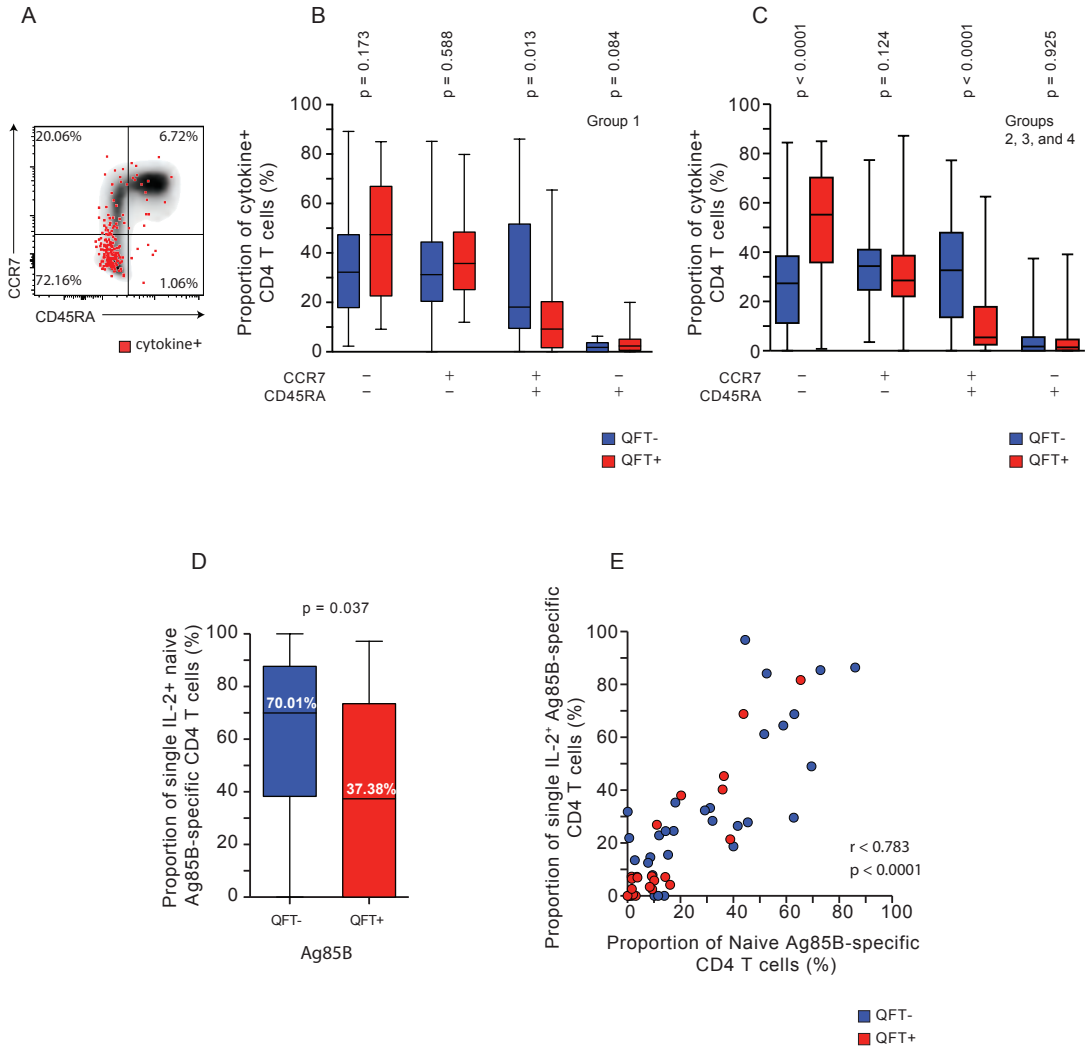

Figure 32. Baseline memory phenotypes Ag85B-specific CD4 T cells in QFT⁻ and QFT⁺ adolescents. (A) A representative flow cytometry plot of CCR7 and CD45RA expression by total CD4 T cells (grey background) or by Ag85B-specific Th1 cytokine$^+$ CD4 T cells (red dots). Numbers indicate the proportions of Ag85B-specific Th1 cytokine$^+$ CD4 T cells falling into each quadrant. The proportions of Th1 cytokine$^+$ Ag85B-specific CD4 T cells expressing each combination of CCR7 and CD45RA in QFT⁻ and QFT$^+$ adolescents in Group 1 (B) or Groups 2, 3, and 4 (C) prior to H1:IC31 vaccination. (D) The proportion of single IL-2 producing Ag85B-specific CD4 T cells displaying the naïve phenotype in QFT⁻ and QFT$^+$ adolescents in Group 1 prior to H1:IC31 vaccination. (E) The correlation of the proportion of single IL-2$^+$Ag85B-specific CD4 T cells and the proportion of total Th1 cytokine-expressing Ag85B-specific CD4 T cells displaying the naïve phenotype in QFT⁻ and QFT$^+$ adolescents in Group 1 prior to H1:IC31 vaccination. P-values were calculated using the Mann Whitney U test (B, C, and D) or Spearman correlation (E). P-values are unadjusted for multiple comparisons.

Primary H1:IC31 vaccination induces higher frequencies of Ag85B and ESAT-6-specific CD4 T cells in QFT$^+$ adolescents compared to QFT$^-$.

Next, we wanted to determine the effect of underlying M.tb infection on the H1:IC31 induced CD4 T cell response. To achieve this, whole blood collected 14, 56, 70, and 224 days after H1:IC31 vaccination was incubated with ESAT-6 or Ag85B and the frequencies of Th1 cytokine expressing CD4 T cells were measured (Figure 33A). We observed that 14 days after primary H1:IC31 vaccination QFT$^+$ adolescents had higher frequencies of Ag85B and ESAT-6-specific Th1 cytokine$^+$ CD4 T cells than QFT$^-$ adolescents. Notably, QFT$^+$ adolescents had higher frequencies of ESAT-6-specific Th1 cytokine$^+$ CD4 T cells throughout the study, compared to QFT$^-$ adolescents. Following the secondary H1:IC31 vaccination, Ag85B-specific Th1 cytokine$^+$ CD4 T cell frequencies were not different in QFT$^+$ and QFT$^-$ adolescents, and remained at comparable levels until the end of study (day 224). We then asked if frequencies of antigen-specific CD4 T cells induced by H1:IC31 were durable. Frequencies of both Ag85B and ESAT-6-specific Th1 cytokine$^+$ CD4 T cells were higher on day 224 compared to day 0 in QFT$^-$ adolescents. In QFT$^+$ adolescents frequencies of Ag85B-specific Th1 cytokine$^+$ were also higher on day 224 compared to day 0. However, frequencies of ESAT-6-specific Th1 cytokine$^+$ CD4 T cells observed on day 224 were not different to baseline (day 0).

We then measured the frequencies of Ag85B and ESAT-6-specific CD4 T cells using a panel of HLA class II tetramers (Figure 33B). Similar kinetics were observed when HLA class II tetramers were used to measure the Ag85B and ESAT-6-specific CD4 T cell responses induced by H1:IC31 (Figure 33C). However, there were some

noticeable differences in the CD4 T cell response measured by tetramers, compared to ICS. Firstly, 14 days after primary H1:IC31 vaccination, frequencies of Ag85B and ESAT-6-specific tetramer^{+} CD4 T cells were similar ($p = 0.067$) in QFT^{+} adolescents, while higher frequencies of ESAT-6-specific Th1 cytokine^{+} CD4 T cells had been observed in QFT^{+} adolescents ($p < 0.0001$). Secondly, 14 days after secondary vaccination (day 70) we observed higher frequencies of Ag85B-specific tetramer^{+} CD4 T cells in QFT^{+} adolescents compared to QFT^{-} ($p = 0.002$). However, frequencies of Ag85B-specific tetramer^{+} CD4 T cells were not different at the remaining time points (i.e. days 112 and 224) in both groups of adolescents. Lastly, frequencies of ESAT-6-specific tetramer^{+} CD4 T cells remained similar following secondary H1:IC31 vaccination.

The response to secondary H1:IC31 vaccination was different in QFT^{-} and QFT^{+} adolescents. QFT^{-} adolescents had increased frequencies of both Ag85B and ESAT-6-specific Th1 cytokine^{+} cells on day 70 compared to day 14 ($p = 0.004$ and $p = 0.02$, respectively). By contrast, QFT^{+} adolescents had similar frequencies of Ag85B-specific Th1 cytokine^{+} cells on day 70 compared to day 14 ($p = 0.462$) and lower frequencies of ESAT-6-specific Th1 cytokine^{+} cells ($p = 0.0003$). Similar results were observed with Ag85B and ESAT-6-specific tetramer^{+} CD4 T cells. When we compared the fold change in frequencies of Th1 cytokine^{+} and tetramer^{+} Ag85B and ESAT-6-specific CD4 T cells following primary (day 14) and secondary (day 70) vaccinations, QFT^{-} adolescents had a larger fold change compared to QFT^{+} adolescents. (Figure 34A and Figure 34B). Together these data suggest that peak frequencies of H1-specific CD4 T cells are achieved after primary vaccination in QFT^{+} adolescents but in QFT^{-} adolescents peak responses are achieved after

secondary vaccination.

Our data suggest that H1-specific CD4 T cells in adolescents with underlying *M.tb* infection are more poised to expand within 14 days following a single H1:IC31 vaccination. However, upon a second vaccination, these cells appear to have diminished capacity to expand, compared with those in persons without *M.tb* infection. These results prompted us to identify whether underlying infection had an effect on other attributes of H1-specific CD4 T cell responses following vaccination. To achieve this, we utilized microfluidic high throughput qPCR to interrogate H1-specific CD4 T cells at the various time points following vaccination.

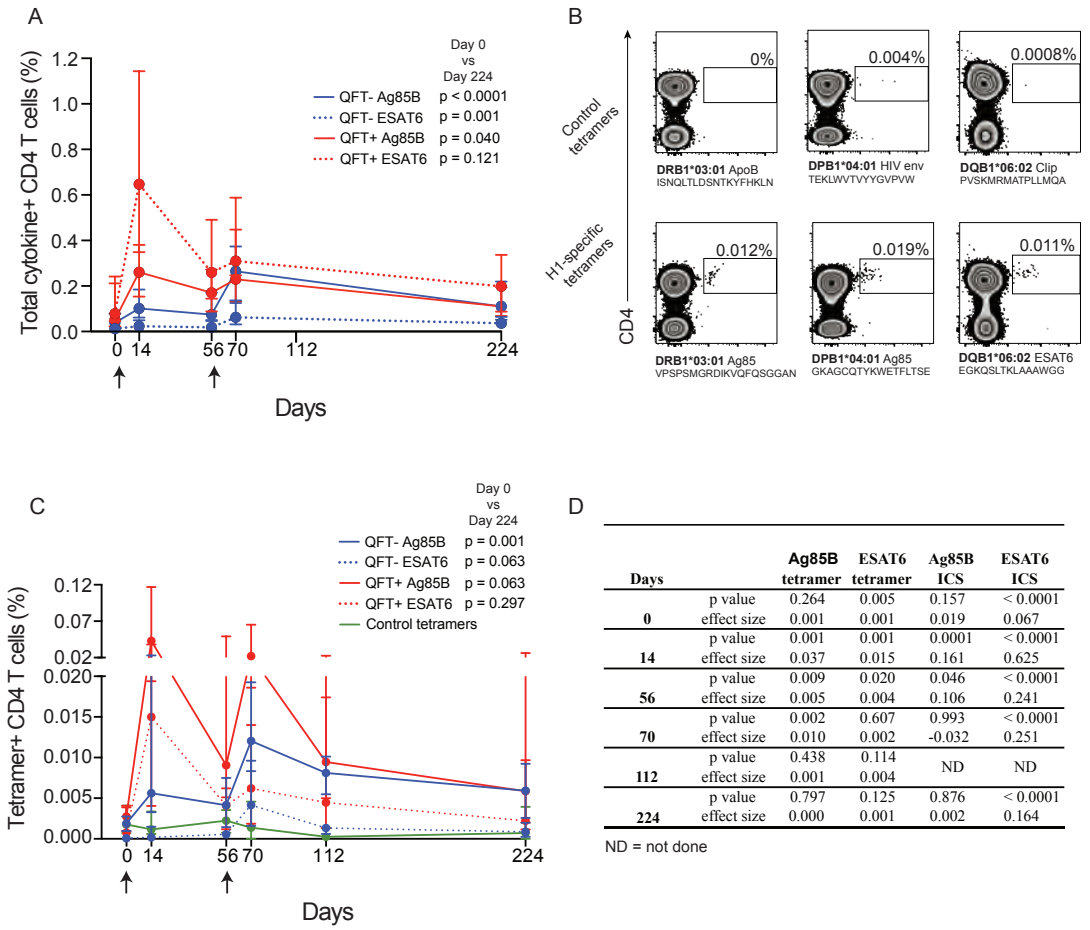

Days		Ag85B tetramer	ESAT6 tetramer	Ag85B ICS	ESAT6 ICS
0	p value	0.264	0.005	0.157	< 0.0001
	effect size	0.001	0.001	0.019	0.067
14	p value	0.001	0.001	0.0001	< 0.0001
	effect size	0.037	0.015	0.161	0.625
56	p value	0.009	0.020	0.046	< 0.0001
	effect size	0.005	0.004	0.106	0.241
70	p value	0.002	0.607	0.993	< 0.0001
	effect size	0.010	0.002	-0.032	0.251
112	p value	0.438	0.114	ND	ND
	effect size	0.001	0.004		
224	p value	0.797	0.125	0.876	< 0.0001
	effect size	0.000	0.001	0.002	0.164

ND = not done

Figure 33. Distinct kinetics of Ag85B and ESAT-6-specific CD4 T cell responses following primary and secondary H1:IC31 vaccination in *M.tb*-infected and uninfected adolescents. (A) Median frequencies (error bars denote IQR) of Th1 cytokine-expressing Ag85B and ESAT-6-specific CD4 T cells, detected by ICS. (B) Flow cytometry plots showing representative staining of CD4 T cells from H1:IC31 vaccinated adolescents (day 14) with HLA class II tetramers either bearing Ag85B peptides (DRB1*0301 and DPB1*0401-restricted epitopes) or ESAT-6 peptides (DQB1*0602-restricted), denoted as H1-specific tetramers. Control tetramer staining was performed using tetramers matched by HLA allele bearing peptides from antigens to which CD4 T cell responses are not expected. Numbers in each plot indicate the frequencies of tetramer$^+$ CD4 T cells. (C) Median frequencies (error bars denote IQR) of Ag85B and ESAT-6-specific tetramer+ CD4 T cells following H1:IC31 vaccination. The green line represents the median frequencies (error bars denote IQR) of all three control tetramers combined. (D) Comparisons of antigen-specific CD4 T cell frequencies between QFT$^-$ and QFT$^+$ adolescents at each study time point. Effect size was determined by taking the difference (Δ) between frequencies in QFT$^-$ and QFT$^+$ adolescents. P values were calculated with Wilcoxon signed-rank (A and C) or Mann Whitney U tests (D) and have not been adjusted for multiple comparisons.

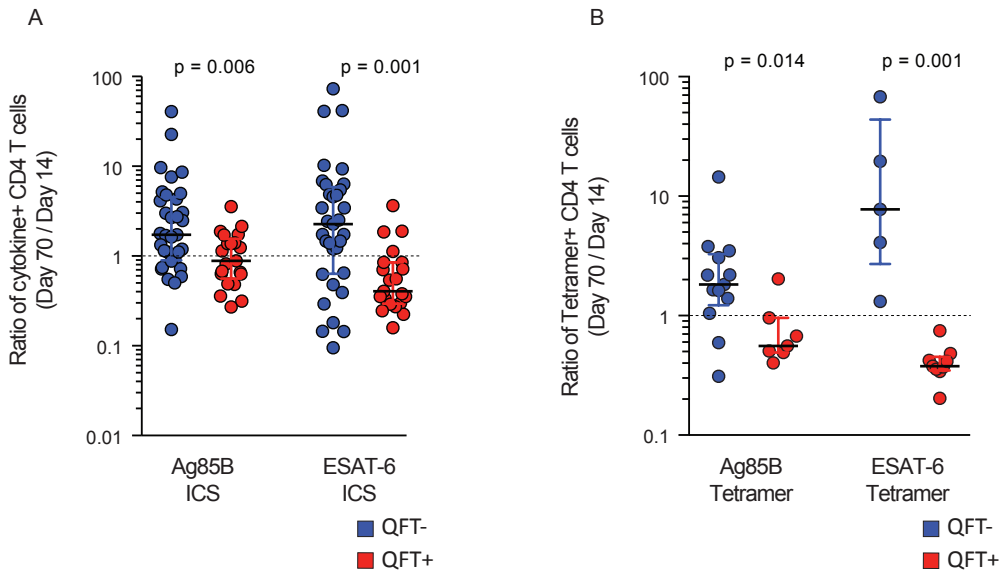

Figure 34. Higher fold change in Ag85B and ESAT-6-specific CD4 T cells following secondary H1:IC31 vaccination in uninfected adolescents. Ratios of Ag85B and ESAT-6-specific CD4 T cell frequencies detected by ICS (A) or HLA class II tetramer staining (B) in day 70 samples, relative to day 14. Values above 1 (dotted line) represent increased responses after the second vaccination on day 56, relative to the response after the first vaccination. Horizontal lines and whiskers are the median and IQR, respectively. P values were calculated with Mann Whitney U test and have not been adjusted for multiple comparisons

Although the BioMark Fluidigm platform has been used to measure mRNA transcript level within single cells, due to technical limitations (e.g. poor sensitivity between 2 to 10 cells, as shown in Chapter 3) we choose to measure expression of mRNA transcripts in populations of H1-specific tetramer$^+$ CD4 T cells collected at time points before and after vaccination in each donor. Based on prior experience, we anticipated that the number of H1-specific tetramer$^+$ CD4 T cells before vaccination and at later time points (i.e. days 112 and 224 after vaccination) would be very low and often too few to sort and reliably analyse. We therefore, needed to determine a cut-off value for the number of sorted cells to allow robust transcriptomic analyses. Furthermore, because rare transcripts are more likely to be detected as the number of cells increases (Dominguez et al. 2013), we had to determine a maximum number of sorted cells to mitigate the risk of detecting transcriptomic differences due to number of cells sorted. From previous work we observed that the numbers of transcripts

detected in populations of 25 to 50 bulk naïve, central memory, or effector memory CD4 T cells appeared stable within each population (Figure 35A). Moreover, using an unsupervised clustering approach, the 25 and 50-cell samples clustered according to memory phenotype and not according to number of cells sorted (Figure 35B). This suggests that the variability in expression data between 25 and 50 cells was minimal and did not influence the transcriptional profile of cells. Reassuringly, other investigators have also observed that transcriptomic signatures that distinguish bulk monocytes, T cells, and B cells are readily recognized in samples of 25 or more sorted cells (Dominguez et al. 2013). We therefore set the minimum and maximum number of sorted tetramer^{+} CD4 T cells required for transcriptomic analysis to 25 and 50 cells.

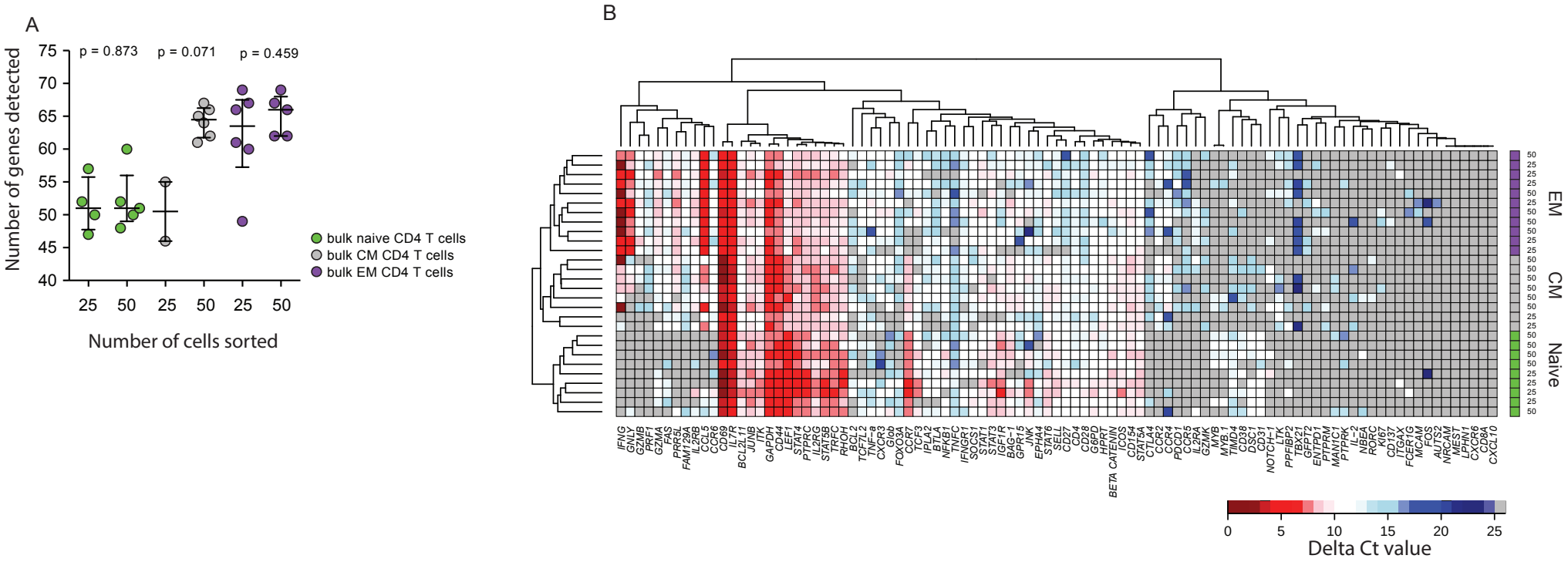

Figure 35. Comparable detection and mRNA expression within bulk CD4 T cell subsets of 25 or 50 cells. (A) The number of mRNA transcripts detected (Ct < 40) within each subset. The horizontal lines indicate medians and the error bars represent IQR. P values were calculated using the Mann Whitney U test and are unadjusted for multiple comparisons. (B) Unsupervised hierarchical clustering of bulk CD4 T cell subsets based on Euclidean distance.

We also wanted to ensure that transcriptomic analysis was performed on genuine H1-specific CD4 T cells with frequencies well above those of CD4 T cells that stained with irrelevant antigen control tetramers (i.e. background staining). To derive the frequency cut-off value we calculated the median frequency of control tetramer^{+} CD4 T cells plus 4 median absolute deviations (MAD) from the median frequencies of control tetramer^{+} CD4 T cells. The median frequency observed for control tetramer^{+} CD4 T cells was 0.001% (Figure 36A) and the MAD was 0.001% (data not shown). Therefore, the minimum frequency (median + 4 MADs) required for transcriptomic analysis of Ag85B or ESAT-6-specific tetramer^{+} CD4 T cells was 0.005%. Coincidentally this cut-off value was also the median frequency of H1 tetramer^{+} CD4 T cells when data from all H1-specific tetramers and time points were included (Figure 36A). Using both the number of cells sorted and the frequency of H1-specific tetramer+ cut-off criteria, 96 samples out of a possible 148 samples were included in our transcriptomic analysis (Figure 36B and Figure 36C). The majority of transcripts were detected in at least half of the samples analysed and only 6 transcripts were detected in less than 25% of samples (Figure 36D). We were unable to investigate the H1-specific CD4 T cell response prior to vaccination (day 0) due to very few samples (0 in QFT^{-} and 2 in QFT^{+}) that met the inclusion cut-off values (Figure 36B).

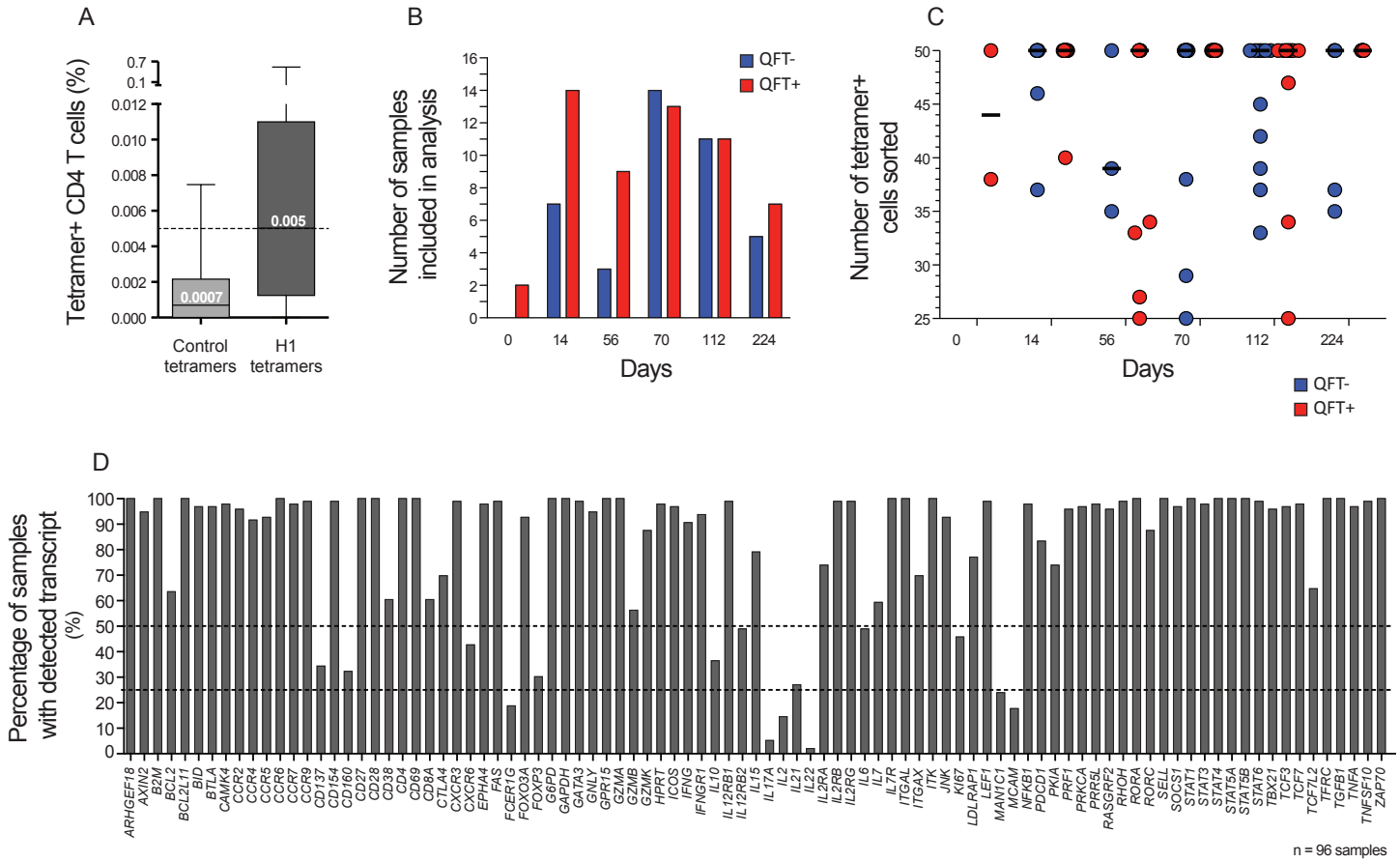

Figure 36. Overall performance of H1-specific tetramer staining and samples included for transcriptomic analysis. (A) Summary data of control and H1-specific tetramer staining throughout the study period. (B) Number of samples with an H1-specific tetramer+ frequency ≥0.005 and ≥ 25 sorted cells in QFT⁻⁻ and QFT+ adolescents. (C) Number of H1-specific tetramer+ cells sorted in QFT⁻⁻ and QFT+ adolescents. (D) The proportion of samples with a detectable (Et >0) level of expression for each mRNA transcript.

Primary vaccination induces H1-specific CD4 T cells in QFT⁻ adolescents with reduced effector functions but a higher proliferative capacity compared to QFT⁺.

Having observed that primary vaccination induced higher frequencies of Ag85B and ESAT-6-specific CD4 T cells in QFT^+ adolescents, compared to QFT^- adolescents (Figure 33D), we wanted to know what other acute response attributes were different between these groups. We compared the expression levels of mRNA transcripts on day 14 in H1-specific CD4 T cells in QFT^- and QFT^+ adolescents. A total of 15 mRNA transcripts were differentially expressed ($p < 0.05$) (Figure 37A). H1-specific CD4 T cells from QFT^+ adolescents expressed higher mRNA transcript levels of the cytotoxic molecules, perforin, granzyme K, granzyme A, and granulysin compared to H1-specific cells from QFT^- adolescents. H1-specific CD4 T cells from QFT^+ adolescents also expressed higher levels of the chemokine receptor, *CXCR3*. H1-specific CD4 cells from QFT^- adolescents expressed higher levels of the cell division marker, *KI67*, and the activation marker, *CD38*, compared to QFT^+ adolescents. Interestingly, H1-specific CD4 T cells from QFT^- adolescents also expressed higher levels of *ICOS*, *PDCD1* (PD-1), and *IL-21* compared to QFT^+ adolescents. These are markers commonly used to distinguish follicular helper CD4 T (Tfh) cells (Crotty 2011). However, work recently performed in mouse models of *M.tb* has revealed a central memory subset of *M.tb*-specific CD4 T cells with Tfh features, including PD-1 and ICOS. Furthermore, a subset of antigen-specific CD4 T cells displaying a similar phenotype was induced when mice received the subunit vaccine H1:CAF01 and was associated with improved and long term bacterial control (Lindenstrom et al. 2013). This subset of cells, which some classify as CM cells, has been shown to retain memory properties despite chronic antigen stimulation (Sakai et al. 2014; Reiley et al. 2010; Moguche et al. 2015).

We therefore asked whether the gene expression profile of H1-specific CD4 T cells from QFT^{-} adolescents was consistent with that of CM cells. We compared the expression levels of the 15 mRNA transcripts found to be differentially expressed in QFT^{-} and QFT^{+} adolescents in bulk EM and CM (Figure 37B). We observed higher mRNA expression of perforin, granzyme K, granzyme A, granulysin, and CXCR3 in bulk EM, compared to CM CD4 T cells. This suggests that, following primary H1:IC31 vaccination, H1-specific CD4 T cells from QFT^{+} adolescents have a larger proportion of EM cells, compared to QFT^{-} adolescents. H1-specific CD4 T cells from QFT^{-} preferentially expressed a profile of activated Tfh-like memory cells (ICOS, PD-1 and IL-21), while sharing some gene expression profiles with typical CM cells (ICOS, CD38, and RHOH). Interestingly, our analysis of bulk CM and EM revealed that *PD-1* expression was higher in EM (Figure 37B). Our bulk sorts did not include anti-CD27 antibody, therefore effector T cells (Teff) were not excluded from the EM population. It is possible that in the context of bulk memory cells, higher PD-1 expression levels may be due to the presence of exhausted virus-specific effector cells, and is a reflection of the regulatory role PD-1 in during effector responses.

Given that H1-specific CD4 T cells from QFT^{+} and QFT^{-} displayed transcriptional profiles consistent with EM and CM phenotypes, respectively, we compared the memory phenotypes of H1-specific CD4 T cells using expression of CCR7 and CD45RA (Figure 37C). A larger proportion of H1-specific CD4 T cells expressed an EM phenotype in QFT^{+} adolescents. By contrast, a larger proportion of H1-specific CD4 T cells expressed a CM phenotype in QFT^{-} adolescents, compared to QFT^{+} adolescents. Interestingly, larger proportions of H1-specific CD4 T cells expressing a

naïve phenotype were also detected in QFT^{-} adolescents. In agreement with the larger proportion EM cells, we observed higher proportions of polyfunctional, IFN-γ^{+}TNF-α^{+}IL-2^{+}, H1-specific CD4 T cells in QFT^{+} adolescents, while larger proportions of single IL-2 producing H1-specific CD4 T cells were observed in QFT^{-} adolescents (Figure 37D).

Together, the transcriptomic, CCR7 and CD45RA surface expression, and cytokine co-expression data suggest that following primary H1 vaccination, adolescents with underlying *M.tb* infection have a larger and more EM H1-specific CD4 T cell response than uninfected adolescents.

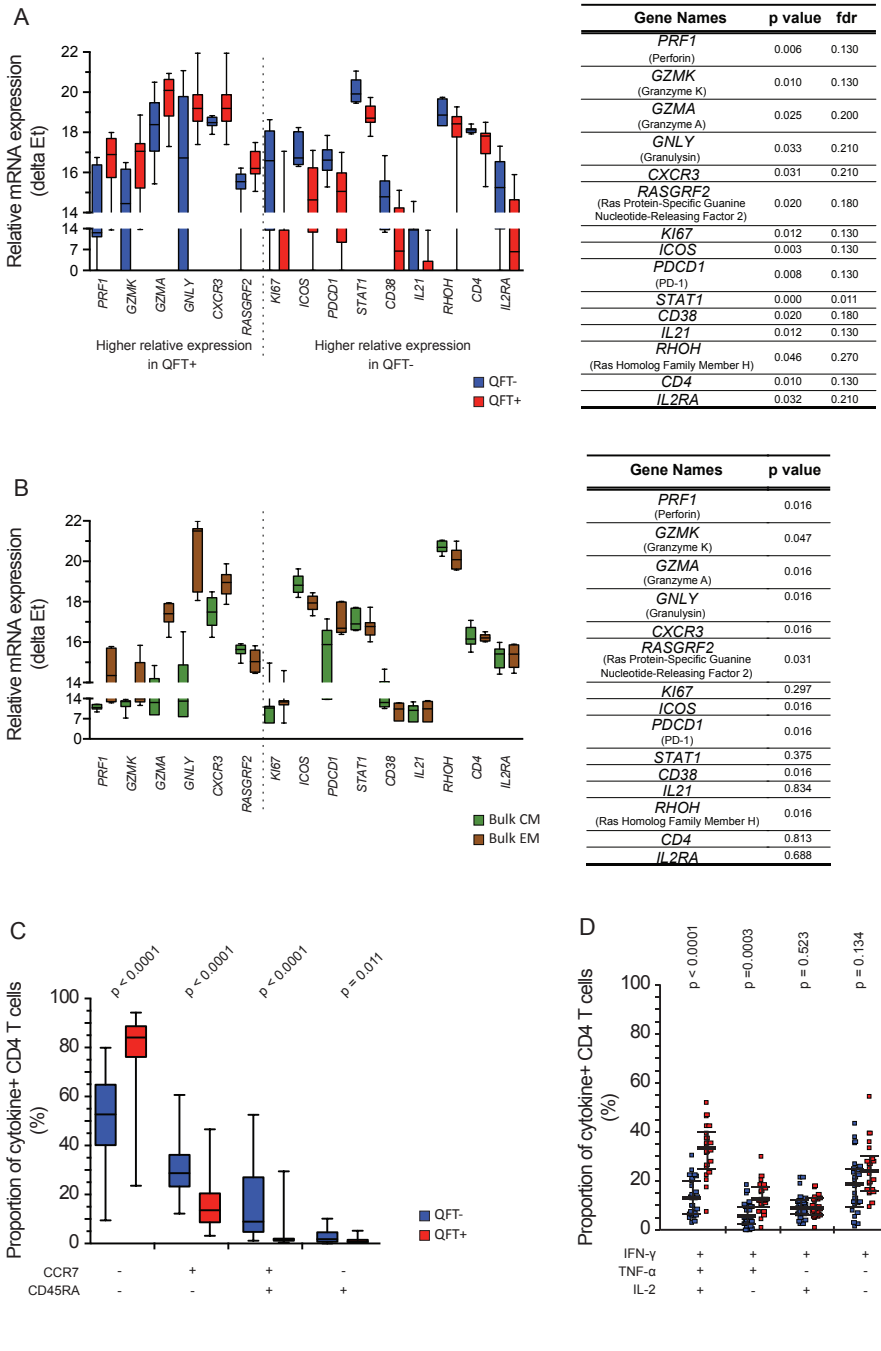

Gene Names	p value	fdr
PRF1 (Perforin)	0.006	0.130
GZMK (Granzyme K)	0.010	0.130
GZMA (Granzyme A)	0.025	0.200
GNLY (Granulysin)	0.033	0.210
CXCR3	0.031	0.210
RASGRF2 (Ras Protein-Specific Guanine Nucleotide-Releasing Factor 2)	0.020	0.180
KI67	0.012	0.130
ICOS	0.003	0.130
PDCD1 (PD-1)	0.008	0.130
STAT1	0.000	0.011
CD38	0.020	0.180
IL21	0.012	0.130
RHOH (Ras Homolog Family Member H)	0.046	0.270
CD4	0.010	0.130
IL2RA	0.032	0.210

Gene Names	p value
PRF1 (Perforin)	0.016
GZMK (Granzyme K)	0.047
GZMA (Granzyme A)	0.016
GNLY (Granulysin)	0.016
CXCR3	0.016
RASGRF2 (Ras Protein-Specific Guanine Nucleotide-Releasing Factor 2)	0.031
KI67	0.297
ICOS	0.016
PDCD1 (PD-1)	0.016
STAT1	0.375
CD38	0.016
IL21	0.834
RHOH (Ras Homolog Family Member H)	0.016
CD4	0.813
IL2RA	0.688

Figure 37. Transcriptomic, functional, and phenotypic profiles of H1-specific CD4 T cells induced by primary vaccination are different in *M.tb*-infected and uninfected adolescents. (A) Transcriptomic profiles of H1-specific CD4 T cells from *M.tb*-infected and uninfected adolescents measured 14 days after H1:IC31 vaccination. Ag85B or ESAT-6-specific CD4 T cells were detected by HLA class II tetramers and sorted by FACS for microfluidic qPCR. mRNA expression data are shown as delta Et values, relative to B2M expression. Only genes with differentially expressed mRNA transcripts at $p < 0.05$ are shown. FDRs were calculated using the Benjamini-Hochberg method. (B) mRNA expression levels of those genes differentially expressed in H1-specific CD4 T cells, in sorted bulk central memory (CCR7+CD45RA-) or effector memory (CCR7-CD45RA-) CD4 T cells (n = 7). (C) Proportions of Th1 cytokine+ H1-specific CD4 T cells expressing each combination of CCR7 and CD45RA. Horizontal lines indicate medians, boxes the IQR and whiskers the range. (D) Median (error bars represent IQR) proportions of H1-specific CD4 T cells co-expressing IFN-γ, TNF-α, and IL-2 in *M.tb*-infected and uninfected adolescents. Groups were compared using Mann Whitney U tests (A, C, and D) or Wilcoxon signed-rank (B). Unadjusted p values are shown.

Persistence of the effector bias in M.tb infected adolescents.

Since the secondary H1:IC31 vaccination induced the peak response only in QFT^{-} adolescents, we asked whether secondary vaccination induces different levels of EM cells in QFT^{-} and QFT^{+} adolescents. To do this we compared proportions of EM H1-specific CD4 T cells on day 70 and day 14. As expected, proportions of H1-specific cells expressing the EM phenotype increased in QFT^{-} adolescents following the secondary H1:IC31 vaccination ($p = 0.002$). However, the secondary vaccination did not increase the proportion of cells expressing the EM phenotype in QFT^{+} adolescents; to the contrary, we observed a trend toward lower proportions of EM cells ($p = 0.046$).

To understand this better, we determined the transcriptomic profile of H1-specific cells in QFT^{-} and QFT^{+} adolescents following the secondary vaccination. Since secondary vaccination increased the proportion of EM H1-specific CD4 T cells in QFT^{-} adolescents only, we hypothesised that this second vaccination would induce expression of genes associated with T cell effector functions and EM CD4 T cells in QFT^{-} adolescents. We determined the fold change in expression of mRNA transcripts on day 70 compared to day 14 by using the comparative Ct method. H1-specific CD4 T cells from QFT^{-} adolescents increased (higher fold change $p < 0.05$) expression of the cytotoxic molecule, perforin, the chemokine receptors, *CCR6* and *CCR9*, the G protein-coupled receptor, *GPR15*, and the low density lipoprotein receptor adaptor protein 1, *LDLRAP1* (Figure 38). All other EM-associated mRNAs were not different. However, expression of *ICOS*, *GATA3*, and *RHOH* was lower in QFT^{-} adolescents (Figure 38). Lower *ICOS* and *RHOH* expression had previously been observed in bulk EM, when compared to bulk CM cells (Figure 37B). It should

be noted, however, that the q-values calculated following correction for multiple comparisons using the Benjamini-Hochberg method were large (i.e. >20%).

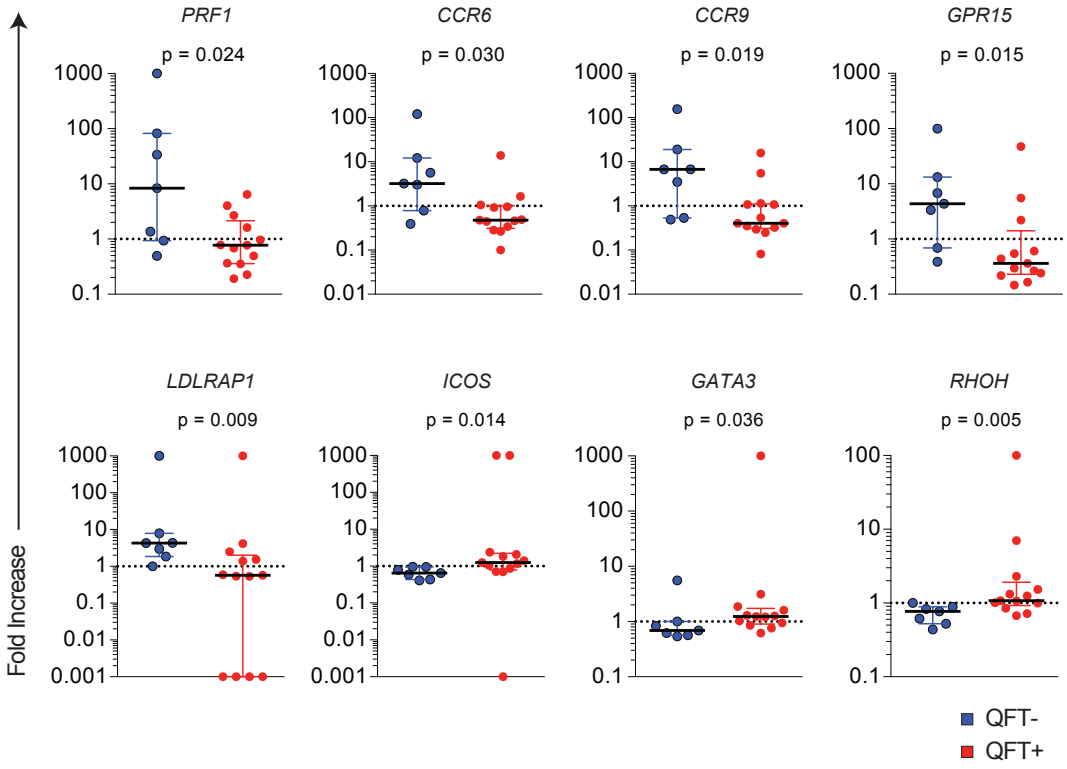

Figure 38. Transcriptomic changes of H1-specific CD4 T cells between the first and secondary vaccination are different in *M.tb*-infected and uninfected adolescents. The fold change in level of mRNA expression on day 70, relative to day 14, in QFT^{-} and QFT^{+} adolescents. Fold change values were calculated using the comparative delta delta Ct method. The horizontal lines indicate medians and the error bars represent IQR. P values were calculated using the Mann Whitney U test and are unadjusted for multiple comparisons.

We were limited in the number of QFT^{-} samples for which we could calculate the fold change after the secondary vaccination, because following primary vaccination only 7 samples, all Ag85B-specific CD4 T cells, from QFT^{-} adolescents met the inclusion criteria for transcriptomic analyses. However, following secondary vaccination 14 samples from QFT^{-} adolescents met the inclusion criteria (Figure 36B). Nineteen mRNA transcripts were differentially expressed between QFT^{-} and QFT^{+} adolescents on day 70 (Figure 39A). While expression of perforin, granzyme A, granulysin, and CXCR3 was not different on day 70 between the two groups

(Figure 39B), H1-specific CD4 T cells from QFT^{-} adolescents expressed *CCR7*, *BTLA*, *CAMK4*, *STAT6* and *JNK* at higher levels day 70 (Figure 39A). Interestingly, these genes were also expressed at higher levels in bulk CM compared to EM (Figure 39C). These results suggest that, even after two doses of H1:IC31, H1-specific CD4 T cell responses in QFT^{-} adolescents were more biased toward a CM phenotype compared to cells from QFT^{+} adolescents, or alternatively, H1-specific cells from QFT^{+} adolescents were more biased toward an EM phenotype.

In line with these observations, proportions of EM and polyfunctional IFN-γ^{+}TNF-α^{+}IL-2^{+} H1-specific cells remained higher in QFT^{+} adolescents ($p = 0.013$ and $p < 0.0001$ respectively) on day 70. However, proportions of H1-specific cells expressing a CCR7^{+}CD45RA^{-} CM phenotype were similar between the two groups ($p = 0.161$). Proportions of single IL-2 producing cells remained higher in QFT^{-} adolescents on day 70 ($p < 0.0001$). Together these data suggest that while secondary vaccination induced an increase in the EM response in QFT^{-}, QFT^{+} adolescents maintained a higher EM-like response. Furthermore, although not evident based on surface marker expression of CCR7 and CD45RA, the cytokine and transcriptomic profiles are suggestive of a bias towards central memory cells in QFT^{-} adolescents on day 70, even 14 days after the secondary vaccination, when the H1-specific response peaked.

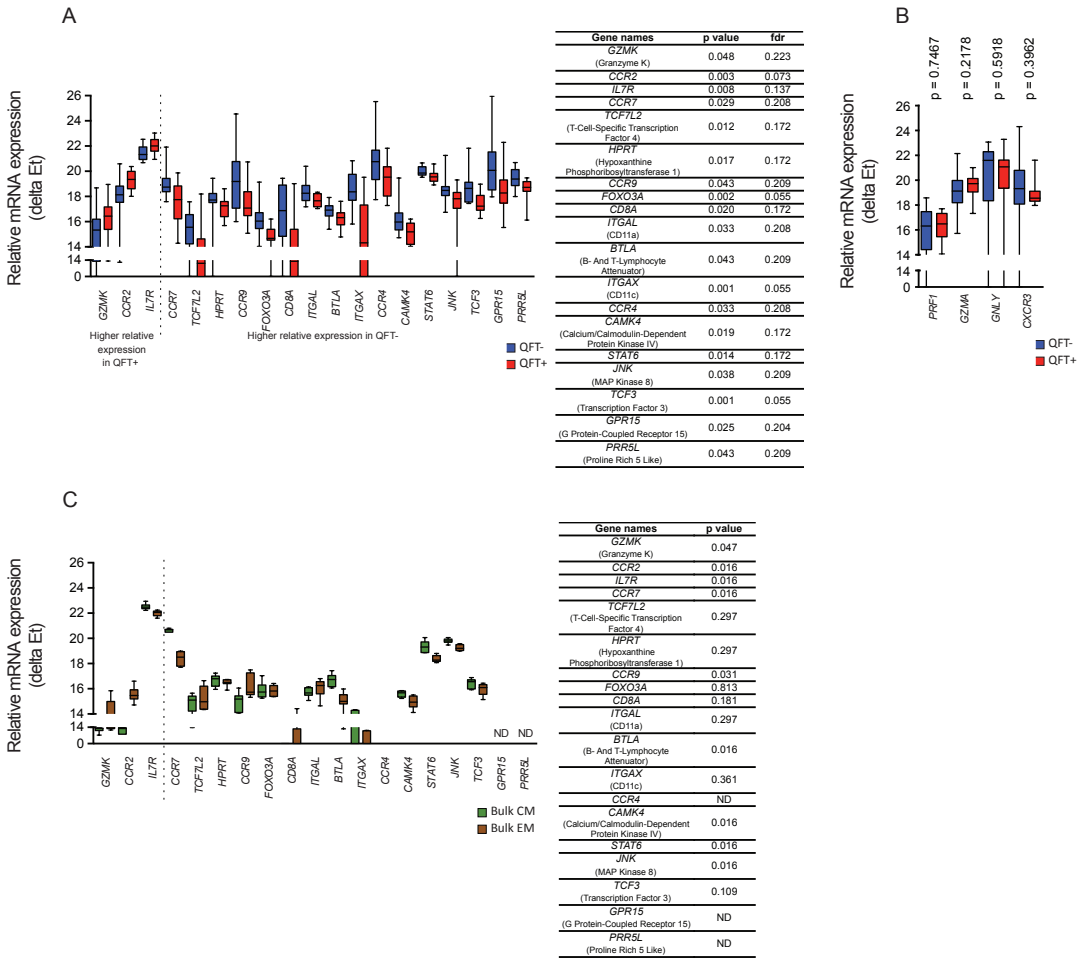

Gene names	p value	fdr
GZMK (Granzyme K)	0.048	0.223
CCR2	0.003	0.073
IL7R	0.008	0.137
CCR7	0.029	0.208
TCF7L2 (T-Cell-Specific Transcription Factor 4)	0.012	0.172
HPRT (Hypoxanthine Phosphoribosyltransferase 1)	0.017	0.172
CCR9	0.043	0.209
FOXO3A	0.002	0.055
CD8A	0.020	0.172
ITGAL (CD11a)	0.033	0.208
BTLA (B- And T-Lymphocyte Attenuator)	0.043	0.209
ITGAX (CD11c)	0.001	0.055
CCR4	0.033	0.208
CAMK4 (Calcium/Calmodulin-Dependent Protein Kinase IV)	0.019	0.172
STAT6	0.014	0.172
JNK (MAP Kinase 8)	0.038	0.209
TCF3 (Transcription Factor 3)	0.001	0.055
GPR15 (G Protein-Coupled Receptor 15)	0.025	0.204
PRR5L (Proline Rich 5 Like)	0.043	0.209

Gene names	p value
GZMK (Granzyme K)	0.047
CCR2	0.016
IL7R	0.016
CCR7	0.016
TCF7L2 (T-Cell-Specific Transcription Factor 4)	0.297
HPRT (Hypoxanthine Phosphoribosyltransferase 1)	0.297
CCR9	0.031
FOXO3A	0.813
CD8A	0.181
ITGAL (CD11a)	0.297
BTLA (B- And T-Lymphocyte Attenuator)	0.016
ITGAX (CD11c)	0.361
CCR4	ND
CAMK4 (Calcium/Calmodulin-Dependent Protein Kinase IV)	0.016
STAT6	0.016
JNK (MAP Kinase 8)	0.016
TCF3 (Transcription Factor 3)	0.109
GPR15 (G Protein-Coupled Receptor 15)	ND
PRR5L (Proline Rich 5 Like)	ND

Figure 39. Transcriptomic analysis of circulating H1-specific CD4 T cells following secondary vaccination. (A) Differentially expressed mRNA transcripts in H1-specific CD4 T cells from QFT^- and QFT^+ on day 70 (14 days after second vaccination). Ag85B or ESAT-6-specific CD4 T cells were detected by HLA class II tetramers and sorted by FACS for microfluidic qPCR and are shown as delta Et values, relative to *B2M* expression. Only genes with differentially expressed mRNA transcripts at $p < 0.05$ are shown. FDRs were calculated using the Benjamini-Hochberg method. (B) Relative expression of *PRF1* (Perforin), *GZMA* (Granzyme A), *GNLY* (Granulysin), and *CXCR3* in H1-specific CD4 T cells from QFT^- and QFT^+ on day 70. (C) mRNA expression levels of those genes differentially expressed in H1-specific CD4 T cells, in sorted bulk CM (CCR7+CD45RA-) and EM (CCR7-CD45RA-) CD4 T cells (n = 7). Horizontal lines indicate medians, boxes the IQR and whiskers the range. Groups were compared using Mann Whitney U (A) or Wilcoxon signed-rank (B) tests. Unadjusted p values are shown. ND = not done

We then asked how stable the distinct memory phenotypes and cytokine profiles of QFT^+ and QFT^- adolescents were. QFT^+ adolescents had persistently higher proportions of EM H1-specific cells throughout the trial follow-up period (Figure 40A). Conversely, H1-specific CD4 T cells consistently expressed a CM biased phenotype in QFT- adolescents, compared to QFT^+ adolescents, throughout the entire study period, with the exception on day 70 (Figure 40B). Similarly, proportions of polyfunctional IFN-γ^+TNF-α^+IL-2^+ H1-specific CD4 T cells were higher at all time points measured in QFT^+ adolescents (Figure 40C), while QFT^- adolescents had larger proportions of single IL-2 producing H1-specific CD4 T cells (Figure 40D). Interestingly, the proportions of TNF-α^+IL-2^+ cells within Th1 cytokine$^+$ H1-specific CD4 T cells steadily increased following H1:IC31 vaccination in QFT^- adolescents, but a transient increase was observed in QFT^+ adolescents (Figure 40E). Together these data suggest that underlying *M.tb* infection drives a persistent bias towards EM in H1-specific CD4 T cells response in QFT^+ adolescents, and that most QFT^+ adolescents must indeed be actively infected with *M.tb*.

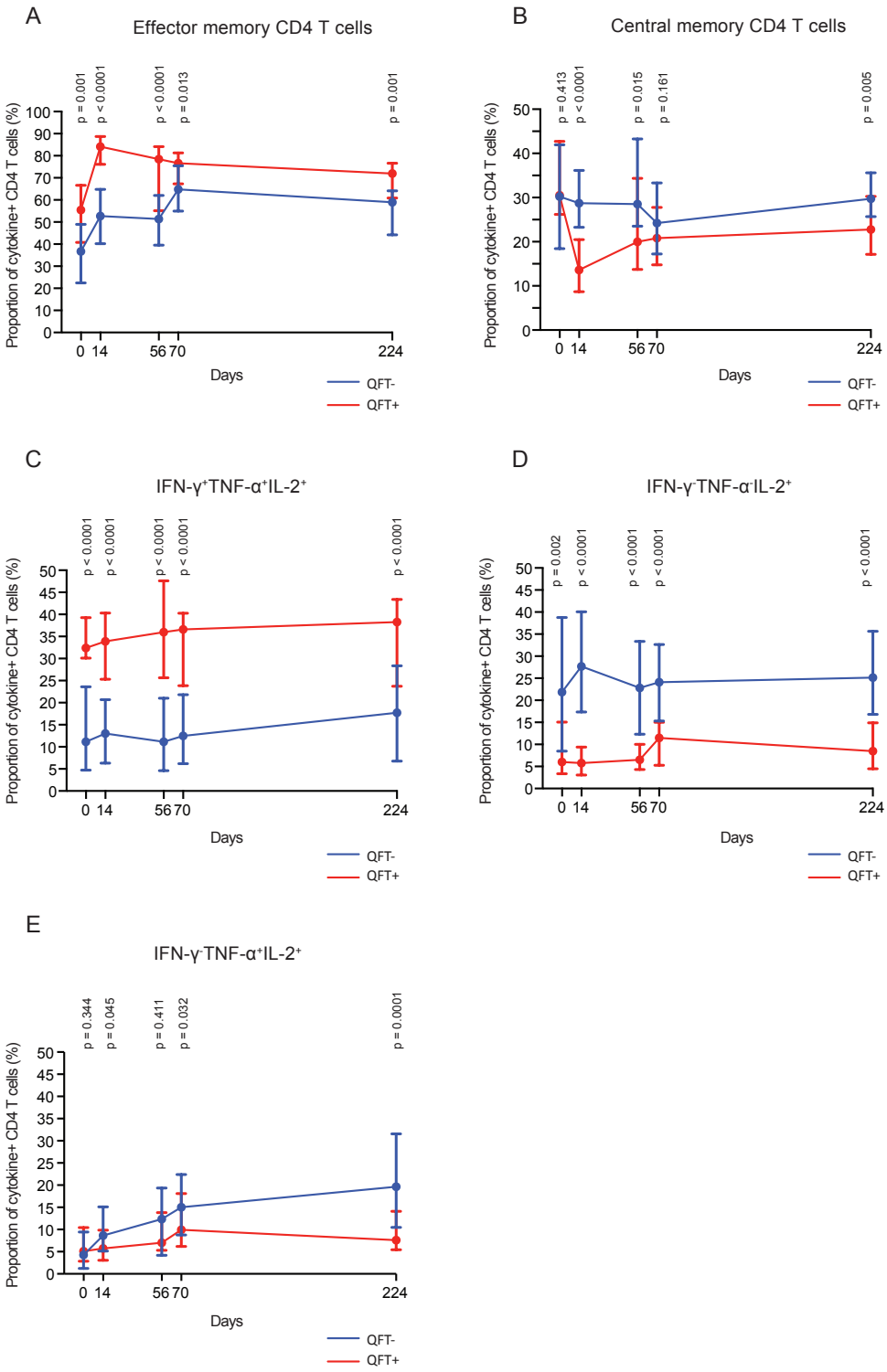

Figure 40. Memory phenotype and cytokine expression profiles of H1-specific CD4 T cells remain consistently different between *M.tb* infected and uninfected adolescents during study follow-up. Median (error bars represent IQR) proportions of Th1 cytokine$^+$ H1-specific CD4 T cells expressing (A) a CCR7-CD45RA- effector memory phenotype or (B) a CCR7+CD45RA- central memory phenotype at all trial time points in *M.tb*-infected and uninfected adolescents. Median (error bars represent IQR) proportions of (C) IFN-γ^+TNF-α^+IL-2^+, (D) IFN-γ^-TNF-α^-IL-2^+, and (E) IFN-γ^-TNF-α^+IL-2^+, H1-specific CD4 T cells following H1 vaccination at all trial time points in *M.tb*-infected and uninfected adolescents. Responses between *M.tb*-infected and uninfected adolescents were compared at each time point using the Mann Whitney U test. P values were not adjusted for multiple comparisons.

The findings that underlying *M.tb* infection biased H1-specific CD4 T cells toward an EM phenotype prompted us to investigate effects the mRNA expression profile of H1-specific CD4 T cells on day 112. We selected day 112 because we reasoned at this time point the vaccine associated activation effect would have waned. Expression of *GZMK*, *GZMA*, *CCR2*, and *CCR5*, genes associated with EM cells, was higher in QFT^{+} adolescents compared to QFT^{-} adolescents, while expression of *ICOS* and *AXIN2*, genes associated with CM cells, was higher in QFT^{-} adolescents (Figure 41A and Figure 41B). It should be noted that the q-values describing differences in expression were large. However, the transcriptomic data were again consistent with the memory phenotypes differences observed in H1-specific CD4 T cells in QFT^{-} and QFT^{+} adolescents.

Recently, results from the mouse model of *M.tb* infection have demonstrated enhanced bacterial control following a BCG prime-H1:CAF01 boost, which was associated with the maintenance of IL-2^{+} producing CM CD4 T cells during infection (Lindenstrom et al. 2013). We therefore asked if H1:IC31 vaccination induced durable changes to the cytokine profile that would be apparent at the last follow-up time point (day 224), and to determine the effect of underlying *M.tb* infection on this memory response. We compared proportions of cells producing any combination of IFN-γ, TNF-α, and/or IL-2 prior to vaccination (day 0) and after vaccination (day 224). After Bonferroni correction, only proportions of IFN-γ^{-}TNF-α^{+}IL-2^{+} H1-specific CD4 T cells in QFT^{-} adolescents were influenced in a durable manner by H1:IC31, all other subsets remain unchanged (Figure 42). Altogether these data strongly suggest that underlying *M.tb* infection in QFT^{+} adolescents drives and EM H1-specific CD4 T cell response that displays both a $CCR7^{-}CD45RA^{-}$ EM

phenotype and polyfunctional profile despite two H1:IC31 vaccinations. Underlying *M.tb* infection appeared to overwhelm any vaccine related possible changes in the cytokine profile of H1-specific CD4 T cells following H1:IC31 vaccination. By contrast, in the absence of *M.tb* infection, a novel and highly durable TNF-α^{+}IL-2^{+} CD4 T cell subset was induced by H1:IC31.

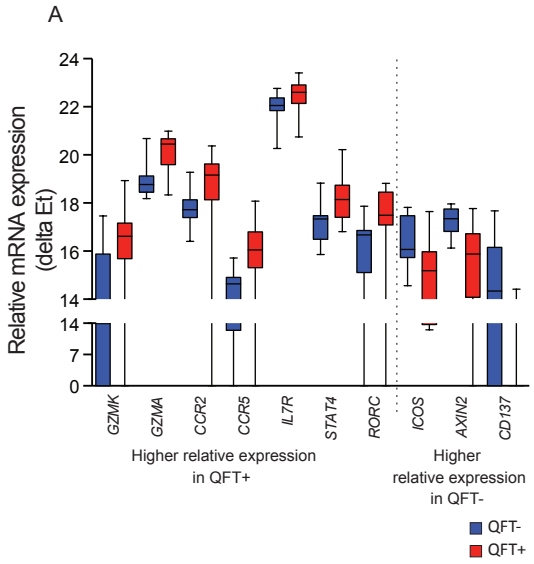

Gene Names	p value	fdr
AXIN2	0.004	0.333
GZMK (Granzyme K)	0.011	0.333
IL7R	0.047	0.420
STAT4	0.034	0.374
ICOS	0.047	0.420
CD137	0.021	0.346
RORC	0.028	0.353
CCR2	0.023	0.346
CCR5	0.008	0.333
GZMA (Granzyme A)	0.023	0.346

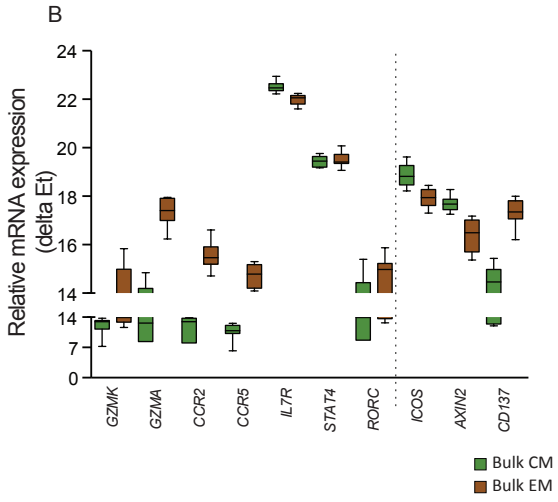

Gene Names	p value
AXIN2	0.016
GZMK (Granzyme K)	0.047
IL7R	0.016
STAT4	0.688
ICOS	0.016
CD137	0.016
RORC	0.031
CCR2	0.016
CCR5	0.016
GZMA (Granzyme K)	0.016

Figure 41. Transcriptomic analysis of circulating H1-specific CD4 T cells at day 112 following H1 vaccination. (A) Differentially expressed mRNA transcripts in HLA class II tetramer-sorted H1-specific CD4 T cells from *M.tb*-infected and uninfected adolescents on day 112 (56 days after the second vaccination). Expression levels are shown as delta Et values. Only genes with differentially expressed mRNA transcripts at $p < 0.05$ are shown. FDRs were calculated using the Benjamini-Hochberg method. (B) mRNA expression levels of those genes differentially expressed in H1-specific CD4 T cells, in sorted bulk CM (CCR7+CD45RA-) and EM (CCR7-CD45RA-) CD4 T cells (n =7). Horizontal lines indicate medians, boxes the IQR and whiskers the range. Groups were compared using the Mann Whitney U tests (A) or Wilcoxon signed-rank (B). Unadjusted p values are shown.

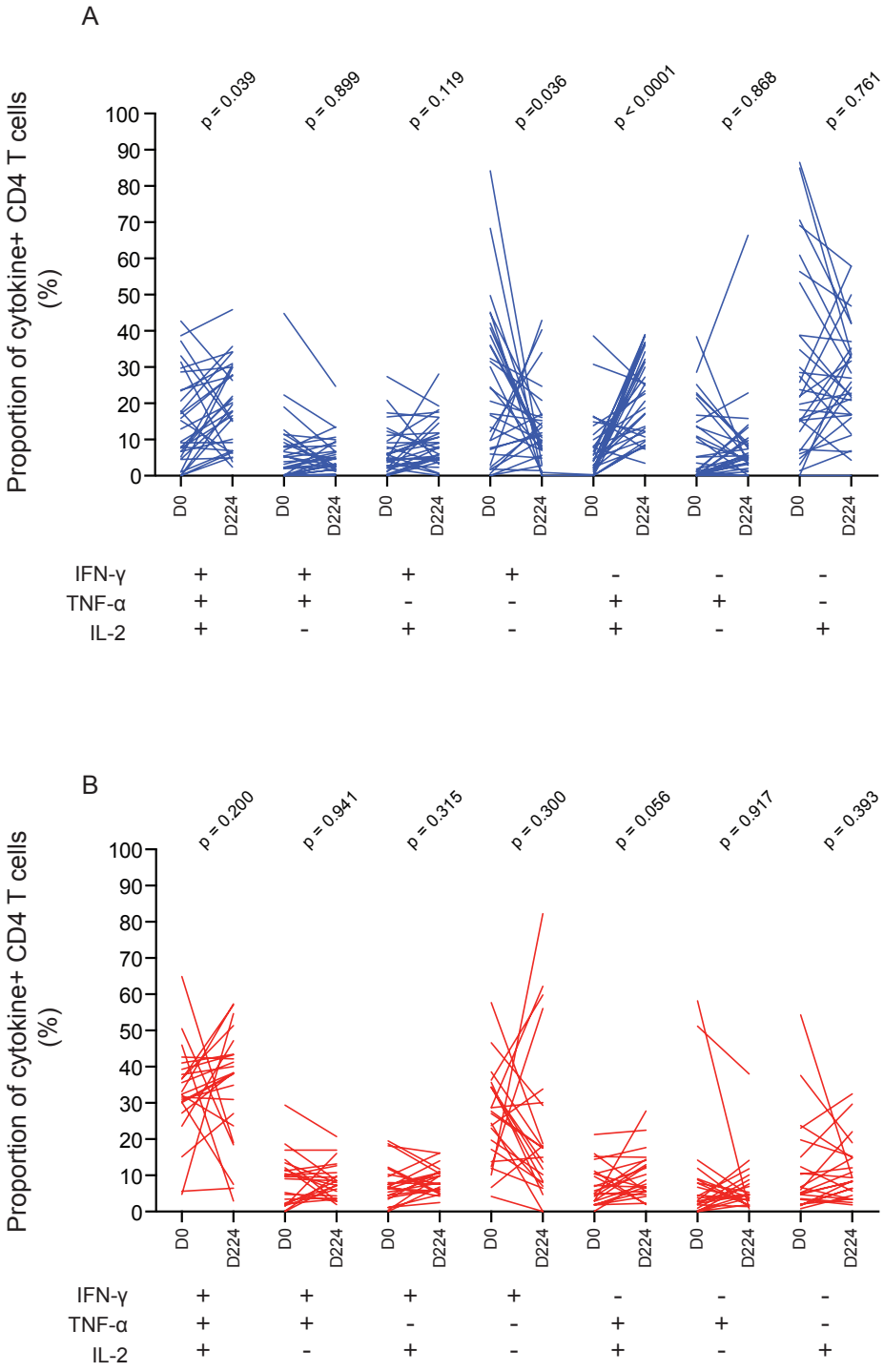

Figure 42. Long term effects of H1:IC31 vaccination on the proportions of cytokine producing subsets within the H1-specific CD4 T cell population. The proportions of H1-specific CD4 T cells co-expressing IFN-γ, TNF-α, and IL-2 in (A) uninfected and (B) *M.tb*-infected adolescents on day 0 and day 224. Groups were compared using the Wilcoxon signed-rank. Unadjusted p values are shown.

Ag85B and ESAT-6-specific CD4 T cells exhibit markedly distinct transcriptomic profiles, memory phenotypes and cytokine expression patterns in M.tb infected adolescents

Our data strongly suggests that underlying latent *M.tb* infection, and presumably *M.tb*-associated persistent antigen exposure, drive H1-specific CD4 T cells towards EM differentiation in QFT^+ adolescents. Since *M.tb* infection of mice results in higher frequencies of ESAT-6-specific CD4 T cells compared to Ag85B (Rogerson et al. 2006), we reasoned that ESAT-6 and Ag85B may be differentially contributing to the antigen driven differentiation of H1-specific CD4 T cells. To determine if *M.tb* may express ESAT-6 and Ag85B at different levels, we mined a publically available RNA expression dataset of cultured *M.tb* clinical isolates and lab adapted strains (http://www.tbdb.org/pubdata/publications//418/2885/exptsetno_2885.tar.gz) (Gao et al. 2005) and compared expression levels of *fbpB* (Ag85B) and *esat6* mRNA. *Esat6* was consistently expressed at higher levels, compared to *fbpB* in these isolates (Figure 43). Further, data from *M.tb* isolated from infected mouse lungs confirmed that at the RNA level ESAT-6 is expressed at higher levels than Ag85B in vivo (Rogerson et al. 2006; Aagaard et al. 2011). We then asked whether we could identify differences in the Ag85B and ESAT-6-specific CD4 T cell responses in QFT^+ adolescents, and to determine if differential antigen load may help explain these differences.

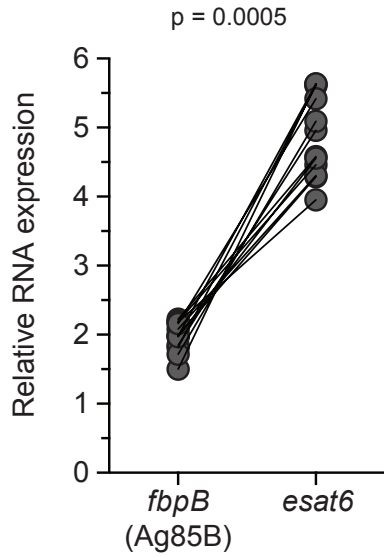

Figure 43. Higher RNA expression of ESAT-6 compared to Ag85B in *M.tb* clinical isolates. The expression levels of ESAT-6 and Ag85B RNA mined from a publically available RNA expression dataset of 7H9 broth cultured clinical isolates in the exponential phase. P value was calculated using the Wilcoxon signed-rank.

Prior to H1 vaccination baseline frequencies of Ag85B and ESAT-6-specific CD4 T cells were not different in QFT^+ adolescents (Figure 44A). However, proportions of ESAT-6-specific CD4 T cells expressing the $CCR7^-CD45RA^-$ EM phenotype at baseline appeared to be greater, compared to Ag85B-specific cells (Figure 44B). We also observed that, prior to vaccination, proportions of single IFN-γ producing ESAT-6-specific CD4 T cells appeared higher, compared to Ag85B-specific cells, while proportions of single IL-2 producing Ag85B-specific CD4 T cells were higher compared to ESAT-6 (Figure 44C).

To determine if these patterns could be confirmed, we compared the frequencies, memory phenotype, and cytokine profiles of Ag85B and ESAT-6-specific CD4 T cells in QFT^+ adolescents in Groups 2, 3, and 4. Frequencies of Ag85B and ESAT-6-specific cells prior to vaccination were not different (Figure 45A). In contrast to Group 1, adolescents in Groups 2, 3, and 4 had similar proportions of Ag85B and

ESAT-6-specific cells expressing the EM phenotype, but Ag85B-specific cells had a larger proportion of $CCR7^{+}CD45RA^{+}$ "naïve-like" cells (Figure 45B), suggesting a similar pattern of more differentiated ESAT-6-specific cells. Lastly, ESAT-6-specific CD4 T cells had larger proportions of polyfunctional IFN-γ^{+}TNF-α^{+}IL-2^{+} cells, while Ag85B-specific cells had higher proportions of single IL-2 producing cells (Figure 45C). Together these data support the hypothesis that differential expression of Ag85B and ESAT-6 during *M.tb* infection may preferentially activate and drive differentiation of ESAT-6-specific cells, while Ag85B-specific cells were exposed to antigen at a much lower level. We then sought to determine if these effects were detectable after H1:IC31 vaccination.

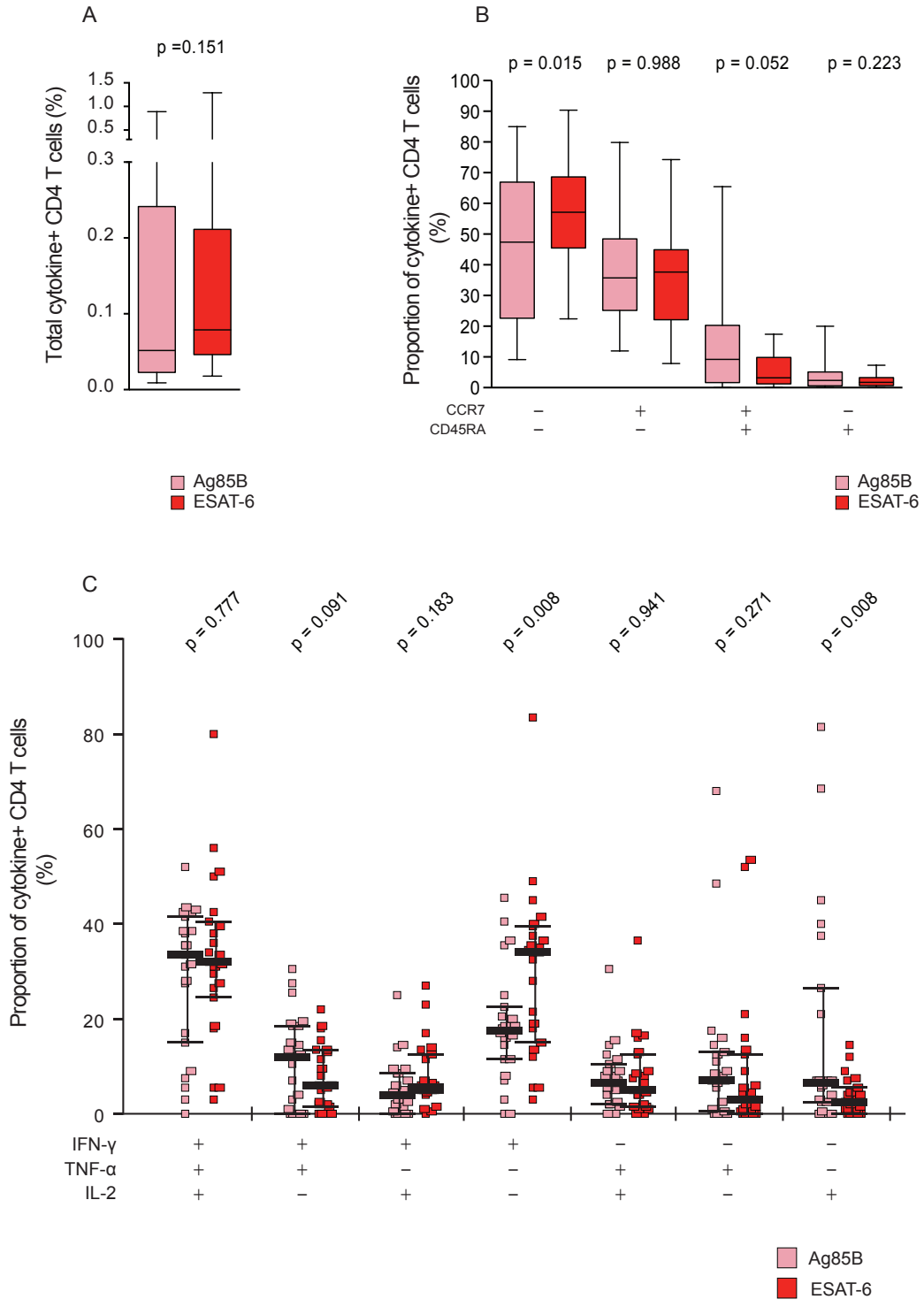

Figure 44. Baseline characteristics of Ag85B and ESAT-6-specific CD4 T cell response in QFT$^+$ adolescents in Group 1 prior to vaccination. (A) Total frequency of Th1 cytokine+ CD4 T cells in QFT+ adolescents on day 0. Proportion of Th1 cytokine+ Ag85B and ESAT-6-specific CD4 T cells expressing each combination of (B) CCR7 and CD45RA or (C) IFN-γ, TNF-α, and/or IL-2. P values were calculated using the Wilcoxon signed-rank test. Unadjusted p values are shown.

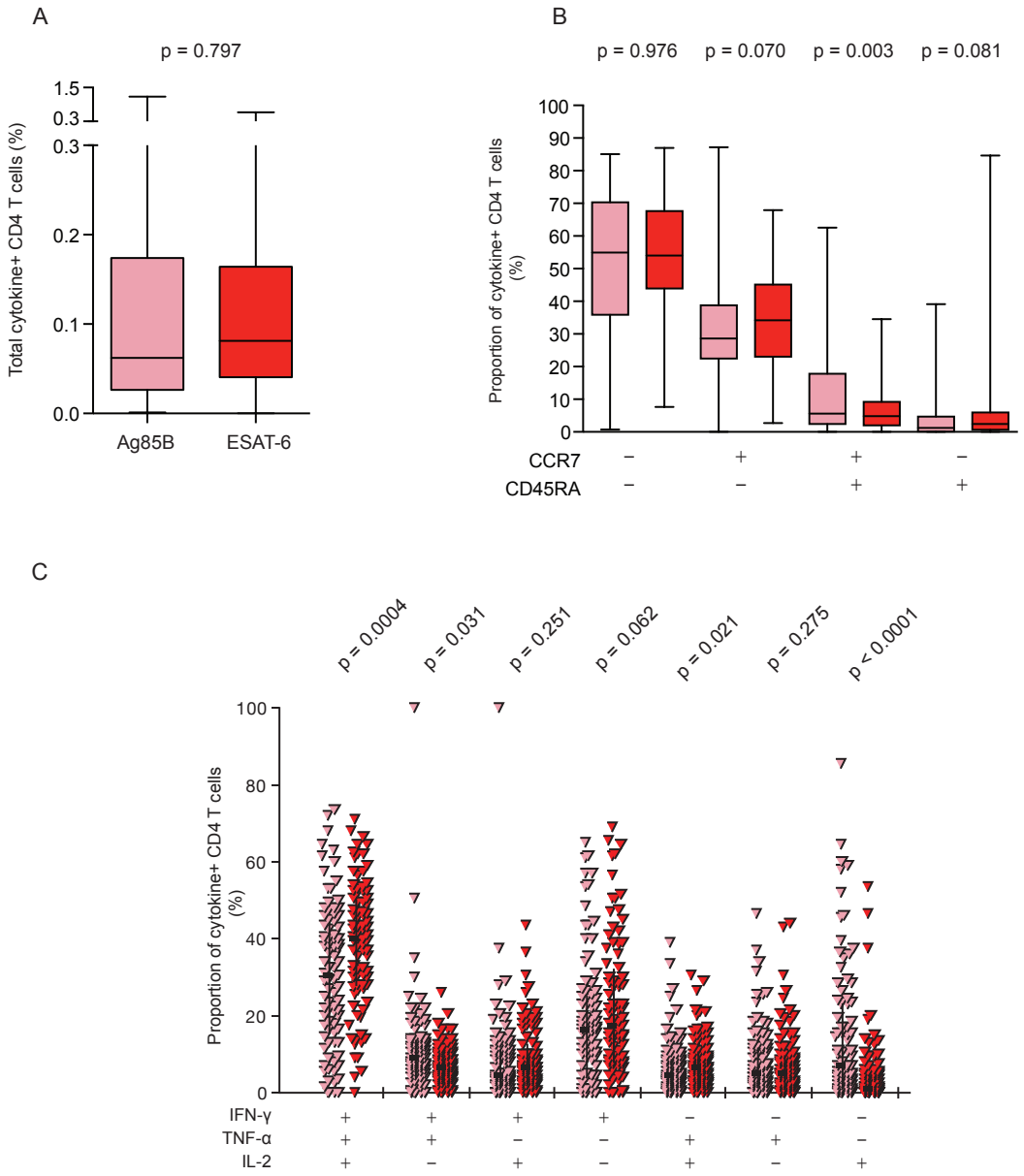

Figure 45. Baseline characteristics of Ag85B and ESAT-6-specific CD4 T cell response in QFT$^+$ adolescents in Groups 2, 3, and 4 prior to vaccination. (A) Total frequency of Th1 cytokine+ CD4 T cells in QFT+ adolescents on day 0. Proportion of Th1 cytokine+ Ag85B and ESAT-6-specific CD4 T cells expressing each combination of (B) CCR7 and CD45RA or (C) IFN-γ, TNF-α, and/or IL-2. P values were calculated using the Wilcoxon signed-rank test. Unadjusted p values are shown.

Following primary vaccination distinct characteristics of Ag85B and ESAT-6-specific CD4 T cells were observed in QFT$^+$ adolescents. Primary H1 vaccination induced a higher frequency of ESAT-6 specific CD4 T cells compared to Ag85B-specific cells ($p < 0.0001$) (Figure 33A). Furthermore, ESAT-6 and Ag85B-specific CD4 T cells had distinct transcriptomic profiles after primary H1:IC31 vaccination (Figure 46A). Interestingly, *GZMA*, ICOS, *CAMK4*, and *LEF1* were among the genes differentially

expressed in Ag85B and ESAT-6-specific CD4 T cells. We had already established that bulk EM cells expressed *GZMA* at higher levels, compared to CM, while CM cells expressed *ICOS* and *CAMK4* at higher levels, compared to EM. We then compared the expression of the transcription factor, *LEF1* in bulk CM and EM cells. *LEF1* was expressed at a higher level in CM compared to EM cells ($p = 0.016$ unadjusted p value). It must be noted that unlike the comparison of transcriptomic differences following primary vaccination between H1-specific CD4 T cells in QFT^{-} and QFT^{+} (Figure 37B), many of the genes that were differentially expressed between Ag85B and ESAT-6-specific cells were not differentially expressed between bulk CM and EM cells.

However, following primary vaccination ESAT-6-specific CD4 T cells had larger proportions of cells expressing an EM phenotype compared to Ag85B-specific cells, while Ag85B-specific cells had larger proportions of cells expressing a CM and "naïve" phenotypes after Bonferroni correction (Figure 46B). Proportions of IFN-γ^{+}TNF-α^{+}IL-2^{-} within the ESAT-6-specific CD4 T cells was also greater than those of Ag85B-specific cells, (Figure 46C), while polyfunctional IFN-γ^{+}TNF-α^{+}IL-2^{+} and single IFN-γ producing cells predominated the ESAT-6-specific CD4 T cell response. Finally, Ag85B-specific cells were characterised by larger proportions of IFN-γ^{-}TNF-α^{+}IL-2^{+} and single IL-2 producing CD4 T cells (Figure 46C).

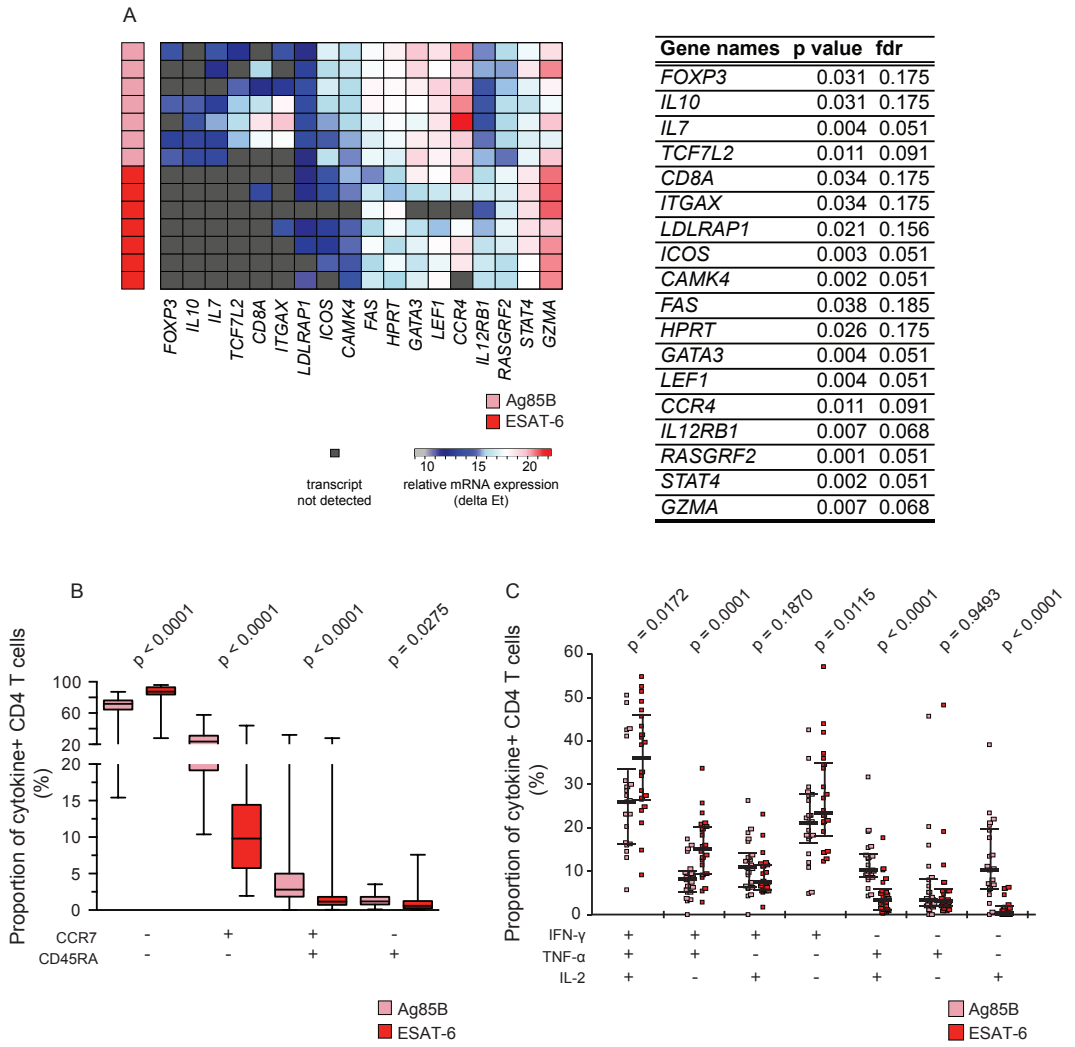

Gene names	p value	fdr
FOXP3	0.031	0.175
IL10	0.031	0.175
IL7	0.004	0.051
TCF7L2	0.011	0.091
CD8A	0.034	0.175
ITGAX	0.034	0.175
LDLRAP1	0.021	0.156
ICOS	0.003	0.051
CAMK4	0.002	0.051
FAS	0.038	0.185
HPRT	0.026	0.175
GATA3	0.004	0.051
LEF1	0.004	0.051
CCR4	0.011	0.091
IL12RB1	0.007	0.068
RASGRF2	0.001	0.051
STAT4	0.002	0.051
GZMA	0.007	0.068

Figure 46. ESAT-6-specific CD4 T cells display markedly more effector-like characteristics than Ag85B-specific CD4 T cells following H1:IC31 vaccination. (A) Supervised heatmap showing differentially expressed mRNA transcripts in HLA class II tetramer-sorted Ag85B-specific and ESAT-6-specific CD4 T cells from QFT+ adolescents on day 14. Expression levels are shown as delta Et values. Only genes with differentially expressed mRNA transcripts at $p < 0.05$ were included. FDRs were calculated using the Benjamini-Hochberg method. (B) Proportions of Th1-cytokine+ Ag85B-specific and ESAT-6-specific CD4 T cells displaying each combination of CCR7 and CD45RA expression in QFT+ adolescents on day 14. Horizontal lines indicate medians, boxes the IQR and whiskers the range. (C) Median (error bars denote IQR) proportions of Ag85B and ESAT-6-specific CD4 T cells producing each combination of IFN-γ, TNF-α, and IL-2 in QFT+ adolescents on day 14. Groups were compared using the Mann Whitney U tests (A) or Wilcoxon signed-rank (B and C). Unadjusted p values are shown (B and C).

These response characteristics were remarkably durable. Proportions of EM ESAT-6-specific CD4 T cells remained higher than Ag85B-specific cells while the proportion of CM Ag85B-specific CD4 T cells remained higher compared to ESAT-6-specific cells throughout trial follow-up (Figure 47A and Figure 47B). Polyfunctional IFN-γ^{+}TNF-α^{+}IL-2^{+} cells were also preferentially associated with ESAT-6-specific CD4 T cells compared to Ag85B-specific cells (Figure 47C). Proportions of IFN-γ^{-}TNF-α^{+}IL-2^{+} and IFN-γ^{-}TNF-α^{-}IL-2^{+} Ag85B-specific CD4 T cells remained higher than ESAT-6-specific CD4 T cells throughout follow-up (Figure 47D and Figure 47E). Although proportions of IFN-γ^{+}TNF-α^{+}IL-2^{-} and IFN-γ^{+}TNF-α^{-}IL-2^{-} were different between Ag85B and ESAT-6-specific CD4 T cells on day 14, these differences did not persist throughout the study period (Appendix Figure 3A and 3B). We confirmed these distinct patterns in ESAT-6 and Ag85B-specific CD4 T cells using data from QFT+ adolescents enrolled in Group 3 of the H1:IC31 trial, who received a single 15μg dose of H1:IC31 (Figure 48) as well as QFT^{+} adults who participated in a phase I trial of H56:IC31 also conducted at the SATVI field site and analysed using the same antibody panel and qualified whole blood ICS assay (Luabeya et al. 2015; Kagina et al. 2015) (Figure 49). Together, these data suggest that individuals with latent *M.tb* infection have qualitatively different ESAT-6 and Ag85B-specific CD4 T cell responses that appear to be unaffected by vaccination. These differences may be associated with differential exposure to antigen load.

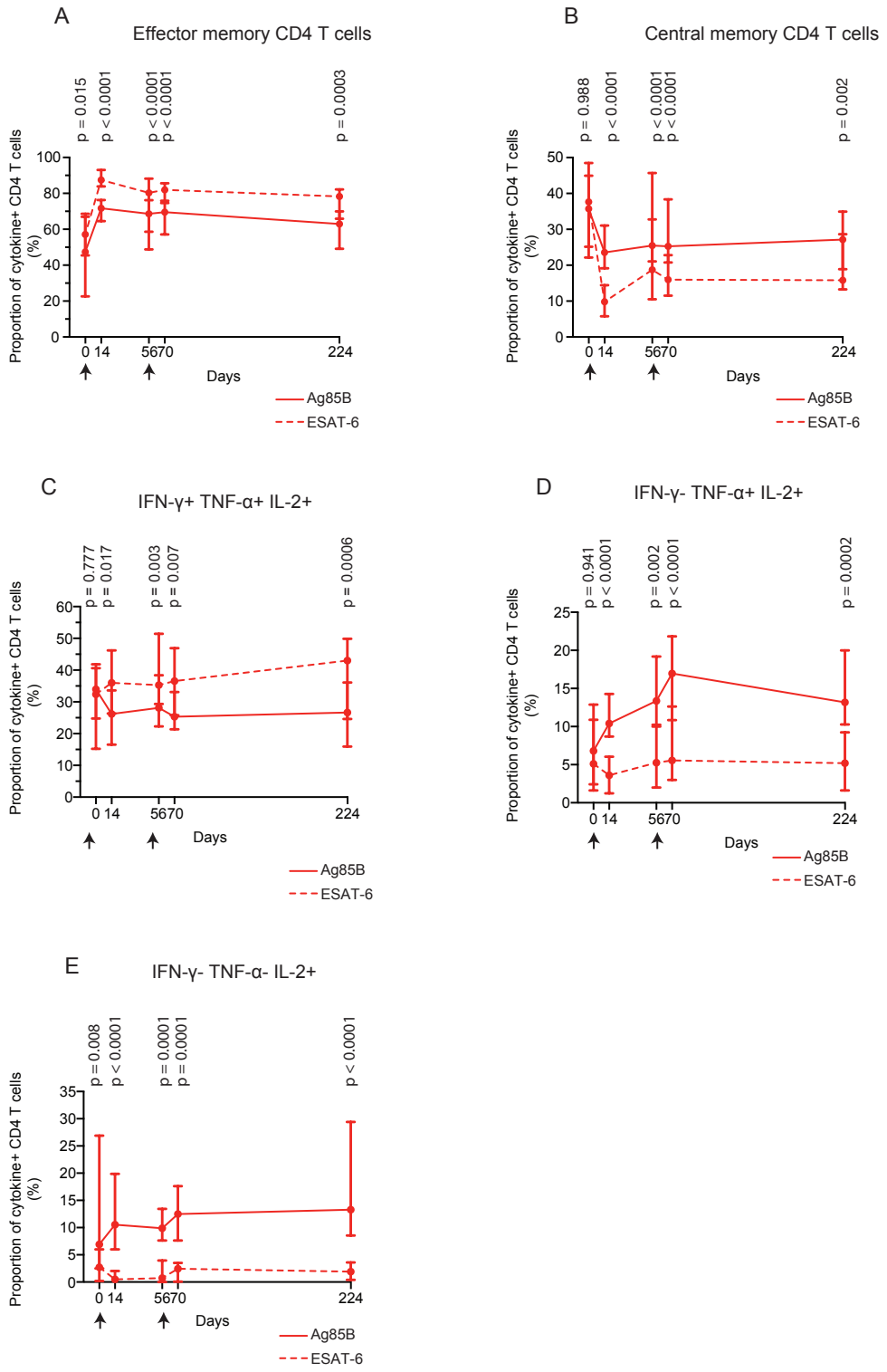

Figure 47. Memory phenotype and cytokine co-expression profiles of ESAT-6 and Ag85B-specific CD4 T cells in QFT+ adolescents are consistently different throughout the follow-up period. Median (error bars denote IQR) proportions of cytokine+ Ag85B-specific and ESAT-6-specific CD4 T cells expressing a (A) CCR7-CD45RA-effector memory phenotype, (B) a CCR7+CD45RA-central memory phenotype in *M.tb*-infected adolescents. Median (error bars denote IQR) proportions of Ag85B-specific and ESAT-6-specific (C) IFN-γ^+ TNF-α^+ IL-2^+, (D) IFN-γ^- TNF-α^+ IL-2^+, (E) IFN-γ^- TNF-α^- IL-2^+ CD4 T cells following H1:IC31 vaccination. P values were calculated using the Wilcoxon signed-rank test. Unadjusted p values are shown. The arrows indicated the days when H1:IC31 was given.

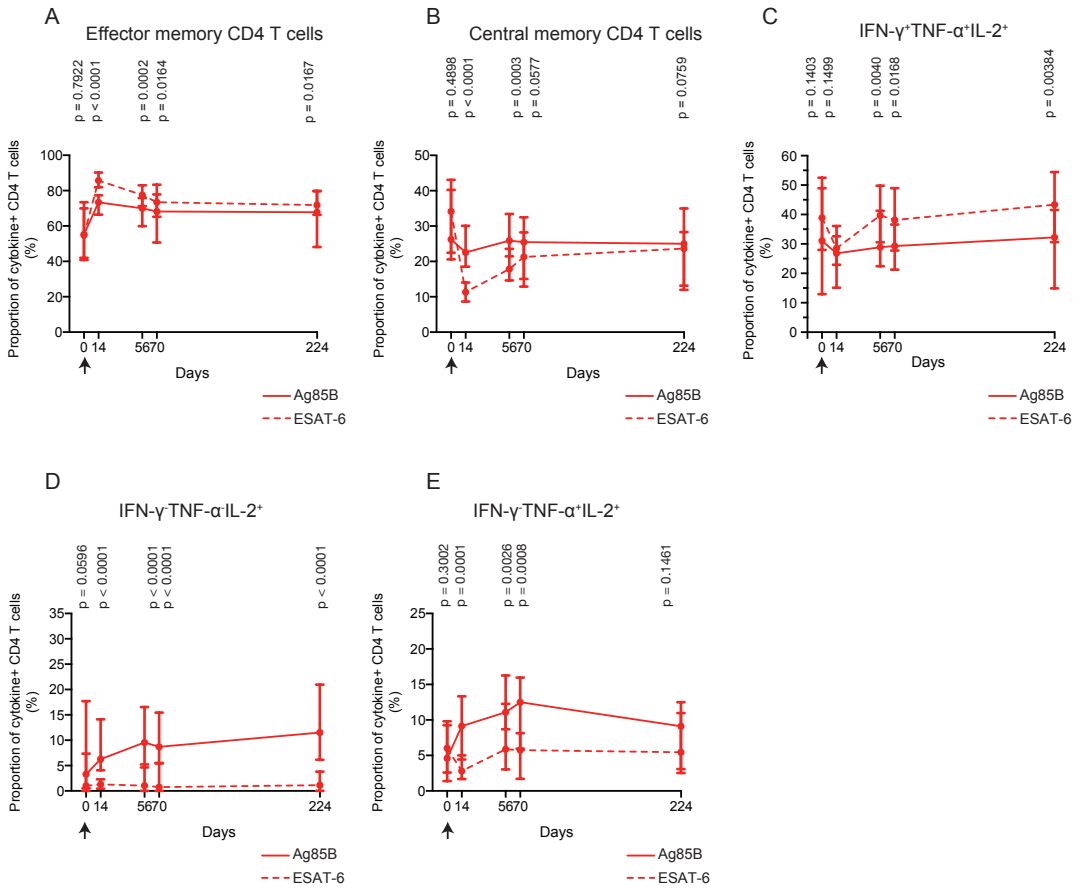

Figure 48. Confirmation that ESAT-6-specific CD4 T cells display markedly more effector-like characteristics than Ag85B-specific CD4 T cells in QFT+ adolescents enrolled in Group 3 of THYB-04 vaccine trail (*refer to consort Figure 23*). The proportions of cytokine+ Ag85B-specific and ESAT-6-specific CD4 T cells expressing the (A) CCR7-CD45RA-effector memory phenotype, (B) a CCR7+CD45RA-central memory phenotype (C) IFN-γ^+ TNF-α^+ IL-2^+, (D) IFN-γ^- TNF-α^+ IL-2^+, and (E) IFN-γ^- TNF-α^- IL-2^+ in QFT+ adolescents in Group 3. P values were calculated using the Wilcoxon signed-rank test. Unadjusted p values are shown. The arrows indicated the days when H1:IC31 was given.

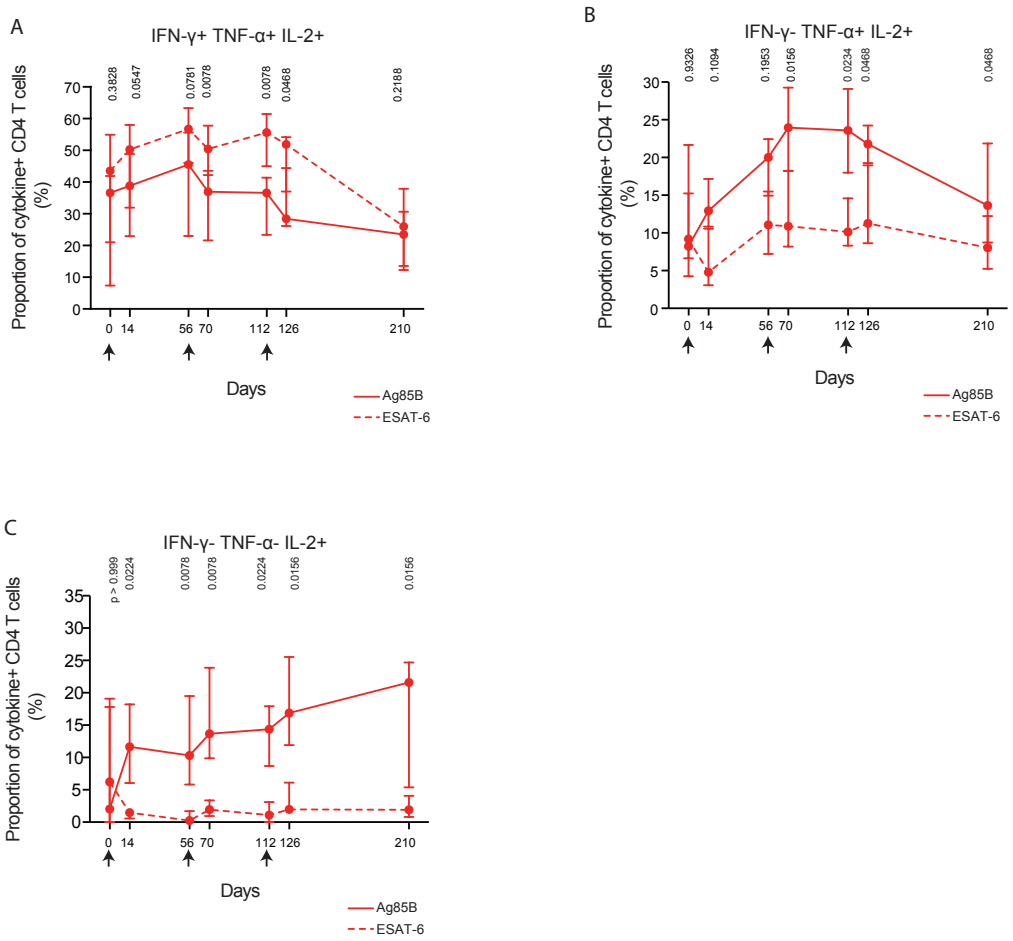

Figure 49. Confirmation that ESAT-6-specific CD4 T cells display markedly more effector-like characteristics than Ag85B-specific CD4 T cells in QFT+ adults vaccinated with H56:IC31 (Luabeya et al. 2015). The trial was registered on ClinicalTrials.gov (NCT01967134). The proportions of Ag85B-specific and ESAT-6-specific CD4 T cells expressing (A) IFN-γ^+ TNF-α^+ IL-2^+, (B) IFN-γ^- TNF-α^+ IL-2^+, and (C) IFN-γ^- TNF-α^- IL-2^+ in QFT+ adults vaccinated with H56. P values were calculated using the Wilcoxon signed-rank test. Unadjusted p values are shown. The arrows indicated the days when H56:IC31 was given.

In the absence of infection, H1:IC31 vaccination induced durable changes in H1-specific CD4 T cells in QFT$^-$ adolescents only (Figure 42A). Additionally, ESAT-6-specific CD4 T cells appeared to drive the effector response in infected adolescents. As such, we sought to determine if durable changes to the H1-specific response due to H1:IC31 vaccination were masked by the ESAT-6-specific response in QFT$^+$ adolescents (Figure 42B). We reasoned that lower expression of Ag85B during *M.tb* infection would make the Ag85B-specific response more malleable to modification by H1:IC31 vaccination in QFT$^+$ adolescents, compared to the ESAT-6-specific

response. We had previously observed that H1:IC31 vaccination increased proportions of TNF-α^+IL-2^+ H1-specific CD4 T cells in QFT^- adolescents, but no durable changes were observed in QFT^+ adolescents (Figure 42). However, when we compared Ag85B-specific CD4 T cells on day 224 to baseline in QFT^+ adolescents, proportions of IFN-γ^+IL-2^+ increased and there was also a trend toward increased proportions of TNF-α^+IL-2^+ cells ($p = 0.030$ and $p = 0.070$, respectively, adjusted p values) (Figure 50A). By contrast, and in agreement with our earlier observations, no differences were observed in cytokine profiles of ESAT-6-specific CD4 T cells on day 224, compared to baseline (Figure 50B).

The cytokine profiles of Ag85B-specific CD4 T cells in QFT^- and QFT^+ adolescents on day 224 were not markedly different in Group 1; none remained significant following Bonferroni correction (Figure 51A). However, in Groups 2, 3, and 4 the cytokine profiles of Ag85B-specific on day 224 in QFT^- and QFT^+ were different. QFT^+ adolescents had higher proportions of IFN-γ^+TNF-α^+IL-2^+ Ag85B-specific CD4 T cells, while proportions of TNF-α^+IL-2^+ and single IL-2^+ Ag85B-specific cells were higher in QFT^- adolescents (Figure 51B). Proportions of other cytokine subsets in Ag85B-specific CD4 T cells were not different in QFT^- and QFT^+ adolescents (data not shown). Proportions of IFN-γ^+TNF-α^+IL-2^+ were higher in ESAT-6-specific CD4 T cells, compared to Ag85B-specific cells in QFT^+ adolescents in Groups 2, 3, and 4 on day 224, while proportions of TNF-α^+IL-2^+ and single IL-2^+ were higher in Ag85B-specific CD4 T cells (Figure 51B). Altogether, these results suggest that underlying *M.tb* infection biased both Ag85B and ESAT-6 towards more a more EM phenotype, but the ESAT-6-specific response is predominantly responsible for driving the EM biased H1-specific response observed in QFT^+

adolescents.

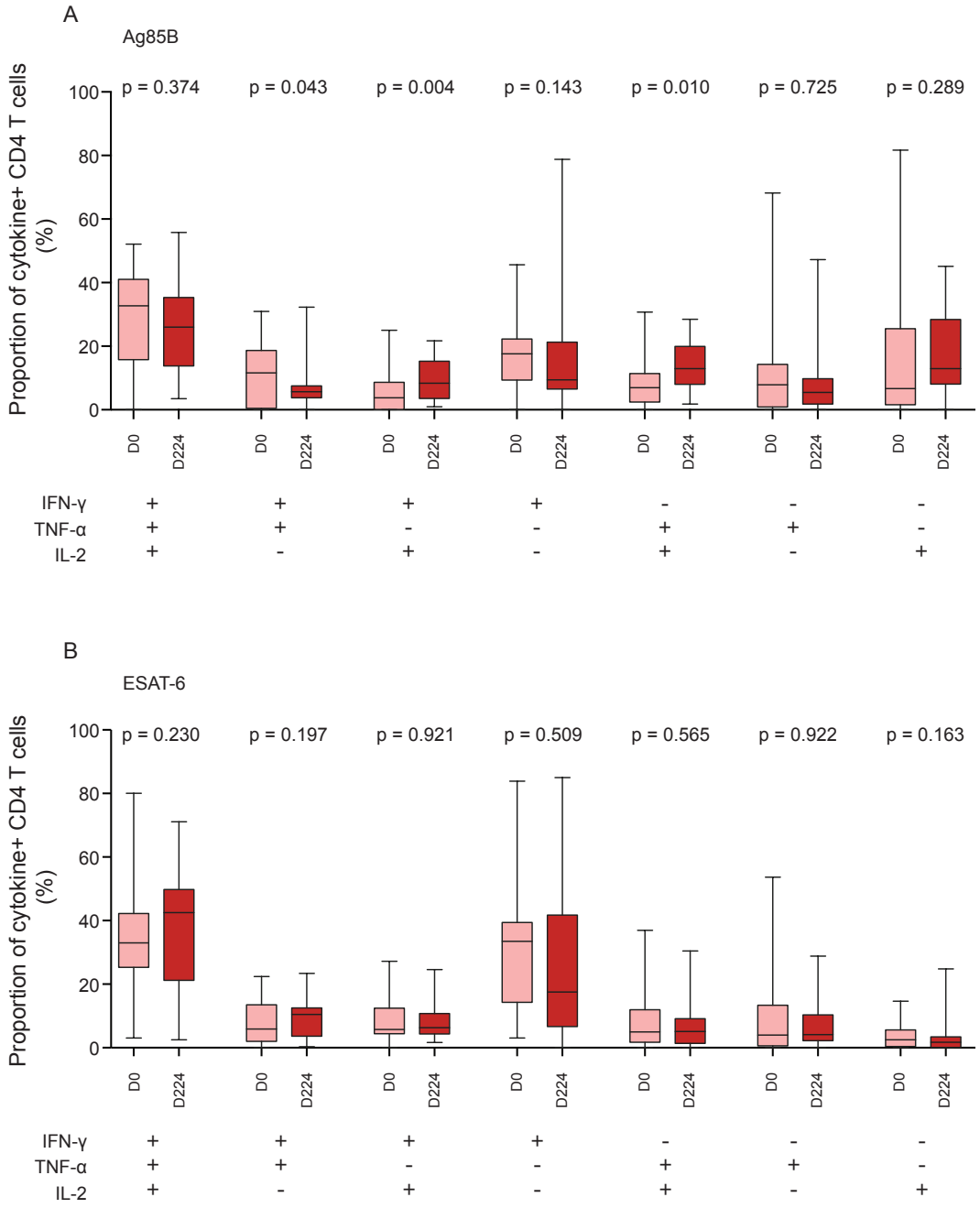

Figure 50. H1:IC31 induces durable changes in Ag85B but not ESAT-6-specific CD4 T cells in QFT$^+$ adolescents. Proportions of (A) Ag85B or (B) ESAT-6-specific CD4 T cells co-expressing IFN-γ, TNF-α, and IL-2 in QFT$^+$ adolescents on day 0 and day 224. Groups were compared using the Wilcoxon signed-rank. Unadjusted p values are shown.

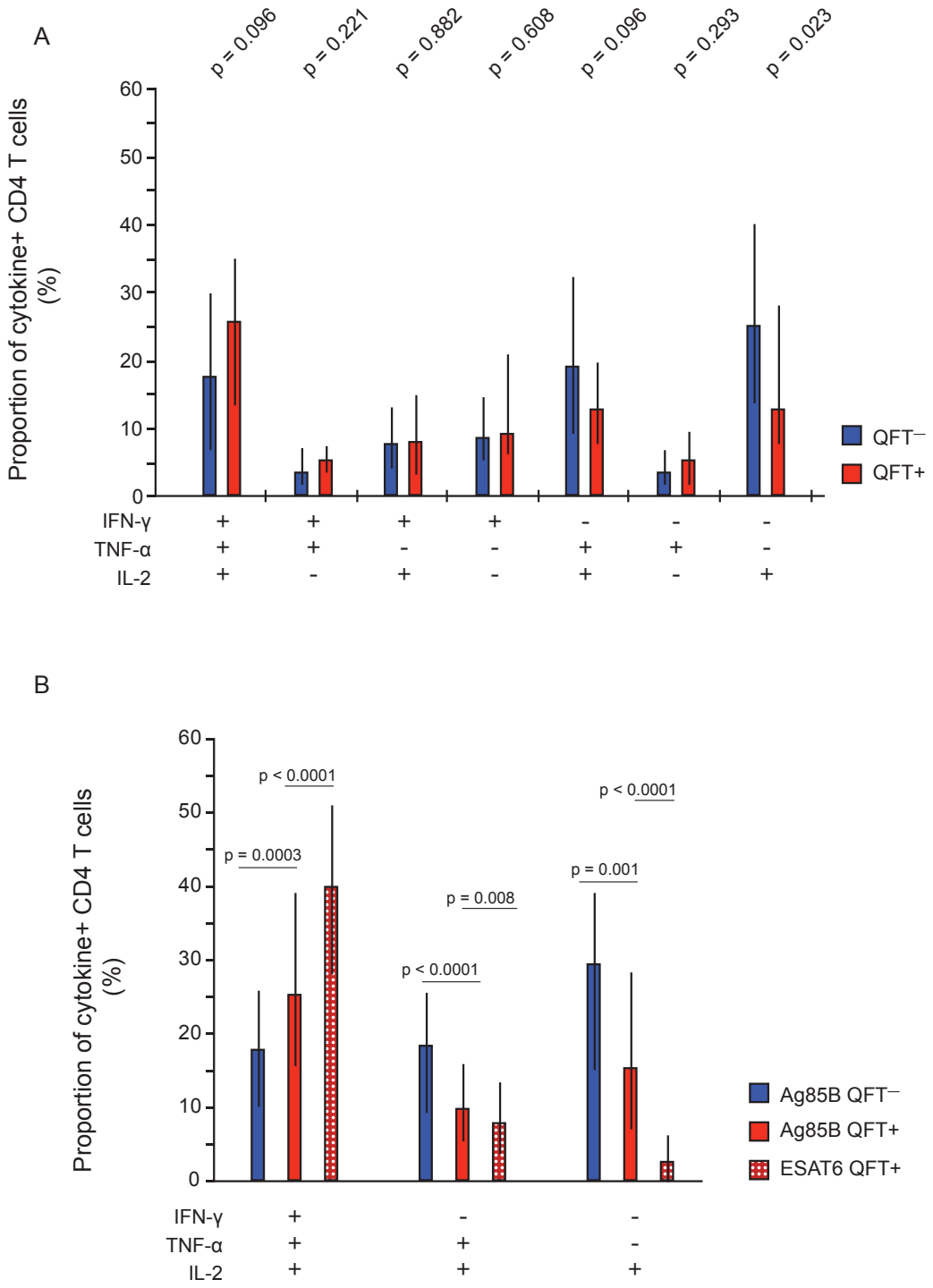

Figure 51. The cytokine profiles of Ag85B-specific CD4 T cells in QFT^{-} and QFT^{+} adolescents on day 224 are not different. (A) Relative proportions of Ag85B-specific CD4 T cells expressing each combination of IFN-γ, TNF-α, and/or IL-2 in QFT^{-} and QFT^{+} adolescents in Group 1 on day 224. (B) Relative proportions of IFN-γ^{+}TNF-α^{+}IL-2^{+}, TNF-α^{+}IL-2^{+} or single IL-2^{+} Ag85B-specific CD4 T cells in QFT^{-} adolescents and Ag85B and ESAT-6 in QFT^{+} adolescents in Groups 2, 3, and 4. Bars indicate medians and error bars indicate IQR. P-values were calculated using the Mann Whitney U test to compare Ag85B-specific responses in QFT^{-} and QFT^{+} adolescents and the Wilcoxon singed-rank test was used to compare Ag85B and ESAT-6 responses in QFT^{+} adolescents. P values are unadjusted for multiple comparisons.

Discussion

The overall aim of this chapter was to investigate the characteristics of mycobacteria-specific CD4 T cells induced by the H1:IC31 vaccine and to determine the effects of underlying infection. To achieve this, we combined the whole blood ICS assay, a qualified assay routinely used in our lab (Kagina et al. 2015; Hanekom et al. 2004) to measure vaccine immunogenicity, and a microfluidic high throughput qPCR assay to perform an in-depth transcriptomic analysis of H1:IC31 induced CD4 T cells in adolescents with and without latent *M.tb* infection. We found that underlying *M.tb* infection had profound and durable effects on the H1-specific CD4 T cells, which appeared to overpower functional and phenotypic effects of vaccination. Results from our analysis revealed the following: (1) There was a durable increase in frequencies of H1-specific CD4 T cells following vaccination in uninfected adolescents and a marginal increase in infected adolescents. (2) Underlying *M.tb* infection appeared to drive differentiation of H1-specific CD4 T cells to an effector-like phenotype and function. (3) The profile of cytokine production within the H1-specific CD4 T cell population remained remarkably stable after vaccination in infected adolescents, while in uninfected adolescents a durable TNF-α^{+}IL-2^{+} subset emerged after vaccination. (4) In *M.tb* infected adolescents ESAT-6-specific CD4 T cells displayed markedly more effector-like characteristics than Ag85B-specific CD4 T cells, and appears to drive the differences observed between infected and uninfected adolescents.

A previous trial that compared the H1-specific responses in *M.tb* infected and uninfected adults showed similar kinetics to the kinetics we observed. The investigators showed that primary vaccination induced higher frequencies of H1-

specific T cells in latently infected persons compared to uninfected persons (van Dissel et al. 2011). Similarly, a more recent study performed by colleagues at SATVI also demonstrated higher frequencies of H56-specific CD4 T cells following primary H56:IC31 vaccination in latently infected adults, compared to uninfected adults (Luabeya et al. 2015). The higher frequencies of H1-specific CD4 T cells in infected individuals following vaccination suggest that the H1-specific CD4 T cell population in infected persons is more poised to rapidly expand upon vaccination. Level of antigen exposure is known to influence the differentiation of memory CD4 T cells, with higher levels of antigen exposure associated with EM, compared to CM (Farber et al. 2013). A common model suggests division of labor between the EM and CM cells, with EM exhibiting rapid effector functions following antigen recall, while CM display delayed acquisition of effector function, but have a greater proliferative potential (Sallusto et al. 2004).

It is likely that persistent antigen exposure during latent infection chronically stimulates H1-specific CD4 T cells and resulting in preferential differentiation of EM cells in latently infected adolescents. The presence of a larger proportion of single IL-2 producing H1-specific CD4 T cells in uninfected adolescents likely reflects less sustained antigen exposure and maintenance of CM cells supports this interpretation. We therefore conclude that the higher frequency of H1-specific CD4 T cells following primary vaccination in *M.tb* infected compared to uninfected adolescents, reflects the higher proportion of EM H1-specific CD4 T cells in infected adolescents prior to vaccination. Furthermore, the lack of significant boosting following secondary vaccination in infected adolescents likely reflects the reduced proliferative capacity of these effector cells or alternatively, greater induction of negative signaling

in the face of heightened antigen stimulation. By contrast, the presence of a less differentiated H1-specific CD4 T cell memory population in uninfected adolescents is more amenable to significant boosting following secondary H1:IC31 vaccination. Notably, H1-specific CD4 T cells from infected adolescents did not show signs of functional exhaustion, even after two doses of H1:IC31, as a large proportion of cells remained polyfunctional, and few re-expressed CD45RA, a marker of terminally differentiated T cells (Henson et al. 2012).

We observed a vaccine induced durable increase in the proportions of H1-specific TNF-α^{+}IL-2^{+} only in QFT^{-} adolescents, while there was a trend towards increased proportions of Ag85B-specific TNF-α^{+}IL-2^{+} in QFT^{+} adolescents. This is consistent with a murine study of H1 vaccination. H1:CAF01 boosting of a BCG primed response in mice resulted in improved maintenance of memory IFN-γ^{+}TNF-α^{+}IL-2^{+} triple cytokine positive and TNF-α^{+}IL-2^{+} double cytokine positive subsets, and mice that received the boost had reduced bacterial burdens (Lindenstrom et al. 2013). In a recent phase I trial, we observed that antigen-specific TNF-α^{+}IL-2^{+} CD4 T cells had a dominant CM phenotype following three doses of H56:IC31 in QFT^{-} and QFT^{+} adults (Luabeya et al. 2015). However, in the current H1 adolescent trial, TNF-α^{+}IL-2^{+} cells predominantly expressed the EM phenotype (Appendix 4). It is not clear why the data from these two trials is not consistent. It should be noted that the study populations were different (adults vs. adolescents) and in the H56:IC31 study adults received three doses of vaccines, while in the current trial adolescent received two doses of H1:IC31.

Interestingly, our transcriptomic analysis of H1-specific CD4 T cells revealed that

following primary vaccination PD-1, ICOS, and IL-21 mRNA transcripts were expressed at higher levels in uninfected adolescents compared to infected adolescents. This was intriguing because expression of these markers is typically associated with T follicular helper cells (Tfh) (Pratama & Vinuesa 2014). A subset of *M.tb*-specific CD4 T cells expressing PD-1 but not KLRG1 has been associated with better control of *M.tb* in mice (Reiley et al. 2010; Moguche et al. 2015; Sakai et al. 2014). These cells also display a greater potential to migrate to the lung parenchyma and greater proliferative capabilities during infection. One of these studies performed a comprehensive characterization of this subset, and showed that these cells also expressed ICOS, shared features of Tfh, such as dependence on Bcl-6 expression, and also memory T cells, such as persistence in the absence of antigen and generating a heterogeneous pool of antigen-specific cells during the recall response (Moguche et al. 2015). The functional capability to generate a diverse pool of antigen-specific cells suggests that PD-1^{+}KLRG1^{-} cells are not terminally differentiated and may be important in the generation of effector CD4 T cells during antigen recall. Indeed, in mice that received a BCG prime-H1:CAF01 boost, a subset of KLRG1^{-} CM cells was associated with improved control of *M.tb* infection. The authors proposed that the enhanced control mediated by these memory cells likely stemmed from resistance to functional exhaustion and replenishment of effector T cells during chronic infection (Lindenstrom et al. 2013). These data support the hypothesis that CM response we observed in QFT^{-} adolescents share functional, transcriptomic, and phenotypic features with ICOS/Bcl-6-dependent PD-1^{+} CM cells described in mice.

Although we did not measure surface expression of PD-1, ICOS, or KLRG1 on H1-

specific CD4 T cells, in a previous clinical trial the cell surface expression of PD-1 on antigen-specific CD4 T cells was measured following vaccination with the subunit vaccine, M72/AS01$_E$. Interestingly, at 7 days post-vaccination PD-1 expression was higher in uninfected adolescents compared to adolescents with latent *M.tb* infection (Penn-Nicholson, Geldenhuys, et al. 2015). Surface expression levels of PD-1, as measured by MFI on M72-specific CD4 T cells, prior to a second M72/AS01$_E$ vaccination, strongly correlated with the fold increase in the frequency of M72-specific CD4 cells (Appendix Figure 5). It is tempting to speculate that in addition to having a larger proportion of cells that display a classical CM phenotype (i.e. CCR7$^+$CD45RA$^-$) prior to secondary vaccination, uninfected adolescents also possessed a larger proportion of cells that display this recently described PD-1$^+$ICOS$^+$KLRG1$^-$ CM-like phenotype. More detailed investigations at the single cell level will be required to determine if PD-1$^+$ICOS$^+$BCL-6$^+$KLRG1$^-$ memory cells are also present in humans.

Lastly, we observed qualitative differences in the Ag85B and ESAT-6-specific CD4 T cell response in *M.tb* infected adolescents. Although, not pronounced prior to H1:IC31 vaccination, ESAT-6-specific cells had more differentiated EM properties, compared to Ag85B-specific cells. This difference was confirmed using data from a separate group of *M.tb* infected adolescents enrolled in the H1:IC31 trial and an independent cohort of *M.tb* infected adults (Luabeya et al. 2015). The differences observed in response to Ag85B and ESAT-6 likely reflects differential expression of these proteins during *M.tb* infection. While the expression patterns in the human lung is currently unknown, expression of ESAT-6 RNA transcripts is significantly higher than Ag85B transcripts in the lungs of infected mice (Rogerson et al. 2006; Aagaard

et al. 2011). Higher frequencies of ESAT-6-specific CD4 T cells than Ag85B-specific CD4 T cells in mice infected with *M.tb* (Rogerson et al. 2006), further support the view that ESAT-6 leads to more persistent antigen exposure and likely greater differentiation of ESAT-6-specific T cells.

In light of the fact that no current assay directly detects *M.tb* in latently infected persons, our findings are noteworthy. An important limitation of IGRA's is that these tests rely on the presence of an immune response to *M.tb*-specific antigens. However, since memory responses to antigens commonly persist following antigen clearance — the basis of vaccination— such tests can still be positive in the absence of persistent *M.tb* infection. The more differentiated effector response we observed in the ESAT-6-specific CD4 T cell population in latently infected adolescents likely reflects persistent expression of ESAT-6, and not Ag85B, in infected adolescents. This provides strong evidence in favour of QFT^{+} adolescents harboring an active and persistent *M.tb* infection. Measuring the differentiation state of Ag85B and ESAT-6-specific CD4 T cells may provide a useful framework to investigate conversion and reversion of TST and/or QFT.

We have shown that a combination of innovative high throughput approaches can yield insights that provide better understanding of the CD4 T cell responses induced by novel tuberculosis vaccines in humans. A limitation of this study was the lack of experiments to confirm that the protein products of differentially expressed genes were indeed expressed differently. This is an obvious area for future studies. Another limitation stems from the requirement for individuals to express specific HLA alleles that allow matched HLA class II tetramer staining and sorting. This

limited the number of samples available for tetramer staining and transcriptomic analysis. Moreover, the relatively low frequencies of tetramer$^+$ CD4 T cells, which in some cases were too low to allow reliable analysis, further reduced our sample size. Lastly, our transcriptomic approach did not provide single cell resolution, but rather the average expression of sorted cells. Future studies using single cell transcriptomic analysis would reveal to what degree antigen-specific cells display heterogeneity. However, despite these limitations, important insights into the H1:IC31 induced response and the effects of underlying *M.tb* infection were gained in this study.

Our data suggest that underlying *M.tb* infection has a profound impact on the H1-specific CD4 T cell response, which appears to overpower H1:IC31 induced effects. However, in the vast majority of latently infected and immunocompetent persons the *M.tb* induced immune response is sufficient to prevent tuberculosis, because only 5-10% of infected persons are at risk of developing tuberculosis disease. A meta-analysis of 18 cohort studies suggested that upon *M.tb* exposure, being latently infected with *M.tb* offers up to 79% protection against development of active tuberculosis upon re-exposure, relative to not being *M.tb* infected. This was calculated from the risk of developing TB following infection or re-infection among *M.tb* uninfected and *M.tb* infected persons, respectively (Andrews et al. 2012). In light of this, altering the immune response in these latently infected individuals may have negative consequences. The fact that H1:IC31 did not markedly modulate the ESAT-6-specific CD4 T cell response may be advantageous. However, modulation of the immune response may be needed to prevent progression to active tuberculosis in the 5-10% of people at risk of developing the disease. This study has highlighted key differences in H1-specific CD4 T cells following H1:IC31 vaccination due to

underlying *M.tb* infection and provided strong evidence of differential antigen exposure during infection. These data underscores the need to further investigate vaccine response in regions endemic for tuberculosis, where a substantial proportion of adolescents and adults are already infected.

Chapter 5. General conclusion

More comprehensive analyses of vaccine induced immune responses and the effects of underlying *M.tb* infection are required for better understanding and generation of novel hypotheses in tuberculosis vaccine design and development. The aim of this thesis was to generate such understanding. We first determined the impact of acquiring *M.tb* infection on the pattern and number of CD4 T cell epitopes recognised within mycobacterial antigens. We then designed HLA class II tetramers to probe and characterise mycobacteria-specific CD4 T cells in adolescents with and without latent *M.tb* infection following H1:IC31 vaccination. Our results support a number of interesting conclusions.

The first major finding is that the pattern and number of CD4 T cell epitopes do not change following *M.tb* infection in BCG vaccinated adolescents. We reason that knowledge of CD4 T epitopes recognised before and after infection will be useful in our understanding of the CD4 T cell response induced by *M.tb* and will provide insights into vaccine design and development. We acknowledge that the sample size in our longitudinal analysis may be too small to detect real differences in the number of epitopes recognised with Ag85A and Ag85B. However, we did detect the same immunodominant regions within these antigens before and after infection. Interestingly, immunodominance has been described in these regions in populations with different genetic backgrounds (Mustafa et al. 2000), suggesting that these regions are targeted by persons with different HLA class II alleles. This level of epitope promiscuity is intriguing. In light of data that suggests that more protective subdominant or "cryptic" epitopes within the ESAT-6 antigen are revealed only when the dominant regions have been removed (Aagaard et al. 2009; Woodworth et al.

2014). An important question is whether CD4 T cells that recognise such subdominant epitopes exist in the human. It would be interesting to determine whether vaccinating individuals with Ag85A and/or Ag85B subunit proteins that lack regions shown to be immunodominant will result in the appearance of "cyptic" Ag85 epitopes. It should be stressed that the diversity of MHC class II molecules in inbred mice is lower compared to humans; therefore it may not be possible to determine and identify "protective" subdominant epitopes is a human population with a diverse HLA class II repertoires (Woodworth et al. 2014).

The second major finding of this work is that underlying infection drives a more effector-like H1-specific CD4 T response after H1:IC31 vaccination, and ESAT-6-specific cells appear to preferentially drive this response (Figure 52). This finding has several implications for vaccine design and development. Compelling data suggest that upon re-exposure to *M.tb*, persons with established latent infection are more protected, compared to uninfected persons exposed to *M.tb* (Andrews et al. 2012). Perhaps, by maintaining a population of mycobacteria-specific EM CD4 T cells, latently infected persons, upon re-exposure have antigen-specific CD4 T cells with immediate effector functions that are already present in the lungs that can rapidly migrate to the lungs, where they can initiate killing or control of the invading *M.tb*. Therefore, developing vaccines that can mimic immune responses naturally induced by latent infection may be advantageous.

Mimicking the response induced by latent infection with the current arsenal of tuberculosis vaccines may be difficult, because the vaccine expressed antigens are eventually cleared. There are however, intriguing approaches that are using the chronic virus, Cytomegalovirus (CMV), as a vaccine vector to generate sustained and

persistent antigen expression in vaccinated animals. These studies have shown that CMV vectored vaccine induced antigen-specific T cells that are highly differentiated toward an EM response, improving the level of protection in the rhesus macaques model of SIV infection (Hansen et al. 2011; Hansen et al. 2009). The induction of such cells was through a rhesus cytomegalovirus (RhCMV) vectored vaccine that persisted in vaccinated macaques, thus one can draw parallels with persistent antigen exposure driven by latent *M.tb* infection and exposure driven by the RhCMV vectored vaccine. Recently, work performed using similar vectored vaccines expressing mycobacterial-antigens have yielded promising results (da Costa et al. 2015). However, caution must be taken in the development of such vaccines, especially if these vaccines will be primarily used in a population were there is a high risk of HIV infection. There is a risk that immune compromise due to HIV infection may result in serious adverse events due to the persisting CMV vaccine vector in persons not already infected with CMV.

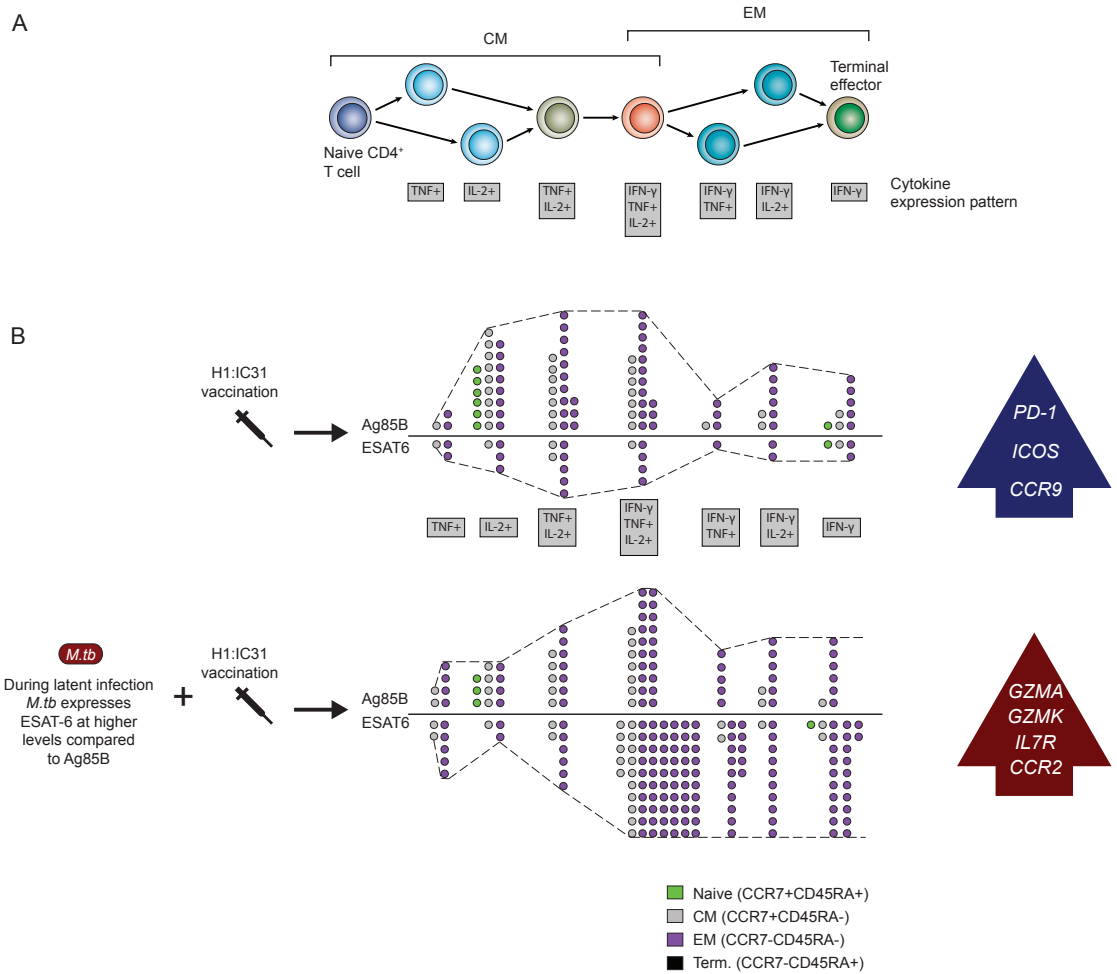

Figure 52. Influence of underlying *M.tb* infection on the Ag85B and ESAT-specific CD4 T cell response induced by H1:IC31 in adolescents. (A) The cytokine pattern, long-term memory potential, and magnitude of effector functions of antigen-experienced CD4 T cells at various stages of differentiation (Modified from Seder et. al *Nature Reviews Immunology* 2008). (B) Graphical depiction of Ag85B and ESAT-6-specific CD4 T cells response and the distinct functional, phenotypic, and transcriptomic characteristics observed in the THYB04 study. The number of circles indicates the magnitude of antigen-specific CD4 T cells in uninfected and latently infected adolescents, stratified by cytokine expression pattern and memory phenotype. mRNA transcripts expressed higher in QFT^{-} (blue arrow) or higher in QFT^{+} (red arrow) at least at 2 time points during the trial follow-up period.

It is very striking that in latently infected adolescents the prevailing H1-specific CD4 T cell response following two doses of H1:IC31 vaccination was remarkably similar to the response prior to vaccination. Whether this is favourable or not is unclear in the absence of T cell correlates of protection against tuberculosis. It is also noteworthy that we did not observe any evidence of functional exhaustion of T cells in adolescents with latent infection even after two doses of H1:IC31, as a large majority of H1-specific CD4 T cells were capable of producing multiple cytokines simultaneously and did not re-express CD45RA, a marker typically re-expressed by exhausted T cells (Henson et al. 2012).

Another important finding in this study was the differential expression of PD-1 and ICOS within H1-specfic CD4 T cells in infected and uninfected adolescents. Given the important role that PD-1^{+}ICOS^{+}KLRG1^{-} CM *M.tb*-specific CD4 T cells have been shown to play in replenishing antigen specific cells during *M.tb* infection (Lindenstrom et al. 2013; Moguche et al. 2015; Reiley et al. 2010; Sakai et al. 2014), generating memory CD4 T cells that display the PD-1^{+}KLRG1^{-} pattern through vaccination may be favourable. The role of the PD-1^{+}KLRG1^{-} subset was described in the mouse model of chronic infection; a model more appropriate for active tuberculosis than latent infection. Therefore, future work should measure antigen-specific PD-1^{+}KLRG1^{-} CD4 T cells induced by novel tuberculosis vaccines and also investigate the role of PD-1^{+}KLRG1^{-} *M.tb*-specific CD4 T cells during progression to active tuberculosis from latent infection. Given that these cells have been shown to preferentially traffic to the lung parenchyma (Sakai et al. 2014; Moguche et al. 2015), studies that attempt to characterise this subset in human infection may not detect these

cells, as they would have been sequestered away from the peripheral blood. Despite this potential limitation this is an avenue that warrants investigation. Together, these data suggest that achieving a balanced response of EM and CM *M.tb*-specific CD4 T cells through vaccination is favourable.

Lastly, this study provided strong evidence of on-going *M.tb* infection in QFT^{+} adolescents, and more importantly, suggested that differential antigen exposure influences the character of antigen-specific CD4 T cell response during infection. ESAT-6-specific CD4 T cells appeared to be driving the higher effector H1-specific response observed in infected adolescents following vaccination (Figure 52). We only compared Ag85B and ESAT-6 responses in infected adolescents. It is important that responses to other antigens that are differentially expressed should also be characterised. Given that ESAT-6 and CFP-10 are expressed as an operon (Berthet et al. 1998), we speculate, that like the ESAT-6-specific CD4 T cell response, the CFP-10-specific response will be different compared to the Ag85B-specific response. It is also important to determine whether Ag85B and ESAT-6-responses during active tuberculosis reflect differential antigen exposure.

Functional and phenotypic differences in the Ag85B and ESAT-6-response in persons with underlying infection and the stability of the number and pattern of CD4 T cell epitopes within Ag85A and Ag85B may be a reflection of low expression of Ag85A and AG85B. The revelation that differential antigen exposure during *M.tb* infection may influence the response in CD4 T cells specific for these antigens has important implications in terms of vaccine design and development. Vaccine-induced Ag85B-specific T cell responses may not be as effective as ESAT-6-specific cells because, in

M.tb infected persons Ag85B is expressed at relatively lower levels compared to ESAT-6. This may be a reason why the MVA85A boost in infants did not improve protection against tuberculosis. While vaccine-induced CD4 T cells that target highly expressed antigens such as ESAT-6 may yield favourable results, caution should be taken. One can speculate that vaccines that target such cells may be inducing cells that are susceptible to exhaustion during chronic antigen exposure. Studies that utilise animal models are needed to determine whether cells that target highly expressed or lowly expressed antigens are more protective and how they respond functionally to levels of antigen.

This study has highlighted key differences in the H1:IC31 induced response due to underlying infection. We have developed innovative tools and approaches and identified potential markers that allows for better understanding and interpretation of CD4 T cells responses and characteristics induced by novel tuberculosis vaccines. Our data provides compelling evidence of on-going antigen exposure in QFT^{+} adolescents and questions the selection of some of the antigens currently targeted by novel tuberculosis vaccines.

References

Aagaard, C. et al., 2011. A multistage tuberculosis vaccine that confers efficient protection before and after exposure. *Nature Medicine*, 17(2), pp.189–194.

Aagaard, C.S. et al., 2009. Quality and vaccine efficacy of CD4+ T cell responses directed to dominant and subdominant epitopes in ESAT-6 from Mycobacterium tuberculosis. *J Immunol*, 183(4), pp.2659–2668.

Abu-Raddad, L.J. et al., 2009. Epidemiological benefits of more-effective tuberculosis vaccines, drugs, and diagnostics. *Proceedings of the National Academy of Sciences*, 106(33), pp.13980–13985.

Achkar, J.M., Chan, J. & Casadevall, A., 2015. B cells and antibodies in the defense against Mycobacterium tuberculosis infection. *Immunological reviews*, 264(1), pp.167–181.

Adekambi, T. et al., 2012. Distinct Effector Memory CD4+ T Cell Signatures in Latent Mycobacterium tuberculosis Infection, BCG Vaccination and Clinically Resolved Tuberculosis D. Goletti, ed. *PLoS ONE*, 7(4), p.e36046.

Aderaye, G. et al., 2004. The relationship between disease pattern and disease burden by chest radiography, M. tuberculosis load, and HIV status in patients with pulmonary tuberculosis in Addis Ababa. *Infection*, 32(6), pp.333–338.

Agger, E.M. et al., 2008. Cationic liposomes formulated with synthetic mycobacterial cordfactor (CAF01): a versatile adjuvant for vaccines with different immunological requirements. *PloS one*, 3(9), p.e3116.

Agger, E.M. et al., 2006. Protective immunity to tuberculosis with Ag85B-ESAT-6 in a synthetic cationic adjuvant system IC31. *Vaccine*, 24(26), pp.5452–60.

Aggerbeck, H. et al., 2013. Randomised Clinical Trial Investigating the Specificity of a Novel Skin Test (C-Tb) for Diagnosis of M. tuberculosis Infection D. Goletti, ed. *PLoS ONE*, 8(5), p.e64215.

Akolo, C. et al., 2010. Treatment of latent tuberculosis infection in HIV infected persons. *Cochrane database of systematic reviews (Online)*, (1), p.CD000171.

Allen, S. et al., 1992. Two-year incidence of tuberculosis in cohorts of HIV-infected and uninfected urban Rwandan women. *Am Rev Respir Dis*, 146(6), pp.1439–1444.

Alving, C.R. et al., 2012. Adjuvants for human vaccines. *Current Opinion in Immunology*, 24(3), pp.310–315.

Andersen, P. & Woodworth, J.S., 2014. Tuberculosis vaccines – rethinking the current paradigm. *Trends in Immunology*, 35(8), pp.387–395.

Andrews, J.R. et al., 2012. Risk of progression to active tuberculosis following reinfection with Mycobacterium tuberculosis. *Clinical infectious diseases : an official publication of the Infectious Diseases Society of America*, 54(6), pp.784–91.

Arlehamn, C.L. et al., 2014. Transcriptional Profile of Tuberculosis Antigen-Specific T Cells Reveals Novel Multifunctional Features. *The Journal of Immunology*, 193(6), pp.2931–2940.

Arlehamn, C.S. et al., 2013. Memory T Cells in Latent Mycobacterium tuberculosis Infection Are Directed against Three Antigenic Islands and Largely Contained in a CXCR3+CCR6+ Th1 Subset P. Salgame, ed. *PLoS Pathogens*, 9(1), p.e1003130.

Baechler, E.C. et al., 2004. Expression levels for many genes in human peripheral blood cells are

highly sensitive to ex vivo incubation. *Genes and Immunity*, 5(5), pp.347–353.

Baena, a & Porcelli, S. a, 2009. Evasion and subversion of antigen presentation by Mycobacterium tuberculosis. *Tissue antigens*, 74(3), pp.189–204.

Baldwin, S.L. et al., 2013. Protection against Tuberculosis with Homologous or Heterologous Protein/Vector Vaccine Approaches Is Not Dependent on CD8+ T Cells. *The Journal of Immunology*, 191(5), pp.2514–2525.

Baldwin, S.L. et al., 2012. The importance of adjuvant formulation in the development of a tuberculosis vaccine. *Journal of immunology (Baltimore, Md. : 1950)*, 188, pp.2189–97.

Barber, D.L. et al., 2006. Restoring function in exhausted CD8 T cells during chronic viral infection. *Nature*, 439(7077), pp.682–687.

Barry, C.E. et al., 2009. The spectrum of latent tuberculosis: rethinking the biology and intervention strategies. *Nature reviews. Microbiology*, 7(12), pp.845–55.

Becattini, S. et al., 2015. Functional heterogeneity of human memory CD4+ T cell clones primed by pathogens or vaccines. *Science*, 347(6220), pp.400–406.

Behar, S.M. et al., 2011. Apoptosis is an innate defense function of macrophages against Mycobacterium tuberculosis. *Mucosal Immunology*, 4(3), pp.279–287.

Belisle, J.T. et al., 1997. Role of the major antigen of Mycobacterium tuberculosis in cell wall biogenesis. *Science (New York, N.Y.)*, 276(5317), pp.1420–1422.

Berard, M. & Tough, D.F., 2002. Qualitative differences between naive and memory T cells. *Immunology*, 106(2), pp.127–138.

Bernardo, L. et al., 2011. The two component adjuvant IC31® potentiates the protective immunity induced by a dengue 2 recombinant fusion protein in mice. *Vaccine*, 29(25), pp.4256–63.

Berry, M.P.R. et al., 2010. An interferon-inducible neutrophil-driven blood transcriptional signature in human tuberculosis. *Nature*, 466(7309), pp.973–977.

Berthet, F.X. et al., 1998. A Mycobacterium tuberculosis operon encoding ESAT-6 and a novel low-molecular-mass culture filtrate protein (CFP-10). *Microbiology*, 144(11), pp.3195–3203.

Billeskov, R. et al., 2013. Comparing Adjuvanted H28 and Modified Vaccinia Virus Ankara Expressing H28 in a Mouse and a Non-Human Primate Tuberculosis Model T. J. Scriba, ed. *PLoS ONE*, 8(8), p.e72185.

Boniface, J.J. et al., 1998. Initiation of signal transduction through the T cell receptor requires the multivalent engagement of peptide/MHC ligands. *Immunity*, 9(4), pp.459–466.

van den Boogaard, J. et al., 2009. New Drugs against Tuberculosis: Problems, Progress, and Evaluation of Agents in Clinical Development. *Antimicrobial Agents and Chemotherapy*, 53(3), pp.849–862.

Bouaziz, J.-D. et al., 2010. IL-10 produced by activated human B cells regulates CD4+ T-cell activation in vitro. *European Journal of Immunology*, 40(10), pp.2686–2691.

Branch, A., 1927. THE MOST RECENT EXPERIMENTS WITH “BACILLE CALMETTE GUERIN.” *Canadian Medical Association Journal*, 17(6), pp.720–721.

Brandt, L. et al., 2002. Failure of the Mycobacterium bovis BCG Vaccine : Some Species of Environmental Mycobacteria Block Multiplication of BCG and Induction of Protective Immunity to Tuberculosis Failure of the Mycobacterium bovis BCG Vaccine : Some Species of Environmental Myc. *INFECTION AND IMMUNITY*, 70(2), pp.672–678.

Buettner, M. et al., 2005. Inverse Correlation of Maturity and Antibacterial Activity in Human Dendritic Cells. *The Journal of Immunology*, 174(7), pp.4203–4209.

Burl, S. et al., 2010. Delaying Bacillus Calmette-Guerin Vaccination from Birth to 4 1/2 Months of Age Reduces Postvaccination Th1 and IL-17 Responses but Leads to Comparable Mycobacterial Responses at 9 Months of Age. *The Journal of Immunology*, 185(4), pp.2620–2628.

Caccamo, N. et al., 2006. Phenotypical and functional analysis of memory and effector human CD8 T cells specific for mycobacterial antigens. *Journal of immunology (Baltimore, Md. : 1950)*, 177(3), pp.1780–5.

Canaday, D.H. et al., 2001. CD4+ and CD8+ T Cells Kill Intracellular Mycobacterium tuberculosis by a Perforin and Fas/Fas Ligand-Independent Mechanism. *The Journal of Immunology*, 167(5), pp.2734–2742.

Carpenter, C. et al., 2015. A side-by-side comparison of T cell reactivity to fifty-nine Mycobacterium tuberculosis antigens in diverse populations from five continents. *Tuberculosis*.

Castillo, E.F. et al., 2012. Autophagy protects against active tuberculosis by suppressing bacterial burden and inflammation. *Proceedings of the National Academy of Sciences*, 109(46), pp.E3168–E3176.

Chen, M. et al., 2008. Lipid mediators in innate immunity against tuberculosis: opposing roles of PGE2 and LXA4 in the induction of macrophage death. *Journal of Experimental Medicine*, 205(12), pp.2791–2801.

Cho, S. et al., 2000. Antimicrobial activity of MHC class I-restricted CD8+ T cells in human tuberculosis. *Proceedings of the National Academy of Sciences of the United States of America*, 97(22), pp.12210–12215.

Clemens, D.L. & Horwitz, M.A., 1995. Characterization of the Mycobacterium tuberculosis phagosome and evidence that phagosomal maturation is inhibited. *The Journal of experimental medicine*, 181(1), pp.257–270.

Cochran, J.R., Cameron, T.O. & Stern, L.J., 2000. The relationship of MHC-peptide binding and T cell activation probed using chemically defined MHC class II oligomers. *Immunity*, 12(3), pp.241–250.

Colditz, G.A. et al., 1995. The efficacy of bacillus Calmette-Guerin vaccination of newborns and infants in the prevention of tuberculosis: meta-analyses of the published literature. *Pediatrics*, 96(1 Pt 1), pp.29–35.

Comas, I. et al., 2010. Human T cell epitopes of Mycobacterium tuberculosis are evolutionarily hyperconserved. *Nat Genet*, 42(6), pp.498–503.

Constant, S.L., 1999. B lymphocytes as antigen-presenting cells for CD4+ T cell priming in vivo. *The Journal of Immunology*, 162(10), pp.5695–5703.

Cooper, A.M. et al., 1993. Disseminated tuberculosis in interferon gamma gene-disrupted mice. *The Journal of experimental medicine*, 178(6), pp.2243–2247.

Cooper, A.M. et al., 1997. Interleukin 12 (IL-12) is crucial to the development of protective immunity in mice intravenously infected with mycobacterium tuberculosis. *The Journal of experimental medicine*, 186(1), pp.39–45.

da Costa, C., Walker, B. & Bonavia, A., 2015. Tuberculosis Vaccines – state of the art, and novel approaches to vaccine development. *International Journal of Infectious Diseases*, 32, pp.5–12.

van Crevel, R., Ottenhoff, T.H.M. & van der Meer, J.W.M., 2002. Innate Immunity to Mycobacterium tuberculosis. *Clinical Microbiology Reviews*, 15(2), pp.294–309.

Crotty, S., 2011. Follicular Helper CD4 T Cells (T_{FH}). *Annual Review of Immunology*, 29(1), pp.621–663.

Curotto de Lafaille, M.A. & Lafaille, J.J., 2009. Natural and Adaptive Foxp3+ Regulatory T Cells: More of the Same or a Division of Labor? *Immunity*, 30(5), pp.626–635.

Daniel, T.M., 2006. The history of tuberculosis. *Respir Med*, 100(11), pp.1862–1870.

Day, C.L. et al., 2011. Functional Capacity of Mycobacterium tuberculosis-Specific T Cell Responses in Humans Is Associated with Mycobacterial Load. *J Immunol*, 187(5), pp.2222–2232.

Day, C.L. et al., 2013. Induction and Regulation of T-Cell Immunity by the Novel Tuberculosis Vaccine M72/AS01 in South African Adults. *American Journal of Respiratory and Critical Care Medicine*, 188(4), pp.492–502.

Day, C.L. et al., 2006. PD-1 expression on HIV-specific T cells is associated with T-cell exhaustion and disease progression. *Nature*, 443(7109), pp.350–354.

Demissie, A. et al., 2004. Healthy Individuals That Control a Latent Infection with Mycobacterium tuberculosis Express High Levels of Th1 Cytokines and the IL-4 Antagonist IL-4 2. *The Journal of Immunology*, 172(11), pp.6938–6943.

Deretic, V. ed., 2008. *Autophagosome and phagosome / edited by Vojo Deretic*, Totowa, NJ: Humana Press.

Dheda, K. et al., 2014. Global control of tuberculosis: from extensively drug-resistant to untreatable tuberculosis. *The Lancet Respiratory Medicine*, 2(4), pp.321–338.

Dietrich, J. et al., 2006. Mucosal administration of Ag85B-ESAT-6 protects against infection with Mycobacterium tuberculosis and boosts prior bacillus Calmette-Guerin immunity. *Journal of immunology (Baltimore, Md. : 1950)*, 177(9), pp.6353–60.

Dintwe, O.B. et al., 2013. Heterologous vaccination against human tuberculosis modulates antigen-specific $CD4^+$ T-cell function: Clinical immunology. *European Journal of Immunology*, 43(9), pp.2409–2420.

van Dissel, J.T. et al., 2010. Ag85B–ESAT-6 adjuvanted with IC31® promotes strong and long-lived Mycobacterium tuberculosis specific T cell responses in naïve human volunteers. *Vaccine*, 28(20), pp.3571–3581.

van Dissel, J.T. et al., 2011. Ag85B–ESAT-6 adjuvanted with IC31® promotes strong and long-lived Mycobacterium tuberculosis specific T cell responses in volunteers with previous BCG vaccination or tuberculosis infection. *Vaccine*, 29(11), pp.2100–2109.

Dominguez, M.H. et al., 2013. Highly multiplexed quantitation of gene expression on single cells. *Journal of immunological methods*, 391(1-2), pp.133–45.

Dorman, S.E., 2010. New Diagnostic Tests for Tuberculosis: Bench, Bedside, and Beyond. *Clinical Infectious Diseases*, 50(s3), pp.S173–S177.

Ehlers, S. & Schaible, U.E., 2013. The Granuloma in Tuberculosis: Dynamics of a Host–Pathogen Collusion. *Frontiers in Immunology*, 3.

Elkington, P. et al., 2011. MMP-1 drives immunopathology in human tuberculosis and transgenic mice. *J Clin Invest*, 121(5), pp.1827–1833.

Elkington, P.T., D'Armiento, J.M. & Friedland, J.S., 2011. Tuberculosis Immunopathology: The Neglected Role of Extracellular Matrix Destruction. *Science Translational Medicine*, 3(71), pp.71ps6–71ps6.

Elvang, T. et al., 2009. CD4 and CD8 T cell responses to the M. tuberculosis Ag85B-TB10.4 promoted by adjuvanted subunit, adenovector or heterologous prime boost vaccination. *PLoS ONE*, 4(4), p.e5139.

Endharti, A.T. et al., 2011. CD8+CD122+ regulatory T cells (Tregs) and CD4+ Tregs cooperatively prevent and cure CD4+ cell-induced colitis. *J Immunol*, 186(1), pp.41–52.

Eruslanov, E.B. et al., 2005. Neutrophil responses to Mycobacterium tuberculosis infection in genetically susceptible and resistant mice. *Infection and Immunity*, 73(3), pp.1744–1753.

Eum, S.-Y. et al., 2010. Neutrophils are the predominant infected phagocytic cells in the airways of patients with active pulmonary TB. *Chest*, 137, pp.122–128.

Fabri, M. et al., 2011. Vitamin D Is Required for IFN- -Mediated Antimicrobial Activity of Human Macrophages. *Science Translational Medicine*, 3(104), pp.104ra102–104ra102.

Farber, D.L., Yudanin, N.A. & Restifo, N.P., 2013. Human memory T cells: generation, compartmentalization and homeostasis. *Nature Reviews Immunology*, 14(1), pp.24–35.

Fennelly, K.P. et al., 2012. Variability of Infectious Aerosols Produced during Coughing by Patients with Pulmonary Tuberculosis. *American Journal of Respiratory and Critical Care Medicine*, 186(5), pp.450–457.

Fernando, S.L. & Britton, W.J., 2006. Genetic susceptibility to mycobacterial disease in humans. *Immunology and Cell Biology*, 84(2), pp.125–137.

Ferron, G.A., 1994. Aerosol properties and lung deposition. *European Respiratory Journal*, 7(8), pp.1392–1394.

Fiorentino, D.F. et al., 1991. IL-10 acts on the antigen-presenting cell to inhibit cytokine production by Th1 cells. *J Immunol*, 146(10), pp.3444–3451.

Flatz, L. et al., 2011. Single-cell gene-expression pro fi ling reveals qualitatively distinct CD8 T cells elicited by different gene-based vaccines. , pp.8–13.

Flatz, L. et al., 2011. Single-cell gene-expression profiling reveals qualitatively distinct CD8 T cells elicited by different gene-based vaccines. *Proc Natl Acad Sci U S A*, 108(14), pp.5724–5729.

Flynn, J.L. et al., 1993. An essential role for interferon gamma in resistance to Mycobacterium tuberculosis infection. *J Exp Med*, 178(6), pp.2249–2254.

Flynn, J.L. et al., 2015. Immunology studies in non-human primate models of tuberculosis. *Immunological reviews*, 264(1), pp.60–73.

Flynn, J.L. et al., 1995. Increases Resistance of BALB/c Mice to.

Flynn, J.L. et al., 1992. Major histocompatibility complex class I-restricted T cells are required for resistance to Mycobacterium tuberculosis infection. *Proc Natl Acad Sci U S A*, 89(24), pp.12013–12017.

Flynn, J.L. et al., 1995. Tumor necrosis factor-alpha is required in the protective immune response against Mycobacterium tuberculosis in mice. *Immunity*, 2(6), pp.561–572.

Francis, D.P., 2010. Successes and failures: Worldwide vaccine development and application. *Biologicals : journal of the International Association of Biological Standardization*, 38(5),

pp.523–8.

Gallegos, A.M. et al., 2011. A Gamma Interferon Independent Mechanism of CD4 T Cell Mediated Control of M. tuberculosis Infection in vivo. *PLoS Pathog*, 7(5), p.e1002052.

Gao, Q. et al., 2005. Gene expression diversity among Mycobacterium tuberculosis clinical isolates. *Microbiology (Reading, England)*, 151(Pt 1), pp.5–14.

García-Basteiro, A.L. & Cobelens, F., 2015. Triage tests: a new priority for tuberculosis diagnostics. *The Lancet Respiratory Medicine*, Vol 3, pp.177–178.

Geldenhuys, H. et al., 2015. The tuberculosis vaccine H4:IC31 is safe and induces a persistent polyfunctional CD4 T cell response in South African adults: A randomized controlled trial. *Vaccine*, (August).

Gideon, H.P. et al., 2015. Variability in Tuberculosis Granuloma T Cell Responses Exists, but a Balance of Pro- and Anti-inflammatory Cytokines Is Associated with Sterilization D. M. Lewinsohn, ed. *PLOS Pathogens*, 11(1), p.e1004603.

Gomez-Reino, J.J. et al., 2003. Treatment of rheumatoid arthritis with tumor necrosis factor inhibitors may predispose to significant increase in tuberculosis risk: a multicenter active-surveillance report. *Arthritis Rheum*, 48(8), pp.2122–2127.

Gopal, R., Rangel-Moreno, J., et al., 2014. Mucosal pre-exposure to Th17-inducing adjuvants exacerbates pathology after influenza infection. *American Journal of Pathology*, 184(1), pp.55–63.

Gopal, R., Monin, L., et al., 2014. Unexpected Role for IL-17 in Protective Immunity against Hypervirulent Mycobacterium tuberculosis HN878 Infection. *PLoS Pathogens*, 10(5).

Goral, S., 2011. The three-signal hypothesis of lymphocyte activation/targets for immunosuppression. *Dialysis & Transplantation*, 40(1), pp.14–16.

Green, A.M. et al., 2010. CD4(+) regulatory T cells in a cynomolgus macaque model of Mycobacterium tuberculosis infection. *J Infect Dis*, 202(4), pp.533–541.

Grosset, J., 2003. Mycobacterium tuberculosis in the Extracellular Compartment: an Underestimated Adversary. *Antimicrobial Agents and Chemotherapy*, 47(3), pp.833–836.

Guirado, E. & Schlesinger, L.S., 2013. Modeling the Mycobacterium tuberculosis Granuloma – the Critical Battlefield in Host Immunity and Disease. *Frontiers in Immunology*, 4.

Guo, G. et al., 2010. Resolution of Cell Fate Decisions Revealed by Single-Cell Gene Expression Analysis from Zygote to Blastocyst. *Developmental Cell*, 18(4), pp.675–685.

Gutierrez, M.G. et al., 2004. Autophagy is a defense mechanism inhibiting BCG and Mycobacterium tuberculosis survival in infected macrophages. *Cell*, 119(6), pp.753–66.

Guyot-Revol, V. et al., 2006. Regulatory T cells are expanded in blood and disease sites in patients with tuberculosis. *Am J Respir Crit Care Med*, 173(7), pp.803–810.

Haining, W.N. et al., 2008. High-throughput gene expression profiling of memory differentiation in primary human T cells. *BMC Immunology*, 9(1), p.44.

Hanekom, W. a. et al., 2004. Novel application of a whole blood intracellular cytokine detection assay to quantitate specific T-cell frequency in field studies. *Journal of Immunological Methods*, 291(1-2), pp.185–195.

Hansen, S.G. et al., 2009. Effector memory T cell responses are associated with protection of rhesus

monkeys from mucosal simian immunodeficiency virus challenge. *Nat Med*, 15(3), pp.293–299.

Hansen, S.G. et al., 2011. Profound early control of highly pathogenic SIV by an effector memory T-cell vaccine. *Nature*, 473(7348), pp.523–527.

He, X.Y. et al., 2010. T regulatory cells and Th1/Th2 cytokines in peripheral blood from tuberculosis patients. *Eur J Clin Microbiol Infect Dis*, 29(6), pp.643–650.

Henson, S.M., Riddell, N.E. & Akbar, A.N., 2012. Properties of end-stage human T cells defined by CD45RA re-expression. *Current Opinion in Immunology*, 24(4), pp.476–481.

Herbst, S., Schaible, U.E. & Schneider, B.E., 2011. Interferon Gamma Activated Macrophages Kill Mycobacteria by Nitric Oxide Induced Apoptosis L. Tailleux, ed. *PLoS ONE*, 6(5), p.e19105.

Hesseling, A.C. et al., 2009. Disseminated bacille Calmette-Guérin disease in HIV-infected South African infants. *Bulletin of the World Health Organization*, 87(7), pp.505–511.

Heuer, J.G. et al., 2005. Adoptive transfer of in vitro-stimulated CD4+CD25+ regulatory T cells increases bacterial clearance and improves survival in polymicrobial sepsis. *J Immunol*, 174(11), pp.7141–7146.

Hsieh, C.S. et al., 1992. Differential regulation of T helper phenotype development by interleukins 4 and 10 in an alpha beta T-cell-receptor transgenic system. *Proc Natl Acad Sci U S A*, 89(13), pp.6065–6069.

Hussell, T. & Bell, T.J., 2014. Alveolar macrophages: plasticity in a tissue-specific context. *Nature Reviews Immunology*, 14(2), pp.81–93.

Irvine, D.J. et al., 2002. Direct observation of ligand recognition by T cells. *Nature*, 419(6909), pp.845–849.

Jonjic, S., 2010. Functional plasticity and robustness are essential characteristics of biological systems: Lessons learned from KLRG1-deficient mice. *European Journal of Immunology*, 40(5), pp.1241–1243.

Kagina, B.M. et al., 2015. Qualification of a whole blood intracellular cytokine staining assay to measure mycobacteria-specific CD4 and CD8 T cell immunity by flow cytometry. *Journal of Immunological Methods*, 417, pp.22–33.

Kagina, B.M. et al., 2010. Specific T cell frequency and cytokine expression profile do not correlate with protection against tuberculosis after bacillus Calmette-Guerin vaccination of newborns. *Am J Respir Crit Care Med*, 182(8), pp.1073–1079.

Kagina, B.M.N. et al., 2010. Specific T cell frequency and cytokine expression profile do not correlate with protection against tuberculosis after bacillus Calmette-Guérin vaccination of newborns. *American journal of respiratory and critical care medicine*, 182(8), pp.1073–9.

Kaiko, G.E. et al., 2008. Immunological decision-making: how does the immune system decide to mount a helper T-cell response? *Immunology*, 123(3), pp.326–338.

Karp, C.L., Wilson, C.B. & Stuart, L.M., 2015. Tuberculosis vaccines: barriers and prospects on the quest for a transformative tool. *Immunological reviews*, 264(1), pp.363–381.

Kaufmann, S.H., Hussey, G. & Lambert, P.-H., 2010. New vaccines for tuberculosis. *The Lancet*, 375(9731), pp.2110–2119.

Keane, J. et al., 2001. Tuberculosis associated with infliximab, a tumor necrosis factor alpha-neutralizing agent. *N Engl J Med*, 345(15), pp.1098–1104.

Khader, S.A. et al., 2007. IL-23 and IL-17 in the establishment of protective pulmonary CD4+ T cell responses after vaccination and during Mycobacterium tuberculosis challenge. *Nat Immunol*, 8(4), pp.369–377.

Kim, M.-J. et al., 2010. Caseation of human tuberculosis granulomas correlates with elevated host lipid metabolism: Lipid metabolism in human tuberculous granulomas. *EMBO Molecular Medicine*, 2(7), pp.258–274.

Kinchen, J.M. & Ravichandran, K.S., 2008. Phagosome maturation: going through the acid test. *Nature Reviews Molecular Cell Biology*, 9(10), pp.781–795.

Knight, G.M. et al., 2014. Impact and cost-effectiveness of new tuberculosis vaccines in low- and middle-income countries. *Proceedings of the National Academy of Sciences*, 111(43), pp.15520–15525.

Kozakiewicz, L. et al., 2013. The role of B cells and humoral immunity in mycobacterium Tuberculosis infection. *Advances in Experimental Medicine and Biology*, 783, pp.225–250.

Kwok, W.W. et al., 2012. Frequency of epitope-specific naive CD4(+) T cells correlates with immunodominance in the human memory repertoire. *Journal of immunology (Baltimore, Md. : 1950)*, 188(6), pp.2537–44.

Lawn, S.D. & Nicol, M.P., 2011. Xpert ® MTB/RIF assay: development, evaluation and implementation of a new rapid molecular diagnostic for tuberculosis and rifampicin resistance. *Future Microbiology*, 6(9), pp.1067–1082.

Lewis, K.N. et al., 2003. Deletion of RD1 from Mycobacterium tuberculosis mimics bacille Calmette-Guerin attenuation. *Journal of Infectious Diseases*, 187(1), pp.117–123.

Leyten, E.M. et al., 2007. Discrepancy between Mycobacterium tuberculosis-specific gamma interferon release assays using short and prolonged in vitro incubation. *Clin Vaccine Immunol*, 14(7), pp.880–885.

Lin, P.L., Rutledge, T., et al., 2012. CD4 T Cell Depletion Exacerbates Acute *Mycobacterium tuberculosis* While Reactivation of Latent Infection Is Dependent on Severity of Tissue Depletion in Cynomolgus Macaques. *AIDS Research and Human Retroviruses*, 28(12), pp.1693–1702.

Lin, P.L. et al., 2009. Quantitative Comparison of Active and Latent Tuberculosis in the Cynomolgus Macaque Model. *Infection and Immunity*, 77(10), pp.4631–4642.

Lin, P.L., Dietrich, J., et al., 2012. The multistage vaccine H56 boosts the effects of BCG to protect cynomolgus macaques against active tuberculosis and reactivation of latent Mycobacterium tuberculosis infection. *Journal of Clinical Investigation*, 122(1), pp.303–314.

Lin, P.L. & Flynn, J.L., 2015. CD8 T cells and Mycobacterium tuberculosis infection. *Seminars in Immunopathology*.

Lindenstrom, T. et al., 2013. Control of Chronic Mycobacterium tuberculosis Infection by CD4 KLRG1- IL-2-Secreting Central Memory Cells. *The Journal of Immunology*, 190(12), pp.6311–6319.

Lowe, D.M. et al., 2012. Neutrophils in tuberculosis: friend or foe? *Trends in Immunology*, 33(1), pp.14–25.

Luabeya, A.K.K. et al., 2015. First-in-human trial of the post-exposure tuberculosis vaccine H56:IC31 in Mycobacterium tuberculosis infected and non-infected healthy adults. *Vaccine*, 33, pp.4130–

4140.

Maglione, P.J. & Chan, J., 2009. How B cells shape the immune response against Mycobacterium tuberculosis. *European Journal of Immunology*, 39(3), pp.676–686.

Maglione, P.J., Xu, J. & Chan, J., 2007. B Cells Moderate Inflammatory Progression and Enhance Bacterial Containment upon Pulmonary Challenge with Mycobacterium tuberculosis. *The Journal of Immunology*, 178(11), pp.7222–7234.

Mahmoud, A.A. & Ali, A.H.K., 2014. Vitamin D receptor gene polymorphism and 25 hydroxy vitamin D levels in Egyptian patients with pulmonary tuberculosis. *Egyptian Journal of Chest Diseases and Tuberculosis*, 63(3), pp.651–655.

Mahomed, H. et al., 2011. Predictive factors for latent tuberculosis infection among adolescents in a high-burden area in South Africa. *Int J Tuberc Lung Dis*, 15(3), pp.331–336.

Mahomed, H. et al., 2011. The Tuberculin Skin Test versus QuantiFERON TB Gold® in Predicting Tuberculosis Disease in an Adolescent Cohort Study in South Africa M. Pai, ed. *PLoS ONE*, 6(3), p.e17984.

Majlessi, L. et al., 2005. Influence of ESAT-6 Secretion System 1 (RD1) of Mycobacterium tuberculosis on the Interaction between Mycobacteria and the Host Immune System. *The Journal of Immunology*, 174(6), pp.3570–3579.

Mane, V.P. et al., 2008. Systematic method for determining an ideal housekeeping gene for real-time PCR analysis. *Journal of biomolecular techniques: JBT*, 19(5), p.342.

Mangtani, P. et al., 2014. Protection by BCG Vaccine Against Tuberculosis: A Systematic Review of Randomized Controlled Trials. *Clinical Infectious Diseases*, 58(4), pp.470–480.

Mariotti, S. & Nisini, R., 2009. Generation of Human T Cell Clones. *T Cell Protocols*, 514, pp.65–93.

Mattila, J.T. et al., 2015. Granzyme B-expressing neutrophils correlate with bacterial load in granulomas from M ycobacterium tuberculosis -infected cynomolgus macaques: Granuloma neutrophils express granzyme B. *Cellular Microbiology*, p.n/a–n/a.

McNerney, R. et al., 2012. Tuberculosis Diagnostics and Biomarkers: Needs, Challenges, Recent Advances, and Opportunities. *Journal of Infectious Diseases*, 205(suppl 2), pp.S147–S158.

McShane, H., 2014. Editorial Commentary: Understanding BCG Is the Key to Improving It. *Clinical Infectious Diseases*, 58(4), pp.481–482.

McShane, H. et al., 2004. Recombinant modified vaccinia virus Ankara expressing antigen 85A boosts BCG-primed and naturally acquired antimycobacterial immunity in humans. *Nature Medicine*, 10(11), pp.1240–1244.

Meintjes, G. et al., 2009. Novel relationship between tuberculosis immune reconstitution inflammatory syndrome and antitubercular drug resistance. *Clin Infect Dis*, 48(5), pp.667–676.

Menzies, D., 1999. Interpretation of repeated tuberculin tests: boosting, conversion, and reversion. *American journal of respiratory and critical care medicine*, 159(1), pp.15–21.

Mikhak, Z., Strassner, J.P. & Luster, A.D., 2013. Lung dendritic cells imprint T cell lung homing and promote lung immunity through the chemokine receptor CCR4. *Journal of Experimental Medicine*, 210(9), pp.1855–1869.

Moguche, A.O. et al., 2015. ICOS and Bcl6-dependent pathways maintain a CD4 T cell population with memory-like properties during tuberculosis. *Journal of Experimental Medicine*, 212(5),

pp.715–728.

Mosmann, T.R. et al., 1986. Two types of murine helper T cell clone. I. Definition according to profiles of lymphokine activities and secreted proteins. *J Immunol*, 136(7), pp.2348–2357.

Van Der Most, R.G. et al., 2003. Changing immunodominance patterns in antiviral CD8 T-cell responses after loss of epitope presentation or chronic antigenic stimulation. *Virology*, 315(1), pp.93–102.

Muller, I. et al., 1987. Impaired resistance to Mycobacterium tuberculosis infection after selective in vivo depletion of L3T4+ and Lyt-2+ T cells. *Infect Immun*, 55(9), pp.2037–2041.

Mustafa, A.S. et al., 2000. Identification and HLA Restriction of Naturally Derived Th1-Cell Epitopes from the Secreted Mycobacterium tuberculosisAntigen 85B Recognized by Antigen-Specific Human CD4+ T-Cell Lines. *Infection and immunity*, 68(7), pp.3933–3940.

Nepom, G.T., 2012. MHC Class II Tetramers. *The Journal of Immunology*, 188(6), pp.2477–2482.

North, R.J., 1998. Mice incapable of making IL-4 or IL-10 display normal resistance to infection with Mycobacterium tuberculosis. *Clinical and Experimental Immunology*, 113(1), pp.55–58.

O'Garra, A. et al., 2004. IL-10-producing and naturally occurring CD4+ Tregs: limiting collateral damage. *The Journal of clinical investigation*, 114(10), pp.1372–1378.

O'Garra, A. et al., 2013. The Immune Response in Tuberculosis. *Annual Review of Immunology*, 31(1), pp.475–527.

Oettinger, T. et al., 1999. Development of the Mycobacterium bovis BCG vaccine: review of the historical and biochemical evidence for a genealogical tree. *Tuber Lung Dis*, 79(4), pp.243–250.

Olafsdottir, T.A. et al., 2012. Novel Protein-Based Pneumococcal Vaccines Administered with the Th1-Promoting Adjuvant IC31 Induce Protective Immunity against Pneumococcal Disease in Neonatal Mice. *Infection and Immunity*, 80(1), pp.461–468.

Olaru, I.D. et al., 2015. Novel drugs against tuberculosis: a clinician's perspective. *European Respiratory Journal*, 45(4), pp.1119–1131.

Orme, I.M., 2010. The Achilles heel of BCG. *Tuberculosis*, 90(6), pp.329–332.

Ozawa, S. et al., 2012. Cost-effectiveness and economic benefits of vaccines in low- and middle-income countries: A systematic review. *Vaccine*, 31(1), pp.96–108.

Ozeki, Y. et al., 2010. Transient role of CD4+CD25+ regulatory T cells in mycobacterial infection in mice. *International Immunology*, 22(3), pp.179–189.

Palaci, M. et al., 2007. Cavitary disease and quantitative sputum bacillary load in cases of pulmonary tuberculosis. *Journal of Clinical Microbiology*, 45(12), pp.4064–4066.

Pattacini, L. et al., 2012. A novel HIV vaccine adjuvanted by IC31 induces robust and persistent humoral and cellular immunity. *PLoS ONE*, 7(7), pp.1–11.

Pedrosa, J. et al., 2000. Neutrophils play a protective nonphagocytic role in systemic Mycobacterium tuberculosis infection of mice. *Infection and immunity*, 68, pp.577–583.

Penn-Nicholson, A., Nemes, E., et al., 2015. Mycobacterium tuberculosis-specific CD4 T cells are the principal source of IFN-γ in QuantiFERON assays in healthy persons. *Tuberculosis*, 95(3), pp.350–351.

Penn-Nicholson, A., Geldenhuys, H., et al., 2015. Safety and immunogenicity of candidate vaccine

M72/AS01E in adolescents in a TB endemic setting. *Vaccine*, 33(32), pp.4025–4034.

Perfetto, S.P. et al., 2010. Amine-Reactive Dyes for Dead Cell Discrimination in Fixed Samples. In J. P. Robinson et al., eds. Hoboken, NJ, USA: John Wiley & Sons, Inc.

Van Pinxteren, L.A.H. et al., 2000. Control of latent Mycobacterium tuberculosis infection is dependent on CD8 T cells. *European Journal of Immunology*, 30(12), pp.3689–3698.

Plotkin, S.A., Orenstein, W.A. & Offit, P.A., 2008. *Vaccines*, Saunders/Elsevier.

Pratama, A. & Vinuesa, C.G., 2014. Control of TFH cell numbers: why and how? *Immunology and cell biology*, 92(1), pp.40–8.

Pym, A.S. et al., 2002. Loss of RD1 contributed to the attenuation of the live tuberculosis vaccines Mycobacterium bovis BCG and Mycobacterium microti. *Molecular Microbiology*, 46(3), pp.709–717.

Querec, T.D. et al., 2009. Systems biology approach predicts immunogenicity of the yellow fever vaccine in humans. *Nat Immunol*, 10(1), pp.116–125.

Quinn, K.M. et al., 2008. Accelerating the secondary immune response by inactivating CD4(+)CD25(+) T regulatory cells prior to BCG vaccination does not enhance protection against tuberculosis. *European journal of immunology*, 38(3), pp.695–705.

Quinn, K.M. et al., 2006. Inactivation of CD4+ CD25+ regulatory T cells during early mycobacterial infection increases cytokine production but does not affect pathogen load. *Immunology and cell biology*, 84(5), pp.467–74.

R Development Core Team, 2014. R: A Language and Environment for Statistical Computing. *R Foundation for Statistical Computing Vienna Austria*, 0, pp.{ISBN} 3–900051–07–0.

Ramakrishnan, L., 2012. Revisiting the role of the granuloma in tuberculosis. *Nature Reviews Immunology*.

Reece, S.T. et al., 2011. Improved long-term protection against Mycobacterium tuberculosis Beijing/W in mice after intra-dermal inoculation of recombinant BCG expressing latency associated antigens. *Vaccine*, 29(47), pp.8740–4.

Reiley, W.W. et al., 2010. Distinct functions of antigen-specific CD4 T cells during murine Mycobacterium tuberculosis infection. *Proceedings of the National Academy of Sciences*, 107(45), pp.19408–19413.

Reither, K. et al., 2014. Safety and Immunogenicity of H1/IC31®, an Adjuvanted TB Subunit Vaccine, in HIV-Infected Adults with CD4+ Lymphocyte Counts Greater than 350 cells/mm3: A Phase II, Multi-Centre, Double-Blind, Randomized, Placebo-Controlled Trial A. Landay, ed. *PLoS ONE*, 9(12), p.e114602.

Resende Co, T. et al., 2007. Intestinal helminth co-infection has a negative impact on both anti-Mycobacterium tuberculosis immunity and clinical response to tuberculosis therapy. *Clin Exp Immunol*, 147(1), pp.45–52.

Riedl, K. et al., 2008. The novel adjuvant IC31 strongly improves influenza vaccine-specific cellular and humoral immune responses in young adult and aged mice. *Vaccine*, 26(27-28), pp.3461–3468.

Rogerson, B.J. et al., 2006. Expression levels of Mycobacterium tuberculosis antigen-encoding genes versus production levels of antigen-specific T cells during stationary level lung infection in mice. *Immunology*, 118(2), pp.195–201.

Rozot, V. et al., 2014. Combined Use of Mycobacterium tuberculosis-Specific CD4 and CD8 T-Cell Responses Is a Powerful Diagnostic Tool of Active Tuberculosis. *Clinical Infectious Diseases*, 60(3), pp.432–437.

Rozot, V. et al., 2013. *Mycobacterium tuberculosis* -specific CD8 $^{+}$ T cells are functionally and phenotypically different between latent infection and active disease: Immunity to infection. *European Journal of Immunology*, 43(6), pp.1568–1577.

Russell, D.G., 2007. Who puts the tubercle in tuberculosis? *Nature reviews. Microbiology*, 5, pp.39–47.

Sakai, S. et al., 2014. Cutting Edge: Control of Mycobacterium tuberculosis Infection by a Subset of Lung Parenchyma-Homing CD4 T Cells. *The Journal of Immunology*, 192(7), pp.2965–2969.

Sallusto, F. et al., 1999. Two subsets of memory T lymphocytes with distinct homing potentials and effector functions. *Nature*, 401(6754), pp.708–712.

Sallusto, F., Geginat, J. & Lanzavecchia, A., 2004. Central Memory and Effector Memory T Cell Subsets : Function, Generation, and Maintenance. *Annual Review of Immunology*, 22(1), pp.745–763.

Sallusto, F. & Lanzavecchia, A., 2009. Heterogeneity of CD4+ memory T cells: Functional modules for tailored immunity. *European Journal of Immunology*, 39(8), pp.2076–2082.

Sander, C.R. et al., 2009. Safety and Immunogenicity of a New Tuberculosis Vaccine, MVA85A, in *Mycobacterium tuberculosis* –infected Individuals. *American Journal of Respiratory and Critical Care Medicine*, 179(8), pp.724–733.

Satti, I. et al., 2014. Safety and immunogenicity of a candidate tuberculosis vaccine MVA85A delivered by aerosol in BCG-vaccinated healthy adults: a phase 1, double-blind, randomised controlled trial. *The Lancet Infectious Diseases*, 14(10), pp.939–946.

Scalapino, K.J. et al., 2006. Suppression of disease in New Zealand Black/New Zealand White lupus-prone mice by adoptive transfer of ex vivo expanded regulatory T cells. *J Immunol*, 177(3), pp.1451–1459.

Schellack, C. et al., 2006. IC31, a novel adjuvant signaling via TLR9, induces potent cellular and humoral immune responses. *Vaccine*, 24(26), pp.5461–5472.

Schmittgen, T.D. & Livak, K.J., 2008. Analyzing real-time PCR data by the comparative C T method. , 3(6), pp.1101–1108.

Schoenen, H. et al., 2010. Cutting Edge: Mincle Is Essential for Recognition and Adjuvanticity of the Mycobacterial Cord Factor and its Synthetic Analog Trehalose-Dibehenate. *The Journal of Immunology*, 184(6), pp.2756–2760.

Scriba, T.J. et al., 2012. A Phase IIa Trial of the New Tuberculosis Vaccine, MVA85A, in HIV- and/or *Mycobacterium tuberculosis* –infected Adults. *American Journal of Respiratory and Critical Care Medicine*, 185(7), pp.769–778.

Scriba, T.J. et al., 2008. Distinct, specific IL-17- and IL-22-producing CD4+ T cell subsets contribute to the human anti-mycobacterial immune response. *J Immunol*, 180(3), pp.1962–1970.

Scriba, T.J., Zhang, H.T., et al., 2005. HIV-1-specific CD4+ T lymphocyte turnover and activation increase upon viral rebound. *J Clin Invest*, 115(2), pp.443–450.

Scriba, T.J., Purbhoo, M., et al., 2005. Ultrasensitive detection and phenotyping of CD4+ T cells with optimized HLA class II tetramer staining. *J Immunol*, 175(10), pp.6334–6343.

Seder, R.A., Darrah, P.A. & Roederer, M., 2008. T-cell quality in memory and protection: implications for vaccine design. *Nature Reviews Immunology*, 8(April), pp.247 – 258.

September, S.M. et al., 2004. Diversity of Nontuberculoid Mycobacterium Species in Biofilms of Urban and Semiurban Drinking Water Distribution Systems Diversity of Nontuberculoid Mycobacterium Species in Biofilms of Urban and Semiurban Drinking Water Distribution Systems †. *Applied and environmental microbiology*, 70(12), pp.7571–73.

Serbina, N. V & Flynn, J.L., 2001. CD8(+) T cells participate in the memory immune response to Mycobacterium tuberculosis. *Infect Immun*, 69(7), pp.4320–4328.

Sidney, J. et al., 2001. Measurement of MHC/Peptide Interactions by Gel Filtration. In John Wiley & Sons, Inc.

Simon, A. et al., 2000. Function-related regulation of the stability of MHC proteins. *Biophysical journal*, 79(5), pp.2305–2313.

Soares, A.P. et al., 2008. Bacillus Calmette-Guerin vaccination of human newborns induces T cells with complex cytokine and phenotypic profiles. *J Immunol*, 180(5), pp.3569–3577.

Soares, A.P. et al., 2013. Longitudinal Changes in CD4+ T-Cell Memory Responses Induced by BCG Vaccination of Newborns. *Journal of Infectious Diseases*, 207(7), pp.1084–1094.

Songane, M. et al., 2012. The role of autophagy in host defence against Mycobacterium tuberculosis infection. *Tuberculosis*, 92(5), pp.388–396.

Stenger, S., 1998. An Antimicrobial Activity of Cytolytic T Cells Mediated by Granulysin. *Science*, 282(5386), pp.121–125.

Szabo, S.J. et al., 2000. A novel transcription factor, T-bet, directs Th1 lineage commitment. *Cell*, 100(6), pp.655–69.

Tameris, M.D. et al., 2013. Safety and efficacy of MVA85A, a new tuberculosis vaccine, in infants previously vaccinated with BCG: a randomised, placebo-controlled phase 2b trial. *Lancet*, 381(9871), pp.1021–1028.

Tena-Coki, N.G. et al., 2010. CD4 and CD8 T-cell responses to mycobacterial antigens in African children. *Am J Respir Crit Care Med*, 182(1), pp.120–129.

Tian, T. et al., 2005. In vivo depletion of CD11c+ cells delays the CD4+ T cell response to Mycobacterium tuberculosis and exacerbates the outcome of infection. *Journal of immunology (Baltimore, Md. : 1950)*, 175(5), pp.3268–3272.

Tobin, D.M. et al., 2010. The lta4h Locus Modulates Susceptibility to Mycobacterial Infection in Zebrafish and Humans. *Cell*, 140(5), pp.717–730.

Torrado, E. & Cooper, A.M., 2010. IL-17 and Th17 cells in tuberculosis. *Cytokine Growth Factor Rev*, 21(6), pp.455–462.

Tostmann, A. et al., 2008. Tuberculosis Transmission by Patients with Smear-Negative Pulmonary Tuberculosis in a Large Cohort in The Netherlands. *Clinical Infectious Diseases*, 47(9), pp.1135–1142.

Tsao, T.C. et al., 2000. Imbalances between tumor necrosis factor-alpha and its soluble receptor forms, and interleukin-1beta and interleukin-1 receptor antagonist in BAL fluid of cavitary pulmonary tuberculosis. *Chest*, 117(1), pp.103–9.

Urdahl, K.B., Shafiani, S. & Ernst, J.D., 2011. Initiation and regulation of T-cell responses in

tuberculosis. *Mucosal Immunology*, 4(3), pp.288–293.

Vergne, I. et al., 2005. Mechanism of phagolysosome biogenesis block by viable Mycobacterium tuberculosis. *Proceedings of the National Academy of Sciences of the United States of America*, 102(11), pp.4033–4038.

Vieira, O., Botelho, R. & Grinstein, S., 2002. Phagosome maturation: aging gracefully. *Biochem. J*, 366, pp.689–704.

Vogelzang, A. et al., 2014. Central Memory CD4+ T Cells Are Responsible for the Recombinant Bacillus Calmette-Guerin ureC::hly Vaccine's Superior Protection Against Tuberculosis. *Journal of Infectious Diseases*, 210(12), pp.1928–1937.

Wang, P. et al., 2008. A systematic assessment of MHC class II peptide binding predictions and evaluation of a consensus approach. *PLoS Computational Biology*, 4(4).

Wang, T. et al., 2012. Selection of Suitable Housekeeping Genes for Real-Time Quantitative PCR in CD4+ Lymphocytes from Asthmatics with or without Depression K. Ito, ed. *PLoS ONE*, 7(10), p.e48367.

Warnes, G.R. et al., 2015. gplots: Various R Programming Tools for Plotting Data. *R package version 2.17.0.*, p.2015.

Weidt, G. et al., 1998. Relationship among immunodominance of single CD8+ T cell epitopes, virus load, and kinetics of primary antiviral CTL response. *Journal of immunology (Baltimore, Md. : 1950)*, 160(6), pp.2923–2931.

Welin, A. & Lerm, M., 2012. Inside or outside the phagosome? The controversy of the intracellular localization of Mycobacterium tuberculosis. *Tuberculosis*, 92(2), pp.113–120.

Weng, N., Araki, Y. & Subedi, K., 2012. The molecular basis of the memory T cell response: differential gene expression and its epigenetic regulation. *Nature Reviews Immunology*, 12(4), pp.306–315.

White, A.K. et al., 2011. High-throughput microfluidic single-cell RT-qPCR. *Proceedings of the National Academy of Sciences*, 108(34), pp.13999–14004.

WHO, 2014. Global tuberculosis report 2014. Available at: http://apps.who.int/iris/bitstream/10665/137094/1/9789241564809_eng.pdf?ua=1 [Accessed May 18, 2015].

Wilkinson, R.J. et al., 2000. Influence of vitamin D deficiency and vitamin D receptor polymorphisms on tuberculosis among Gujarati Asians in west London: a case-control study. *Lancet*, 355(9204), pp.618–621.

Willinger, T. et al., 2006. Human Naive CD8 T Cells Down-Regulate Expression of the WNT Pathway Transcription Factors Lymphoid Enhancer Binding Factor 1 and Transcription Factor 7 (T Cell Factor-1) following Antigen Encounter In Vitro and In Vivo. *The Journal of Immunology*, 176(3), pp.1439–1446.

Wolf, A.J. et al., 2007. Mycobacterium tuberculosis Infects Dendritic Cells with High Frequency and Impairs Their Function In Vivo. *The Journal of Immunology*, 179(4), pp.2509–2519.

Wood, R. et al., 2012. Indoor Social Networks in a South African Township: Potential Contribution of Location to Tuberculosis Transmission P. Tang, ed. *PLoS ONE*, 7(6), p.e39246.

Wood, R., Maartens, G. & Lombard, C.J., 2000. Risk factors for developing tuberculosis in HIV-1-infected adults from communities with a low or very high incidence of tuberculosis. *J Acquir*

Immune Defic Syndr, 23(1), pp.75–80.

Woodworth, J.S. et al., 2014. Protective CD4 T Cells Targeting Cryptic Epitopes of Mycobacterium tuberculosis Resist Infection-Driven Terminal Differentiation. *The Journal of Immunology*, 192(7), pp.3247–3258.

Woodworth, J.S., Wu, Y. & Behar, S.M., 2008. Mycobacterium tuberculosis-specific CD8+ T cells require perforin to kill target cells and provide protection in vivo. *J Immunol*, 181(12), pp.8595–8603.

Wooldridge, L. et al., 2009. Tricks with tetramers: how to get the most from multimeric peptide-MHC. *Immunology*, 126(2), pp.147–164.

Workman, C.J. et al., 2009. The development and function of regulatory T cells. *Cellular and Molecular Life Sciences*, 66(16), pp.2603–2622.

Yamamoto, S. & Yamamoto, T., 2007. Historical review of BCG vaccine in Japan. *Japanese Journal of Infectious Diseases*, 60(6), pp.331–336.

Yamamura, M. et al., 1991. Defining protective responses to pathogens: cytokine profiles in leprosy lesions. *Science*, 254(5029), pp.277–279.

Zhang, M. et al., 1995. T-cell cytokine responses in human infection with Mycobacterium tuberculosis. *Infect Immun*, 63(8), pp.3231–3234.

Zhang, W. et al., 2013. Genome sequencing and analysis of BCG vaccine strains. *PloS one*, 8(8), p.e71243.

Zhang, X. et al., 2009. Coactivation of Syk Kinase and MyD88 Adaptor Protein Pathways by Bacteria Promotes Regulatory Properties of Neutrophils. *Immunity*, 31(5), pp.761–771.

Zheng, W. & Flavell, R.A., 1997. The transcription factor GATA-3 is necessary and sufficient for Th2 cytokine gene expression in CD4 T cells. *Cell*, 89, pp.587–596.

Zhu, J., Yamane, H. & Paul, W.E., 2010. Differentiation of effector CD4 T cell populations (*). *Annual review of immunology*, 28, pp.445–489.

Zielinski, C.E. et al., 2011. Dissecting the human immunologic memory for pathogens. *Immunological reviews*, 240(1), pp.40–51.

Zumla, A. et al., 2015. Tuberculosis treatment and management—an update on treatment regimens, trials, new drugs, and adjunct therapies. *The Lancet Respiratory Medicine*, 3(3), pp.220–234.

Zumla, A. et al., 2013. Tuberculosis. *The New England journal of medicine*, 368(8), pp.745–55.

Zumla, A. & James, D.G., 1996. Granulomatous infections: etiology and classification. *Clinical infectious diseases*, 23(1), pp.146–158.

Appendix

#	Amino Acid Sequence
1	MTEQQWNFAGIEAAA
2	WNFAGIEAAASAIQG
3	IEAAASAIQGNVTSI
4	SAIQGNVTSIHSLLD
5	NVTSIHSLLDEGKQS
6	HSLLDEGKQSLTKLA
7	EGKQSLTKLAAAWGG
8	LTKLAAAWGGSGSEA
9	AAWGGSGSEAYQGVQ
10	SGSEAYQGVQQKWDA
11	YQGVQQKWDATATEL
12	QKWDATATELNNALQ
13	TATELNNALQNLART
14	NNALQNLARTISEAG
15	NLARTISEAGQAMAS
16	ISEAGQAMASTEGNV
17	QAMASTEGNVTGMFA

#	Amino Acid Sequence	#	Amino Acid Sequence	#	Amino Acid Sequence	#	Amino Acid Sequence
1	MQLVDRVRGAVTGMS	21	FEWYDQSGLSVVMPV	41	AMGPTLIGLAMGDAG	61	DSGTHSWEYWGAQLN
2	RVRGAVTGMSRRLVV	22	QSGLSVVMPVGGQSS	42	LIGLAMGDAGGYKAS	62	SWEYWGAQLNAMKPD
3	VTGMSRRLVVGAVGA	23	VVMPVGGQSSFYSDW	43	MGDAGGYKASDMWGP	63	GAQLNAMKPDLQRAL
4	RRLVVGAVGAALVSG	24	GGQSSFYSDWYQPAC	44	GYKASDMWGPKEDPA	64	AMKPDLQRALGATPN
5	GAVGAALVSGLVGAV	25	FYSDWYQPACGKAGC	45	DMWGPKEDPAWQRND	65	LQRALGATPNTGPAP
6	ALVSGLVGAVGGTAT	26	YQPACGKAGCQTYKW	46	KEDPAWQRNDPLLNV	66	GATPNTGPAPQGA
7	LVGAVGGTATAGAFS	27	GKAGCQTYKWETFLT	47	WQRNDPLLNVGKLIA		
8	GGTATAGAFSRPGLP	28	QTYKWETFLTSELPG	48	PLLNVGKLIANNTRV		
9	AGAFSRPGLPVEYLQ	29	ETFLTSELPGWLQAN	49	GKLIANNTRVWVYCG		
10	RPGLPVEYLQVPSPS	30	SELPGWLQANRHVKP	50	NNTRVWVYCGNGKPS		
11	VEYLQVPSPSMGRDI	31	WLQANRHVKPTGSAV	51	WVYCGNGKPSDLGGN		
12	VPSPSMGRDIKVQFQ	32	RHVKPTGSAVVGLSM	52	NGKPSDLGGNNLPAK		
13	MGRDIKVQFQSGGAN	33	TGSAVVGLSMAASSA	53	DLGGNNLPAKFLEGF		
14	KVQFQSGGANSPALY	34	VGLSMAASSALTLAI	54	NLPAKFLEGFVRTSN		
15	SGGANSPALYLLDGL	35	AASSALTLAIYHPQQ	55	FLEGFVRTSNIKFQD		
16	SPALYLLDGLRAQDD	36	LTLAIYHPQQFVYAG	56	VRTSNIKFQDAYNAG		
17	LLDGLRAQDDFSGWD	37	YHPQQFVYAGAMSGL	57	IKFQDAYNAGGGHNG		
18	RAQDDFSGWDINTPA	38	FVYAGAMSGLLDPSQ	58	AYNAGGGHNGVFDFP		
19	FSGWDINTPAFEWYD	39	AMSGLLDPSQAMGPT	59	GGHNGVFDFPDSGTH		
20	INTPAFEWYDQSGLS	40	LDPSQAMGPTLIGLA	60	VFDFPDSGTHSWEYW		

#	Amino Acid Sequence	#	Amino Acid Sequence	#	Amino Acid Sequence	#	Amino Acid Sequence
1	MTDVSRKIRAWGRRL	21	YYQSGLSIVMPVGGQ	41	PSLIGLAMGDAGGYK	61	THSWEYWGAQLNAMK
2	RKIRAWGRRLMIGTA	22	LSIVMPVGGQSSFYS	42	LAMGDAGGYKAADMW	62	YWGAQLNAMKGDLQS
3	WGRRLMIGTAAAVVL	23	PVGGQSSFYSDWYSP	43	AGGYKAADMWGPSSD	63	LNAMKGDLQSSLGAG
4	MIGTAAAVVLPGLVG	24	SSFYSDWYSPACGKA	44	AADMWGPSSDPAWER		
5	AAVVLPGLVGLAGGA	25	DWYSPACGKAGCQTY	45	GPSSDPAWERNDPTQ		
6	PGLVGLAGGAATAGA	26	ACGKAGCQTYKWETF	46	PAWERNDPTQQIPKL		
7	LAGGAATAGAFSRPG	27	GCQTYKWETFLTSEL	47	NDPTQQIPKLVANNT		
8	ATAGAFSRPGLPVEY	28	KWETFLTSELPQWLS	48	QIPKLVANNTRLWVY		
9	FSRPGLPVEYLQVPS	29	LTSELPQWLSANRAV	49	VANNTRLWVYCGNGT		
10	LPVEYLQVPSPSMGR	30	PQWLSANRAVKPTGS	50	RLWVYCGNGTPNELG		
11	LQVPSPSMGRDIKVQ	31	ANRAVKPTGSAAIGL	51	CGNGTPNELGGANIP		
12	PSMGRDIKVQFQSGG	32	KPTGSAAIGLSMAGS	52	PNELGGANIPAEFLE		
13	DIKVQFQSGGNNSPA	33	AAIGLSMAGSSAMIL	53	GANIPAEFLENFVRS		
14	FQSGGNNSPAVYLLD	34	SMAGSSAMILAAYHP	54	AEFLENFVRSSNLKF		
15	NNSPAVYLLDGLRAQ	35	SAMILAAYHPQQFIY	55	NFVRSSNLKFQDAYN		
16	VYLLDGLRAQDDYNG	36	AAYHPQQFIYAGSLS	56	SNLKFQDAYNAAGGH		
17	GLRAQDDYNGWDINT	37	QQFIYAGSLSALLDP	57	QDAYNAAGGHNAVFN		
18	DDYNGWDINTPAFEW	38	AGSLSALLDPSQGMG	58	AAGGHNAVFNFPPNG		
19	WDINTPAFEWYYQSG	39	ALLDPSQGMGPSLIG	59	NAVFNFPPNGTHSWE		
20	PAFEWYYQSGLSIVM	40	SQGMGPSLIGLAMGD	60	FPPNGTHSWEYWGAQ		

Appendix Figure 1. 15mer peptide sequences overlapping by 10 amino acids spanning (A) ESAT-6, (B) Ag85A , and (C) Ag85B.

```
Ag85A MQLVDRVRGAVTGMSRRLVVGAVGAALVSGLVGAVGGTATAGAFSRPGLPVEYLQVPSPSMGRDIKVQFQSGGANSPALYLLDGLRAQDDFSGWDINTPAFEWYDQS
           V        RRL  G   A    GLVG  GG ATAGAFSRPGLPVEYLQVPSPSMGRDIKVQFQSGG NSPA YLLDGLRAQDD  GWDINTPAFEWY QS
Ag85B    MTDVSRKIRAWGRRLMIGTAAAVVLPGLVGLAGGAATAGAFSRPGLPVEYLQVPSPSMGRDIKVQFQSGGNNSPAVYLLDGLRAQDDYNGWDINTPAFEWYYQS

Ag85A GLSVVMPVGGQSSFYSDWYQPACGKAGCQTYKWETFLTSELPGWLQANRHVKPTGSAVVGLSMAASSALTLAIYHPQQFVYAGAMSGLLDPSQAMGPTLIGLAMGDA
      GLS VMPVGGQSSFYSDWY PACGKAGCQTYKWETFLTSELP WL ANR VKPTGSA  GLSMA SSA  LA YHPQQF YAG  S LLDPSQ MGP LIGLAMGDA
Ag85B GLSIVMPVGGQSSFYSDWYSPACGKAGCQTYKWETFLTSELPQWLSANRAVKPTGSAAIGLSMAGSSAMILAAYHPQQFIYAGSLSALLDPSQGMGPSLIGLAMGDA

Ag85A GGYKASDMWGPKEDPAWQRNDPLLNVGKLIANNTRVWVYCGNGKPSDLGGNNLPAKFLEGFVRTSNIKFQDAYNAGGGHNGVFDFPDSGTHSWEYWGAQLNAMKPDL
      GGYKA DMWGP  DPAW RNDP     KL ANNTR WVYCGNG P  LGG N PA FLE FVR SN KFQDAYNA GGHN VF FP  GTHSWEYWGAQLNAMK DL
Ag85B GGYKAADMWGPSSDPAWERNDPTQQIPKLVANNTRLWVYCGNGTPNELGGANIPAEFLENFVRSSNLKFQDAYNAAGGHNAVFNFPPNGTHSWEYWGAQLNAMKGDL

Ag85A QRALGATPNTGPAPQGA
      Q  LGA
Ag85B QSSLGAG
```

Appendix Figure 2: Homology between Ag85A and Ag85B. The optimal sequence alignment of Ag85A (top) and Ag85B (bottom) is shown in red (middle).

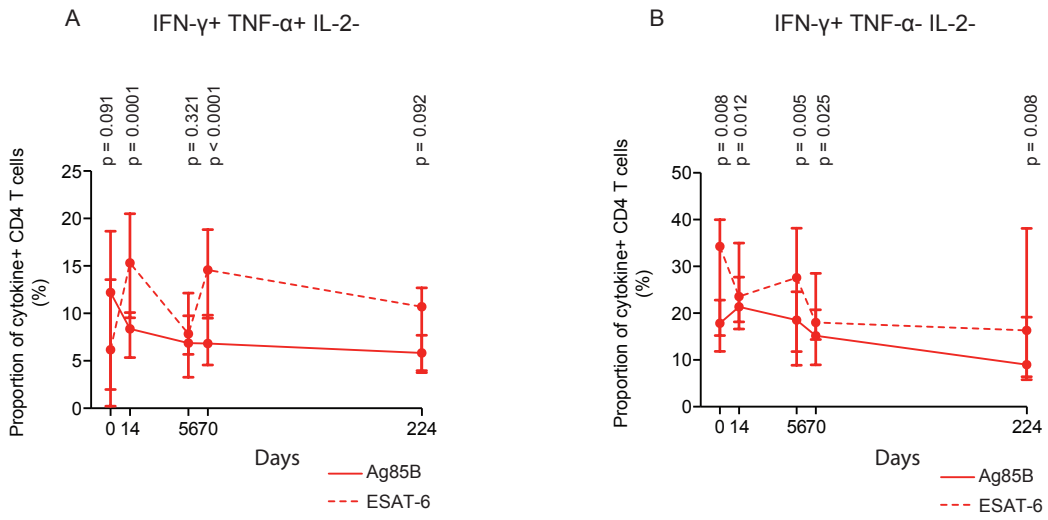

Appendix Figure 3. The proportions of (A) IFN-γ^{+}TNF-α^{+}IL-2^{-} and (B) IFN-γ^{+}TNF-α^{-}IL-2^{-} Ag85B and ESAT-6-specific CD4 T cells in QFT+ adolescents. P values were calculated using the Wilcoxon signed-rank test. Unadjusted p values are shown.

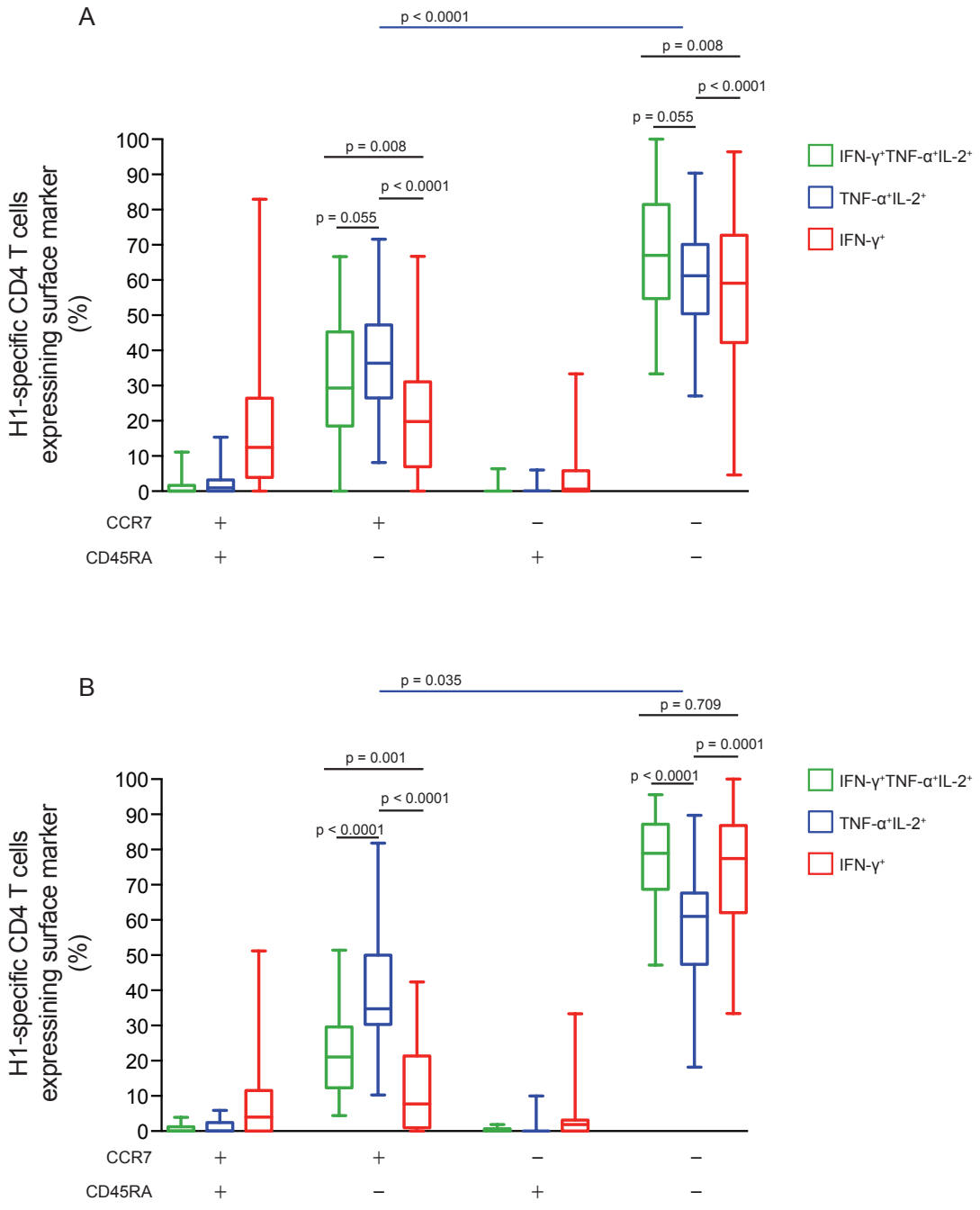

Appendix Figure 4. The proportion of IFN-γ^{+}TNF-α^{+}IL-2^{+} (green), IFN-γ^{-}TNF-α^{+}IL-2^{+} (blue), and IFN-γ^{+}TNF-α^{-}IL-2^{-} (red) H1-specific CD4 T cells in Group 1 expressing all combinations of CCR7 and CD45RA on day 224.

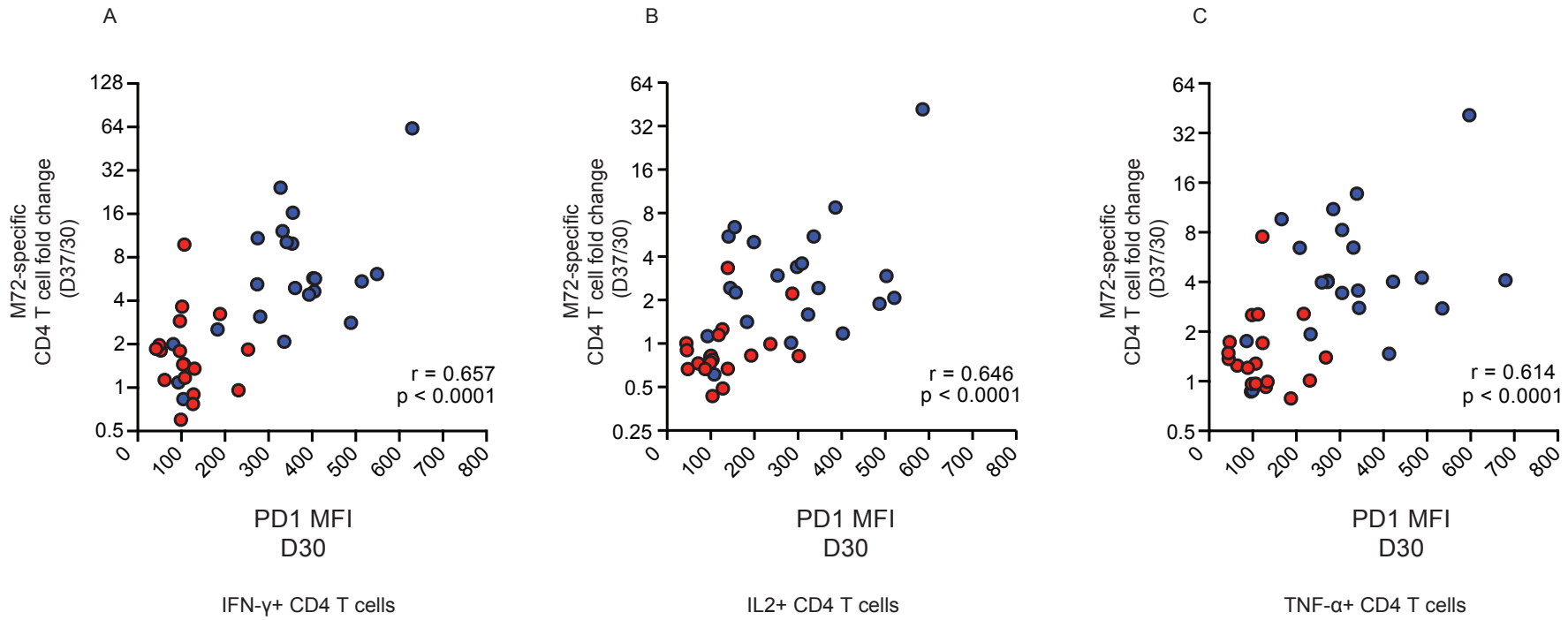

Appendix Figure 5. The correlation of PD-1 MFI on M72-specific CD4 T cells on day 30 and the fold increase in (A) IFN-γ^+ (B) TNF-α^+ (C) IL-2^+ M72-specific CD4 T cells following secondary vaccination. P and r values were calculated using the Spearman's rank correlation.